USC
UNIVERSIDADE
DE SANTIAGO
DE COMPOSTELA

CENTRO INTERNACIONAL DE ESTUDOS
DE DOUTORAMENTO E AVANZADOS
DA USC (CIEDUS)

TESE DE DOUTORAMENTO

DOUBLE AND MULTIPLE STELLAR SYSTEMS: OBSERVATIONAL TECHNIQUES, DATA ADMINISTRATION AND SCIENTIFIC RESULTS

Jorge Gómez Crespo

ESCOLA DE DOUTORAMENTO INTERNACIONAL

PROGRAMA DE DOUTORAMENTO EN MATEMÁTICAS

SANTIAGO DE COMPOSTELA

2018

USC
UNIVERSIDADE
DE SANTIAGO
DE COMPOSTELA

DECLARACIÓN DO AUTOR DA TESE

DOUBLE AND MULTIPLE STELLAR SYSTEMS: OBSERVATIONAL TECHNIQUES, DATA ADMINISTRATION AND SCIENTIFIC RESULTS

D. Jorge Gómez Crespo

Presento a miña tese, seguindo o procedemento axeitado ao Regulamento, e declaro que:

1) A tese abarca os resultados da elaboración do meu traballo.
2) De selo caso, na tese faise referencia ás colaboracións que tivo este traballo.
3) A tese é a versión definitiva presentada para a súa defensa e coincide coa versión enviada en formato electrónico.
4) Confirmo que a tese non incorre en ningún tipo de plaxio doutros autores nin de traballos presentados por min para a obtención doutros títulos.

En Santiago de Compostela, 5 de novembro de 2018

Asdo. Jorge Gómez Crespo

USC
UNIVERSIDADE
DE SANTIAGO
DE COMPOSTELA

AUTORIZACIÓN DO DIRECTOR DA TESE

DOUBLE AND MULTIPLE STELLAR SYSTEMS: OBSERVATIONAL TECHNIQUES, DATA ADMINISTRATION AND SCIENTIFIC RESULTS

D. José Ángel Docobo Durántez, Catedrático de Astronomía do Departamento de Matemática Aplicada da Universidade de Santiago de Compostela

INFORMA:

Que a presente tese, correspóndese co traballo realizado por D. ***Jorge Gómez Crespo****, baixo a miña dirección, e autorizo a súa presentación, considerando que reúne os requisitos esixidos no Regulamento de Estudos de Doutoramento da USC, e que como director desta non incorre nas causas de abstención establecidas na Lei 40/2015.*

En Santiago de Compostela, 5 de novembro de 2018

Asdo. José Ángel Docobo Durántez

USC
UNIVERSIDADE
DE SANTIAGO
DE COMPOSTELA

Acknowledgements

I thank J.A. Docobo, the Director of this dissertation, for his assistance and collaboration. He introduced me to the field of Astronomy and, since then, he has motivated and guided me. His work and support was fundamental for the completion of the projects and research articles presented herein. I especially want to thank J.A. Docobo for having facilitated my research visits to the Byurakan Astrophysical Observatory (BAO) in Armenia, the Special Astrophysical Observatory (SAO-RAS) in Russia, the Southern Astrophysical Research (SOAR) Telescope in Chile, and the Telescope Fabra-ROA at Montsec (TFRM) in Spain, which were essential for the completion of this dissertation project.

Noray Melikian of the BAO supervised my apprenticeship in Astronomy and Astrophysics during my first year of the doctoral program in Armenia as well as during the observation campaigns that we carried out with the BAO 2.6m telescope as he took charge of the logistics and my well being. Thanks to him, my research stays there were productive at the scientific level as well as at a personal level.

I also thank the other scientists with whom I have collaborated. They are: P. P. Campo, M. Andrade, V. Tamazian, L. Picotti, and L. M. Scott (OARMA); A. A. Karapetian, S. A. Khazaryan, H. A. Harutyunian, M. Gevorgyan, G. M. Paronyan, T. H. Movsissian, and K. S. Gigoyan (BAO); Y.Y. Balega, D. A. Rastegaev, V. V. Dyachenko, A. F. Maksimov, E. V. Malogolovets, and E. Philippova (SAO); R. A. Méndez, E. Costa (Universidad de Chile); A. Tokovinin (AURA/CTIO/NOAO); E. P. Horch (Southern Connecticut State University and Lowell Observatory); D. del Ser, M.ª T. Merino, and the entire team at TFRM, led by Jorge Nuñez. I wish to express my profound appreciation to all of the astronomical institutions that I visited during my doctoral research period for the hospitality extended.

The Astrophysics Data System Bibliographic Services of NASA, the Washington Double Star Catalog, the SIMBAD database, the catalog access tools of Vizier, IRAF, LaTeX, and Anaconda have made this work possible.

Many thanks to my family and, especially, to my parents and my sister. I also thank Lara for all of her support and care that she has given me throughout these years.

Last but not least, I thank Raz, Lira, Ernesto, Pilar, Miriam, Laura, Miguel, Mireia, Melissa, Lucho, Lima, Quique, Basa, Gati, Tasio, Virginia, Irene, Andrea, Abraham, Marta, Petra, Karla, Carlos, Enric, Pablo, Varum, Francis, Hasmik, Diego, David, Betxi, Nati, Lourdes, Lía, Gabriel, Susana, Mónica, Noelia, Deivid, Mero, Becho, Sori, Nacho, Charly, Castro, Elías, Peti, López, Malías, Paco, Jamaoh, Luis A., Casti, David, Rosa, Xavi, Juan David, Bea, Sergio, and María José.

My sincere thanks to all!

USC
UNIVERSIDADE
DE SANTIAGO
DE COMPOSTELA

A Lucía, Ana, Servando, Raz y Lira.

USC
UNIVERSIDADE
DE SANTIAGO
DE COMPOSTELA

Short Abstract

Title

DOUBLE AND MULTIPLE STELLAR SYSTEMS: OBSERVATIONAL TECHNIQUES, DATA ADMINISTRATION AND SCIENTIFIC RESULTS

Short Abstract

This dissertation, written as a compendium of research articles, was proposed and supervised by J.A. Docobo, Full Professor in Astronomy and Director of the Ramon María Aller Astronomical Observatory of the University of Santiago de Compostela. The focus is on the practical application of speckle interferometry techniques, including the initiation and development of several observational campaigns employing OARMA's eMCCD speckle camera attached to the 2.6m telescope at BAO. Additionally, we present 26 orbits of accessible binaries of the Southern hemisphere based on SOAR speckle data. Also, the orbital information of the double-line spectroscopic binaries, HD 183255, HD 114882, and HD 30712, together with new speckle measurements performed using large telescopes, allowed us to determine the main physical parameters of these systems.

Apart from that, emission and photometric results related with the regions Cep OB3 and Cyg OB7 are presented.

USC
UNIVERSIDADE
DE SANTIAGO
DE COMPOSTELA

Abstract

This dissertation was written by Jorge Gomez Crespo as a compendium of research articles under the supervision of J.A. Docobo, a Full Professor in Astronomy and Director of the Ramon María Aller Astronomical Observatory of the University of Santiago de Compostela, Spain. In order to provide the reader a correct scientific context, we have included an Introduction in which the scientific context regarding the study of double and multiple star systems and their physical and dynamical properties is presented. Within this wide field, we have centered our research on imaging techniques, particularly, Speckle Interferometry (SI). Today, SI is the most productive amongst the high resolution techniques used to obtain relative positions and differential photometry of binaries, which are the first steps in visual binary research. The author, in collaboration with his Dissertation director and members of OARMA, has continually conducted research in this field since his enrollment in the USC Doctoral program in Mathematics (Astronomy). Thanks to his work and collaboration with prestigious international scientists, such as, Y. Y. Balega, R. A. Méndez, E. P. Horch, and N. D. Melikian, we have been able to accomplish a large part of the tasks that were proposed at the beginning of this educational period.

In addition, three chapters are included that summarize the principal concepts relative to observation from the Earth's surface, the techniques and technology of imaging, the instrumentation used in Astronomy to investigate double and multiple systems and provide precise observations that guarantee determined orbits, the methodology developed and used in the observation campaigns in Armenia, and different aspects relative to the treatment of images obtained with CCD and eMCCD cameras.

The first year of the Doctorate was supported by the European Commission by means of an Erasmus Mundus Alrakis II scholarship. The scholarship allowed the author to take advantage of a research visit in Armenia, to work in the Byurakan Astrophysical Observatory, and to collaborate with Profesor N. D. Melikian who supervised the visit. Professor Melikian has dedicated his career to the study of Young Stellar Objects and to regions of stellar formation.

It is important to mention, the author attended various observation campaigns at prestigious international centers such as SAO (Russia) and SOAR (Chile) and with experience acquired at these institutions, we were able to begin a series of SI observation campaigns with the 2.6 m telescope at the Byurakan Astrophysical Observatory in which the eMCCD camera of OARMA was left on deposit at the Armenian observatory.

In the chapter entitled Imaging, the theory that is necessary to understand the ways in which atmospheric turbulence creates difficulties for observation when a telescope of more than 1 m is used. Due to atmospheric turbulence, classic resolution does not scale with aperture. In order to evaluate the quality of an astronomical image, several principal concepts have been introduced. They include the disc de Airy, the disc of seeing, the FWHM, and the PSF. Next,

we explain three techniques that are used to correct for the atmospheric effects and reach the theoretical diffraction limit:

- Adaptive Optics (AO): primarily used in the infrared.
- Speckle Interferometry (SI): Useful with all types of telescopes and, fundamentally, for observations in the visible.
- Lucky Imaging (LI): especially useful for telescopes of $\leqslant$3 m because efficiency is lost with larger telescopes.

Although this work is centered on SI, it is important to detail some basic aspects of other imaging techniques applied to stellar observation and the detection of exoplanets. In this way, the reader may have an idea of the set of strategies used for star observation and their applications when detecting and resolving double and multiple systems. Moreover, SI can be used in combination with AO systems as is the case with the observations acquired with the 4.1 m at SOAR that was used for two of the articles presented herein. For that reason, it is important to detail these general concepts that control the design and function of AO.

Within the context of this dissertation, it is important to highlight that LI and SI today use the same type of eMCCD cameras and, therefore, the reduction processes are similar. Moreover, the Shift-and- Add algorithms that characterize LI are also used with SI in order to calculate the disc of seeing and to be able to evaluate the quality of the observations.

The techniques for the detection of exoplanets serve to show how the observation techniques and image treatment that are used in imaging have evolved in recent years. They are now adapted to the difficulties presented by these low brightness objects that are often hidden by the halo of the host star itself.

In the first chapter, a complete bibliographic review of SI research since its inception is presented. In it, the original article is summarized in which it was realized, for the first time, that this technique was recognized (Labeyrie, 1970), the different research groups that used it were mentioned and the applications related to the study of an ample range of astronomical phenomenon and celestial objects were cited. We differentiated the first decades of observation with SI in which photographic paper, CCDs, and ICCDs were used from the modern epoch in which the use of eMCCD technology is used for detection. As mentioned, the objective of this chapter is to provide the reader with a series of concepts and knowledge that will permit an understanding of the trajectory and importance of SI.

In the chapter on Instrumentation, the principal instruments that have accompanied the observation of double star systems since its initiation are reviewed. Although the first double system was detected for its light curve by photometric technology, the study of visual double star systems was historically associated with filar micrometers as shown by more than 150 years of research reports. For that reason, this work would be incomplete if we did not describe its design and name some of the researchers that contributed notably to the study of

double and multiple systems using micrometric observations. The revolution brought on by Michelson and interferometry is also treated in this document in which the different types of interferometers are described and the moment that SI was initiated is highlighted.

The exposure time characteristics of SI were not efficient until the photon Charge-Coupled Devices (CCDs) appeared. SI has developed along with the evolution and improvement of CCDs. For that reason, the function of CCDs and ICCDs are also detailed. In order to obtain scientifically valid results of the CCD images, the noise present in them must be eliminated. The reduction process used has been carefully detailed as well as the calibration images needed for its execution. Here, we present a brief description of the ICCD camera that OARMA used for its first SI observation campaigns until the eMCCD PhotonMAX 512 detector was acquired. In this text, we present the characteristics of eMCCD technology, its peculiarities when reducing noise, the design of the OARMA eMCCD camera and how it is mounted on and dismounted from the 2.6 m telescope at Byurakan at the beginning and the ending of our observation campaigns today.

The content of this chapter is designed to permit the reader to understand how the quality of astronomical observations depends to a great degree on the technical characteristics of the detectors utilized. We also emphasize the importance of knowing the necessary reduction processes and to be be very careful with their execution.

In the chapter on campaigns, we focus on the methodological part that accompanies the development of new observation campaigns at SAO and BAO. The process of acquiring the images, the calibration of the pixel size, and the deviation of the camera in its installation is explained and that is accompanied by a description of a night of observation. The reduction and analysis processes that are applied to the acquired images at both observatories is also detailed. Our collaboration with the SAO SI research group, the people involved in our BAO campaigns, and the principal SI observer at SOAR, A. Tokovinin, has been fundamental.

As the processes of reduction and analysis of the observations acquired during the SAO and BAO campaigns have not been completely finalized, we cannot yet reveal all of the results achieved. We are able to report quantitative date referent to the quantity of objects of interest that were registered as well as the acquired calibration images. In the case of the observations at BAO, a part of those results have been previously published in a recently recovered journal of the Armenian Observatory itself. In this communication, we describe the camera and the results obtained until the end of 2017. The data that corresponds to the last campaign of May-June 2018 is presented here for the first time.

The principal chapter of the dissertation is presented next. We begin by emphasizing the importance that the detection of new components has for modern Astronomy. We also explain how the calculus of orbits in double and multiple systems contributes information to different branches of Astronomy concerning the fundamental parameters on which our knowledge of the stars and, in particular, the models of stellar evolution are based. Regarding the importance of our observation campaigns, we include three articles regarding research

which used measurements obtained with SI. In the first, by means of our collaboration with the Professor and Researcher at the University of Chile, R. A. Mendez, we were able to obtain observation time at SOAR. In that line of activity, the author traveled to La Serena (Chile) in order to participate in image acquisition. With the results obtained, we improved the orbits of 12 austral systems at the same time that we contributed scientific information relative to the physical properties of those systems. The analytic method of J.A. Docobo was used for the calculation of all of the orbits.

To said collaboration, E. Costa, a researcher associated with the University of Chile, has recently joined our collaborative group. Along with the Director of this dissertation, J.A. Docobo, P.P. Campo, and the Chilean researchers, we have published another article contributing 14 more orbits. These orbits correspond to systems that are, in their majority, located in the Southern hemisphere. In this work, we add an initial study of the ages of the components of these systems and here we show their evolutionary tracks as well as the diagrams that compare the current temperature and luminosity of these components with the temperatures and luminosity expected throughout their evolution in stars of the same mass and metallicity.

The third article was written in collaboration with E. P. Horch, a researcher at the Lowell Observatory and Southern Connecticut University. This prestigious scientist has had a long career in SI. Using data obtained in his observation campaigns along with other information that we contributed from our SAO campaigns, we have been able determine the physical characteristics relative to the mass and orbital parallax of the three systems with high precision that present the particularity of also being double line spectroscopic binaries.

This type of closed binaries are generally difficult to detect visually, When possible, thanks to the methodology developed by the OARMA researchers, J. A. Docobo, P. P. Campo, and M. Andrade, it has been possible for us to calculate a visual orbit that adjusts to the spectroscopic orbit and improve it. Moreover, in these systems the mass of the components can be calculated separately and the orbital parallaxes can be compared to the data provided by Gaia.

The three articles have been published in high impact scientific journals in Astronomy such as The Astronomical Journal and Monthly Notices of the Royal Astronomical Society.

Finally, in the last chapter, we present the collaborations that the author of this dissertation has completed with N. D. Melikian and A. A. Karapetian. Together, we have published three studies concerning two regions of stellar formation, Cep OB3 and Cyg OB7. Said articles are centered on stars with emissions in H_α in these zones and in the detection of variability by means of differential photometry and the study of light curves. Among the results, an unusual flare was detected in V 733 Cep, a FU Ori type star. These collaborations were published in a scientific journal of lesser impact than those previously indexed in JSON.We mention that, due to the sad loss of A.A.Karapetian, he was not able to participate in the third article.

The dissertation shows a large part of the acquired knowledge of the author during his doctoral period. In addition to the works presented here, it is important to add that there are other articles in progress that we were not able to complete before the due date for finalizing the Doctorate. Those others contain the reduction and analysis of the data acquired via SI with the 6 m telescope at SAO and the 2.6 m telescope at BAO as well as the reduction and analysis of the light curves of the images given by the Baker-Nunn type telescope of the Fabra-ROA Telescope at Monsec. In the field of spectroscopy, we have the images obtained with the GMOS on the 8.1m telescope at Gemini South. These images should be reduced and it is our intention to analyze the resulting spectra in order to determine the spectral class of these multiple systems. This information along with the orbital, metallicity, and photometric information that is available will permit us to better understand the evolutionary stage and the physical characteristics of these systems.

All of these contributions demonstrate the great quantity of techniques and associated knowledge that the author has acquired throughout this stage of education. Scientifically, the quality of the same has been recognized by means of 6 articles, three of them in international highly prestigious scientific journals that historically are ranked in the first quartile in the field in terms of impact, although, in some year, they may descend to the top locations in the second.

Lastly, we point out that all of the research developed here and carried out by means of our international collaborations is within the frame of the lines included in the research Project: Study of Close Binaries of Special Dynamical and Astrophysical Interest in the Gaia Era, for which the Director of this Dissertation, Jose Angel Docobo, is responsible.

USC
UNIVERSIDADE
DE SANTIAGO
DE COMPOSTELA

Resumen

Esta tesis ha sido realizada por Jorge Gómez Crespo en la modalidad de compendio de artículos de investigación bajo la supervisión del catedrático en Astronomía y director del Observatorio Astronómico Ramón María Aller (OARMA) J. A Docobo. Para dotar de coherencia y sentido a la misma, hemos incluido una Introducción donde exponemos el contexto científico donde se enmarca: el estudio de sistemas dobles y múltiples a través de sus propiedades físicas y dinámicas. Dentro de este amplio campo de trabajo hemos centrado nuestros estudios en las técnicas de imaging, particularmente, en la Interferometría Speckle (SI). La SI es a día de hoy la técnica más productivas de alta resolución para obtener posiciones relativas y fotometría diferencial de binarias, es decir, el primer paso en la investigación de binarias visuales. El que suscribe, en colaboración con su director de tesis y el personal del OARMA, ha desarrollado una labor continuada en el estudio de este campo desde su matriculación en el programa de doctorado de la USC en Matemáticas por la línea de Astronomía. Gracias a esta labor y a la colaboración con prestigiosos científicos internacionales como son, entre otros, Y. Y. Balega, R. A. Méndez, E. P. Horch y N. D. Melikian, hemos podido completar gran parte de las tareas que nos propusimos al comienzo de este periodo formativo.

Además, hemos incluido tres capítulos que resumen los conceptos principales relativos a la observación desde la superficie terrestre, las técnicas y tecnologías de imaging, la instrumentación empleada en astronomía para dotar a los sistemas dobles y múltiples de observaciones precisas que sirvan para determinar con garantías sus órbitas, la metodología observacional que empleamos en las campañas de observación que hemos desarrollado en Armenia, así como, diferentes aspectos relativos al tratamiento de las imágenes obtenidas con cámaras CCD y eMCCD.

El primer año de doctorado fue apoyado por la Comisión Europea mediante la beca Erasmus Mundus Alrakis II. Esta beca me permitió instalarme en Armenia, trabajar en el Byurakan Astrophysical Observatory y comenzar a colaborar con el profesor N. D. Melikian, el cual supervisó mi estancia allí. Este científico dedica su carrera al estudio de Young Stellar Objects y regiones de formación estelar.

Así mismo, entre las tareas desarrolladas destaca la asistencia a campañas de observación en centros de prestigioso nivel internacional como son SAO (Rusia) y SOAR (Chile). Gracias a la experiencia adquirida en estas instituciones, hemos podido comenzar una serie de campañas de observación con Interferometría Speckle en el telescopio de 2.6 m del Byurakan Astrophysical Observatory. En ellas, empleamos la cámara eMCCD del OARMA, una PhotonMAX 512 de Princeton Instruments que se haya en depósito en el observatorio armenio.

En el capítulo de Imaging se resume la teoría necesaria para entender como la turbulencia atmosférica dificulta las observaciones cuando se emplean telescopios con un tamaña superior a un metro. Estas dificultades repercuten en la pérdida de capacidad de resolución de los

telescopios de forma que esta deja de mejorar conforme aumenta el tamaño del espejo. Para evaluar la calidad de una imagen astronómica hemos introducido los principales conceptos que se emplean: el disco de Airy, el disco de seeing, la FWHM y la PSF. A continuación, explicamos tres técnicas que sirven para corregir los efectos de la atmósfera y alcanzar el límite de difracción teórico:

- Óptica Adaptativa: se emplea principalmente en el infrarrojo.
- Interferometría Speckle: útil para todo tipo de telescopios y, fundamentalmente, para observaciones en el rango visible.
- Lucky Imaging: especialmente útil hasta telescopios de tres metros ya que pierde eficiencia para tamaños superiores.

Aunque este trabajo se focaliza en la Interferometría Speckle, nos parece importante detallar aspectos básicos de las otras técnicas de imaging aplicado a la observación estelar y a la detección de exoplanetas para que el lector tenga una visión de conjunto de que estrategias se emplean para la observación estelar y sus aplicaciones a la hora de detectar y resolver sistemas dobles y múltiples. Además, la Interferometría Speckle se puede utilizar en combinación con sistemas de Óptica Adaptativa, como es el caso de las observaciones adquiridas en el telescopio de 4.1m de SOAR que hemos empleado en dos de los artículos aquí presentados. Es por ello que detallar los conceptos generales que rigen el diseño y funcionamiento de la Óptica Adaptativa era necesario.

En el contexto de esta tesis es importante resaltar que, el Lucky Imaging y la Interferometría Speckle usan en la actualidad el mismo tipo de cámaras electro-multiplicadoras (eMCCDs) por lo que sus procesos de reducción son similares. Además, los algoritmos de Shift-and-Add que caracterizan al Lucky Imaging también se utilizan en Interferometría Speckle para calcular el disco de seeing y poder evaluar la calidad de las observaciones.

Las técnicas expuestas para la detección de exoplanetas sirven para mostrar como las técnicas de observación y de tratamiento de imagen que se emplean en imaging han evolucionado en los últimos años para adaptarse a las dificultades que presentan este tipo de objetos de bajo brillo muchas veces ocultos por el propio halo de la estrella que los alberga.

Volviendo al objeto de la presente memoria, en este primer capítulo incluimos también una completa revisión bibliográfica de la Interferometría Speckle desde sus orígenes. En ella, resumimos el artículo original donde por primera vez se da cuenta de esta técnica (Labeyrie, 1970), comentamos los diferentes grupos de investigación que la emplearon, y citamos las aplicaciones que se le han dado para el estudio de una amplia gama de fenómenos astronómicos y objetos celestes. Diferenciamos entre las primeras décadas de observación con Interferometría Speckle donde se empleaban papel fotográfico, CCDs e ICCDs, de la época moderna donde se ha generalizado el uso de detectores con tecnología eMCCD. Como decíamos el objetivo de este capítulo consiste en dotar al lector de una serie de conceptos

y conocimientos que le permitan entender la trayectoria e importancia de la Interferomtería Speckle y que de este modo pueda valorar lo que sigue.

En el capítulo de instrumentación revisamos los principales instrumentos que han acompañado la observación de los sistemas dobles desde sus comienzos. Aunque el primer sistema doble fue detectado por su curva de luz, y por tanto de forma fotométrica, el estudio de los sistemas dobles visuales ha estado históricamente ligado al micrómetro de hilos. Más de 150 años de observaciones así lo atestiguan. Es por ello, que este trabajo estaría incompleto si no describiésemos su diseño y nombráramos algunos investigadores que han contribuido notablemente al estudio de los sistemas dobles y múltiples mediante observaciones micrométricas. La revolución que supuso el inicio de la interferometría gracias a Michelson queda también reflejada en la tesis. Describimos los distintos tipos de interferómetros que se han creado desde sus comienzos y enfatizamos el momento en el que nace la Interferometría Speckle.

Las características de la Interferometría Speckle en cuanto a los tiempos de exposición hace que no sea realmente eficiente hasta la aparición de los detectores de conteo. El desarrollo de la Interferometría Speckle ha ido de la mano de la evolución y mejora de las CCDs. Es por ello que también detallamos el funcionamiento de las CCDs y de las ICCDs, siendo estas últimas, CCDs dotadas de un tubo que multiplica los fotones detectados.

Para conseguir resultados científicamente válidos de las imágenes obtenidas con CCDs, los ruidos presentes en las mismas han de ser eliminados. El proceso de reducción que se emplea ha sido detallado cuidadosamente, así como, las imágenes de calibración que se necesitan para ejecutarlo. Antes de pasar a la tecnología eMCCD hacemos una breve descripción de la cámara ICCD que empleaba el OARMA en sus primeras campañas de observación en Interferometría Speckle hasta la adquisición del detector eMCCD PhotonMAX 512.

En el texto se presentan las características de la tecnología eMCCD, sus peculiaridades a la hora de reducir sus ruidos, el diseño de la cámara eMCCD del OARMA y como ésta se instala y se desmonta en el telescopio de 2.6 m de Byurakan al inicio y final de nuestras actuales campañas de observación.

Todo lo expuesto en este capítulo permite al lector entender como la calidad de las observaciones astronómicas depende en gran medida de las características técnicas de los detectores empleados. Enfatizamos también la importancia de conocer los procesos de reducción necesarios y de ser muy cuidadosos en su ejecución.

En el capítulo de campañas nos centramos en la parte metodológica que acompaña el desarrollo de nuestras campañas de observación en el SAO y en el BAO. El proceso de adquisición de las imágenes, la calibración del tamaño de pixel y de la desviación de la cámara en su instalación se acompaña de la descripción de una noche de observación. Además, detallamos los procesos de reducción y análisis que se aplican a las imágenes adquiridas en ambos observatorios. Para todo ello ha sido fundamental nuestra colaboración con el grupo de

investigación en Interferometría Speckle del SAO, con el personal involucrado en nuestras campañas en BAO y con el observador principal en Interferometría Speckle en SOAR, A. Tokovinin.

Como el proceso de reducción y análisis de las observaciones adquiridas durante las campañas de SAO y BAO no está completamente finalizado, no podemos revelar todavía los resultados alcanzados. Eso sí, exponemos datos cuantitativos referentes a la cantidad de objetos de interés registrados, así como, de las imágenes de calibración adquiridas. En el caso de las observaciones que hemos realizado en el BAO, parte de estos resultados han sido publicados anteriormente en una revista propia que el observatorio armenio ha recuperado recientemente. En esta comunicación describimos la cámara y los resultados alcanzados hasta finales de 2017. Los datos correspondientes a la última campaña de Mayo-Junio de 2018 se exponen en el presente documento por vez primera.

A continuación viene el capítulo principal de esta tesis. En este capítulo comenzamos enfatizando la importancia que la detección de nuevas componentes tiene en la astronomía moderna. Explicamos también como el cálculo de órbitas en los sistemas dobles y múltiples dota a diferentes ramas de la astronomía de los parámetros fundamentales sobre el que se cimienta nuestro conocimiento de los astros y en particular de los modelos de evolución estelar. Con el fin de demostrar la importancia de nuestras campañas de observación incluimos tres artículos donde se emplean medidas obtenidas con Interferometría Speckle. En el primero de ellos, mediante nuestra colaboración con el profesor e investigador de la Universidad de Chile, R. A. Méndez pudimos obtener tiempo de observación en SOAR. De este modo, quién suscribe se desplazó a La Serena (Chile) para participar en la adquisición de las imágenes. Con los resultados obtenidos mejoramos las órbitas de 12 sistemas australes, al tiempo que aportamos información científica relevante sobre las propiedades físicas de estos sistemas. Para el cálculo de todas las órbitas hicimos uso del método analítico de J. A. Docobo.

A esta colaboración se ha unido recientemente el investigador adscrito a la Universidad de Chile E. Costa. Junto al director de esta tesis, J. A. Docobo, mi compañero de doctorado P. P. Campo, y los investigadores chilenos hemos publicado otro artículo aportando 14 órbitas más. Estas órbitas corresponden a sistemas mayoritariamente localizados en el hemisferio sur, aunque no todos. En esta contribución añadimos un estudio inicial de las edades de las componentes de estos sistemas y aquí lo completamos mostrando sus evolutionary tracks así como los diagramas que comparan la temperatura y la luminosidad actual de estas componentes con las temperaturas y luminosidades esperadas a lo largo de su evolución en estrellas con la misma masa y metalicidad.

El tercer artículo ha sido escrito en colaboración con E. P. Horch, investigador del Lowel Observatory y de la Southern Connecticut University. Este prestigioso científico lleva una larga carrera ligada principalmente a la Interferometría Speckle. Usando datos obtenidos en sus campañas de observación junto con otros aportados por nosotros gracias a nuestras campañas en SAO, hemos podido determinar con gran exactitud los parámetros físicos

relativos a masa y paralaje orbital de tres sistemas que presentan la particularidad de ser también binarias espectrocópicas de doble línea. Este tipo de binarias cerradas son en general difíciles de detectar visualmente. Cuando esto es posible, gracias a la metodología desarrollada en los últimos años por los investigadores del OARMA, J. A. Docobo, P. P. Campo, y M. Andrade, nos ha sido posible calcular una órbita visual que se adecue a la órbita espectroscópica y que permita mejorar ésta. Además, en estos sistemas se puede calcular la masa de las componentes por separado y comparar las paralajes orbitales con los datos proporcionados por Gaia.

Estos tres artículos han sido publicados en revistas de alto impacto científico en Astronomía como son The Astronomical Journal y Monthly Notices of the Royal Astronomical Society.

Finalmente, en el último capítulo presentamos las colaboraciones que el autor de la tesis ha completado con N. D. Melikian y A. A Karapetian. Juntos, hemos publicado tres estudios sobre dos regiones de formación estelar, Cep OB3 y Cyg OB7. Estos artículos se centran en las estrellas con emisiones en H_α en estas zonas y en la detección de variabilidad mediante fotometría diferencial y el estudio de curvas de luz. Entre los resultados alcanzados destaca un inusual flare detectado en V 733 Cep, una estrella tipo FU Ori. Estas colaboraciones han sido publicadas en una revista de menor impacto científico que los anteriores pero indexada en el JSON. Comentar que el tristemente fallecido A. A. Karapetian no pudo participar en el tercero de los artículos.

Esta tesis muestra gran parte de los conocimientos adquiridos por el autor a lo largo de su periodo doctoral. A los trabajos aquí expuestos hay que añadirle aquellos que todavía están en marcha y no ha sido posible completar antes de la fecha obligatoria de finalización del doctorado. Estos trabajos incluyen la reducción y análisis de los datos adquiridos mediante Interferometría Speckle en el telescopio de 6m del SAO y en 2.6m de BAO. También la reducción y análisis de las curvas de luz de las imágenes que nos proporcionó el telescopio Baker-Nunn del Telescopio Fabra-ROA at Monsec. En el campo de la espectroscopía disponemos de imágenes obtenidas con GMOS en el telescopio de 8.1m de Gemini Sur. Estas imágenes deben ser reducidas y es nuestra intención analizar los espectros resultantes para determinar la clase espectral de estos sistemas múltiples. Esta información junto con la información orbital, de metalicidad y fotométrica disponible nos permitirá conocer mejor la etapa evolutiva y las características físicas de estos sistemas.

Todos estas contribuciones muestran la gran cantidad de técnicas y conocimientos que el que suscribe ha adquirido a lo largo de esta etapa de su formación. A nivel científico la calidad de los mismos ha sido reconocida mediante la publicación de 6 artículos, tres de ellos en revistas internacionales de elevado prestigio científico que historicamente se sitúan en el primer cuartil de su campo en cuanto a impacto, aunque algún año puedan descender a los primeros puestos del segundo.

Por último, hacer constar que toda la investigación aquí desarrollada y llevada a cabo a través de nuestras colaboraciones internacionales, se enmarca dentro de las líneas incluidas en el

proyecto de investigación: *Study of Close Binaries of Special Dynamical and Astrophysical Interest in the Gaia Era*, del que es responsable el director de esta tesis José Ángel Docobo.

CONTENTS

USC
UNIVERSIDADE
DE SANTIAGO
DE COMPOSTELA

LIST OF FIGURES

USC
UNIVERSIDADE
DE SANTIAGO
DE COMPOSTELA

LIST OF TABLES

USC
UNIVERSIDADE
DE SANTIAGO
DE COMPOSTELA

LIST OF ABBREVIATIONS

ACF	**A**uto**C**orrelation **F**unction
ADI	**A**ngular **D**ifferential **I**maging
AO	**A**daptive **O**ptics
BTA	**B**olshoi **T**eleskop **A**lt-azimutalnyi
BAO	**B**yurakan **A**strophysical **O**bservatory
CCD	**C**harged-**C**oupled **D**evice
CHARA	**C**enter (for)**H**igh **A**ngular **R**esolution **A**stronomy
DSSI	**D**ifferential **S**peckle **S**urvey **I**nstrument
eMCCD	**e**lectron **M**ultiplying **C**harged-**C**oupled **D**evice
FWHM	**F**ull **W**idth (at) **H**alf **M**aximum
FOV	**F**ield **O**f **V**iew
GMOS	**G**emini **M**ulti-**O**bject **S**pectrographs
GSU	**G**eorgia **S**tate **U**niversity
HRCAM	**H**igh **R**esolution **CAM**era
ICCD	**I**ntensified **C**harged-**C**oupled **D**evice
LI	**L**ucky **I**maging
LOCI	**L**ocally **O**ptimized **C**ombination (of) **I**mages
OARMA	**O**bservatorio **A**stronómico **R**amón **M**aría **A**ller
PS	**P**ower **S**pectrum
PSF	**P**oint **S**pread **F**unction
RAS	**R**ussian **A**cademy (of) **S**cience
SAO	**S**pecial **A**strophysical **O**bservatory
SI	**S**peckle **I**nterferometry
SNR	**S**ignal-to-**N**oise **R**atio
SOAR	**SO**uthern **A**strophysical **R**esearch (Telescope)
SSDI	**S**imultaneous **S**pectral **D**ifferential **I**maging
STF	**S**peckle **T**ransfer **F**unction
TLOCI	**T**emplate **L**ocally **O**ptimized **C**ombination (of) **I**mages
TFRM	**T**elescope **F**abra-**R**OA (at) **M**onsec
USNO	**U**nited **S**tates **N**aval **O**bservatory

USC
UNIVERSIDADE
DE SANTIAGO
DE COMPOSTELA

Introduction

The study of double and multiple stars is an important field of research in Astronomy from a mathematical point of view (Astrodynamics) as well as from the perspective of Physics (Astrophysics). In fact, from the calculation of orbits along with other observable parameters such as spectra, magnitudes, and parallaxes, these stellar systems constitute a rich source of information in terms of obtaining the fundamental parameters in stellar physics. We must not forget that the mass of a star will indicate its evolutionary path and the only empirical way to assign said mass of a singular star is by using those aforementioned determinations for double and multiple stars. It is thanks to the orbital motions and the precise calculation of orbits based on visual, spectroscopic, and photometric observations that we are able to assign realistic masses not only to stars but to exoplanets and planetary satellites as well.

In addition, the dynamics of double stars permits the study of other phenomena of great interest in Astrophysics such as the transfer and the loss of mass of the components, certain relativistic effects, flare components, gravitational waves, the detection of stellar subcomponents, or the determination of the physical properties of recently discovered exoplanets. For that reason it is extremely necessary to obtain high quality orbits which can only be achieved by using very precise observational data as much as possible.

In general terms, we can define a double star as being two stars that are physically associated by a mutual gravitational attraction and, as a consequence of this fact, each one of the stars describes a Keplerian orbit around the center of mass of the system. These orbits, called absolute orbits, are equivalent to the denominated relative orbit, that is, that which results from the consideration of the principal star of the system as being fixed. In this manner, in accordance with the Two Body Problem, the other star (the secondary component) describes an elliptical Keplerian orbit around the principal which occupies one focal point of the ellipse.

Nevertheless, the direction of our line of view directed at the double star does not have to be perpendicular to its orbital plane. As a consequence, what we see from Earth is a projection of the relative orbit on the plane that is perpendicular to our line of vision. In theory, this projection would be conical but due to the great distances between the stars, we can consider it to be a cylindrical projection. In this way, the "observed orbit" is also an ellipse which is called the apparent orbit. In the cylindrical projection, the center of the ellipse is conserved but, in general, the focus are not conserved for which reason the apparent orbit of the principal star of the system simply occupies an interior point of the ellipse.

Usually, the brightest star of the pair is considered to be the principal star but it often occurs that the brightness and magnitude are similar for both components therefore giving rise to problems in the identification of the principal and the secondary components. In those doubtful cases, that which has the greater right ascension (an astronomical coordinate) is taken to be the principal but, confusion between them occurs on numerous occasions which can lead too different orbital solutions.

On the other hand, the term, double star, may be ambiguous given that there are cases of optical pairs in which there is no physical relation between the two stars that seem to us to be very close simply due to an effect of perspective relative to our position as observers. Therefore, the convention is to name those stars with clear orbital evidence as "binaries", leaving the name "double stars" as a generalization applicable to optical pairs as well as binaries. In this sense, it is useful to remember that double stars have been relevant as such in the heart of the International Astronomical Union (IAU) since its constitution in 1909 which coordinates Astronomical research at a world level. Until 2015, there were two Commissions responsible for the study of Double Stars, Number 26 (Double and Multiple Stars) and Number 42 (Close Binaries).

At the General Assembly of the IAU celebrated in Hawaii, both Commissions merged into the actual G1, with the name of "Binary and Multiple Stars". The Director of this Doctoral Dissertation, Jose Angel Docobo, was President of Commission 26 during the period from 2009 to 2012.

Although the better classification that should be made for binaries may be that with respect to the distance between the components, separated, semiseparated, and in contact, what is certain is that generally the traditional classification continues to be utilized as a function of the technique used to discover and study it. In that way, we have the visuals, the spectroscopics, and the eclipsing. For the first, observations in the past were conducted with a micrometer or, today, with CCD cameras in conjunction with high resolution techniques such as speckle interferometry (SI) which is a principal theme of this study and by means of which the limit of the resolution of the telescope may be reached. The final result of the process is to be able to obtain the position of the secondary star with respect to the principal using its polar coordinates. With adequate software, in many cases it is possible to deduce the difference of magnitude between the components (differential photometry). A particular case of this type of binary occurs when one of the components is much brighter than the other, in such a way that its companion cannot be observed. However, its presence can be known by the periodic motion of the primary as measured with respect to the other apparently close stars. This type is called an "astrometric binary". Astrometric Binaries are usually detected in program studying absolute astrometry by periodicities in the proper motion and/or parallax.

In the case of spectroscopic binaries, the observational technique consists of registering Doppler displacements in the lines of the spectrum and, from there, to transform into radial velocity data by means of the expression:

$$v_r = \frac{c(\lambda' - \lambda)}{\lambda}, \tag{1}$$

where “c”, as usual, is the speed of light, λ' is the observed wave length, and λ is the correspondent to the same spectral line measured in the laboratory.

Finally, eclipsing binaries are those in which our line-of-sight is contained within (or is close to) the orbital plane in such a way that the orbiting of the binary produces mutual eclipses between the components. In general, the last two groups mentioned present very small orbital periods on the order of days or weeks while the visuals are characterized by orbital periods of months, years, and decades, with some exceptions.

Although it is commonplace that many of the eclipsing are also spectroscopic, the relations between these and the visuals were practically nonexistent due to reasons associated with the resolution capacity of the telescope. The situation is the same in every case but the distance between the components varies considerably. Nevertheless, thanks to the SI technology of today, many of the spectroscopic binaries have now been resolved optically. Once the orbits have been calculated, it is then possible to employ a very effective methodology in order to determine the separate masses of the components as well as the orbital parallax, a highly precise parameter that yields the distance of the binary and that serves for comparison with the parallax measurements generated by the Hipparcos and Gaia space telescopes. Concerning this issue, it will come into play in another point of this Doctoral Thesis, applying it to the HD183255, HD 114882, and HD 30712 binaries.

The major problem with visual observation is not only the necessity to use large telescopes that give us high theoretical resolutions such as tenths or hundredths of a second of arc. An even more important difficulty that is added to observations conducted on the surface of the Earth is the presence of an atmosphere that exists between the stars and ourselves. This is a dynamic medium that is highly turbulent and which changes almost constantly. Variations in temperature and composition as well as the density between the large masses of air that make up the atmosphere produce variations in the refraction index between the layers which gives place to the fact that the straight path of a luminous beam emitted by a star and traveling through empty space will be deformed by the atmosphere and display a distorted image.

To give us an idea, in optimal atmospheric conditions, a 60 cm. aperture telescope can be used to resolve two stars, the angular separation of which is 0”20. Under adverse conditions, the capacity to separate a double source of light may increase incrementally up to 3”. As we explain in detail in I.1, the presence of the distortion of the light caused by the atmosphere is a serious problem which must be considered in the observation of double stars. The size of the telescope is no longer determinant when it is approximately bigger than 1 meter of diameter. Hundreds of professional and amateur observers have had to live with this problem for the past 250 years of visual double star observation.

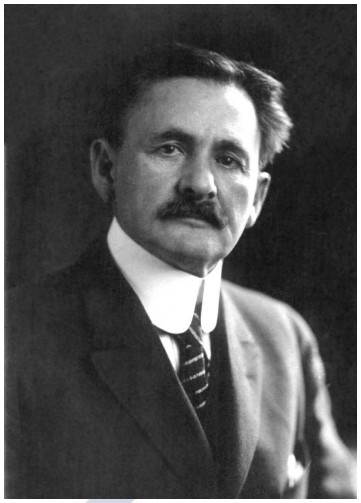

FIGURE 1: Photograph of Novel Albert Abraham Michelson
from English Wikipedia

Hundreds of thousands of micrometric observations carried out by pioneers as W. Herschel, W. Struve, W. R. Dawes, E. Dembowski, O. Struve, or O. Herschel, as well as those after them, e.g., S. E. Burnham, R. G. Aitken, E. Doolittle., W. J. Hussey, G. Van Biesbroeck, R. Jonckheere, T. J. J. See, W. H. Van den Bos, R. M. Aller, among others, and more recently by W. F. Rabe, P. Baize, G. P. Kuiper, F. Holden, P. Muller, G. M. Popovic, D. J. Zulević, P. Couteau, W. D. Heintz, C. E. Worley, J.A. Docobo or J. F. Ling, have been the observational base that has allowed us to progress in the study of visual binaries (Docobo, 2016). The first step to make the astrometric measurements more objective was taken by A.A. Michelson at the beginning of the last century (Michelson, 1920). Said author began to call attention to the possibility of measuring the diameters of satellites and asteroids within the solar system, as well as stars, by means of the observation of the interferometry fringes produced in the telescope focus when only two portions of the objective were utilized. Around the year 1891, Michelson successfully applied this technique in order to directly determine the sizes of the satellites of Jupiter. But it was not until 1919 when he applied this method to stellar observations. Those pioneering observations were carried out in the observatories of Yerkes and Mount Wilson (II.4) and they yielded the first successful results, albeit with bad weather observation conditions.

Next, Anderson (1920) followed the suggestion of Barr (1900) and, using the same interferometric technique employed by Michelson, he was able to optically resolve the star, Capella, with a separation of only 0”05. This star was classified as a spectroscopic binary and its binary nature was known. Nevertheless, the new visual measurements contributed by Anderson permitted the improvement of its orbit as well as the masses deduced for each one of its components. Later, P.W. Merrill and Anderson himself (Merrill, 1922) resolved κ Ursae Majoris and, at the request of R.G. Aitken, the same was done with ν^2 Boötis. An

ample list of binaries were studied with this innovative technique which, in that period, gave unprecedented resolutions. It is worth to mention that its main weakness is that it is only effective with bright stars.

Photographic plates and the first CCD cameras were instruments broadly used in the determination of parallaxes as well as in the observation of wide pairs and astrometric binaries. However, the impact was minimal regarding the resolution of close binaries. The size of the grain in the case of photography as well as the first photodetectors of the CCDs did not improve the situation. Actually, they negatively affected the capacity of resolution of the micrometers.

In the middle of the past century, the South African astronomer, W.S. Finsen, developed an ocular interferometer (II.6) that allowed for the measurement of binary systems, finally discovering a total of 73 (Docobo and Andrade, 2013; Finsen, 1964a, 1971). However, the precision reached was not optimal in many cases. It is important to note that many of the techniques and tricks that Michelson, Anderson, Merrill, or later, Finsen used, or even created, have been recovered or rediscovered. Nowadays, some of these tactics improve the observations that attempt to reach high resolution, both in the field of stellar observation as well as in the search for exoplanets.The origins of the guide and calibration stars, the use of a star itself or of its ghost double for the reduction of the images, long base interferometry or interferometric masks can take us back to the period of the first half of the 19th Century when observations were conducted with nothing more than the human eye and, in the best of cases, by experienced observers using a system of threads systematically situated between the objectives.

Nevertheless, the appearance of the Speckle Interferometry (SI, Labeyrie (1970)) was determinant as it completely revolutionized the panorama of visual double stars in terms of what is referred to as observational precision.

Labeyrie proposed a method for the analysis of the effects produced in a natural manner by the aperture of large telescopes and thereby corrected for the effects of a turbulent atmosphere. In general, long exposures produce a loss of spatial information when various close sources of light are present as a result of the superimposition of interference patterns on the seeing disk. On the other hand, SI is based on taking images during very short exposure times in such a way that the light that is accumulated on the CCD has crossed through the atmosphere and the optical path of the telescope, suffering similar turbulent conditions. In each one of these images, “speckles” are observed (see Figure 4). If the exposure time is more than a few tenths of a millisecond, these speckles will accumulate giving way to the formation of the seeing disc. If we save a sufficient number of these short exposure images and we average them after to calculate the Fourier Transform of each, we obtain a resulting image lying in the space of the frequencies. Studying this image, we are able to determine the singularity or the multiplicity of the observed light source. When the atmospheric conditions are not very adverse, one can arrive at the diffraction limit of the telescope by using this technique.

FIGURE 2: Caption from W. S. Finsen's article An Eyepiece interferometer

In this manner, in the case of multiple stars with a greater diameter of the main mirror of the telescope, i.e. the size of the telescope, there will be an increased capacity to separate the components of the system and, from that, to measure their relative positions. The use of this technique has been limited for various reasons. For example, short exposure intervals restrict the range of the stars to the most relatively bright.

Until recently, it was common to use intensifiers in order to increase the signal before being read by the CCDs until, hardly twenty years ago, when they began to extend to the use of the eMCCD technology cameras which themselves increase the received signal II.5. Said cameras permit acquisition with short exposure times on the order of a few milliseconds and with a very good signal to noise relation. Thanks to these detectors, today we are able to register stars up to a magnitude 15 using 8m class telescopes. Moreover, the difference of magnitude among the components of the system is an important factor to consider because it clearly affects the capacity to detect the less bright components. An approximate limit for this maximum magnitude difference is of average about four or five magnitudes, values that can be slightly higher when the principal component is moderate bright.

On the other hand, there has never been an excessive amount of large telescopes. In addition, if we add the fact that other observational techniques exist that benefit from the size of the telescope, we have the situation that the observational time that is available for this type of

FIGURE 3: Photograph of Antoine Labeyrie

observations is limited as the competition to access a 4m class or higher telescope has always been high. This problem is especially acute in the Southern hemisphere.

There is another technical question that deserves to be highlighted. It is the fact that, principally for economic reasons, until now there have never been many research groups that use SI. The software implicated in the reduction and the analysis of the specklegram blocks have been created ad-hoc for and by each of these teams. Public access has been practically null. The majority of said groups have opted for sharing the final results of observations in the form of position measurements and differences of magnitude to allow the use of their own reduction and analysis software, offered in the form of an open code.

Moreover, the threat of Adaptive Optics (AO, I.3.1) has threatened on SI for decades (Hartkopf, 1992). When this technique passed the theoretical stage and could be used for nonmilitary ends, the hopes of the scientific community were high as they believed that they could reach the theoretical limits of diffraction in telescopes of a class superior to 1 m. Nevertheless, after decades of development, due to its inherent limitations in the visible range, AO has not yet achieved the elimination of the necessity of other techniques now understood to be complementary such as SI and Lucky Imaging.

As mentioned earlier, the presence of large telescopes as well as of research groups studying binaries has been, until recently, considerably superior in the Northern hemisphere (Hartkopf and McAlister, 1991). Due to the work carried out at SOAR during the past 10 years (Tokovinin, 2018b), this difference has clearly decreased. Before, the SI observation campaigns in the South were of a punctual nature (Hartkopf et al., 1993, 1996; Horch, Franz, and Ninkov, 2000; Horch, Ninkov, and Franz, 2001; Horch et al., 1995b; Horch, Ninkov, and Slawson, 1997; Horch et al., 2006; McAlister, Hartkopf, and Franz, 1990).

In Spain, the first observations of double stars were made with micrometers in Cataluña at the end of the XIX century by R. Patxot and J. Comas Solá. But the person who really introduced the study of double stars was Ramon María Aller Ulloa. He first worked in his personal observatory in Lalín and, later, he moved his observatory to the campus of the University of Santiago de Compostela (USC) at the Residence (today, Campus Vida). In both installations,

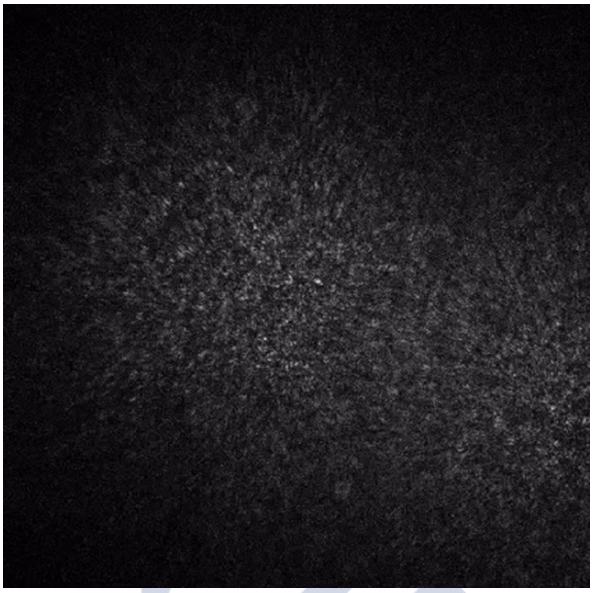

FIGURE 4: Double star specklegram obtained with an eMCCD camera

he used his personal Steinheil refractor which he later donated to USC. This instrument was acquired in Germany in 1924 and installed in Lalín one year later. It was moved to Santiago in 1944, almost 5 years after D. Ramon arrived at the University of Santiago de Compostela in order to teach Analytic Geometry and Mathematical Analysis in the Faculty of Sciences (Docobo, 2016).

His first micrometric meaurements were presented in the principal European Astronomical journal at that time, the Astronomische Nachrichten, where he published six articles (Aller, 1930, 1934, 1935a,b, 1936, 1939). Moreover, Father Aller was the author of the first orbit calculated in Spain, that of the STT 77 system of 1935, which was followed by many more. Apart from that, and among many other scientific contributions, he discovered four visual double stars and created a research group in this branch of Astronomy at the Observatory of USC in 1943.

Sadly, the work of this Full Professor and priest Aller was not continued as desired due to the fact that there was no other Professor of Astronomy able to substitute for him after his death in 1966. The Observatory endured years of economic and personnel hardship together with the total absence of a scientific direction. In order to have a better understanding of the life and work of Ramon María Aller, one may access the biographies and other works prepared by Professors Enrique Vidal Abascal (Vidal, 1979) and Jose Ángel Docobo Durantez (Docobo, 1991a, 2016) as well as the Doctoral Dissertation of Cecilia Doporto Regueira, written under the direction of Professor Docobo (see the MINERVA repository) and defended in 2017: The Human Projection of Ramon María Aller Ulloa, his scientific legacy and the Museum House of Lalín.

At the end of 1981 when the Director of the above-mentioned Doctoral Dissertation, Jose Ángel Docobo, took over responsibility for the research work of the Center while, at the same time, taking charge of the physical recuperation of the Observatory. In effect and in spite of the efforts of the research assistant of C.S.I.C., Jesus Manuel Costa, the Center was in a terrible physical condition and both the library as well as the instrumentation urgently needed to be updated.

Baptized in 1983, the Observatorio Astronómico Ramon María Aller (OARMA) was under the intense dedication of Professor Docobo as the Observatory recuperated the principal line of research, that is to say, double stars. By means of the first completed research projects, it was possible for OARMA researchers to travel to other Observatories such as Fabra in Barcelona and the Astronomical Center of Yebes in order to carry out observing campaigns. In the first case, a 38 cm aperture refractor was used to perform micrometer measurements and, in the second, photographic plates produced by a double astrograph of 20 cm were employed. In addition, J.Á. Docobo considered it to be essential that doctoral students and OARMA collaborators would travel outside of the country in order to be in touch with outstanding specialists and to know and use more powerful instrumentation. Josefina Ling was able to enjoy a 3 month stay in 1986 in the Nice Observatory with Dr. Paul Couteau. Later, J.A. Docobo and J.F Ling carried out various micrometric campaigns in Nice, at Pic du Midi. Later, once a micrometer was acquired, it was installed in the 1.52 cm. Spanish telescope at Calar Alto (Sierra de Filabres, Almeria, Spain).

As a result of these observation campaigns and the consequent calculation of orbits, they published many scientific articles between 1983 and 2000 (Abad, Docobo, and della Prugna, 1998; Costa and Docobo, 1983; Couteau, Docobo, and Ling, 1993; Couteau et al., 1989; Docobo and Prieto, 1995; Docobo, 1988, 1991b, 1996, 1998, 2000; Docobo and Balega, 1998; Docobo and Costa, 1986, 1987a,b,c, 1988a,b, 1989a,b,c, 1990a,b,c,d, 1991, 1992; Docobo and Ling, 1991, 1992a,b,c, 1993a,b,c, 1994a,b,c, 1995a,b, 1996a,b, 1997a,b,c, 1998a,b,c, 1999a,b,c, 2000a,b,c; Docobo, Ling, and Prieto, 1994; Docobo and Prieto, 1991a,b, 1992, 1993a,b, 1994, 1996a,b; Docobo and Tamazian, 1998; Docobo and Vasyuk, 2000; Docobo et al., 1991, 1999, 2000b; Ling and Lanchares, 1993; Ling and Prieto, 2000).

In terms of orbit calculation, this process was facilitated by the 1985 publication of the analytic method of Docobo, of which we will speak further on.

The case is that the micrometric measurements were losing weight/importance at the end of the past century during a process in which the disappearance of emblematic figures such as P. Baize, W.D. Heintz. C.E. Worley, or P. Coteau as well as the “strength” of techniques such as SI that had been moved forward by pioneers such as H.A. McAlister, Y.Y. Balega and their respective CHARA teams (Atlanta, USA) and SAO (Russia), and also remembering other outstanding figures in this field auch as D. Bonneau, A. Tokovinin, W. F. Van Altena, etc.

The move of OARMA for SI began thanks to the decision of J.A. Docobo in the early 1990s. He made the first contacts with McAlister in order to attempt to obtain a speckle camera but he

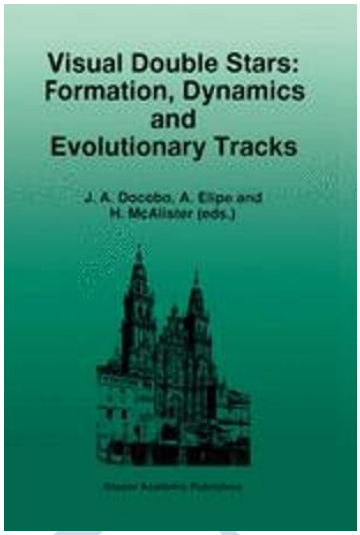

FIGURE 5: Proceedings of the International Workshop, Visual Double Stars, Formation, Dynamics, and Evolutionary Tracks

found that the prices were prohibitive at that time. Nevertheless, he sent C. Prieto to Atlanta in 1991 for a three month research visit which permitted her not only to familiarize herself with the technique but to also be able to participate in observation campaigns, including in Chile.

Thanks to the role that OARMA played in the organization of the 1996 International Workshop: VISUAL DOUBLE STARS, FORMATION, DYNAMICS, AND EVOLUTIONARY TRACKS (Docobo, Elipe, and McAlister (1997), Figure 5) where the most outstanding researchers in Celestial Mechanics and Double Stars met in Santiago de Compostela, a collaboration agreement was able to be established with Yuri Balega, the new Director of SAO. The Russian center promised to construct an ICCD camera for the Observatory in Santiago de Compostela which was able to be installed in the 1.52 m and the 3.5 m telescopes at the Centro Hispano-Aleman at Calar Alto, beginning in 1998 (Docobo et al., 2001, 2004, 2008). Vahktang Tamazian, who had joined OARMA two years earlier, also played an important role in this project.

In the following years, the collaboration with SAO intensified via common observation campaigns with the 6 m. aperture Russian telescope (BTA, Figure 6), including a research stay of one of the OARMA collaborators, Jose Blanco, at SAO, resulting in various joint publications and continuing with a proposal to construct a new eMCCD camera that would yield relative positions of binaries as well as the differences of magnitude between their components, information that is fundamental for the study of the physical properties of these bodies. This camera was finally acquired by means of financing provided simultaneously by both research projects of OARMA granted by the Spanish Ministry of Education and the Xunta of Galicia, respectively.

The camera was used successfully with the 0.62 m. OARMA telescope but Docobo understood very well that it was necessary to take more advantage of the instrument by attaching it to at least a 2m class telescope. Then the possibility occurred to solve the issue by working with another OARMA collaborator, Norair D. Melikian of the Byurakan Astrophysical Observatory (BAO) of Armenia.

In January 2010, the Professors H.A. Harutyunyan, Director of BAO and J.A. Docobo, Director of OARMA, signed a collaboration agreement which included the transportation, installation, and use of the OARMA speckle camera attached to the BAO 2.6m telescope, agreeing on at least one observation campaign per year for five years. The agreement was later extended.

The first installation of the camera was not successful due to technical questions although the process was supervised by the engineer that had designed it, A.F. Maksimov. Following that, the telescope and the dome of BAO went through a long period of scientific inactivity while both where improved. This fact created the situation that the beginning of the campaigns was suspended and delayed without a fixed date. Meanwhile, SAO continued completing annual SI campaigns as the Time Allocation Committee accepted the observation programs proposed by OARMA.

The principal objective of this Doctoral Dissertation is, on one hand, to demonstrate all of the work developed by us in the field of SI. This not only involves the development of mathematical algorithms to be incorporated into new data reduction software which is a fundamental aspect necessary to obtain the astrometric positions and the magnitude difference. It also involves all of the experience accumulated during more than four years using the eMCCD camera at BAO, participating in observation campaigns at SAO and SOAR, and finally obtaining data to be utilized in orbit calculation. Lastly, it involves showing the applications of all this background in the collection of relevant astronomical data by means of the corresponding mathematical tools that were reflected in three scientific articles, which are the cornerstone of this dissertation.

In effect, after an ERASMUS scholarship was awarded in 2013, the Director of this work considered it to be a unique opportunity for the academic destination to be BAO. There the scholarship recipient would have the opportunity to study photometry with N. Melikian as well as to initiate the works that will allow to finally carry out the SI campaigns with the OARMA eMCCD camera that was located in storage at the Armenian center.

This difficult experience was made compatible by means of attendance at three speckle campaigns at SAO in which D. Rastegaev and V.V. Dyachenko demonstrated the most important practical facets to be kept in mind. These include the selection of exposure time, the filter, and the position of the prisms of atmospheric dispersion in conjunction with the processes of decision-making at the moment of selecting the stars to be observed which principally depends on atmospheric conditions and the position of the light sources in the celestial sphere. Moreover, E.V. Malogolovets instructed us in the management of the software that

FIGURE 6: The 6m
Bolshoi Teleskop Alt-azimutalnyi (BTA) dome
Credit: Tyavin Paul under CC BY-SA 3.0

they use there for the reduction and analysis of the acquired images. All of the work described above was conducted under the supervision of Y.Y. Balega who was in constant contact with Professor Docobo.

Taking advantage of these observation campaigns, all of the observational data registered since 2012 that pertained to the observation times assigned to OARMA was able to be recollected that, for reasons of work overload and lack of funds, had not been reduced.This delay in obtaining the positional and photometric results created the situation that we proposed the development of our own reduction software in order to complete this work with the most adequate and friendly algorithms.

Apart from these fundamental experiences in my education in modern Astronomy including working with leading groups at an international level, the ample contacts of my Dissertation Director permitted me to do similar work in the austral hemisphere. The idea to be able to conduct SI observations in the South had already been considered in the current research project of the Ministry that had been proposed by J.A. Docobo who had previously made contact with Professor Rene A. Mendez of the University of Chile. In 2015, Docobo understood that it was the appropriate moment that my scientific experience should be complemented with a research visit in Chile with access to the SOAR telescope. It was there that A. Tokovinin was developing tremendous observation work as well as carrying out the calculation of orbits with visual and spectroscopic binaries and multiple systems, especially triple systems. All of that was in perfect harmony with the subject of my dissertation.

During our stay in La Serena, I had the opportunity to carry out observations for several nights with A. A. Tokovinin, learning how the different software was employed in order to optimize the campaigns. In particular, it was useful to know how to manage the algorithms that they use there, above all with reference to the realization of differential photometry (Tokovinin, Mason, and Hartkopf, 2010). The result of this was the publication of 26 orbits in two articles, Gomez et al. (2016) and Docobo et al. (2018a) (section IV.2.1).

It is important to note that the process of obtaining high precision data is focused in the utilization of it for their scientific application by means of ad-hoc procedures in order to

finally deduce relevant information concerning the physical properties of these stars.

Using all of the observations carried out, micrometrically and then with our cameras and/or thanks to the agreements with other observatories and speckle interferometry research groups, the OARMA team has been able to calculate orbits from the 1930 (Aller, 1930) to the same 2018 (Docobo, Tamazian, and Campo, 2018; Docobo et al., 2018b). All of them were previously announced in the Information Circulars of Commission 26 of the IAU, Commission G1 (before No. 26). We have always employed the method created by J.A. Docobo (Docobo, 1985, 2012). This versatile algorithm mathematically supposes the natural way to analytically determine the seven orbital elements and, at the same time, it represents a generalization of the previous methods of Thiele-Innes-Van den Bos and Cid (Cid Palacios, 1958; Thiele, 1883; van den Bos, 1926, 1932).

The Thiele-Innes-Van den Bos method was the first used to calculate the elliptical orbit of a binary star based on three complete observations, $(\theta, \rho; t)$. This method also requires the utilization of the constant of the areas of the apparent orbit, C, that is obtained from the rest of the available observations.

In 1958, a disciple of Ramon María Aller, Rafael Cid also presented an analytical method that only uses observational data which are the same as the previously mentioned from three complete observations $(\theta_i, \rho_i; t_i)_{i=1,2,3}$ but an incomplete observation of the form $(\theta_4; t)$ is added. It is obvious that if we change the value of C in a progressive manner using the Thiele-Innes-Bos method or we change the fourth angle using the Cid method, a series of different orbits are produced, all of them passing through the three given observational points. In other words, three observations define a set (possibly empty) of relative Keplerian orbits whose correspondent apparent orbits all pass through the three base points. We call this set of orbits, $\mathcal{E}$, where each orbit is defined by its seven orbital elements, that is, $P, T, e, a'', i, \Omega, \omega$. The method designed by Docobo follows this idea that, thanks to a more simple mathematical algorithm, permits the establishment of an application between the interval $(0,2\pi)$ and the set, $\mathcal{E}$. If one or some of the base observations belong to different revolutions, it becomes necessary to substitute the interval $(0,2\pi)$ for $(0,\infty)$. The definitive orbit, e.g.Figure 7, for a concrete system within the set of orbits generated is selected based on different criteria such as those that give realistic mass values for the spectral types of the components, those that minimize the residuals in θ and ρ with the rest of the available observations for the system, or for those in which the resulting dynamical parallax corresponds with other parallaxes obtained by a different manner (Gaia, Hipparcos, ...). For each orbit of the set $\mathcal{E}$, it is posible to calculate the corresponding value of C. For this reason the Thiele-Innes-Van den Bos method can be considered as a particular case of Docobo's method.

Another use of Docobo's method for orbit calculation has been recently published (Docobo, Tamazian, and Campo, 2018). In that article, the calculus of the orbital parameters in accordance with the selection criteria is explained in detail. The weights assigned to each type of observation are those suggested by Docobo and Ling (2003).

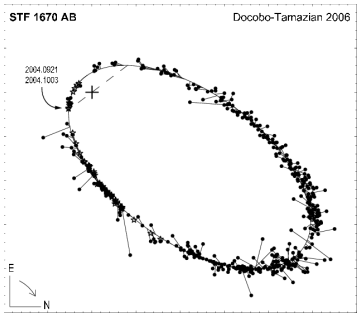

FIGURE 7: STF 1670 AB orbit calculated with Docobo's analytical method

Of special interest are the close pairs for which we can calculate the visual orbit (generally obtained with speckle measurements) and, at the same time, the spectroscopic orbit (better using double lined spectroscopic binaries). J. A. Docobo proposed to fix the attention on this class of binaries (Docobo et al., 2016, 2017a, 2018b) as it provides not only the individual masses of their components, but the orbital parallax as well (deduced from both orbits as we saw previously), due to the fact that this last value is an excellent test for comparing with the parallax measurements updated by Gaia.

In addition to these articles, we must add the methodology proposed by Docobo et al. (2014) that permit the determination of the three-dimensional (3D) orbit for those systems that, in addition to a spectroscopic orbit, also have at least one visual measurement. Normally this would be a measurement obtained with speckle interferometry as well as necessarily having a precise value for the parallax of Gaia preferably, or of Hipparcos.

As an application of the aforementioned, we present this report: "The Three-dimensional Orbit, Orbital Parallax, and Individual Masses of the Double-lined Spectroscopic Binaries HD 183255, HD 114882, and HD 30712" (Docobo et al., 2018a) (IV.3), whose authors are J.A. Docobo, P.P. Campo, E.P. Horch, and the author of this dissertation. In this article, we make use of observations carried out on the 8m Gemini North telescope and the 6m BTA at SAO (see III.2). It was possible to obtain the 3D orbits of the three spectroscopic systems where the dynamic parallax fits notably with that provided by the satellites. As they are systems with spectroscopic orbits, we have been able to calculate very precise values for the masses of each component which is something that is only possible with this type of system which is both visual and spectroscopic at the same time.

It is important to highlight that, in the context of this dissertation, two observations obtained with the BTA in Russia were reduced and the apparent positions of the systems were calculated using the software that has been developed by the author of this memory in the last years, this being the first article in which it is used. As the process of calibration is not yet complete, the errors in the values of θ and ρ have been directly calculated from the error of the size of the pixel. A more careful calculus of error must wait until we complete the methodology for the

calculus of the difference of magnitude, although notable differences between the errors are not expected within the range used in this article and those that new routines may provide.

This dissertation is organized in the following manner. After this Introduction, we present Chapter I *Imaging*, the difficulties that are associated with Earth-based observations and atmospheric interference are discussed. That is followed by a summary of the theory of turbulence applied to the atmosphere as well as concepts that are relative to the determination of the quality of the astronomical image.The discussion continues with an explanation of the set of techniques and technologies that permit the correction of effects of atmospheric turbulence when we use telescopes that are larger than 1 meter. Adaptive Optics (AO) is presented as the technology that permits the correction of atmospheric turbulence effects by means of optical systems and actuators that deform the main mirror of the telescope. After that, the origins of Speckle Interferometry (SI) observational projects that have been carried out since 1970 to today, and how the appearance of eMCCD cameras and their combination with AO systems benefits this technique. The technique known as Lucky Imaging (LI) is also summarized which also allows us to approach the resolution limit of telescopes up to a size of 3 m. and can be understood as an evolution of the Shift-And-Add techniques that consists of reaching subpixel precision. Lastly, brief comments are presented regarding the techniques and algorithms of imaging used to detect the presence of exoplanets.

Chapter II *Instrumentation*, begins with the explanation of the instrumental evolution beginning with the use of micrometers, moving to the origins of interferometry, and ending with the eMCCD cameras of today. Details are explained regarding the physical functioning and the different components of camera types CCD, ICCD, and eMCCD. The principles that are followed relative to the reduction of images taken with said cameras in order to eliminate noise in the images are explained. In particular, the design and functioning of the ICCD and eMCCD of OARMA, the last which is equipped with a PhotonMax 512 detector by Princeton Instruments is presented. In this same chapter, the installation onto the telescope and the initial configuration of the PhotonMax are also detailed.

In Chapter III *Observational Campaigns with SI*, the importance of observations in Astronomy, especially those that facilitate the determination of the multiplicity of systems such as those that permit the calculation orbits of double and multiple systems is emphasized. The different methodologies applied in the observation campaigns with SI at the Special Astrophysical Observatory (SAO) and at the Byurakan Astrophysical Observatory (BAO) are explained. These methodologies are divided into those that are applied in the process of taking images, those that we use in the reduction process, and others that are used in the analysis process data that is free of noise. The experience of one night of observation is described in detail. In terms of reduction, the technical information and the generic nature of it is not repeated as it was discussed in the previous chapter. Herein, we only detail the particularities that we have applied to our reductions and the reasons for them. The analysis of the images is explained in terms of the calculation of the Power Spectrum, the Autocorrelation Function, and everything that is necessary in order to derive the positional and photometric parameters

from the reduced speckle blocks. A brief summary is also presented of the campaigns conducted at SAO and at BAO. A communication published in a journal edited by BAO is also included.

In Chapter IV *Published articles using SI*, three articles are presented that were published in high impact, international journals.These articles are the product of scientific collaboration established By OARMA with different international SI research groups. In the first two, a total of 26 orbits produced by observations at the Southern Astrophysical Research (SOAR) Telescope along with the scientific use of the same are discussed which translates fundamentally into the accumulation of information relevant to the physical and dynamic properties of all of these systems. The third article reports a study of three close systems with known spectroscopic orbits where the existence of speckle registers permitted not only the improvements of the orbits but also the more precise determination of parameters that are important such as the mass of each component as well as the parallax. The results of the parallax have been contrasted with those provided by the Gaia space mission today that reach coherent results within the limitations that affect the Gaia measurements in the case of non-singular systems.

Chapter V, *Articles about the pohotometric study of stellar regions Cep OB3 and Cyg OB7*, contains a review of the articles that were produced as a result of the collaborations of the author with N.D. Melikian. These articles report the search for stars that demonstrate H_α emissions in the Cep OB3 and Cyg OB7 regions of stellar formation. These regions are rich in the number of variable stars, in particular, T Tauri type stars. In addition to the H_α emission detections, both articles include photometric data of the observed stellar objects. Moreover, a flare similar to those presented by type UV Ceti type stars was investigated in a FU Ori type star known as V 733 Cep or "Persson Star".

Finally, the bibliographic references utilized in the development of this dissertation as well as the final conclusions (V.2) are presented.

Chapter I

Imaging

Throughout this chapter, basic aspects of astronomical observation are described that refer to observations within the range of visible light that are carried out on the Earth's surface with the objective of the "direct" detection of celestial bodies. In order to understand the importance and the difficulties that these activities present, we begin by emphasizing the effects of atmospheric disturbance and how this affects the propagation of light. We explain the physical processes behind the turbulent medium that the light crosses until it reaches the telescope and we equip these phenomena with a mathematical theory to achieve a better understanding of it. The polynomials of Zernike are introduced as the best mathematical tool for the description and correction of the aberrations produced at the light wavefront with adaptive optics circular systems. We point out which are the most important aspects to analyze and to measure the quality of the image created on the main focal point of the telescope and that will be lately registered in the detectors.

Next, we offer a brief summary of the principal techniques that allow us to correct the atmospheric turbulence in the stellar observation with only one telescope: Adaptive Optics (AO), Lucky Imaging (LI), and Speckle Interferometry (SI). We emphasize the ways in which the use of eMCCD cameras (whose technical features will be detailed in the next chapter) have permitted the continual development of more Speckle Interferometry (SI) programs. Those are mostly oriented to the discovery of new stellar components as well as the following of binaries now known. The data stocked in these campaigns is used by the international astronomical community in the calculation of their orbits with maximum precision. The orbits offer us basic physical parameters, including stellar masses, heavily important to understand key astrophysical features. Finally, we summarize some of the techniques that are used today for the detection of exoplanets: ADI, LOCI, SSDI, and TLOCI.

The sections that refer to LI and AO can be considered to be introductions to those aspects. The reader should combine the information collected here by means of other sources if he or she wants to have a complete and profound perspective of these topics.

We have presented SI based on the initiatory theoretical article of 1970 by Labeyrie and applied on-sky almost immediately by himself and his collaborators. The specific processes

that are necessary to conduct SI observation campaigns as well as the software necessary to reduce and analyze the speckle images (specklegrams) are presented in another chapter that is related to our practical work in the field.

The revision and exposition of the SI reference literature is intended to be the most complete possible for the years from 1970 to 2000. Programs of recent decades that use eMCCD technology have been indicated in a separate section. In this section, we also mention the applications of this technique in the field when searching for exoplanets. Given that almost five decades of literature concerning SI exists, we may have neglected to mention some relevant work but that has not been our intention.

In the section that refers to the imaging of exoplanets or "exoimaging", an observational technique known as Angular Differential Imaging (ADI) and two algorithms (LOCI and TLOCI) that are used to improve results are discussed. Although more methods and proposed algorithms exist or are in development to be used to carry out the imaging of exoplanets, the objective of this section is to point to a field of research today in which the most classic techniques, already explained within this dissertation, continue to be used and improved in order to achieve new limits of resolution. We have centered on this series of developments that are interrelated to some degree in order to be able to explain these techniques and algorithms in a simple manner without having to introduce too many new concepts.

I.1 Atmospheric Turbulence and the Propagation of Light

Even on calm nights, we can appreciate small variations, scintillations, in the intensity of the stars. This effect is produced by the passage of light through different layers of the atmosphere, which we can label as a turbulent medium. Moreover, this transit does not only affect the intensity. It also affects the size and the form with which we perceive them. In general, we refer to these distortions as atmospheric "seeing". As it is not the objective of this dissertation to develop a detailed model for atmospheric turbulence nor for the propagation of light through the atmosphere, we are going to be very brief here, simply providing a sketch of the key points. The interested reader may go to Roddier (1981) for a more detailed development of this topic.

The astronomical observation of an object consists of the detection of the front of the wave which may be considered to be flat as it enters the atmosphere. As it spreads upon the face of the Earth, it breaks up due to the optical turbulence. This limits the precision of the measurements that are made from telescopes situated on the Earth's surface. The optical distortions are produced by the mixture of the layers of air that have different temperatures. These differences in temperature, and in density as well, provoke variations in the refraction index. Although we can consider that the changes in the temperature of the atmosphere are continuous, it happens that a small volume of air equalizes its temperature with that its

environment more slowly than the time that it takes to blend with it. For that reason, when a small pocket of air at a certain temperature mixes with another layer of the atmosphere with a different temperature, a change is produced in the refraction index in small spatial layers. As light passes through a large number of them, the accumulated effect may be considerably great.

Kolmogorov (1941) developed a physical model of turbulence that can be used to evaluate its effects. This model is constructed upon the following premises. To begin, the energy only enters into a turbulent system at the largest spatial layers and then dissipates into the smallest. The kinetic energy is conserved between the layers. The energy spreads toward the smallest layers through vortices or eddies. That subdivide it which is called the Richardson cascade. When these eddies become sufficiently small, the energy dissipates due to the viscous properties of the medium. Between the largest and the smallest layers, where the dissipation is produced, Kolmogorov predicted a law of potentials for the distribution of the turbulent energy in three dimensions,

$$\Phi(k) \sim \|K\|^{\frac{-11}{3}}, \tag{I.1}$$

where Φ is the density of the spectral energy, k is the wavenumber that corresponds to a spatial scale r with the relation $k = 2\pi/r$.

Experimental evidence exists that confirms the Kolmogorov model of atmospheric turbulence, for example, Nightingale and Buscher (1991). However, other evidence also exists that suggests that the atmosphere does not always obey Kolmogorov's power law with exponent 11/3 (Dayton et al., 1992; Golbraikh et al., 2006; Nicholls, Boreman, and Dainty, 1995). In general, it has been found that the potential may be less than 11/3 but rarely more than that.

Kolmogorov also introduced the use of the function of structure as an instrument for the study of turbulence. The random variables such as the velocity tend not to be stationary, that is, the average value of the random process may vary slowly. We use the function of structure, D_f that is defined as the average of the square of the difference between two locations,

$$D_f(\tau) =< [f(t+\tau) - f(t)]^2 >, \tag{I.2}$$

in order to study the variations between different layers. The function of the structure of Kolmogorov for the field of homogeneous turbulence velocities in three dimensions is:

$$D_v = C_v^2 r^{\frac{2}{3}}, \tag{I.3}$$

where $C_v$is a dependent parameter of the turbulence energy.

The next step is to consider the interaction of light with the turbulent medium. The incidental monochromatic light can be represented by the formula,

$$\psi_0(r,t) = A\exp^{i(\phi_0+2\pi\nu t+k.r)}, \tag{I.4}$$

which experiences perturbation due to the variation of the index of refraction and emerge verifying:

$$\psi_p(r) = (\chi_a(r)\exp^{i\phi_a(r)})\psi_0, \tag{I.5}$$

for any instantaneous observation. χ_a represents the fractional change due to the atmosphere in amplitude, A, and ϕ_a is the perturbation at the wavefront that evolves with the changes in temperature of the turbulent atmosphere.

We are going to consider a sky with no clouds that would partially absorb the light, nor any other difficulty for the transmission of light. In this case, only the variation in the refractive index affects the phase of light. The variations in the amplitude are a secondary effect caused by the diffraction as the light spreads between the turbulent layers and the observer. That is, in order to model a good astronomical localization at visual wavelengths, in general, it is appropriate to preclude the effects of the diffraction and the sparkle of scintillation. This is called the geometric propagation model as it use vectors representing the paths that rays of light follow during their propagation and whose wavefronts advance or recede due to the "phase screen". The phase screen concept is used as a generalization of all the turbulent phase perturbations that affected the wavefronts.

Tatarskii (1961) demonstrates that for a refraction index, n, which has variations induced by the turbulence with a function of the structure,

$$D_n = C_n^2|r|^{\frac{2}{3}}, \tag{I.6}$$

the structure of the atmospheric phase screen ϕ_a takes the form:

$$D_\phi(r) \propto \int_0^z C_n^2(z)dz|r|^{\frac{5}{3}}, \tag{I.7}$$

where $C_n(z)$ is the parameter of the function of structure that varies with the height, z, in accordance with the different intensities in the refraction index for the variation in the turbulence. This integral may be written as a function of only one parameter, r_0, the Fried coherence length or Fried's parameter:

$$D_\phi(r) = 6.88(\frac{r}{r_0})^{\frac{5}{3}}, \tag{I.8}$$

which describes how the mean square phase difference between two points scales with the distance between them (Fried, 1965).

The Fried's parameter corresponds to the diameter that a telescope would have to have in order that the "seeing" has no effect and varies with the wavelength as $\lambda^{6/5}$. As the ratio between the diameter of the telescope and the Fried coherence length increases it occurs that the point spread function (PSF), which would ideally have to be an Airy disc, divides into multiple spots known as "speckles". These speckles are created by the interference between the light of different regions at the length and width of the telescope between which the phase differs by approximately 1 radian. These regions are the popularly known as "coherent cells". So the dimensionless ratio D_{tel}/r_0 can be used to measure the effects of different factors that affects the observations (telescope size, wavelength, atmospheric conditions,...) as a whole.

I.2 Image Quality

The terms that describe the perturbations at the wavefront and image quality are commonly used in Astronomy. For that reason, we will describe them briefly here.

I.2.1 Zernike polynomials

A majority of the optics systems used today employ elements of imaginology as well as circular pupils. The polynomials of Zernike (I.1) are a mathematical tool that allows us to describe the propagation of wavefronts or the differences between optical paths in these systems. A wavefront can be thought of as a surface that shares the same phase and is produced by the radiation from a source of monochromatic light. Given a point of light at an infinite distance, this surface corresponds to a flat wave. The mathematical description given by the polynomials of Zernike is used to define the differences of magnitude and characteristics between the image created by the optical system and that of the original source. This optical aberration may be the result of imperfections in one or various optical elements of the configuration utilized or of the entire system.

The polynomials of Zernike are one of the infinite sets of polynomials that have two variables are orthogonal and continuous on the unit circle. The condition of being continuous is important because, in general, the Zernike polynomials do not have to be orthogonal over a discrete set of points within the unit circle. The normalized expansion of Zernike is used to describe the aberrations and offers a series of important advantages over others. First, the coefficient or the value of each mode represents that average of the difference of squares (rms) of the error of the wavefront attributed to this mode. Second, the coefficients of Zernike that are used to mathematically describe the wavefront are independent of the number of polynomials used, in such a way that any additional number of terms may be calculated without impacting those previously considered. Last, the coefficients of greater magnitude indicate a greater contribution of this particular mode to the the total rms error of

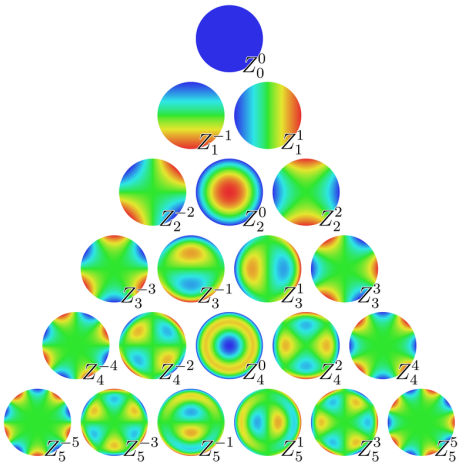

FIGURE I.1: The first order Zernike polynomials, ordered vertically by radial degree and horizontally by azimuthal degree
Credit: Rocchini (Zom-B at en.wikipedia) under CC BY 3.0

the wavefront of the system and, thereby, a greater negative impact in the performance of the system.

We should also comment that the polynomials of Zernike are not always the best to use to model a wavefront. Some effects of astronomical turbulence or effects due to errors of fabrication of optical elements may not be well represented, including those due to a long expansion of the same. For example, when testing conical optical elements, we should add additional terms to Zernike's polynomials in order to represent errors of alignment or, including these modifications, the description obtained may not be optimal. Moreover, in any system with noncircular pupils, the Zernike polynomials for the circular unit will not be orthogonal, above all in the area of the pupil and, therefore, it is not the ideal polynomial sequence.

In any case, supposing that these polynomials are adequate for the optical configuration used, we should point out that the low order polynomials correspond to the changes in the low frequencies along the wavefront. In consonance with the Kolmogorov model, the changes in the largest layers will, on average, always have a greater amplitude. As such, applying a correction, the greatest improvements result from first correcting the lower order terms. From there, the nicknames of adaptive optics, "low order" and "high order". $\mathcal{Z}_0^0$ is the first term of Zernike, it is called "piston" but it is not important when we have only one aperture, mainly it is used when we compare the phase across two interferometric apertures. The following two, $\mathcal{Z}_1^{\{-1,1\}}$, are called "tip-tilt" and together they create a generic form of the wavefront. This form creates the situation that the detected light source moves about in the focal plane. Besides this, all types of distortions are described by higher order terms, such as astigmatism, blurriness, coma, ...

The polynomials of Zernike play a fundamental role in AO because they permit the measurement of aberrations that are present at the wavefronts. The measure is taken in the form of coefficients that accompany each polynomial that approximates the image received in the detector at the wavefront (I.3.1).

I.2.2 Point Spread Function

The propagation function of a point source of light in the detector, commonly called Point Spread Function or just PSF, is defined as the distribution of the intensity of light that is measured on the focal plane of a telescope and which has been emitted by what we call "an unresolved source", i.e., an infinitesimal source of light or a point of light. In practice, it means that the light is emitted by a non multiple star or single-like star not bright enough to saturate the detector pixels.

As we have seen, we can use Zernike polynomials to describe the perturbations of phase in a direct way. Nevertheless, they do not describe the effects of the atmospheric perturbations on the quality of the image and, consequently, on the PSF.

The most common measurements used in Astronomy to assess these distortions are the ratio of Strehl and the full width to half of the maximum or FWHM. It is also common to use the width of the "seeing" which is a special case of the FWHM. Before explaining each one of these measurements, we should introduce the Airy disc and the disc of seeing, how both are related to the Nyquist-Shannon theory of sampling, and the importance of the pixel size of the camera.

I.2.3 Airy disc

The theory explains that, in the absence of turbulence, the wavefront should be flat when it arrives at the pupil of the telescope. This flat wavefront should spread through the optical elements of the telescope and focus a PSF to the limit of diffraction permitted by the diameter of the telescope. The full width at half of the maximum (FWHM) of the PSF to the limit of diffraction for a Cassegrain class telescope with a central occultation of ~0.2 will be:

$$\theta = 0.98\frac{\lambda}{D}, \tag{I.9}$$

where D represents the telescope diameter.

That is, the theoretical PSF for a telescope with a circular or anular aperture is described as the function of Airy, the one that displays the Airy disc, and it has an angular width that depends on the central darkness and it is proportional to the ratio between the observed wavelength and the aperture size, $\frac{\lambda}{D}$. Moreover, Rayleigh criterion indicates that the resolution, understood

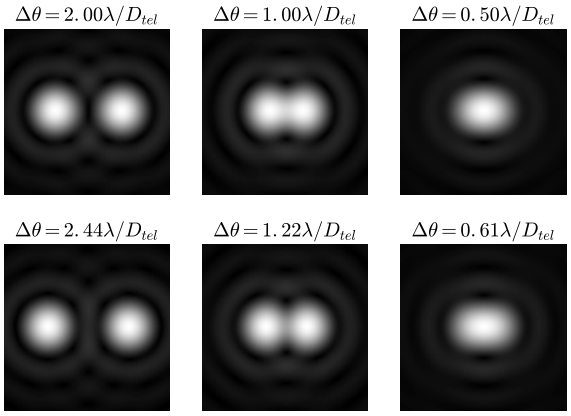

FIGURE I.2: Airy pattern of two sources according to separation

as the capacity to separate two different infinitesimal point light sources, depends on the location of the first minimum of the Airy function, which verifies:

$$\theta \approx 1.22\frac{\lambda}{D}, \tag{I.10}$$

for very small angles.

The criterion states that for separations that are greater than or equal to $1.22\lambda/D$, two points of light can be resolved. That is, they can be observed as two differentiated points of light on the focal plane. With minor separations, the discs of Airy mix together in such a way that is impossible to distinguish if the light source is 1, 2, or more objects with separations between them that are inferior to the angular separation limit (Figure I.2).

I.2.4 The seeing disc

However, reality is quite different. When our camera collects light on the focal plane of a medium to large terrestrial telescope, for example, with an aperture greater than 1 m. (to give an approximate and generally accepted lower limit), the PSF obtained after a long exposure on the order of seconds, do not resemble as the Airy disc. What we observe is known as the "disc of seeing" which is normally modeled using the function of Moffat (Trujillo et al., 2001a,b). The difference that exists between the theoretical case, the expected disc of Airy, and the real case creates the situation that the observed seeing disc causes us to lose information which becomes in less capacity of resolution (Figure I.3).

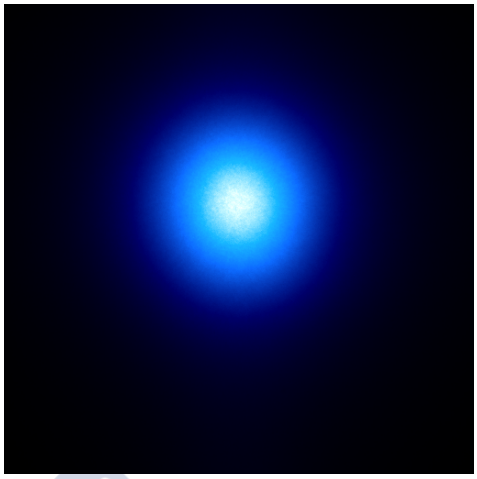

FIGURE I.3: Seeing disk of the system ADS 9688 after SAA specklegrams obtained with the 6m BTA

I.2.5 Pixel size and the theory of Nyquist-Shannon

The pixel size is fundamental when designing an astronomical camera. The width of the desired field, an obtained adequate sample of the PSF, and the signal-noise ratio (SNR or S/N) are the principal aspects to be considered in order to decide which size is most adequate for our scientific interests. Other factors to keep in mind such as the noise of the reading, the capacity to transfer data collected, or the levels of saturation can be considered within one of these characteristics or as a combination of several.

A pixel size that permits us to observe a large part of the sky will receive more photons and, therefore, have a greater signal level. Nevertheless, the Nyquist-Shannon theorem of sampling (Shannon, 1949) explains that in order to be able to save a signal, we need a sampling ratio that is two times greater than the highest frequency present in the sample. In the case of a flat wavefront, entering into a telescope with a perfect optical configuration, the angular size of the corresponding pixel would have to be $\lambda/2D$, with λ being the wavelength and D being the diameter of the primary aperture of the telescope.

I.2.6 Effective PSF

An inherent complexity exists when the pixel integrates a signal on a finite area. The Nyquist-Shannon theory refers to this as an instantaneous or punctual sample. If we use the concept of "effective PSF" Anderson and King (2000) that defines PSF as the result of the convolution between the distribution of the intensity of the light on the focal plane and the response function of the pixel, we can apply the sampling theory to this effective PSF. This concept highlights the fact that, in order to obtain the best resolution, in reality we need to sample the

PSF with pixels of an angular size smaller than $\frac{\lambda}{2D}$. This is due to fact that because of the finite pixel size, the effective PSF will always have a total width of the maximum (FWHM) that is greater than the instrumental FWHM. In any case, being realistic, this is not very practical in the majority of cases.

In order to obtain the largest ratio of the signal sample, we can chose one of two solutions, taking the sample at smaller intervals, reducing the field of vision, or if the signal is stable, take many samples at different phase intervals. If the second option is chosen, then many individual exposures combine to produce an average image.This permits the reduction of need for storage, it facilitates the analysis process, and it produces data sets that can easily be visually inspected. In order to combine the images, we have to look for an algorithm that minimizes the convolutions with the pixel response function which supposes a loss of resolution and, at the same time, permits the application of methods to reject pixels that store corrupt data (dead pixels or very high intensity noise). According to our needs, we can use, for example, the Shift-and-Add (SAA) algorithm or the well known "drizzle algorithm" (Fruchter and Hook, 2002).

I.2.7 Strehl ratio and full width at half maximum (FWHM)

The ratio of Strehl is defined as the quotient between the intensity of the maximum peak of the observed PSF and that which should be observed in the absence of phase perturbations using a perfect optical system. In order to determine this ratio, we must know the total intensity that is sent by a source of light in order to estimate the ideal peak intensity. In order to obtain precise measurements of the Strehl ratio, it is necessary to have many high quality photometric measurements and an adequate sample of the image. The ideal peak of intensity may be approximated using a model of the disc of Airy although this may be difficult if we use a segmented primary mirror especially when the spaces between segments are relatively large.

The second measurement is the total width at half of the maximum or FWHM. As the name indicates, it corresponds with the PSF width at half of the peak intensity. Part of the premise of a symmetrical PSF with respect to the spatial axes, which is a reasonable premise, but does not always have to be completely true.

I.2.8 Seeing width

The width of seeing is nothing more than the FWHM of an image taken using a long exposure time with a sufficiently large aperture in order that atmospheric effects convert the PSF independent of the aperture. This is usually considered to occur when we have values of D_{tel}/r_0 that are greater than 10. The width of seeing depends on the wavelength on which

it is observed, verifying the relation (Tokovinin, 2002):

$$\epsilon = 0.98\frac{\lambda}{r_0}. \tag{I.11}$$

For general use, for example, as a measurement of the conditions of seeing, the calculus of ϵ is restricted to a wavelength of 500nm.

I.2.9 Wavelength dependence

All of the metrics (the Strehl ratio, FWHM, and the width of seeing) for the PSF in the presence of atmospheric and optical perturbations depends on the wavelength on which they are observed. To begin, the differences between the paths of propagation caused by said problems act in different ways on diverse wavelengths. A difference of 200 nm. in the propagation of blue light whose band centers at 400 nm. has a substantial effect, but there is little effect on the infrared "band K" which centers at 2200 nm. On the other hand, the ideal PSF also varies with the wavelength in a way that the greater wavelength will have a larger and flatter PSF. Combining both effects, the ratios of Strehl are much better as the wavelength is greater.

With respect to the width of seeing, as $r_0 \propto \lambda^{\frac{6}{5}}$, this will decrease as we observe longer wavelengths, following the relation:

$$\epsilon \propto \frac{1}{\lambda^{\frac{1}{5}}}, \tag{I.12}$$

for a given atmospheric turbulence and when $\frac{D_{tel}}{r_0} >> 1$.

I.2.10 The PSF of multiple systems

As commented earlier, the difference that exists between the disc of Airy and the disc of seeing causes a loss of information. On one hand, if the adequate pixel size is maintained for the sampling of the disc of Airy, the result is that the real flow from the source extends to more pixels than expected and the SNR decreases as a consequence of the readout noise. On the other hand, if we increase the pixel size, we lose resolution due to the convolution with the pixel response function. Even in the best case, a well sampled PSF with a high signal level, a greater width of the real image blurs much of the information in the high spatial frequencies. In all scenarios, we lose information that is vital to deal with double and multiple closed star systems. The criteria of Rayleigh is not longer applicable and as the size of the telescope is not important, our capacity for separation depends on atmospheric conditions, “seeing”, present during the observation.

Moreover, if we are studying a multiple system, it is difficult to estimate the ideal intensity for the calculation of the ratio of Strehl. Also, in general, the symmetry hypothesis with respect to the axes on which the FWHM depend will not occur.

I.3 Observational Techniques

To deal with effects provoked by turbulence in the images taken from the Earth's surface, different techniques have been proposed and developed for the past decades. Here we present three of them: Adaptive Optics (AO), Speckle Interferometry (SI), and Lucky Imaging (LI).

I.3.1 Adaptive Optics

Adaptive optics (AO) consists of a series of technological developments that allow the improvement of image quality produced by the light through an optical system, especially telescopes. It has become the most important method today to correct, in real time, the presence of terrestrial atmospheric turbulence.

This type of system can generate an estimation of the deformation of the wave front and update it using a Deformable Mirror (DM) to correct it. AO theory began to be developed in the 60s but its use was not extended until the 90s. The common physical elements of almost all AO systems are listed below.

- The Tip&Tilt Mirror is a flat mirror the inclination of which, at both axes (Tip and Tilt), can be controlled by correcting the average inclination of the wavefront. The variance of the wavefront can be improved by a factor of 10.
- The Deformable Mirror (DM) can be shaped/formed by active mechanisms with the objective of correcting aberrations of a superior order (I.2.1) that affect the wavefront. Although it would be possible to use this mirror to correct the Tip&Tilt, because the aberrations of this type are of greater amplitude and therefore may suppose a mechanical risk for the DM, this tends to be specifically corrected using the type of mirror previously mentioned.
- The Wavefront Sensor (WS) is a fast reading camera attached to a special optical piece and that, by means of an algorithm for the reconstruction of the phase, it can be used to create a continual estimation of the wavefront. Said estimation data is sent to the anterior mirrors in order to quickly correct the positions and adapt them to the turbulences reflected on the wavefront.

The process functions as a closed loop (I.4), in a way that the reading and estimation of the wavefront is produced sufficiently rapidly. The correction of the wavefront can be performed several times until it is substantially modified.

Three fundamental factors exist that control the design and effectiveness of AO:

- The parameter of Fried, r_0, that can be interpreted physically as the aperture on which the average quadratic deviation of the phase is 1 radian. If an AO system is designed to reach a Strehl ratio of 40%, the corrections to be made move on the r_0 scale. The r_0 determines the number of actuators that a DM should have as the quantity depends on $\frac{D_{tel}}{r_0}$.
- The isoplanatic angle, $\theta_0 \propto cos(\nu)\frac{r_0}{h}$, with "h" denoting the average height at which the turbulence occurs as well as the zenith distance, ν. Given a certain direction to correct, the isoplanatic angle describes the maximum angle as measured from that direction within which the corrections carried out are adequate or, in other words, the size of the angle where the phase is approximately constant. It is normally situated in the range of a few arcseconds in the range of the visible spectra and depends in great measure on the height where the turbulences are found.
- The response time with which the average quadratic phase error will be less than 1 radian, $\theta_0 = \frac{r_0}{\gamma}$, where γ denotes the average wind velocity. This is calculated using the Greenwood frequency (Greenwood, 1977) which describes the typical time interval in which the turbulence phase changes. The frequency at which the actuators should modify the DM should be greater than or on the order of the frequency with which the frequency varies.

As commented earlier in I.2, r_0 ,and θ_0, vary with $\lambda^{\frac{6}{5}}$. The consequence is that longer wavelengths need less response time which makes AO development more simple.

Next, we will briefly summarize the general function of AO. One part of the incident light is diverted by a beamsplitter, to a wavefront sensor. The data collected are sent to a control unit that estimates the observed perturbations. This control unit sends commands to the DM and particularly to its actuators, to adapt it, thereby altering the lengths of the optical paths that the light follows to different sections of the wavefront. The DM is set in front of the beamsplitter creating a process that allows testing to know if the correction was adequately carried out. The objective is to achieve a flat wavefront that is free of perturbations as, in this way, not only the telescopic resolution capacity limit is reached but the concentration of light as well is maximized.

Among the most important corrections that this process must make concern the aberrations produced by the average inclination of the wavefront. This inclination produces movement of the centroid of the star on the focal plane. That are known as Tip&Tilt which is the name of the order 1 Zernike polynomials that are those that correspond to this correction. The average angle of inclination and warp provoked by these inclinations is proportional

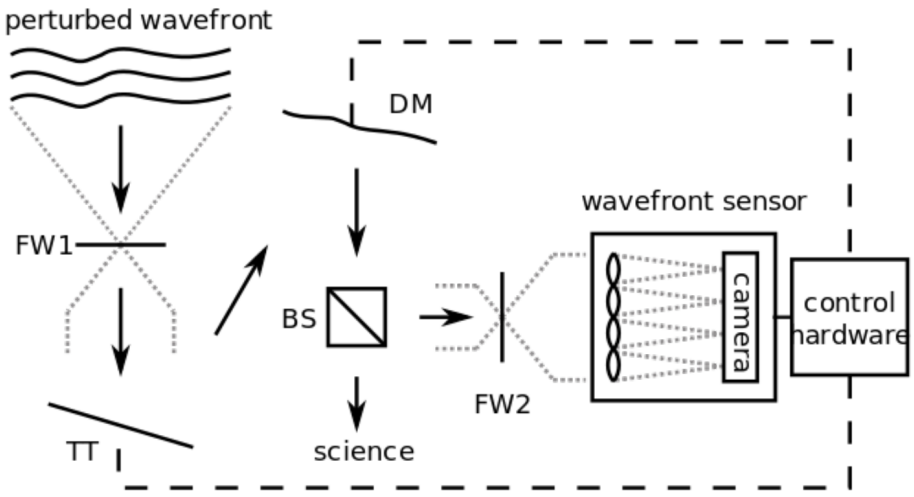

FIGURE I.4: Simplified AO system: the light first hits a tip&tilt (TT) mirror and then a deformable mirror (DM) which corrects the wavefront; part of the light is tapped off by a beamsplitter (BS) to the wavefront sensor and the control hardware which sends updated signals to the DM and TT mirrors.
Credit: 2pem under CC BY-SA 3.0

to λ/D_{tel}^{-3} as measured in radians to the square, in accordance with John W. Hardy "Book Review: Adaptive optics for astronomical telescopes / Oxford U Press, 1998" (2000). The Tip&Tilt decreases as the wavelength increases. Fixing the wavelength, when increasing the telescope size, the displacement of the image increases proportional to the diffraction limit λ/D_{tel}. The displacement of the image is the largest component of the disc of seeing at longer wavelengths.

One of the most important limitations of this technique is the need for a relatively brilliant light source in order that the wavefront sensor detects perturbations with SNRs sufficiently elevated and in less time than that given by the Greenwood frequency. For that reason, Natural Guide Stars (NGS) can be observed which would fall within the 4-14 magnitude range or that would be simulated with potent lasers, Laser Guide Stars (LGS). The fact that LGS must be used in certain zones of the sky without sufficiently bright reference stars makes the design, creation, and study of the technical complexities involved a field of high interest in Astronomy today.

In summary, we emphasize that the AO systems of today only function well with wavelengths that are sufficiently long because the phase perturbations suppose a small fraction of the length of the observed wavelength or, likewise, where the D_{tel}/r_0 ratios are small. Typical observations in the J, H, and K infrared bands yield Strehl ratios of ~0.4-0.7 in K and ~0.2-0.3. in J (Racine, 2006). Telescopes of 10 m. with AO such as the Keck or the VLT reach FWHM resolutions on the order of 0.1 arcseconds, the same as the Hubble Space Telescope,

although the information provided relates to different spectral bands. Tests of new generation AO systems are promising (e.g. Esposito et al. (2010)), but it can not be expected that the resolution capacity would improve drastically in the near future.

I.3.2 Speckle Interferometry

Here we will speak about the development of Speckle Interferometry (SI) with large telescopes since its origins (Labeyrie, 1970) to the eMCCD technology that began a bit more than a decade ago II.5. We cite the first article about SI, "Attainment of Diffraction Limited Resolution in Large Telescopes by Fourier Analysing Speckle Patterns in Star Images" by Labeyrie (1970) who considered that this technique can be understood as an extension of the stellar interferometer of Michelson and be used to measure stellar diameters as well as to resolve and study multiple systems.

The name "speckle" is given to the granulated structures that are observed when a laser is reflected by a diffusing surface. Based on the previous work of Texereau (1962), Labeyrie explained that the images of the stars can form a pattern that seem to be speckles when working with large telescopes. The speckles can be identified with the coherence domains of Bose-Einstein whose analysis applied to the study of star bodies was the basis (Brown and Twiss, 1956) of the technique called "intensity interferometry" (Brown and Twiss, 1954; Brown and Twiss, 1957).

Labeyrie explained that the speckles are produced by effects of interference on the phase of the wavefront caused by atmospheric seeing and can be observed when exposure times are considerably short, without exactly specifying the ranges within which they should move. He defended the opinion that the minimum size of the obtained granules (the observed speckles) is theoretically equal to the Airy disc given by the telescope in the absence of seeing and aberrations. For that reason, the information obtained in the images that shows these granulated structures are larger than the information present in observations where the exposure time leads to the accumulation of speckle forms on the seeing disc.

Using the theory of diffraction to interpret his experiments, he formalized that:

$$I(\alpha, \beta) = O(\alpha, \beta) \otimes |p(\alpha, \beta)|^2, \tag{I.13}$$

in such a way that $I(\alpha, \beta)$, which represents the distribution of intensity in the acquired image, corresponds to the convolution ((⊗ in the original but we use $*$ in the following) produced on the distribution of intensity of the original object $O(\alpha, \beta)$ by the function, $p(\alpha, \beta)$ which is the transformation of Fourier of $P(x, y)$ that represents the aberrated pupil of the telescope.

The Fourier transform of this equation yields:

$$i(x, y) = o(x, y) \cdot \mathcal{A}[P(x, y)], \tag{I.14}$$

where $\mathcal{A}$ is the autocorrelation function of $P(x, y)$. Calculating the squares of the modulus:

$$|i(x, y)|^2 = |o(x, y)|^2 \cdot |\mathcal{A}[P(x, y)]|^2. \tag{I.15}$$

$|\mathcal{A}[P(x, y)]|^2$ represents the Modulation Transfer Function (MTF) of the instrument in the presence of perturbations. Although this function can not be known in a given instant, the temporal average is an easily determined simple function, i.e., measured, and it must be parametrized for the seeing conditions.

Labeyrie also pointed out the importance of using a large number of images in order to improve the signal-noise ratio. This translated to the following equations:

$$\Sigma|i(x, y)|^2 = |o(x, y)|^2 \cdot \Sigma|\mathcal{A}[P(x, y)]|^2, \tag{I.16}$$

$$|o(x, y)|^2 = \Sigma|i(x, y)|^2 / \Sigma|\mathcal{A}[P(x, y)]|^2. \tag{I.17}$$

If we satisfactorily know the MTF, we then question from where are we able to calculate the intensity of the observed object. As Labeyrie commented, the loss of information that refers to the phase creates the situation that unless a symmetry centre exists, the object cannot be completely reconstructed.

Briefly, Labeyrie reiterated that SI should use sequences of photographs obtained with very short exposures in order that the speckles are visible. On one hand, this broke with the common method at that time of using exposure times of various seconds and, moreover, it became interesting to apply it in conjunction with image intensifiers. With that, Labeyrie stated that this technique requires magnification as well as prisms that correct the atmospheric dispersion. Labeyrie explained that short exposure times as well as using prisms to correct the atmospheric dispersion, in addition to magnifications, are the reasons why these granular structures are no usually observed and, therefore, are not well known in the field of astronomical observation. However, he did point out that, on certain occasions, they can be visualized using an eye piece.

Labeyrie did not include results of observations or real images due to the experimental nature of this first article. He indicated that, when applying this technique with a telescope, the resolution limit should be approximately 0”02 and that the minimum order of magnitude would be 7. We must to note that some important technical conditions, as the size of the telescope, under which this limit would be reached are not specified in the text.

Gezari, Labeyrie, and Stachnik (1972) published the first observations obtained with this technique and established that the limit reached for the observation of stellar diameters is

only 0”016 using a 200 inch telescope (5.08 m.). The resolution limit and the minimum magnitude reached would be 0”01 and $m_v = 9$, i.e., above the initial calculations in the initial article of 1970.

Speckle Interferometry: the first decades

Before SI, only four techniques were known that permitted the measurement of the angular diameters of stars with certain precision (Brown, 1968). On one hand, there were scarce spectroscopic eclipsing binary stars whose spectroscopic orbits, in combination with the photometric transit, allowed the direct calculation of the radius. Double aperture photometry was used for the most common stars and had been conceived and successfully used by Michelson and Pease (1921) and by Anderson (1920). In addition to that technology, lunar occultations (Evans, 1955) and intensity interferometers (Brown and Twiss, 1958) were used.

As we already mentioned, in the first published article where SI astrometrical observations are presented (Gezari, Labeyrie, and Stachnik, 1972), the authors attempted to reproduce the stellar diameter measurements that previously used methods had yielded. As we said, the new technique permitted them to measure stellar diameters of up to 0”016. The important point is that those results proved to be coherent with measurements previously obtained by other astronomers. Moreover, the resolution limit reached using a 5.08 m. telescope was even better than predicted, 0”010 for less bright objects, $\sim m_v$=9. In this study, in addition to diameters, they also tried to determine “limb darkening”, the oblateness, and the polar position parameters in binary stars as well as the difference of magnitude between the components.

The difference of magnitude for each system was obtained using the contrast function that is constructed as follows:

$$C = \frac{(I_{max} - I_{min})}{(I_{max} + I_{min})}, \tag{I.18}$$

and the contrast obtained converts to the difference of magnitude by means of the expression:

$$\Delta m = 2.5 log \frac{1 + (1 - C^2)^{1/2}}{1 - (1 - C^2)^{1/2}}. \tag{I.19}$$

Labeyrie and his collaborators continued that series of articles with Bonneau and Labeyrie (1973) and Labeyrie et al. (1974).

In the first two that correspond to 1972 and 1973, they were able to determine a total of 7 stellar diameters and resolve two closed binary systems. In the third from 1974, they used SI for the first time in a systematic way for the study of double stars. They selected 110 closed components selected for their spectra, their variability, or their binarity whether spectroscopic or astrometric. In total, they resolved 12 systems including three (β Per or Algol C,χ Dra

and τ Per) that were previously known astrometrically, two (γ Per and β CrB) spectroscopic, and three more completely unknown (δ Sco, σ Her, and β Cep). They reached limits of resolution of 0”020 and $\Delta m_v < 5$ magnitudes. They also calculated seven new masses based on earlier position measurements along with those published in this work. It was observed that the new masses for those components sustained the empirical mass-luminosity relation proposed by Harris, Strand, and Worley (1963).

In Harvey and Breckinridge (1973), this technique was used for the first time to study the Sun. As noted in his letter, the principles that control SI are also applicable for the study of details in extended sources and, especially, solar features. In that first effort to use speckle images or specklegrams, they studied the granulation, the faculae, and the penumbral filaments as well as umbral dots of only 180 km. of diameter, achieving results in accordance with earlier models and observations.These first results, along with the advantage of using the total aperture of the telescope which was different than the double aperture technique of Michelson, motivated the authors to affirm that SI was very effective for obtaining information about these small-sized characteristics of the Sun. In later years, the study of solar granulation as well as other solar characteristics has continued (e.g., Aime, Ricort, and Harvey (1978), Druesne et al. (1989), Grec et al. (2007), Harvey and Schwarzschild (1975), Krieg et al. (2000), Ricort and Aime (1979), Ricort et al. (1981), and Wöger, von der Lühe, and Reardon (2008)).

Along with the first practical applications, numerous articles developed the theory that sustained this technique, the most important being Dainty (1973, 1974), Gough and Bates (1974), Knox and Thompson (1974), Korff, Dryden, and Miller (1972), Linfoot and Witcomb (1972), and Liu and Lohmann (1973). It is noteworthy that in Dainty (1974), fundamental aspects were studied in detail such as the function of transference, the signal to noise ratio, and the limit of magnitude where it was demonstrated theoretically and by means of computational models that binary stars up to m_v=16 can be resolved. This limit surpasses that reached by the Michelson interferometer or the intensity interferometer. In Knox and Thompson (1974), the first successful attempt was made to recover the phase information that, in the case of binary stars, allows us to obtain the real information of the observed system, eliminating the ambiguity of 180 degrees that is introduced on the resolution by means of the autocorrelation function. A bit later, Weigelt (1977) proposed another method based on triple autocorrelation or biespectrum with the same end. The bispectrum method will be analyzed and contrasted with other techniques during next decade (Beletic, 1988; Karbelkar, 1988; Karbelkar and Nityananda, 1987).

The first digital photon-counting version of a speckle interferometer camera was used on the 5 m. telescope at Mount Palomar to observe 100 stars (Blazit et al., 1977) reaching a resolution similar to the previous one that used photographic film. That same year, the Special Astrophysical Observatory (SAO) in Russia began working with SI on their 6 m. telescope (Balega and Tikhonov, 1977).

In 1973, C.R. Lynds began the SI program on the 4 m. Mayall telescope of Kitt Peak that led

to the publication,"Digital image reconstruction applied to alpha Orionis", Lynds, Worden, and Harvey (1976). The Lynds program was the precursor of the program that McAlister began in 1975 and that became the most efficient and productive in the 80s and 90s. That program began with the articles by McAlister (1976b) and McAlister (1976a).

In "Spectroscopic binaries as a source for astrometric and speckle interferometric studies." (McAlister, 1976b), they proposed the resolution of 102 spectroscopic binary systems using SI with a 5 m class telescope (73 systems) and a 2m class telescope (29 systems). In addition, they included 10 other astrometric binaries that were supposedly able to be resolved using SI on large telescopes.

The program consisted of obtaining precise astrometric measurements of binary systems using SI directed by McAlister and was carried out at the Kitt Peak National Observatory using a 4m class telescope. His first article reported the resolution of the spectroscopic component AB of the triple visual η Orionis (McAlister, 1976a). Consequently, the new visual measurement improved the orbit. Combining the new visual resolution with existing spectroscopic data, he determined a more exact system mass and he was also able to prove that the mass-luminosity relations of the system components were consistent with Harris, Strand, and Worley (1963).

In "Speckle interferometric measurements of binary stars. I" by McAlister (1977a), the results of 256 observations carried out during 5 nights with adequate atmospheric conditions between September 1975 and January 1976 were published. As the principal motive of the program was to resolve new pairs, the data showed that only one-fourth of the observed objects registered positive for multiplicity. In total, they completed 70 observations of 53 binary systems with a minimum separation of 0"037±0.001 in the case of ADS 3064. The presence of systemic errors was proven by comparing the results obtained with the theoretical positions expected in those systems that have well-known orbits. Of the 70 measurements obtained for the 53 resolved systems, 34 pertained to systems whose orbits were considered to be very high quality at that time.The average residuals were $< \Delta\rho >$=+0"002±0"03 and $< \Delta\theta >$=-0"006±0"014. Next, he eliminated 9 measurements with considerably dubious quality reaching average residuals of $< \Delta\rho >$=-0"001±0"009 and $< \Delta\theta >$=-0"004±0"014. In all cases, the fact that those residuals were less than the dispersions is a clear indicator of the absence of serious systematic errors.

In the following years, teams from France (Bonneau and Foy, 1980a,b; Bonneau et al., 1980), the U.S.A. (Hubbard et al., 1979; McAlister, 1978c, 1979a; McAlister and Degioia, 1979; McAlister and Fekel, 1980), USSR, Great Britain (Morgan, Beckmann, and Scaddan, 1980; Morgan et al., 1978), Germany (Weigelt, 1978a,b), and Australia (Tango et al., 1979) conducted observations. In addition, the first SI observations were carried out in ESO (Ebersberger and Weigelt, 1979). Moreover, during those years, the first near infrared observations were conducted (Selby, Wade, and Sanchez Magro, 1979).

Recalling the famous article of Finsen (1971), "Twenty Years of Doubles-Star Interferometry and its Lessons", McAlister (1983) published "Five years of double star interferometry and its lessons" in which he summarized the quantitative and qualitative data of the first speckle interferometry programs. In five years, collecting the measurements obtained by the groups in Germany, England, and France and above all, those registered by the McAlister group, he obtained 1,366 measurements for 358 binary stars. Of those, half (683) resolved systems of less than 0"2 arcseconds of separation and almost one-quarter (22%) of less than 0"1. More than 58 new binaries were discovered. Approximately 83% were obtained by the Kitt Peak National Observatory group.In said article, the results accumulated up to that time were reported and, moreover, the technical and practical characteristics associated with SI observation campaigns were explained. Among various recommendations and tips, the author suggested that the speckle interferometry cameras be calibrated using a double slit mask, a technique that continues to be practiced today.

As a result of the systematic SI observations of binary stars, McAlister and the Kitt Peak group began to publish a long list of articles, the first of which was "Speckle interferometric measurements of binary stars. I" (McAlister, 1977a) that was preceeded by a catalog of objects of interest (McAlister, 1976b) and by two articles about individual stars (McAlister, 1976a, 1977b). Those were followed by (McAlister, 1978c, 1979a; McAlister and Degioia, 1979; McAlister and Fekel, 1980; McAlister and Hendry, 1982a,b; McAlister et al., 1983) till "Speckle interferometric measurements of binary stars. IX", McAlister et al. (1984).

In addition to measurements, the group also published data corresponding to unresolved stars (Hartkopf and McAlister, 1984; McAlister, 1978a; McAlister and Hendry, 1981), a catalog of reference stars for SI (McAlister and Hartkopf, 1983), and many other articles focused on the astrophysical study of specific star systems (e.g., McAlister (1978b, 1979b, 1981) and McAlister and Hartkopf (1982)).

In 1982, the same group began to develop the new ICCD camera (McAlister, Robinson, and Marcus, 1982) and they published their first observational results in "ICCD speckle observations of binary stars. I - A survey for duplicity among the bright stars" (McAlister et al., 1987a). Many new publications followed concerning observations (Lu et al., 1987; McAlister, Hartkopf, and Franz, 1990; McAlister et al., 1987b, 1989) and orbits (Hartkopf, McAlister, and Franz, 1989; McAlister et al., 1988).

The initial objective of the first article "ICCD speckle observations of binary stars. I - A survey for duplicity among the bright stars" (McAlister et al., 1987a), was to avoid errors in spatial observations that are due to the multiple nature of some stars. The final aim was to provide the Hubble Space Telescope (HST) with a list of single objects that could be used as guiding stars, rejecting double and multiple systems. To that end, they observed 672 stars from the Bright Star Catalog (BST) of Yale in order to determine their multiplicity ratios. As a result, they discovered 52 new binary systems. They observed 60 other known systems and

calculated a frequency of 11% of closed visual binary systems with separations in the range of 0”04-0”25.

As far as we know, McAlister and Hartkopf (1984) published the first catalog of high resolution measurements after SI appeared and in which CHARA, the Center for High Angular Resolution Astronomy, was first mentioned. The mission of this institution is to promote, design, economically support, and operate the future CHARA array (McAlister, 1988) which began “to see the first fringes” in 1999. In articles after “ICCD speckle observations of binary stars. III - A survey for duplicity among high-velocity stars”, (Lu et al., 1987), it was considered that the observations were carried out using the ICCD of CHARA while, in the first, the camera was still referred to as the Georgia State University (GSU) ICCD Speckle Camera.

Working in parallel to the speckle research of CHARA and the German, French, English, Australian, and Russian teams that began their studies with SI in the 70s, in the 80s, SI began to be used to not only study double stars and binary systems but it use extended to a multitude of celestial objects and applications, listed below:

- to observe satellites that pertain to other planets or dwarf planets within the Solar System, (Baier, Hetterich, and Weigelt, 1982; Baier and Weigelt, 1983, 1987; Hetterich and Weigelt, 1983),
- to observe asteroids and study their multiplicity, (Baier, Hetterich, and Weigelt, 1982; Bowell et al., 1981; Drummond et al., 1982; Vakulik et al., 1989),
- QSOs, (Hege et al., 1981),
- the size of the Wolf-Rayet star dust shells,(Allen, Barton, and Wallace, 1981),
- molecular clouds, (Dyck and Howell, 1982),
- Nebula and clusters, (Baier, Ladebeck, and Weigelt, 1985; McCarthy et al., 1982; Weigelt, Baier, and Ladebeck, 1985),
- collaborate in the preparation of the Hipparcos Space Mission , (Argue et al., 1984, 1985),
- to study the Magellan Cloud planetary nebulae, (Barlow et al., 1986; Wood, Bessell, and Dopita, 1985),
- to follow supernovas, (Meikle, Matcher, and Morgan, 1987a,b; Nulsen et al., 1990; Wood et al., 1989),
- to study stellar populations, for example, evolved stars and bipolar nebulae (Dyck et al., 1984), las T Tauri stars (Baier et al., 1985) o las OH/IR stars (Cobb and Fix, 1987).

We should not overlook the appearance of new technical and instrumental tecnology such as the ICCD (McAlister et al., 1985) or speckle spectroscopy (Afanas'jev et al., 1988) developed by the SAO speckle research group.

During the first half of the 90s, new programs such as that of the U.S. Naval Observatory (USNO) (Douglass, Hindsley, and Worley, 1993; Worley and Douglass, 1992) appeared. E Horch began his SI work, developing the Stanford University Speckle Interferometer System (SUSIS) for the MAMA detector (Horch et al., 1992a,b). Devaney (1992) obtained a series of double star observations from La Palma and studied the T Tau system with SI to obtain information about the diffraction limit of the telescope in narrow bands around H_α where the system is resolved and, in the nearby red continuum where the system remained unresolved (Devaney et al., 1995). After SAO published all of the measurements obtained with the 6 m. BTA between 1981 and 1988 (Balega, Balega, and Vasyuk, 1990), they began to regularly publish obtained measurements (Balega, Balega, and Vasyuk, 1991a,b), and they launched a specific program (Balega et al., 1991) oriented to the observation of some stars, all of which are included in the Gliese (1969) Catalog or in its supplement Gliese and Jahreiß (1979) of which there existed known or suspected variations in their radial velocites. They also published in collaboration with a French SI group concerning their detection of the orbital movement of the DF Tau system (Thiebaut et al., 1995) and also gave a first estimation of its masses. For that article, they used measurements of lunar occultations taken by (Chen et al., 1990).

The GSU/CHARA group compiled a new catalog of interferometric measures (Hartkopf and McAlister, 1991) and continued their orbit publications (Gies et al., 1993; Mason et al., 1995; McAlister, Hartkopf, and Mason, 1992; McAlister et al., 1995). In the companion article to the Catalog, they shared statistics such as observations/declinations and observations/year graphics.

Hardly a year after this article, Hartkopf (1992) gave a conference for the IAU Colloq. 135: Complementary Approaches to Double and Multiple Star Research where he contributed updated information that showed the progress realized in obtaining interferometric measurements since its beginning at the end of the 19th century. The principal observers and techniques can be seen in I.5. In I.7, the enormous lack of coverage in the austral declinations can be observed which is due to the fact that most of the SI work was carried out in the northern hemisphere. In I.6, distributions are shown for time and separation until the date of that conference event. In said graphics, we can appreciate the dependence on said graphics with respect to the work of the GSU/CHARA group at that time. One example is that, in the first half of 1982, the group directed by McAlister prepared to move forward with the ICCD technology and also dedicated time to engineering and to the necessary tests of the new camera. At that time of year, it was not possible for them to observe with their customary frequency and, at a world level, only 26 measurements were produced in those 6 months.

In order to mitigate the lack of coverage of SI observations in the southern hemisphere, E.

TABLE 1. Interferometrists Past & Present

Schwarsschild	1895	Michelson interf.	Munich 10-in
Anderson, Merrill	1919–1921	Michelson interf.	Mt. Wilson 2.5-m (6-m baseline)
Maggini	1922–1923	eyepiece interferometer	Catania 13-in
Finsen	1933	Michelson interf.	Johannesburg 26-in
Wilson	1934–1935 1949–1954	eyepiece interferometer	Flower 18-in
Jeffers	1939–1941	eyepiece interferometer	Lick 36-in
Finsen	1954–1969	eyepiece interferometer	Johannesburg 26-in
Gesari, Labeyrie	1970–1973	speckle (photographic)	Hale 5-m, KPNO 4.0-m, KPNO 2.1-m
Wickes, Dicke	1972–1974	Michelson interf.	Mt. Wilson 1.5-m Mt. Wilson 0.6-m
Morgan, Scaddan, Tango	1975–1978	speckle (photographic)	Isaac Newton 2.5-m, SAAO 1.9-m, RGO 1-m
McAlister	1975–1981	speckle (photographic)	KPNO 4-m & 2.1-m
Blasit, Bonneau, Koechlin	1975–1986	speckle (photon-counting TV) (also ICCD in 1986)	SAO 6-m, Hale 5-m, CFH 3.6-m, ESO 3.6-m, Pic du Midi 2-m, Haute–Provence 1.9-m
Schmidt, Angel	1976	1-D speckle (SIT TV)	Steward 2.3-m
Tokovinin	1977	2-point speckle	Crimea 1.25-m
Balega, Dudinov	1977–1980	speckle (photographic)	SAO 6-m
Weigelt, Ebersberger	1977–1983	speckle (photographic)	ESO 3.6-m & 1.5-m, Asiago 1.8-m, Hoher List 1-m
Tokovinin	1978–	photoelectric phase–grating interferometer	Crimea 2.6-m, Mt. Sanglok 1-m, Shternberg 0.7- & 0.6-m
Cocke, Hege	1979–1981	speckle (photographic)	KPNO 4-m, Steward 2.3-m
Morgan, Vine, Argue	1981–1988	speckle (Plumbicon)	AAT 3.9-m, Mt. Stromlo 1.9-m, Lowell 1.8-m
McAlister, Hartkopf	1981–	speckle (ICCD)	KPNO 4-m, CTIO 4-m, CFH 3.6-m, Lick 3-m, Mt. Wilson 2.5-m, Lowell 1.8-m
Balega	1983–	speckle (intensified TV)	SAO 6-m
McCarthy, Leinert, Mariotti	1985–	1-D IR speckle	KPNO 4-m, ESO 3.6-m, Calar Alto 3.5-m, Steward 2.3-m
Yiming, Yaohui	1986	speckle	Yunnan 1-m
Zinnecker, Perrier	1986–	1-D IR speckle	ESO 3.6-m
Isobe	1987	speckle (intensified MOS camera)	San Pedro Martir 2.1-m Shternberg 0.7- & 0.6-m
Bakhtin	1987	speckle?	Abastumani AZT-11
Beckers, McCarthy, Henry	1987–	2-D IR speckle	KPNO 4-m, Steward 2.3-m
Morgan, Horch	1988–	speckle (MAMA)	ESO 3.6-m, Lick 3-m, Steward 2.3-m
Worley, Douglass	1990–	speckle (ICCD)	USNO 0.7-m
Ghez	1990–	2-D IR speckle	Hale 5-m

FIGURE I.5: From W. I. Hartkopf, Twenty Years of Speckle Interferometry

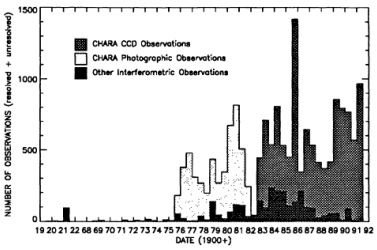

FIGURE 5. Number of speckle measure as a function of time. Note the pronounced gap in early 1982.

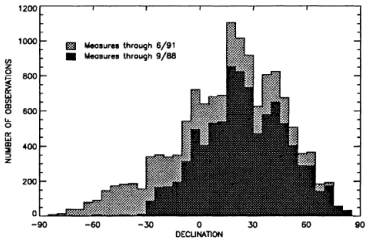

FIGURE 4. Number of speckle measures, as a function of declination. The darker shaded region indicates the distribution through September 1988, the lighter region the improvement in this distribution after regular southern hemisphere observations were begun in early 1989.

FIGURE I.6: From W. I. Hartkopf, Twenty Years of Speckle Interferometry

Horch and W.F. Altena moved the SUSIS that had been used at the Lick Observatory and they installed it on a 76 cm. reflector at El Leoncito, Argentina (Horch et al., 1995a; Horch et al., 1996). In addition to covering austral declinations, these new observations could be combined with the those by Finsen as well as with the new parallax measurements from Hipparcos. This would permit more detailed investigation of the lower portion of the mass-luminosity relation for the mean sequence.

USNO research significantly increased in the late 90's (Douglass, Hindsley, and Worley, 1997; Douglass et al., 1999; Germain, Douglass, and Worley, 1999a,b) and continues today. USNO is one of the more important speckle interferometry research teams and contributes a large quantity of observational data per year to the international community (Douglass et al., 2000; Hartkopf and Mason, 2011, 2015; Hartkopf, Mason, and Rafferty, 2008; Mason and Hartkopf, 2017; Mason, Hartkopf, and Friedman, 2012; Mason, Hartkopf, and Hurowitz, 2013; Mason, Hartkopf, and Wycoff, 2008, 2010, 2011a,b; Mason et al., 2000, 2001a, 2002, 2004a,b, 2006a,b, 2007, 2017). This team usually utilizes ICCD cameras attached to the USNO 26-inch Clark refractor located in Washington, DC. However, this camera has been transported to the KPNO and CTIO 4 m, the Mount Wilson 2.5 m, and the McDonald Observatory 2.1 m telescopes. The USNO and CHARA groups use the same algorithm, Directed Vector Autocorrelation (DVA) (Bagnuolo et al., 1992), to determine the real position of the components. Collaborations between both groups have been continual during the last two decades (e.g., Mason et al. (1999, 2001b)).

We point out the increase in international collaborations of SAO during the last years of the 20th century that led to numerous publications concerning speckle observations using the 6 m. BTA (Balega et al., 1997, 1999; Hofmann et al., 2000; Petrov et al., 1996; Schertl et al., 2000; Schoeller et al., 1998; Weigelt et al., 1998, 1999a,b). The GSU/CHARA group continued with regular publications concerning orbit calculation (Hartkopf, Mason, and McAlister, 1996; Mason, 1997; Mason, Douglass, and Hartkopf, 1999; Mason, McAlister, and Hartkopf, 1996; Mason et al., 1997, 2000).

Leinert et al. (1997) extended his study of multiplicity in close M dwarfs (<5pc) to the

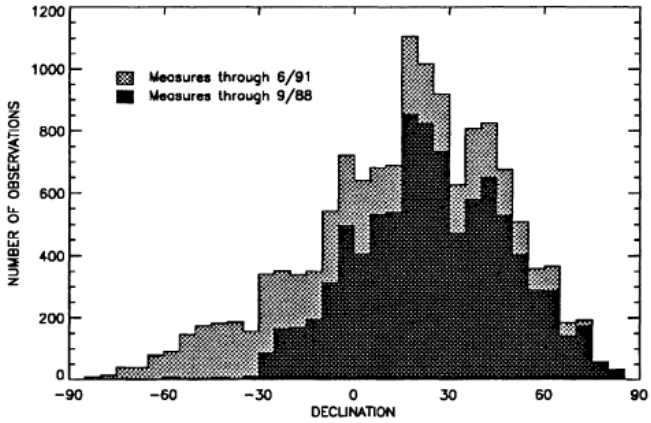

FIGURE 4. Number of speckle measures, as a function of declination. The darker shaded region indicates the distribution through September 1988, the lighter region the improvement in this distribution after regular southern hemisphere observations were begun in early 1989.

FIGURE I.7: From W. I. Hartkopf, Twenty Years of Speckle Interferometry

southern hemisphere (<δ-30) in order to continue his previous investigations with SI in the infrared that began at the beginning of the decade (Henry and McCarthy, 1990). As the known quantity of these objects was very small, they studied a total of 25 brown dwarf stars in the northern hemisphere and 9 in the southern hemisphere with the objective of finding new components.

Duquennoy et al. (1996) continued his studies of multiplicity in the Solar System and published an orbit that combined the spectroscopic and interferometric data in the close infrared to the single line brown dwarf, Gliese 692.I (Tokovinin et al., 1994). The speckle images were taken at Calar Alto with two instruments: a one-dimensional scanning device like that used by Leinert and Haas (1989a,b) and MAGIC (Herbst et al., 1993). Also in Calar Alto, Fors, Horch, and Núñez (2004) applied the drift scanning technique to improve speckle observations with CCDs. This technique had been previously used to obtain lunar occultations at milliseconds sampling rate (Fors, Núñez, and Richichi, 2001; Fors et al., 2004).

Speckle Interferometry with eMCCDs

During the past decades, SI has contributed notably to expand our knowledge of the relative positions of thousands of multiple systems, to discover new nearby components, to better understand the Solar System and its asteroids, to study supernovas and star formation environments, etc. Although there continue to be only a few groups that regularly use SI to systematically study double stars, the technological progress in computation, hardware,

telescopes, pointing, etc. has created the situation that said research can be carried out with continually increasing precision and speed.

In terms of SI development, one of the most important advances has been the appearance of cameras with electro-multiplication technology or eMCCDs (II.5). These technological developments have driven the creation of numerous observation programs that, each year, yield thousands of measurements in the northern hemisphere (e.g., Balega et al. (2013), Balega et al. (2011), Horch et al. (2017), Mason and Hartkopf (2017), Orlov (2015), Prieur et al. (2017), Rastegaev et al. (2014), and Van Altena, Horch, and Casetti-Dinescu (2017)), as well as in the southern hemisphere, (Tokovinin, 2018b; Tokovinin et al., 2018). The van Altena-Horch team conducted austral observations, still using CCD technology or the MAMA instrument. They also have the Differential Speckle Survey Instrument of eMCCD detectors (Horch et al., 2011a,b) and have begun to use it on telescopes of both hemispheres (WYNN, DCT, and both Gemini's North and Sur, (Horch et al., 2018)) due to its portability.

One of the first instruments used to observe using an eMCCD was the High Resolution Camera (HRCam) constructed in 2007 for SOAR (Tokovinin and Cantarutti, 2008), followed by the Astralux (Hippler et al., 2009; Hormuth et al., 2008) used for Lucky Imaging on the 2.2 m. at Calar Alto and the NTT, the speckle camera of the BTA (Maksimov et al., 2009), the previously mentioned DSSI (Horch et al., 2009), Robo-AO (Baranec et al., 2014) or the AOLI (Velasco et al., 2018).

Moreover, the high performance of these devices has led to other applications such as the effective development of Lucky Imaging that we will explain later (I.3.3), or, in the field of exoplanet research, it has facilitated the detection of low brightness companions around the stars that host them (Furlan et al., 2017; Hirsch et al., 2017; Howell et al., 2011, 2016). The precision needed for this work requires the combination of AO with SI and, in that way, one is able to assess the multiplicity of the system in certain cases which affects the relative brilliance of the principal star (e.g., Crossfield et al. (2016)). This implies information that is determinate at the moment of deriving the correct radius of the exoplanet (Ciardi et al., 2015).

As mentioned in I.3.1, due to the technical difficulties involved with this technology in the visible range, the great majority AO observations are carried out on long wavelengths associated with infrared. Nevertheless, it is rare that the obtained Strehl ratios are less than 0.2 arcseconds. However, SI permits reaching the refraction limit of the telescope in the visible range, with the expense of observing a very small field of vision. For that reason, the combination of both techniques improves the performance of AO in the visible and the precision of the speckle instruments by augmenting the SNR and diminishing the Tip&Tilt. With said combination, the limits of detection around the stellar object can be reduced which permits better scrutiny concerning the astrophysical properties of binaries as well as multiple systems. Moreover, increasing the capacity to detect secondary components also

adds credibility to the detections of exoplanets by the transit method as these are affected by the presence or absence of unknown components.

I.3.3 Lucky Imaging

Lucky Imaging (LI) is based on the fact that atmospheric seeing is random as are those moments where seeing is significantly better or worse than average. The time of coherence that is associated with seeing is on the order of tenths of a millisecond. Therefore, to select the best moments for seeing, we should conduct observations with cameras that permit acquisitions in this time range. Fried (1978) is credited with the origin of LI for its article *Probability of getting lucky short-exposure image through turbulence*, although he himself cited an anterior article by R.E. Hufnagel who discussed methods similar to those proposed by Fried to arrive at the conclusion that LI reaches its best results when the ratio, $D_{tel}/r_0 \sim 7$ (According to Fried (1978) this article corresponds to Hufnagel, R.E., 1966 in "Restoration of Atmospherically Degraded Images", Vol. 3, p. 11). As the detectors at that time did not allow for short observations, 20 years had to pass before Astronomy could take advantage of his results. It was the development of eMCCD cameras that we explained in the Chapter II.5 that permitted the capacity to reach acquisition ratios per second and the SNRs necessary for this technique to be applied to a wide range of research today.

In addition to the technical requirements, LI has great computational capacity. After acquiring the images, each one must be cleaned of artifacts produced by the detector, and then analyzed in order to adjust the present atmospheric turbulence. The best images are aligned to correct the Tip&Tilt effects on the image detected on the focal plane and added using the Drizzle algorithm (Fruchter and Hook, 2002). With each accumulated image, the SNR is slightly improved and the limit of observed magnitude increases.

The principal limitation of this technique is the necessity that the aperture of the telescope and the conditions of observation verify that the ratio D_{tel}/r_0 is 7 or slightly less than 7. For higher ratios, the probabilities to obtain images with good seeing diminishes rapidly, following the Fried (1978) equation:

$$P \approx 5.6 \exp^{-0.1557(\frac{D_{tel}}{r_0})^2}. \tag{I.20}$$

The wavelengths that we can observe are limited by the sensibility to light of the eMCCDs which diminishes when the wavelengths move from the visible toward infrared. For typical seeing at observatories located in good astronomical locations, LI restricts a telescope of 3 m. maximum, resulting in images on the order of ~0.1 arcseconds. Nevertheless, LI permits the completion of the empty space that exists in the visible where AO is not efficient. The other option would be to obtain images from space. Today, new types of detectors are being

created for infrared observations, that would permit the implantation of cameras that would use LI on medium-size telescopes (3 - 8 m.) (Rogalski, 2005; Rothman et al., 2009).

One of the main advantages of LI is the price as compared to AO. An eMCCD camera can cost tens of thousands of dollars, while the cost to equip a telescope with AO can be millions of dollars. In addition, it is easier to operate an eMCCD camera and lasers are not required. Another advantage is the acquisition times that, with LI, are very reduced even for thousands of images per field of observation.

To conclude, the isoplanatic angles are larger than the common ones in AO, normally it takes an average of 30 arcseconds for a good seeing, and the guiding stars reach magnitude 16 in the *i* band of the SDSS (Law, Mackay, and Baldwin, 2006). The combination of all of these factors permits coverage of the sky that is superior to that permitted by AO guided by NGS. In any case, both techniques can be complementary. For example, the LI camera of Cambridge in combination with the AO system at PALMAO of the 200 inch Hale telescope at Palomar (Law, Hodgkin, and Mackay, 2008) improved the FWHM that corresponds to 710 nm from 75 to 40 milliarcseconds and improved the Strehl ratio of 0.06 to 0.15.

I.3.4 Imaging techniques for observing exoplanets

The detection of exoplanets, brown dwarfs, or discs in the proximity of stars is essential in order to understand the processes of substellar formation as well as the evolution of them and their relation with the host stars around which they develop. In order to achieve these detections as diminish the proportion of false positives are some of the principal objectives of new generation telescopes of 8 - 10 m. as well as with future telescopes of 30 and 100 meters.

In general, substellar objects are much less bright than the halo provoked by the star after their light crosses the atmosphere. Telescopes on the Earth's surface are affected by the atmospheric consequences in the form of speckles or spots that hide the presence of these dim bodies.

The techniques of direct imaging are among the most effective methods for the detection of exoplanets although indirect methods also exist such as the analysis of radial velocities or the study of transits. The last two only allow us to indirectly infer the presence of these not bright, low mass companions on the basis of changes in the conditions of the star that houses them while we can directly observe the body and definitely confirm their existence with imaging techniques.

Indirect techniques are more sensitive to large exoplanets that have short orbits and are aligned with our vision. Direct imaging complements those aspects because, the ability to directly observe a planet permits us to try to obtain its spectrum as well as study its atmospheric composition and temperature which are key factors for habitability.

The disadvantage of direct techniques, given the technical limits today, is the small number of planet that can be detected with them. This creates the obligation to observe many stars before a detection is obtained. The principal reason is the brilliance-contrast-separation conjugation. The great differences of emission between stars and exoplanets added to the angular separations observed from Earth make it very difficult to achieve a positive result.

The exoplanets for which we are searching do not emit their own light in the visible spectrum; they only reflect the light of their star. The closer that the planet is to the star, the less will be the contrast between them because the reflected light is brighter. However, the closer that the planet is to its star, the less will be the angular separation observed, possibly being below the limit of diffraction of our telescope which would make it impossible to distinguish no matter neither the brightness nor the contrast.

In accord with Guyon et al. (2006), a planet the size of Earth is approximately 10^{-10} times brighter than the star that it orbits and a planet the size of Jupiter is only 10 times more bright than the previous. In general, the separation between these planets and their stars are usually much less than an arcsecond. In order to obtain the contrast by means of astronomical observations, the size of the telescope can be increased in order to increase the light reflected by the planet in a smaller cone (size λ/D). In favorable observation conditions and using a 60m telescope, it is possible to achieve a contrast on the order of 10^8 at distances of 0”2 and a chronograph would help to drop the Airy disc on an order of 3 magnitudes.

Nevertheless, the fact that all planets have their own thermal emission is favorable for direct imaging. Given that the average temperature of an exoplanet is in the range of 100K-700K, we know that, in general, this thermal emission creates the situation that the exoplanets are more brilliant in the near infrared than in the visible. Moreover, this thermal emission does not depend on the separation between the star and the emitting planet. For these reasons, these techniques use filters and efficient detectors in the near infrared and AO offers benefits for the reaching the limit of diffraction of the telescope used.

Another problem that occurs at the time of observing exoplanets with direct methods is associated with the difficulty to distinguish the planet from the background noise. The required duration for these observations creates the conditions that the normal atmospheric turbulence in the atmosphere limits the resolution in the visible and in the near infrared at levels between 0”5-2” depending on the placement of the telescope. To reach the theoretical resolution limit, we must use it in combination with AO technical systems that allow the minimization of the noise present as well as achieve an adequate contrast without introducing artifacts that could be interpreted to be detections. Nevertheless, the overlap of the speckles due to the duration of the observation produces a quasi-static pattern of noise that is mainly due to optical imperfections and the slow evolution of those instrument-AO-telescope alignments. This quasi-static speckle noise is of long duration and it adds coherently as the exposure of the images increases, it converts to be the dominant source of noise (Lafrenière et al., 2007a).

Continuing with our imaginary 60 m. telescope in favorable conditions, the noises present that are normally in the form of quasi-static speckle noise, must be calibrated with a precision of 10% in order to detect a Jupiter and, with 1% in order to detect an exoplanet similar to Earth (Guyon et al., 2006).

Next, we will explain an observational technique known as ADI (Angular Differential Imaging, I.3.4). We refer to the images and observations obtained by using this technique as "ADI images and observations" as appropriate. These images suppose the use of two algorithms to improve the results. LOCI (I.3.4) consists of a process of the selection of ADI images acquired throughout a series of observations of a star that is a candidate for having exoplanets or circumstellar discs as a function of parameters such as luminosity, spectrum, evolutionary phase, or distance with respect to the Solar System. TLOCI depart from LOCI and is used to attempt to achieve a more effective selection and would take note of support images obtained in other nearby wavelengths. With these images, a PSF Template is constructed in order to assist with exoplanet detection. In order to understand TLOCI (Template LOCI, I.3.4), it is important to first explain what constitutes the Simultaneous Spectral Differential Imaging (SSDI, I.3.4) and its combination with ADI images applying LOCI or a version of it known as damped-LOCI.

ADI

Angular Differential Imaging (ADI, Marois et al. (2006)) is a high contrast direct imaging technique that reduces the presence of the quasi-static speckling and facilitates the detection of dim bodies close to a star. The technique consists of acquiring a sequence of images with a fixed orientation of them while the field of vision (FOV) rotates, that is, the terrestrial rotation are not corrected as it is usual in the majority of astronomical observations. To cancel out this rotation that corrects the terrestrial movement has the effect that the telescope and the instrument maintain a fixed observation direction, while the exoplanet and the field of vision observed move continuously and the quasi-static noise produced by the optical elements is generally constant. In addition to the classic process of reduction, a reference PSF is constructed for each image from other images in the sequence selected for certain criteria. Then, this reference of the image is extracted to eliminate the noise. The resulting images are aligned, thereby recovering the same orientation of the field with respect to the celestial sphere and they combine to to augment the S/N ratio. The combination of these images yields an additional gain on the order of the square root of the total number of images used. One of the principal advantages of this technique is that the star itself is used to construct the reference PSF. This means that the PSF comes from a star of the same spectrum and brilliance which creates a more rapid observation process as there is no need to obtain images of other stars for the calibration. Ghost detections and the noise produced by the sky are also eliminated due to the process of removal of the PSF model.

PSF model construction is very important for this technique. Various methods exist as detailed by Marois et al. (2006). The first method is based on selecting the median image of the sequence. If the rotation of the field during the sequence is done in such a way that has been sufficient enough in order to obtain that a point of light that is adjacent to the star has moved at least twice its FWHM, then this point of light will be fully rejected by the median leaving only the average PSF. As the median is taken from a large quantity of images, the pixel-to-pixel noise (i.e., PSF, flat, Poisson noises produced by the sky and the read-out noise of the camera) of the resulting image will be much less than any of the individual images. This process considerably reduces the noise in the ones where the residuals are limited by the pixel-to-pixel noise. Nevertheless, as the sequences of images last around one hour, the presence of quasi-static noise in the reference PSF image does not demonstrate a high correlation with the images to be corrected.

Another method takes the median of only a portion of the images as close in time as possible of the particular image of the sequence that we want to correct, but where there exists a movement of at least 1.5 times the FWHM of the PSF. This minimum movement assures us that the nucleus of the PSF of a possible light source is not reduced with the removal. The time required to produce this minimum rotation is given by the equation:

$$\psi = 0.2506 \frac{\cos A \cos \varphi}{\sin z}, \tag{I.21}$$

where the ratio of the FOV rotation, ψ, in degrees per minute, is obtained from the temporal derivative of the paralactic angle as given en "Book Review: Electronic imaging in astronomy: detectors and instrumentation / Wiley, 1997" (1997). In the equation, A represents the azimuth, z is the zenith distance, and φ is the telescopic latitude. This technique yields a greater attenuation of the quasi-static noise. Nevertheless, the pixel-to-pixel noise in this case is not adequately corrected in the majority of cases.

The combination of both techniques in only one algorithm is presented in Marois et al. (2006) as well as other details with relation to attenuation of noise. This article also explains how it is applied to real observations using the Gemini North telescope with the AO Altair system (Herriot et al., 1998) and the infrared NIRI camera (Hodapp et al., 2000).

In accord with their results, a total attenuation of 20-50 is obtained from one hour of observation if we compare the result of a 30 second exposure. An attenuation of 100 seconds can be achieved with sequences of 2 hour exposures, reaching a contrast of 5-sigmas for differences of 20 magnitudes in separations greater than 8". For a 30 minute sequence, ADI yields a S/N ratio that is 30 times greater than the classical observation techniques. It was concluded that ADI can be used to search for planets of $1 M_{Jup}$ with orbital radii between 50 and 300 AU around young stars (Marois et al., 2006).

In general, ADI consists of taking images in only one bandwidth with short exposure times, in sequences that normally last one hour.

This technique originated as a generalization of the "roll deconvolution" of the HST. This roll deconvolution subtracts two images of the star acquired during the same orbit with the space telescope aimed at an object at different angles. With this technique (Marois et al., 2006), similar improvements were obtained on the order of 50 (Fraquelli et al., 2004; Schneider and Silverstone, 2003), but it was limited by the PSF evolution.

A technique that is similar to ADI and developed independently by Liu (2004) has been used to search for circumstellar discs.

LOCI

Lafrenière et al. (2007a) developed an algorithm to combine ADI images and improve the elimination of quasi-static noise. ADI is based on the idea that the angular position of a planet changes continually while its flux remains constant. The algorithm is called Locally Optimized Combination of Images (LOCI) and it was designed to interact with this form of observation and attenuate the variations in sky transmission, i.e., the PSF smearing due to the rotation of the field of vision and the variations in seeing/Strehl ratio.

Using ADI observations for each image (I_i), from which the objective is to remove the quasi-static Speckle noise, a reference image is created (I^{REF}) using a linear combination of other images from the sequence:

$$I_i^{REF} = \sum_k (c_{k,i} \times I_k). \tag{I.22}$$

The weights ($c_{k,i}$) are obtained by solving the linear equation:

$$Ac_i = b_i, \tag{I.23}$$

where the covariance matrix of the reference images, c_i, is the vector of coefficients and b_i is the vector of correlation of the image to subtract with all reference images. Inverting A,

$$c_i = A^{-1} b_i, \tag{I.24}$$

and multiplying, we obtain the coefficients.

The algorithm consists of determining the set of coefficients that, after subtracting the reference image, the residual noise is minimized.

In order to impede source point self-subtraction, for each image, those images recently taken that experience a rotation of the field of vision of less than 1/2λD are not used to calculate the reference image. The subtraction of the reference image is usually carried out in small anular sections.

Speckle-Optimize Subtraction for Imaging Exoplanets (SOSIE, Marois, Macintosh, and Véran (2010)) uses the formalism of LOCI but it improves the contrast with respect to the original algorithm. If the reference image is too large, in which case it can occur that it is not correlated with the image to subtract, the noise can make the determination of the optimal set of coefficients difficult. In order to solve that, the covariance matrix can be truncated using a single value decomposition (SVD) and/or it can be modified using image selection techniques based on the correlation. An algorithm known as Karhunen-Loeve Image Projection (KLIP, Soummer, Pueyo, and Larkin (2012)) achieves a similar optimization by decomposing the reference image saved in eigenvalues. We muse keep in mind that, for covariance matrices, using the SVD or eigenvalue decomposition are mathematically equivalent, so SOSIE and KILP use the same process of least-square inversion.

SOSIE uses a masking technique to avoid the the LOCI algorithm subtracts the planet from the images when attempting to eliminate noise. In addition, LOCI subtracts the planet from the images when attempting to eliminate noise. Moreover, the idea was proposed to generate a PSF template in order to be able to fit the astrometry and the photomety of the exoplanets thereby permitting the calculation of the curve of contrast without having to inject artificial sources.

SSDI

Before we present TLOCI, we should explain the technique called Simultaneous Spectral Differential Imaging (SSDI).

Racine et al. (1999) presented a detailed study of speckle noise and the limits that this imposes when the objective is to detect planets around stars. Within the different possibilities that the author proposed in order to correct said noise, there exists the option to subtract the speckle pattern. This can be done by using pairs of images taken simultaneously with two narrow filters centered on adjacent wavelengths. The limiting factor then becomes the noise that corresponds to the flat-fielding for frequencies from $\sim \lambda/D$.

Biller et al. (2006) and Marois et al. (2003b) applied this instrumental method to attempt to calibrate and eliminate the speckle noise of the AO images obtained, and they referred to this method as Simultaneous Differential Imaging (SDI) as well as Differential Simultaneous Imaging (DSI). The objective is to isolate the light from the planet from that received from the nearby star. In both studies, this method was applied using VLT, MMT (Biller et al., 2006) and CFHT (Marois et al., 2003b) telescopes. They decided to use the fact that all of the cold exoplanets , $T_{eff} \lesssim$1200K-1470K, are believed to have strong methane absorption

lines (CH_4) around 1.62 μm in the infrared H band. Various simultaneous images were taken within as well as outside of that zone. Next, they used these images to subtract the halo influence and the speckle noise in the resulting images and, in that way, reveal the light emitted by the planetary companions that are normally hidden by the halo. Other specific characteristics that clearly differentiate the spectrum of the planet and of the star can be used in the same manner.

Lafrenière et al. (2006, 2007b) and Marois, Phillion, and Macintosh (2006) called this technique, Simultaneous Spectral Differential Imaging (SSDI). In the initial simulations, the SSDI results showed promise but, when they tried to use it, they realized that the presence of non-common path aberrations produce quasi-static and uncorrelated speckle noise in each optical channel.This impeded an adequate subtraction of the speckle noise. The problem with simulations was that they were based on the idea that all of the aberrations are produced on the pupil plane which, as we have said, is not absolutely true. New simulations use a different approximation known as "Talbot Wavefront Propagation", simulating the effects that the out-of-pupil-plane aberrated optics have at the moment of achieving the suppression of the speckle noise. The simulated results with the Talbot approximation fell to the attenuation of ~10 for any range of angular separation (using the Fraunhofer approximation) to ~10 with a limit of separation of λ/D.

The first applications of this technique selected a limited number of PSFs in different colors and the optimal individual and double differences (SD and DD) were calculated. The DD is the curvature of the flow as a function of the wavelength. If one exoplanet is present in the image, it would have to generate a strong curvature in comparison with the speckles that appear to be linear with respect to the wavelength. Near Infrared Coronographic Imager (NICI, Artigau et al. (2008), Biller et al. (2008), and Chun et al. (2008)) allows to obtain two simultaneous images at different wavelengths and combined ADI and SSDI by simply adding the image in the extra wavelength to the set of ADI images in order to achieve better results using LOCI.

Another algorithm exists that is known as damped-LOCI. First, LOCI is used to obtain an initial detection of the planet and, next, damped-LOCI introduces a penalty term that forces the algorithm to find positive coefficients and maximize the flow in a $\sim \lambda/D$ aperture around the position of the planet. That is, unlike LOCI simple, the inversion of the matrix is not a blind process and that permits the minimization of contamination around the localization of the planet. Obviously, the main problem is the necessity to previously know the position of the planet and also is problematic that when the algorithm works to maximize the flow, the surrounding noise can be maximized in an uncontrollable manner.

TLOCI

In order to be able to visualize exoplanets and circumstellar discs, the noise produced by the halo of the star that host them must be suppressed as much as possible. The difference of magnitude between the star and the exoplanets as well as the closeness between these objects makes their discovery a particularly attractive challenge for modern Astronomy. The standard techniques to achieve these detections using only one band have, until now, consisted of the ADI observational technique as well as in the LOCI algorithm. The new high contrast measurement instruments have been designed to benefit from AO as well as from the multispectral images obtained via integral field spectographs. Having these images available in different bands has led to the creation of new algorithms that take advantage of the possibility to use them along with those obtained using ADI, that is, with rotations of the field of view.

Marois et al. (2014) developed a new algorithm named Template LOCI (TLOCI). This algorithm maximizes the S/N ratio of the possible exoplanets using as input data the spectrum as well as a reference PSF generated by the image of the star that hosts the exoplanet or the disc. With said data, it is able to optimize the reference image and thereby minimize the self-subtraction of the planet without being effective at the moment of suppressing the speckle noise. It is known that quasi-static speckles, i.e., the noise present in the PSF halo, can be coherent with time scales that last from a few seconds to hours and that constitute one of the principal limitations at the moment of suppressing the effects produced by the stellar halo in the AO images (Marois et al., 2003a).

TLOCI is an algorithm developed by the Gemini Planet Imager (GPI, Macintosh et al. (2014)) and it can combine the ADI and SSDI images and, at the same time, reduce deficiencies in the process of subtraction. Similar to LOCI, it is based on the selection of images designed to not contaminate the flow produced by it nor the exoplanets that may be hidden in the images, although the selection process is different than that used by LOCI. From the model of the planet spectrum, TLOCI only uses one parameter to determine to what point the self-subtraction is acceptable. For that, the images are previously normalized before calculating the coefficients, $c_{i,k}$, which translates to the situation that all of the images contain the same total flow.

USC
UNIVERSIDADE
DE SANTIAGO
DE COMPOSTELA

Chapter II

Instrumentation

The present Chapter describes the instruments applied for the observation of binary and multiple stars throughout history, especially the cameras used for the development of different programs of observation by the Observatory after Ramón María Aller in this astronomical field.

Firstly, we shall present the origins and design of the micrometers, in particular: the results obtained with this kind of instruments by the founder of our Observatory and the astronomers who continued his work. Afterwards, we shall offer the readers an introduction to the origin of interferometry thanks to Michelson's contribution in the beginning of the XX century and we shall explain some of different types of the current interferometers.

We shall explain first in general terms, then, taking into account their importance currently in astronomy, in details, the functionality of both CCDs and eMCCDs, focusing on the description of different noises produced by these instruments. At the same time, we shall explain in details the fundamental aspects for the reduction of images in the case of both types of detectors.

At last, we shall proceed with the description of the Observatory's old ICCD camera, currently out of use, as well as the Princeton Instruments eMCCD Photon MAX 512 applied to carry out our observation campaigns in the 2.6 m. telescope at Buyrakan Aastrophysical Observatory (BAO). This description continues with the scrupulous presentation of the technical aspects of the detector, as well as the optical part of the camera, divided into filters, microscopes and prisms, meant to regulate atmospheric dispersion. We shall also specify the aspects to be considered when mounting and demounting the camera on the telescope, as well as the procedures that we applied to plan and perform our observation campaigns.

II.1 Micrometers

In a letter dated on the 28th of December 1666 and published in 1667 in Philosophical Transactions, N 21, pp. 373-375, the French astronomer Adrien Auzout informs that he managed to determine the diameters of the Sun, the Moon and the planets by using his own method, developed jointly with Jean Picard, which allowed of order arcsecond accuracy (Djokić, 1996). Auzout mentions in the same letter that he succeeded in determining the lunar parallax based on the diameter calculated according to this new method. Although the letter's text does not specify how the measurements were fulfilled, the results published make Rochard Towenley wonder who is the inventor of this instrument able to measure the angular distances and is called micrometer for this feature.

In the beginning of the XVII century, Galileo Galilei himself had created devices to measure accurately the sizes of distance in the visible range of his telescopes. The invention of the ocular micrometer is believed to have taken place as soon as the telescopes began being provided with measurement instruments, like quadrants or sextants. In this early period, they were used to determine by means of direct measures the diameters of the closest celestial objects. In a letter published in Philosophical Transactions, N 25, 1667, pp. 457-458, Richard Towenley comes to indicate that it was William Gascoigne who introduced the micrometer in the observational practice in 1640 approximately. This is based on the original correspondence between Gascoigne and his friends explaining the invention and the application of the device for measuring small angular distances. Unfortunately, both Gascoigne's friends and he himself died very young, so the micrometer had to be re-discovered twenty years later by the above French astronomers.

After the discovery of orbital movements existing in double stars by William Herschel, this ocular micrometer evolved to the form known as filar micrometer. A piece with the most common design consists of a micrometer and a reticle with two spider silk threads or, in the absence thereof, thin wires which were parallel. These threads must have the ability to move closer or come apart through a screwing mechanism, forming the micrometer itself. The threads are placed in the focal plane of the ocular micrometer, superimposed over the object or objects observed.

In some other designs, the micrometer disposes of a fixed reticle against which a single thread or a second reticle moves. In case of this configuration, the measurement axis may be adjusted by rotating the ocular micrometer over the telescope tube, according to the position of the two sources. When a thread is placed over the line of view pointing to one of the points of interest and the other one is moved towards the second point, it becomes possible to measure the distance between the threads with the related micrometric instrument. A trigonometric calculation with the object's focal length provides the angular distance between two measured points.

FIGURE II.1: Friedrich Georg Wilhelm von Struve from Wikipedia

Friedrich Georg Wilhelm von Struve was the first astronomer to stand out with his observations of double stars by applying a filar micrometer. Although the phenomenon of the stellar multiplicity was examined for the first time by its inventor W. Herschel and later by his son John Herschel and James South, F. G. W. von Struve exceeded in many aspects the efforts of those who preceded him. All along his life, he was devoted to the observation of double stars, making measurements of 2714 stars only between 1824 and 1837. These observations were published later in his work *Stellarum Duplicium et multiplicium mensurae micrometricae*. He discovered a large quantity of new components and published the first collection thereof in *Catalogus novus stellarum duplicium* (1927). He established in 1839 the Observatory of Pulkovo, running it until his retirement for health problems in 1861, according to the Britannica Enciclopedia Moderna: "...having measured about 3000 binaries during his study of more than 120.000 stars". Besides, Struve was the first one in measuring the parallax of the star Vega, though before Friedrich Bessel had measured a parallax for the first time: that of $61 Cygni$. Otto Struve, Wilhem von Struve's son, continued his work in the position of Director of the Observatory of Pulkovo from 1862 to 1889.

The prestigious astronomer Wulff D. Heintz describes in the Chapter 9 of his classic book "Double stars /Revised edition/", (Heintz, 1978), titled Micrometric Observations, the filar micrometer, exposing its measurement process:

> "The filar micrometer has a field of view as shown in ... It is rotatable, connected

> with a graded circle, so that the position angle can be read at bisection of both stars with one wire (I), or perhaps between a pair of wires (II). The separation measurement (III) use a fixed and a moving wire (read in both positions from a drum connected with the precision screw) corresponds to double the separation. Multiplying it by half the screw value (arc sec per revolution) gives the separation. The orientation of the circle (zero point) is found from a star trailing along the wire used for the angle readings. Repeated settings are recommended for all readings, for the purpose of better accuracy and of checking. The author prefers to take, within one observation, five or six angle and three double- distance readings, moving the wires off position in between the settings in order to reduce the bias. A prism in front of the eyepiece, inverting the field of view, may help to eliminate possible systematic errors, when half of the readings are taken each with and without the prism. For bright stars, or under poor seeing conditions, a stepping-down of the aperture may improve the accuracy, yet the opinion of observers is not unanimous on that point."

In the end of the paragraph, he refers to the double-image micrometers and comparison micrometers which use a double artificial star. The first one generates two images based on a light source, thanks to the application of a birefringent prism (for instance, Muller's design (Muller, 1949)). This device was used to relieve the problems caused by the lack of practice of unexperienced observers when using a filar micrometer, reflected in the presence of systematic errors. Another advantage was the possibility to make a polarized photometric comparison. Its obvious disadvantage, i.e. the reduction of the intensity of the light reaching the eye due to the prism, was compensated by the absence of illumination of the field, which facilitated the sight's adaptation. The micrometers of comparison with double artificial stars were already out of use when Heintz wrote his book in order to detect the errors they used to provoke; however, the author mentioned that they could be useful for less brilliant stars, underlining at the same time that he had no information about the use thereof for the mentioned purpose.

When looking through this text, it is curious to see how some of actual techniques preserve the spirit of these micrometers. One of the examples is the speckle camera DSSI (Horch et al., 2009) which provides images reaching the telescope's diffraction limit simultaneously in two channels, using also a prism to separate the light source. Another example is the adaptive optics with laser guide stars which simulates stars in order to measure the caliber before and/or during the observations.

With no intention to go deep into the details of all the works implemented with different kinds of micrometers since the origins of the astronomy with telescopes, we would like to emphasize that these micrometers have permitted the accumulation of measures with the same kind of used instrument for almost 200 years in the field of double stars. The micrometric measures provided are still applied nowadays for the calculation of orbits, which seeks for quantities of data and the coverage of the star positions in different phases of the orbit that they draw.

When applying them, it is necessary to take into consideration always that the accuracy of these measures varies a lot because of the optic features of different telescopes in use, because of the atmospheric conditions during which the observations are carried out, because of the observer's professionalism and observation routine, because of the site's height above the sea level, between other relevant considerations.

The use of the micrometer survived even the introduction of photographic techniques in the astronomy; it was only quite late in the XX century that its use eventually ceased, as the technology of the Charge-Coupled Devices (CCDs) went developing and gaining solid ground since its birth in 1969. This technological jump from the eye to pixels led from the astronomy of purely visual observation, with all its deficiencies: the inherent necessity to repeat several times the collection of data in every observation, the impossibility of storing for a continuous period of time the telescope's fields of view, the need in an experienced observer, etc., to the modern astronomy where we can observe, store and handle images many times completely automatically, minimizing the human intervention and all the errors that it supposes.

The staff of the Astronomical Observatory after Ramón María Aller (OARMA) ordered to make its latest micrometer, analogous to that employed in Pic du Midi by Dr. Couteau, in the workshops of the Nice Observatory in 1988, in order to obtain astrometric measures. It was applied in the telescope of 1.52 m in Calar Alto (Almeria) and lately in the one of 0.62 m in the OARMA. The results of these observations were published in different scientific articles between (Abad, Docobo, and della Prugna, 1998; Couteau, Docobo, and Ling, 1993; Couteau et al., 1989; Docobo, 1998; Docobo and Ling, 1994a; Docobo and Prieto, 1993a; Ling and Lanchares, 1993; Ling and Prieto, 2000). In the same way that the Steinheil refractor, this device come equipped with two vertical yarns plus another horizontal which allows good performance measurements of both angular separations and positional angles.

II.2 Origins of Interferometry

Thomas Young performed in 1801 his famous Double Slit Experiment in order to try to distinguish between the corpuscular and wave-like natures of the light (II.2). Thanks to this experiment, Young was able to confirm that the light coming from a distant source generated a pattern of interferences or a fringe when diffracted, passing through double slit. This discovery highly contributed to the theory of the wave-like nature of the light. Besides, this knowledge was fundamental to prove in the future the duality of wave and corpuscle.

The experiment is explained below. An electromagnetic monochromatic wave with its wavelength equal to λ may be described per every point, in time and space, as a complex quantity, i.e. provided with amplitude and a phase, $A\exp^{i\phi}$. For more convenience, the amplitude assumed is a steady value A, characteristic for a constant light source, while the

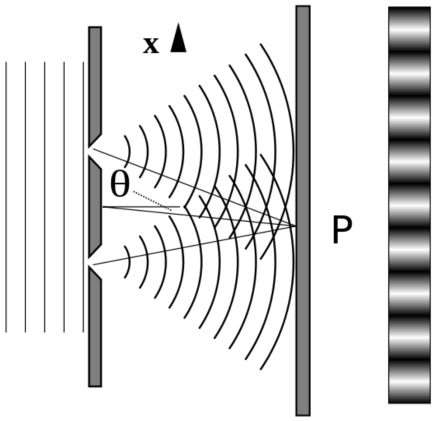

FIGURE II.2: The position on the screen, P, determines the phase difference between the two arriving wavefronts. Waves arriving in phase interfere constructively and produce bright strips in the interference pattern. Waves arriving out of phase interfere destructively and result in dark strips in the pattern. Credit: Lacatosias under CC BY-SA 3.0

phase is allowed to vary depending in time and position. If the wave moves across two different ways and it is recombined later in a P point, the resulting electric field would be equal to the sum:

$$E = E_1 + E_2 = A\exp^{i\phi} + A\exp^{i(\phi-\phi_0)}, \tag{II.1}$$

where the delay ϕ_0 is related with the path difference τ_0:

$$\phi_0 = \frac{2\pi\tau_0}{\lambda}. \tag{II.2}$$

The attribute that we measure on the screen, i.e. the brightness, physically consists in the intensity of the electric field, EE* (in which * stands for conjugate), divided by the quantity of time during which the light is accumulated while measured:

$$EE^* = (E_1 + E_2)(E_1 + E_2)^* = E_1E_1^* + E_2E_2^* + E_1E_2^* + E_2E1^* = A^2 + A^2. \tag{II.3}$$

As a result, we get replacing:

$$EE^* = 2A^2 + 2A^2\cos\phi_0. \tag{II.4}$$

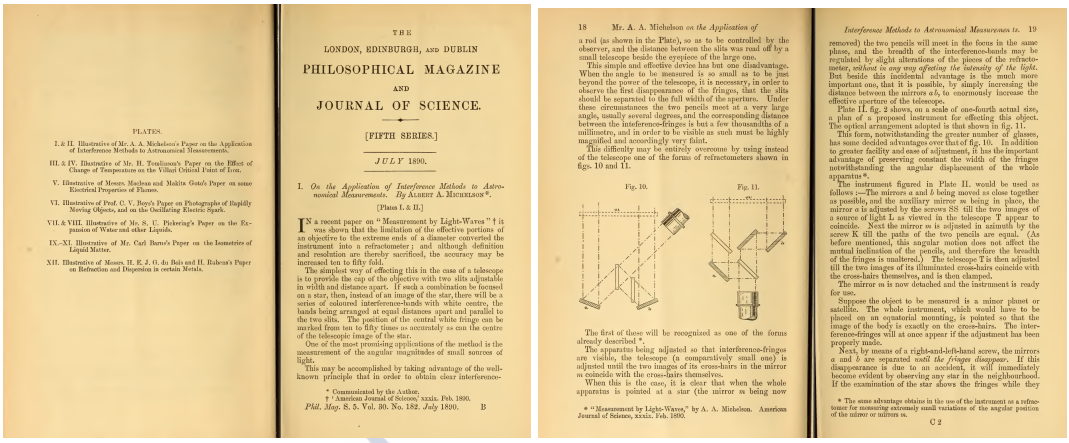

THE
LONDON, EDINBURGH, AND DUBLIN
PHILOSOPHICAL MAGAZINE
AND
JOURNAL OF SCIENCE.
[FIFTH SERIES.]
JULY 1890.

I. *On the Application of Interference Methods to Astronomical Measurements.* By ALBERT A. MICHELSON*.

[Plates I. & II.]

IN a recent paper on "Measurement by Light-Waves" † it was shown that the limitation of the effective portions of an objective to the extreme ends of a diameter converted the instrument into a refractometer; and although definition and resolution are thereby sacrificed, the accuracy may be increased ten to fifty fold.

The simplest way of effecting this in the case of a telescope is to provide the cap of the objective with two slits adjustable in width and distance apart. If such a combination be focused on a star, then, instead of an image of the star, there will be a series of coloured interference-bands with white centre, the bands being arranged at equal distances apart and parallel to the two slits. The position of the central white fringe can be marked from ten to fifty times as accurately as can the centre of the telescopic image of the star.

One of the most promising applications of the method is the measurement of the angular magnitudes of small sources of light.

This may be accomplished by taking advantage of the well-known principle that in order to obtain clear interference-

* Communicated by the Author.
† 'American Journal of Science,' xxxix. Feb. 1890.
Phil. Mag. S. 5. Vol. 30. No. 182. *July* 1890. B

a rod (as shown in the Plate), so as to be controlled by the observer, and the distance between the slits was read off by a small telescope beside the eyepiece of the large one.

This simple and effective device has but one disadvantage. When the angle to be measured is so small as to be just beyond the power of the telescope, it is necessary, in order to observe the first disappearance of the fringes, that the slits should be separated to the full width of the aperture. Under these circumstances the two pencils meet at a very large angle, usually several degrees, and the corresponding distance between the interference-fringes is but a few thousandths of a millimetre, and in order to be visible as such must be highly magnified and accordingly very faint.

This difficulty may be entirely overcome by using instead of the telescope one of the forms of refractometers shown in figs. 10 and 11.

Fig. 10.

Fig. 11.

The first of these will be recognized as one of the forms already described *.

The apparatus being adjusted so that interference-fringes are visible, the telescope (a comparatively small one) is adjusted until the two images of its cross-hairs in the mirror *a* coincide with the cross-hairs themselves.

When this is the case, it is clear that when the whole apparatus is pointed at a star (the mirror *a* being now

* "Measurement by Light-Waves," by A. A. Michelson. American Journal of Science, xxxix. Feb. 1890.

removed) the two pencils will meet in the focus in the same phase, and the breadth of the interference-bands may be regulated by slight alterations of the pieces of the refractometer, *without in any way affecting the intensity of the light.* But beside this incidental advantage is the much more important one, that it is possible, by simply increasing the distance between the mirrors *a b*, to enormously increase the effective aperture of the telescope.

Plate II. fig. 2 shows, on a scale of one-fourth actual size, a plan of a proposed instrument for effecting this object. The optical arrangement adopted is that shown in fig. 11.

This form, notwithstanding the greater number of glasses, has some decided advantages over that of fig. 10. In addition to greater facility and ease of adjustment, it has the important advantage of preserving constant the width of the fringes notwithstanding the angular displacement of the whole apparatus *.

The instrument figured in Plate II. would be used as follows:—The mirrors *a* and *b* being moved as close together as possible, and the auxiliary mirror *m* being in place, the mirror *a* is adjusted by the screws SS till the two images of a source of light L as viewed in the telescope T appear to coincide. Next the mirror *m* is adjusted in azimuth by the screw K till the paths of the two pencils are equal. (As before mentioned, this angular motion does not affect the mutual inclination of the pencils, and therefore the breadth of the fringes is unaltered.) The telescope T is then adjusted till the two images of its illuminated cross-hairs coincide with the cross-hairs themselves, and is then clamped.

The mirror *m* is now detached and the instrument is ready for use.

Suppose the object to be measured is a minor planet or satellite. The whole instrument, which would have to be placed on an equatorial mounting, is pointed so that the image of the body is exactly on the cross-hairs. The interference-fringes will at once appear if the adjustment has been properly made.

Next, by means of a right-and-left-hand screw, the mirrors *a* and *b* are separated *until the fringes disappear.* If this disappearance is due to an accident, it will immediately become evident by observing any star in the neighbourhood. If the examination of the star shows the fringes while they

* The same advantage obtains in the use of the instrument as a refractometer for measuring extremely small variations of the angular position of the mirror or mirrors *a*.

FIGURE II.3: Details of the original paper from Michelson
See Pages 1-21 from Filosophical Magazine for July 1890 (Volume XXX,I)

We may observe in this equation that the phase disappeared, leaving solely the delay phase ϕ_0, produced by the path difference. While the first part of the sum is constant, the second one may vary with ϕ_0 according to the screen or receptor, P, position. At the same time, the intensity EE* is a real quantity, varying from 0 to $4A^2$. This is what causes the alternation of bright and dark zones on the screen where the light is projected.

Although this experiment pretended originally just to prove the wave nature of the light, it ended up becoming the origin of Interferometers. As we noticed, the intensity of the object observed can be determined in a relatively easy way on the screen where the light would appear. This is not a big advantage, as it can be also obtained directly, observing the object. Nevertheless, we can also extract spatial information here. Besides, the capacity to extract this spatial information would depend on the distance between slits. If an optical telescope's capacity to separate light sources depends on the diameter of the mirror aperture, D, being proportional to $\frac{\lambda}{D}$, in case of an interferometer this capacity is expressed by $\frac{\lambda}{B}$, where B is the distance between slits. Taking into account that it is cheaper to make a long baseline interferometer than a telescope with large aperture, this aspect gains a high importance in practice, especially in the development of radioastronomy.

Stellar Interferometry may be defined as the art of using the effects typical to the interference in order to improve the angular resolution of observations, in our case: astronomical observations. Therefore, they seek to optimize the telescope's resolution capacity and to resolve small angular structures in details. The interferometers may be divided in two classes: those configured as an independent mechanical and optical structure, and those consisting in an auxiliary tool connected to the telescope.

The theory supporting the first interferometer of Michelson (1920) was described for the first time in an article of 1890 in Filosophical Magazine for July 1890, (XXX,I) (Figure II.3). The following year, a series of proving observations was put into circulation at Lick

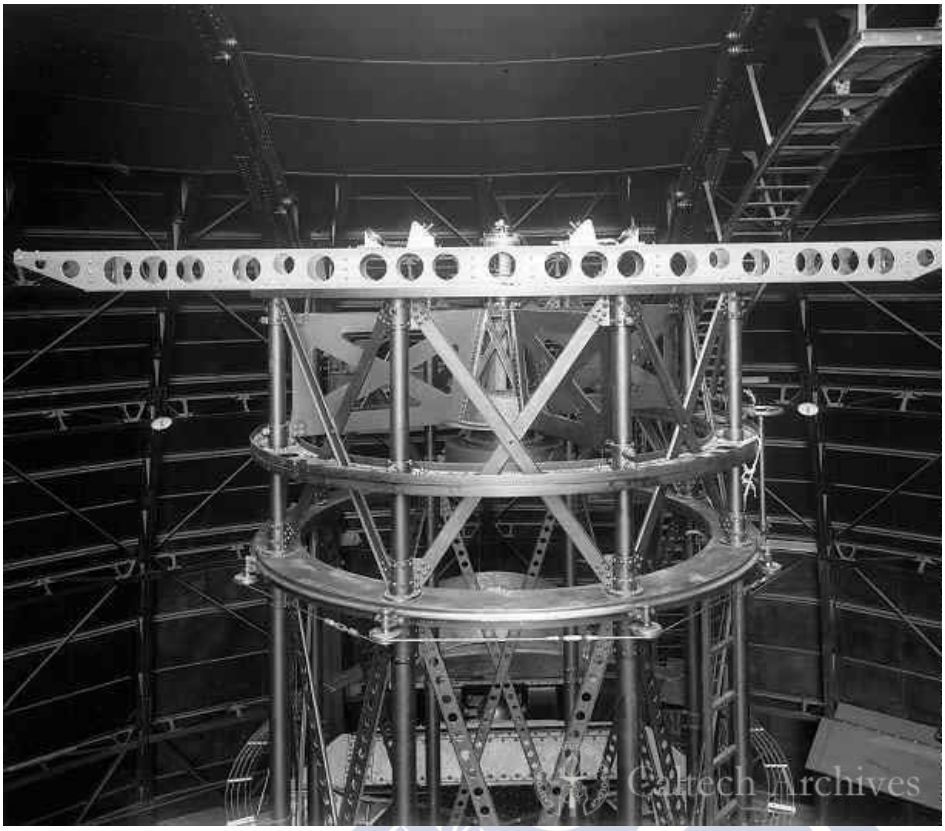

FIGURE II.4: 20' Michelson interferometer on Hooker telescope
Photo by Mt. Wilson and Las Campanas Observatories
From Caltech Archives.

Observatory, aimed at determining the size of Jupiter's satellites and, later, measuring the size of Betelgeuse, meanwhile the first interferometric measurement of a binary was performed by K. Schwarzschild (1896), thus inaugurating the application of the technical innovation created by Michelson to this kind of stars.

The basic design of many actual optical interferometers follows the model developed by Michelson where an ensemble of external mirrors plays the role of slits, altering the optical path length and generating a "d" length base (II.5). The rest of the optical system carries the light, already in the form of two wavefronts, towards the detector. It was Michelson himself who encouraged the observations of Schwarzschild, indicating that this optical configuration could be useful for astrometry on double systems.

It was between 1919 and 1922 when J.A. Anderson and Paul W. Merrill carried out a series of measurements of bright stars, using Michelson's interferometer. As Michelson's primary intention was to measure stellar diameters, J.A. Anderson (1920) was the second one after Schwarzschild who published observations of double stars with telescopes of 60 and 100

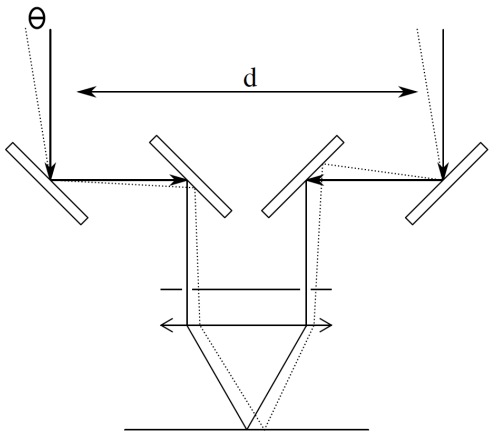

FIGURE II.5: Idea behind the stellar interferometer
Credit: Alex-engraver under CC BY-SA 3.0

inches at the Mount Wilson Observatory (II.4).

Among Anderson (1920) results is their measure of 0”0545 with an error of less than 1 % of *Capella*'s components. In this article, he calculates a first orbit which would be refined soon by Merrill (1922). Merrill too explains that thanks to the experiments that both of them realized in order to find a double artificial star with known separation, using a quartz plate, and to improve the reduction process, they revealed that *κ Ursae Majoris* behaved unusually.

Consulting the literature they discovered that Aitken had appointed in 1907 the double nature of this star, recording three measures of separation: 0”21, 0”25 and 0”15. Thus, the results of Anderson and Merrill published in 1922 confirmed the double nature of this system and measured its position at a moment when its angular separation was about 0”0836, decreasing in a couple of months to 0”077. This is an example of how the Interferometry enlarged the scope of separation after its first steps.

In 1951, the South African astronomer William Stephen Finsen (28 July 1905 – 16 May 1979) developed an ocular interferometer which allowed measuring closed binary systems (Finsen, 1964b, 1971). This pioneer of interferometric observation of binary systems discovered 73 new systems from 1954.

His tool (II.6) consisted in a collimator and interferometer composed of slits, possible to be mounted on any telescope. The results of his observations attracted the attention of the observers of his period; van den Bos himself analyzed the results in 1953, comparing the measures with other ones obtained with micrometers or by means of known orbits (van den Bos, 1953). In his study, van den Bos affirms that the results obtained by Finsen have a high quality and scientific value thanks to his tool.

FIGURE II.6: From W. S. Finsen, An Eyepiece interferometer

The following great innovation corresponds to the intensity interferometer: first, in the field of radio astronomy (Brown and Twiss, 1954; Jennison and Das Gupta, 1953), then, in the optical field (Brown and Twiss, 1957). This system measures the fluctuations in the intensity recorded by two different telescopes. The resistance of the system to atmospheric scintillation is one of its most outstanding features.

The greatest part of these first interferometers was not widely used because of being considered hard to manage and because of the magnitude limits possible to observe. However, the gradual improvement of the optical components, the electronic elements and the appearance of computation provoked a spectacular progress during the following decades.

One of the decisive steps forward was the invention of the Speckle Interferometry (SI, I.3.2) by Labeyrie (1970) and its application in the observation with telescopes from the earthly surface. The name of speckle derives from grainy structures, observed when a laser is reflected by a diffusing surface. Based on the prior work by Texereau (1962), Labeyrie warns that in case of working with large telescopes, the image of stars form a pattern similar to these speckles. Applying the analysis of Fourier and the theory of diffraction, he develops a procedure permitting the recovery of intensity and the spatial information to some extent. This technique allows him to reach the limit of resolution of big telescopes.

One of the main characteristics of the Speckle Interferometry is its employment of sequences

of pictures obtained from exposures of milliseconds range. It brought an end to exposures of several seconds, applied before. Besides, it requires magnification and prisms which would amend the atmospheric dispersion, something not very common in that period either. Labeyrie presents these features as the reason why these grainy structures are not commonly observed and widely known in the field of astronomical studies, although he states that they can be visually remarked in some occasions, when observing stars with lens.

The Speckle Interferometry was used almost immediately for the study of double stars by different research groups: among them, Special Astrophysical Observatory of Russia (SAO) and, especially, the Center for High Angular Resolution Astronomy (CHARA) where Harold A. McAlister managed to split a significant quantity of spectroscopic binaries.

Most modern optical interferometers preserve the design by Michelson, employing as external mirror several complete optical telescopes, such as the VLT which combines 4 telescopes of 8.2 m and four of 1.8 m. In the contemporary literature, it is usual to refer to this kind of optical systems or to multiple radio antenna systems which combine different baseline lengths to resolve celestial objects, like interferometers, disregarding the designs that require one telescope only, as in Finsen's case. It is worth pointing out the relatively modest magnitude limit of multi-aperture interferometry when compared with single-aperture interferometry (i.e., speckle).

However, we are interested within the framework of the present thesis in the interferometry systems used on one single telescope.The Speckle Interferometry, that this work is focused on, is an observational technique permitting to reach for the limit of resolution of the mentioned type of singular telescopes.

One of the main reasons for the use of interferometers composed from many telescopes is the observational limitation supposed in observations with a single mirror. The Table II.1 exposes the limits of observation marked by Rayleigh's criteria for capacity of resolution depending on the diameter.

As we may see in II.1, in order to observe in the infrared and to get a resolution of 0"24, we would need a telescope with a diameter of ~10 m, which is actually impossible to build using one mirror only. Nevertheless, the results that we can get within visible light, with telescopes of 2 m, 4 m, 6 m and 8 m, are still quite interesting and useful. This is where the role of the Speckle Interferometry becomes significant. This technique, either accompanied with AO or in the absence thereof, allows reaching for separation limits permitted by the telescope's diameter. It gives the possibility to detect closed double stars that are the ones that present faster orbital motions. If we are able to separate these close light sources we will be able to determine their position and even to calculate the difference of magnitude between both of them. This technique allows taking advantage of old telescopes from 2 m to 6 m, in a relatively low-cost way, in the same form as in case of installation on a state-of-the-art telescope of 8 m class. Its development was fundamentally conditioned by the evolution of the CCD technology until the last generation's eMCCD detectors.

TABLE II.1: Resolution limits

Telescope		Angular Resolution		
		Visible		Infrared
Single	Size	$\lambda = 500nm$	$\lambda = 800nm$	$\lambda = 10\mu m$
Amateur	0.5 m	0”252	0”403	5”
BAO	2.6 m	0”0484	0”077	0”968
SOAR	4.1 m	0”031	0”049	0”614
SAO	6 m	0”021	0”033	0”419
Gemini	8.1 m	0”0155	0”0248	0”311
Multiple				
GTC	10.4 m	0”0121	0”019	0”242
MACE	21 m	0”006	0”0096	0”12
ELT	39 m	0”0032	0”0052	0”0645

Below, we present in detail the most important aspects of CCDs, ICCDs, and eMCCDs cameras. Finally, the eMCCD PhotonMAX 512B used by OARMA for Speckle Interferometry observations.

II.3 CCDs

The charge-coupled devices or CCDs are fundamental elements in modern astronomy. The main reason thereof is their faculty to offer a reaction in the form of practically linear electrons to the captured light, as well as their quantum efficiency, higher than 80% for several decades in case of the greatest part of the visible spectrum. Currently, some detectors approach almost 100% in some areas of the spectrum. This supposed a radical difference with respect to the photographic materials, plates [placas] and films used earlier. But there is even more: when maintained at low temperature, they generate very little readout noise while they can reach big sizes, that is: afford many pixels or picture elements.

It is worth remarking a certain language ambiguity, rather common and which may lead to confusions. By definition, a pixel is the minimal element of a picture. So the pixel represents the intensity-position pair. This pair corresponds to the intensity detected by a physical element called photodetector and located in a certain position inside of the CCD. The CCDs are usually matrix-configured, therefore, a row and a column correspond to every photodetector in the matrix of photodetectors, configuring altogether the CCD. As a rule, the

matrix position of every photodetector is preserved in the final image. The intensity results from the readout of detected photons and their conversion into analogous units or ADUs. The language abuse consists in employing "pixel" both to define this intensity-position pair, i.e. the minimal element of an image, and to refer to the physical place where the signal is captured, i.e. the photodetector.

The CCDs are based on a photoelectric effect. When the light falls on a CCD, its silicon substrate absorbs some proportion of the photons from its structure, and a (photo-)electron is released per photon absorbed. Therefore, the quantity of the electrons produced is proportional to the quantity of the light received. The ratio between the photons received and the electrons generated is known as the detector's quantum efficiency. The electrons released are captured thanks to positive voltage which attracts them towards an electrode, maintaining them inside of a potential well due to the SiO isolator, hindering the release thereof.

A CCD, in fact, is a chain of gate electrodes, each one storing electric charge. Every cell or photosite consists from three gates. When the exposure is over, the charges accumulated in every potential well are transported thanks to the alternative application of positive potential to consecutive gates, so that the charge is moving around, that is: the same gates used for the collection of charges are used now for the transportation process. This process is known as clocking. There is an exit gate in the end of the line, as well as a charge amplifier, meant to convert the charge into voltage, i.e. in analogous signal. And finally, the voltage passes through a unit which converts the analogous signal in digital one (ADU), as a result of which we get the entire final value of the intensity in the given location of the cell or, putting it with the language abuse we referred to, the intensity of pixel.

A usual A/D converter employs 16-bits to convert the analogous signal into digital one. As the CCDs convert photons into electrons, it would be meaningless to talk about negative values for the signal to be converted, so there is no need to specify the sign. This is why the range of the resulted values varies between 0 and $2^{16} - 1 = 65,535$. As a rule, the intensity of a pixel is not equal to the quantity of the detected electrons, but they are related through the gain (inverse): this factor is defined as the ADUs inverse, allocated to $1e^-$ detected,

$$\mathcal{G} = \frac{e^-}{ADU}. \tag{II.5}$$

In the ideal case, when multiplying the pixel's intensity by the gain, we should get the number of the electrons received; however, the reality is rather different as we need to take into account the availability of numerous noises, affecting this factor.

For instance, the conversion of photo-electrons into voltage introduces an additive noise, called readout noise, because the intensity values obtained for every pixel are located in accordance with a Gaussian distribution around the real quantity of the electrons captured. This is one of the main problems when reaching to very high readout speeds, i.e. higher than

10Hz. Such high speeds lead to pixel readout ratios of several Mhz in case of a relatively big CCD. R. N. Tubbs quotes in his Ph.D. thesis thesis readout noises of 50-69 electrons equal to 5.5MHz for a CCD of the period of T. D. Staley 2014 [1].

II.3.1 Basic Aspects for the Calibration of a CCD

In order to fulfill the calibration of a CCD, we shall take a series of calibration images, some of them, in the absence of incident light, i.e. with a closed shutter and/or an optical path of signal, which will let us calibrate the internal problems of the detector, and others, called flats, aimed at ensuring a maximally uniform illumination of the detector and showing the detector's reaction to the light. Usually, we take a lot of calibration images from every type which are combined, using the average or the median, in a single "median" image, after which they are deducted or divided, depending on the case, into the image that we obtained from the object or the stellar field of interest. The different types of calibration images and the process of reduction where they are applied are described below.

- The calibration images taken in the absence of light and during the minimal exposure allowed by the camera or the shutter are called images of bias and they are applied to deduce the pedestal level of intensity or the bias pedestal.
- Depending on the intensity of the object or some of the objects that we would like to observe, our images subject to reduction will be taken with different exposures. In order to amend the dark current generated in the camera during the mentioned times, the pictures will be taken with each of the t_{exp} applied in the scientific observations, but in the absence of light. This kind of images are called darks.
- The flat images are going to show us the reaction of pixels to the light and linearity or, in the absence thereof, between pixel and pixel. In order to obtain them, the camera shall receive uniform illumination. After the calculation of their average or median, they are normalized, so they do not depend extremely on the exposure, although in general, as in case of darks, we shall use the ones that share the t_{exp} with the images that we are planning to reduce. The flats depend on the wavelength, so we must take flats for each band of the spectrum where we plan to observe or where we have observed.

As told before, the common practice is to take various observations of every type and combine them, usually using the median to create "median" images and apply them in reductions. According to a common language abuse, the images obtained and the medians are called the same way, e.g. the median images of many of these pictures are called bias. In order to avoid confusion, we have opted to call maps those resulted from the calculation of the average or median images of many other pictures and used for the reduction, and bias, darks or flats, depending on the case, those obtained with the camera and not subjected to any other process.

[1] both PhD Thesis are not in adsabs.

The process of reduction is summed up in the following equation (Howell, 2000):

$$IRO = \frac{IAO \times MB \times MCO}{MFN}, \tag{II.6}$$

where IRO is the Image Reduced of the Object, IAO is the Image Acquired of the Object, MB is the Map of Bias, MCO is the Map of Dark Current, and MFN is the Map of Flat Normalized. Let us see below how this process eliminates the noises available in the images obtained with CCDs.

The process of readout which converts the charge into voltage ensures at the same time that all the pixels acquired are positive and, therefore, digitised. As we mentioned in the end of Section II.3, this readout implies a noise related to the Gaussian nature, which we call readout noise. Even in the absence of light and in minimal periods of exposure, this noise causes a mismatch which makes the image adopt values different from zero in case of some percentage of pixels. This positive mismatch is called bias pedestal. The map of bias is seeking to show us the average variation of the mentioned pedestal from pixel to pixel and to correct it when we deduct it in order to clean the image acquired of the object.

The longer our exposure time, the more events of thermal character will be added to the true photonic events. This thermal noise cannot be corrected before the processes of conversion into analogous signal and later into ADUs, that is why it is handled just as the true photonic events during the process of readout and conversion. Obviously, it alters the final values of intensity and, as a consequence, the gain. The map of dark current is meant to amend the intensity of the signal produced by the thermal emissions coming from the CCD and other close electronic components for a certain exposure period.

Summarizing, the bias are obtained with short exposures in order to minimize the contribution of the thermal emissions, meanwhile the darks, in general, are taken with the same exposure as the one employed to take the images of objects, because their objective is to represent the thermal noise accumulated after a certain period of time. Both types of images are taken with no light, either by hindering its access to the detector or leaving specific zones in the margins of the detector with no illumination. These zones are called “offsets”.

Considering that images of the necessary calibration are not available, there are procedures allowing the deduction of the map of bias on the basis of the darks, taken with different exposures, and another one to extrapolate the bias to zero when our camera or shutter do not allow really short exposures, e.g., based on a succession of maps of bias with different short times of exposure we can study how the pedestal decreases as the time is decreasing and build with this information a map of bias with zero exposure.

The images of flats require uniform illumination. It can be ensured in different ways: by means of images from the telescope dome illuminated uniformly; by means of specific illumination systems placed above the telescope; or, in the most classic version, taking images of the sky at dusk and dawn, where there is no trail of the Sun on the horizon line, moments called

"blue hours" in astronomy. The maps of flat or flats serve to calculate the sensitivity of the camera before different quantities of incident light and also reveal the presence of external factors altering the mentioned sensitivity, like partial darkening due to dust on the lens. As we are interested in the relation of pixel to pixel and not in the intensity thereof, they have been always applied after being normalized usually by their average and not by their median.

Another extended use is that of superflats and superdarks: these are built with a great number of images of darks or flats, respectively, taken at different times of the observation campaigns. They provide a global average assessment of the effects that we want to amend and they offer the advantage of being simpler to program when planning an observation campaign. Besides, the use of these "general" images saves our time during the reduction, as we do not have to select images of calibration closer in time to the observation we want to reduce. Such differences of speed get appreciable when dealing with a great quantity of data.

Another common correction that may be demanded by our system is the calibration implemented by the shutter's map, realized in two phases: the first phase is the correction for the shutter's effects. This correction is especially important for the photometry in short exposures and very necessary when our shutter partially darkens the images with its movement. As long as there is a shutter in our optical configuration, this correction will improve the rms of the curves of light obtained. It is carried out as follows:

$$ICO = \frac{IAO \times t_{exp}}{MO + t_{exp}}, \tag{II.7}$$

where ICO is the Image Corrected of the Object, IAO is the Image Acquired of the Object, MO stands for Map of Shutter and t_{exp} is the exposure.

The second phase is the already-known equation cited above, meant to reduce the thermal noises and the lack for linearity in the reaction to the light:

$$IRO = \frac{ICO \times MB \times MCO}{MFN}, \tag{II.8}$$

where IRO stands for the Image Reduced of the Object, ICO is the Image Corrected of the Object via the map of shutter, MB stands for Map of Bias, MCO is the Map of the Dark Current, and MFN, the Map of Normalized Flat.

All these calibration images that we described will remain adequate during certain time lapses, usually short ones. The changes of the outside temperature may alter both the bias and the accumulated thermal noises, so we have a range of hours or days. The quantities of dust on the lens is slowly accumulating, causing a continuous deterioration until they are cleaned, changing drastically every moment. The stains with an animal origin are also common on the optical elements, having a completely discreet character. The only exception

are the superdarks and superflats which may be a good model for a long term, even though they must be inevitably revised and recalculated at a certain moment too.

The OARMA team carried out different campaigns observing relatively wide binaries using CCDs cameras mounted on Calar Alto 1,23 and 1,52 m. telescopes. The results have been published in different astronomical journals (Abad, Docobo, and della Prugna, 1998; Abad et al., 2004; Docobo et al., 2000a).

II.4 ICCDs

A last generation ICCD camera is based on the combination of a high-performance CCD camera and an intensifier of image, located between the access of the light and the CCD itself.

Based on the photons received, the intensifier generates electrons which are later amplified and turned into photons again. The first conversion "from photon to electron" is fulfilled via a photocathode which releases electrons thanks to the photoelectric effect produced when the photons hit its surface. The photocathode is built in a manner that makes the electrons be released on the opposite side to where the light is received. Then the generated electrons move faster in the microchannel plate (MCP), where a process called secondary cascaded emission is produced. The MCP is a plane plate which is usually made from resistant materials and is about 2 mm thick. It is composed from microchannels which form a dense array of parallel small tubes or slots, put across the plate from one front to another, and separated from each other by a distance of some 15 micrometers. The diameter of each such tube is about 10 micrometers, coming up to 6 micrometers in MCPs of high resolution. The plate is normally placed in a leaning position, or the tubes present an inclination of about 8° between two fronts, with respect to the normal inclination. This inclination provokes the production of more electrons per each electron impacting the surface at the plate access.

Every electron that hits the MCP releases numerous electrons which move towards a fluorescent screen of high voltage, which carried out the conversion from electron into photon. These photons released are issued towards the CCD. The vacuum in the tube and the big differential of voltage in this first part of the tube makes the electrons move straight between the photocathode and the MCP. It preserves the collimation of light. Thousands of new electrons are issued per every electron hitting the MCP, fastened again by the difference of potential, although smaller than the previous one, between the MCP and the fluorescent screen. The fluorescent releases a photon per each electron it receives.

The multiplication capacity of these tools lets them capture images under extremely low-light conditions, within exposure times slower than 200 ps. Therefore, the total flow detected by the exposure is very small. It becomes possible due to the fact that the so-called gating is allowed precisely by the intensifier.

Gating is one of the differential features of these cameras as compared to CCDs and eMCCDs. In the "gate on" state, the entering light is intensified and converted into photons. In the "gate off" state, the light is not transmitted to the CCD. That is: the gating fulfills the function of a shutter, integrated inside of the ICCDs. The ICCDs make it possible in the scale of picoseconds. The operation of the gating consists in reversing the potential between the photocathode and the anode located at the height of the MCP by means of a high-intensity voltage signal having the form of a square wave. The size of this square wave determines the gate time, which is equivalent to the shutter speed. In case of no voltage, the door remains closed and, therefore, the electrons generated by the photocathode are held inside of it. When applying the appropriate voltage in the form of a square wave, the MCP receives the electrons during the difference of time between the moment when the wavefront arrives in the anode and the moment when its tail does.

This ability of gating in the range of picoseconds widely exceeds the capacities of the frame transfer technology, typical of eMCCDs and some CCDs, which deals with the range of few milliseconds. It makes these cameras ideal for achieving ultra-high speed imaging. Such a speed is necessary, for example, to observe the wavefront in combustions or explosions. The capacity of setting the opening time, for instance, the start of a process, also permits to measure the events with high accuracy, based on the synchronization with the camera.

These instruments kept constantly developing since their operation was suggested by G. Holst and H. De Boer in 1928. The major part of the evolution was accompanied by their military use, mainly meant for the night vision. Actually the greatest part of the models in use belongs to the third generation or version.

II.4.1 ICCD Camera of the OARMA

As already discussed in the Introduction , the OARMA's predilection for the SI started thanks to the decision of J. A. Docobo made in the beginning of the 90-s. He established the first contacts with McAlister, trying to obtain a speckle camera, but the prices he found were prohibitive for OARMA at that moment.

Using the economical advantages provided by the general program to commemorate the University of Santiago de Compostela's 500th year in 1995–1996, the Prof. Docobo organized a international meeting which gathered the most important researchers at world level of Celestial Mechanics and Double Stars. The International Workshop VISUAL DOUBLE STARS, FORMATION, DYNAMICS, AND EVOLUTIONARY TRACKS by AORMA in 1996 (Figure 5) allowed also to establish a cooperation agreement with Yuri Y. Balega, Director of the SAO until recently, between another scientifical contacts. Thanks to the funds supplied by the Xunta de Galicia (Regional Government of Galicia) during the call for research grants of the Research Infrastructure of the General Secretary of I+D in 1998, the OARMA was able to acquire its first speckle camera from SAO. The camera arrived

in Santiago de Compostela in 1999 and performed almost immediately its first observation campaign on the telescope of 1.52 m placed in the Observation Station at Calar Alto. The following campaigns were carried out in June 2000 and in July 2001. The first results were published in Docobo et al. (2001, 2004, 2008).

The totality of parts making up the camera, its mounting and handling are summed up below, although back in 2002, the Prof. Docobo suggested and directed a Bachelor Degree final report: "The ICCD camera of OARMA". It was developed and presented in details in the Bachelor Dissertation in Mathematics at Ms María Teresa Costado Dios. The mentioned document is available at the library of the OARMA.

The different components of the camera are described below.

Black Box and guiding camera

The light coming from a star reaches for the primary mirror of the telescope disturbed by the atmosphere. Then it passes to the secondary mirror in order to be focused. Afterwards, it enters the so-called Black Box of the camera.

As soon as the light enters this first part of the camera, it finds the mirror or an additional elbow which, being in a certain position, should take the light towards a guide camera settled in a fixed manner, lateral and exterior to the Black Box. This guide camera registers the image and send it to a TV monitor, used to visualize the observed field and to proceed with centre the object. Once the object is centered, the elbow moves and the light should no longer reach for the guide camera, continuing its way into the ICCD camera.

Still in the Black Box, the light shall pass first through an electronic shutter of distant control, synchronized with the CCD. This shutter is in charge of setting the exposure time between 5 and 40 ms. For this purpose, it lets the light pass during these exposures and hinders it from passing between capture and capture, which is known as readout time. It is worth having it closed while localizing the star.

Then it is the turn of the microscopic lenses, applied to magnify the image observed. The idea is to employ an increase which would guarantee a sufficient sampling, in accordance with the theorem of Nyquist-Shannon. For that purpose, the camera possesses two interchangeable lenses of 8 and 20 magnifications. In general, that of 8 is used to center the image again, so that its position in this field is adjusted to the center of the field of the lens of 20 magnifications.

Intensifier

The intensifier provides an intensified image until a certain value, so that the readout noise of the CCD could be considered insignificant. The entrance photocathode is 24 mm thick and

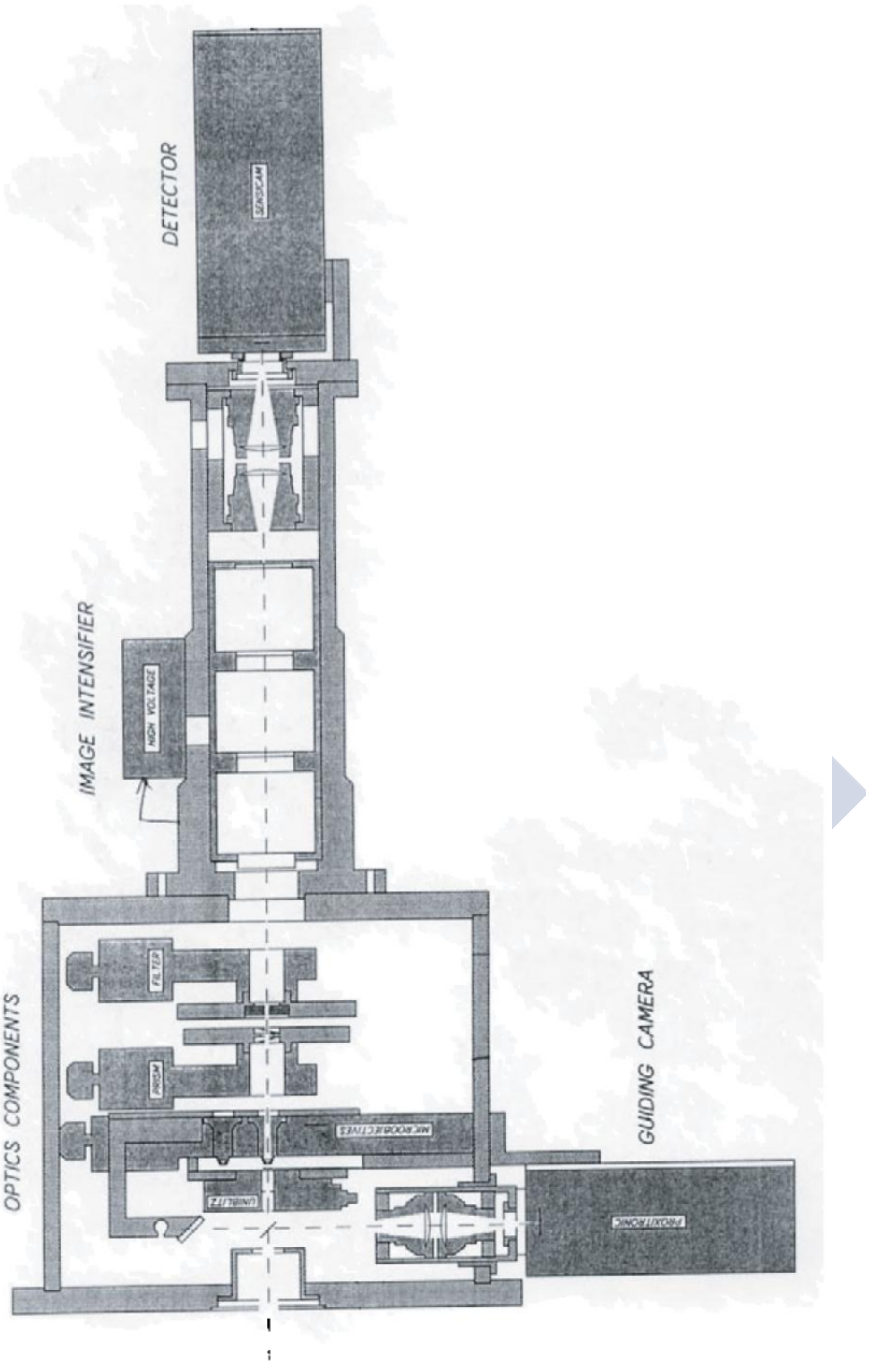

FIGURE II.7: Design of the OARMA's ICCD camera

has a spectral reaction S-25 with a top of sensitivity of 12% at 510 nm and 2% at 800 nm. Its employability depends on its capacity to keep the vacuum inside. The light is converted into current in this vacuum, gets intensified and then is converted into light again. There are two ranges outside: the aperture of diaphragm through which the light passes to make a focus on the CCD, and the focus which shall vary solely when an extreme change of temperature is produced.

Description of Sensicam detector

Sensicam is the CCD detector used by this camera. It was made by PCO Computer Optics (Germany) and it consists from 1280×1024 pixels of 6.7×6.7 μm. It is connected to the image intensifier by means of a couple of lenses with a transfer of f/1.5. The scale is from 0”028 or 0”011 per pixel, with a total field of 5”6 and 14”3, respectively.

Secondary parts

The CCD has its own source of supply, established when installing the tool on a lateral side of the Black Box. The MPS or Motor Power Supply is a box which permits to control the optical part of the camera, that is: the filter wheel, the diaphragms and the pair of magnifiers situated in the Black Box. It counts with four controllers, one from which is supporting, used in case any from the remaining three fails. Its operation is controlled by Mps-Prisma program.

The Distribution Unity (DU) controls the Intensifier and the Sensicam. It is connected to the telescope and the Control Unit (CU) via optical fiber. The CU is established in the telescope’s control room from where the observations are made. It is in charge of controlling the CCD and it gives the possibility to adjust the exposure time, the shutter, as well as to activate the intensification process.

Three monitors are needed in order to continue the observations: one of them is used to manage the programs responsible for the camera control, the second one is a video monitor, reflecting the images supplied by the guide camera, and the third one corresponds to the telescope and serves to control its movement.

Two pairs of cables of optical fiber are required to complete the mounting of the ICCD. The first pair is connected to the Sensicam’s control card, installed on the main computer. The second pair connects the DU and CU.

Besides, there shall be a base or an adapter piece built for every telescope, functioning as a stand for coupling with the telescope.

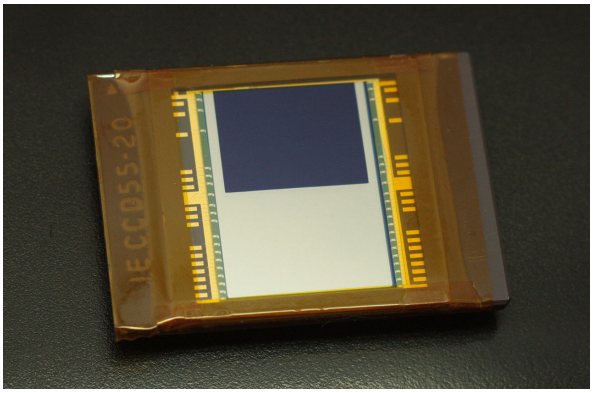

FIGURE II.8: A frame transfer CCD system
Credit: Olli Niemitalo under CC0 1.0

II.5 eMCCDs

The eMCCDs offer a solution to the main problem represented by ordinary CCDs, i.e. they allow achieving a great sensitivity at high readout speeds or short exposure times.

On the one hand, the structure of the CCD applied most of all consists from two parts. The first part is the sensor which captures the image during the acquisition process. Besides, in case of an ordinary CCD, this is where the charge is stored before the readout. Meanwhile the eMCCDs are provided with a specific storage area where the image is transferred and over which the process of readout is produced (Figure II.8). Both areas have usually the same size for obvious reasons, but the storage area in the eMCCDs is covered with an opaque plate, normally made of aluminium, acting like an electronic shutter. While the readout process is implemented over the storage area, the sensor is being exposed once again to the light, collecting information for a new image. This design also serves to increase the speed at which we can take images.

Besides, in case of the eMCCDs, the charge moves across a serial register of many cells before the charge amplifier (producing the analog signal), where it undergoes a signal amplification process which we shall call either multiplication or gain. This increase of the quantity of cells through which the charge is transferred seeks to amplify the noise, generated in a natural way in all the processes of charge transfer or clocking. The mentioned noise is known as spurious charge or Clock-Induced Charge (CIC). Prior to the eMCCD technology, the CIC was considered a noise which should be neutralized or at least amended. However, in case of eMCCD cameras, we take profit of this noise.

The charge clocking implies a minor probability of generating additional charge due to the process called impact ionization. The impact ionization happens when the charge has got enough energy to create another electron-hole in the register of multiplication or gain, i.e. the side of cells through which it is guided towards readout (Figure II.9). Therefore, every

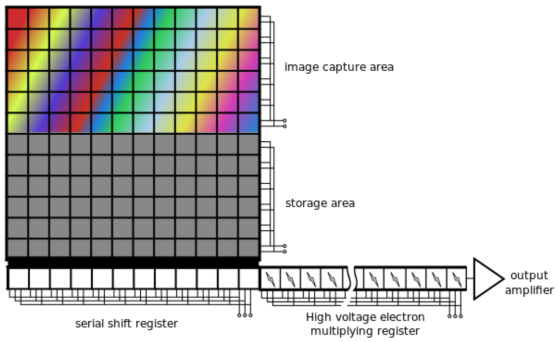

FIGURE II.9: Electrons are transferred serially through the gain stages making up the multiplication register of an eMCCD
The high voltages used induce the creation of additional charge carriers through impact ionization
Credit: Jsanchezd under CC BY-SA 3.0

time a charge is transferred, it is possible to produce an extremely slight amplification in a natural way. In order to take advantage of this effect, the eMCCDs intend to strengthen the impact ionization. In order to increase the probability of such ionization, the charge moves at a larger voltage which provides more energy and facilitates the process of creation of a new pair of electron and hole. Besides, as stated above, the eMCCDs are designed to contain hundreds of cells where the ionization process can take place, so in spite of a small probability inside of a cell, it gets very high by passing through hundreds of cells, and thousands of gain electrons can be achieved. As the probability of multiplying the charge varies according to the temperature in an inversely proportional way, causing a larger probability at lower temperaturas, the eMCCDs are usually cooled in order to reach temperatures lower than $-70°$.

Adjusting the temperature and the voltage applied to the sensor of the eMCCDs, it is possible to obtain gains ranging from a unit (~20V) to thousands (25-50V). In general, we are interested in adjusting it to make it several times larger than the average variation of the readout noise. As a result of the whole process, when we take images at very high readout speeds employing an eMCCD to amplify the signal, the readout noise keeps equivalent to the signal of a photoelectron multiplied some 10 or 20 times, as in a normal CCD, but the signal received is being multiplied in the form of electrons at the factor of 1000 or 2000, significantly increasing the S/N.

II.5.1 Basic Aspects for Calibration of an eMCCD

The eMCCDs are essentially a type of CCD, so the noises described above are also present in the images obtained with these devices. That is why the basic aspects of calibration of an

eMCCD follow the same criteria and processes as those presented above in II.3.1.

It is worth specifying that the absence of shutter in the eMCCDs conditions the lack of necessity to realize that part of the process. Besides, some programs of observation with eMCCD in Speckle Interferometry do not carry out the corrections needed to amend the lack of linearity between pixels, that is: the corrections per map of flats. This is conditioned by the fact that the actual Andor cameras' reaction to the light does not oblige this type of correction.

Nevertheless, as a general rule, the cameras of the previous generations, as in case of Photon MAX 512 of the Princeton Instruments owned by AORMA that we applied during our observation campaigns, require a correction per map of flats for its reduction. In our case, certain peculiarities in the design of detector provoke an overload in the readout area, reflected in the form of the Power Spectrum, and therefore affecting all the images that we could take. When reducing the map of darks, we partially resolve the mentioned defect, but even so, the results will be more appropriate if we carry out reduction per flats in addition.

The following section describes in details the specific sources of noise presented by eMCCDs and how to correct them.

II.5.2 Specific Aspects for Calibration of an eMCCD

In order to ensure a correct calibration of eMCCD, it is necessary to take into account not only all the previous factors, but also other noises like those produced by the CIC due to the high speed of acquisition and the register of multiplication. Both spatial and temporal variations produced in the observations with eMCCDs must be corrected image by image before any other type of joint reductions. The reason are the effects of the electrons multiplication or gain, as they determine for us the level of pedestal which ensures that the photonic events crossing the threshold are not uniform, in case we want to apply the technique of photon counting based on a threshold. Certain algorithms, like the so-called drizzle, combine values of different pixels, assigning them equal weights as a basis, which will result in the loss of information both in the signal and in the noise if these effects typical to eMCCD are not corrected.

T. D. Staley (2014) cites the PhD thesis of Law (2007) [2], indicating that there are methods based on the analysis of the histogram of certain images of calibration for calculating the gain of the camera. His work is focused on the use of eMCCDs for Lucky Imaging (I.3.3), but the mentioned method is equally valid for Speckle Interferometry (I.3.2) and, in general, for any image taken with an eMCCD. Before proceeding with the explanation, we shall talk about the models of probability distribution applied in eMCCDs.

[2] both available on ArXiv.org

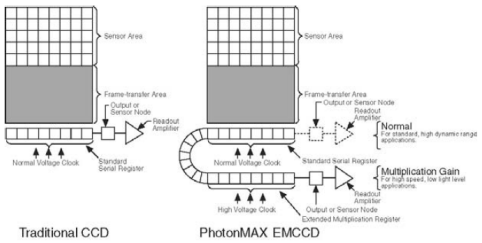

FIGURE II.10: Comparison of traditional CCD and PhotonMAX eMCCD Array Structures

Models of Probability Distribution for eMCCDs

The process of an eMCCD's signal multiplication has a stochastic character and introduces a new source of noise; besides, the high speeds of collection make us have to analyze usually several hundreds or thousands of images per object of interest, obtained in a very short period. It lets us get farther than with CCDs and not only apply some images coming from the measurement of others but also to model the distributions in value of pixels, altering the parameters of the model in order to adapt to the complete histogram of the pixel values obtained. A simple model consists from two parts: one of them molds the stochastic character of the gain process and the second part adds readout noise of Gaussian nature.

Before proceeding, let us introduce the notation presented by Tulloch and Dhillon (2011). The "avalanche multiplication gain" or electron-multiplying gain will be represented by g_A, a dimensionless factor that measures the multiplication between the electrons entering in a series in the register and the electrons leaving it. They use a subscript to distinguish it from the conventional gain of the system applied in the CCDs and denoted with $\mathcal{G}$. The system's gain reflects the quantity of photoelectrons that every ADU represents and, therefore, its units are $\frac{e^-}{ADU}$. They also introduce the term g_0 which denotes the ratio between the electrons accessing the readout process and the ADUs of the output.

An approach of the probability distribution of the exit signal $p(x)$ is offered by (Basden, Haniff, and Mackay, 2003; Matsuo, Teich, and Saleh, 1985) in case of the access signal with n photons where $n \lesssim 15$ and a long enough multiplication register:

$$p(x) = \frac{x^{n-1} \exp(\frac{-x}{g_A})}{g_A^n (n-1)!}. \tag{II.9}$$

Therefore, the average of the exit signal is ng_A and the variance, ng^2. When the photon flow increases, the exit's probability distribution is molded better with a normal distribution having the same average and standard deviation. The variance in the distribution introduces an extra noise in the exit signal, above the photon noise, which follows Poisson's distribution.

The ratio between the signal and the exit's final noise (SNR) in the absence of the readout noise but with photonic noise equals:

$$SNR = \frac{ng_A}{(ng_A^2 + (n^{\frac{1}{2}}g)^2)^{\frac{1}{2}}} = \frac{n^{\frac{1}{2}}}{2^{\frac{1}{2}}}. \tag{II.10}$$

That is: the process of gain introduces an extra factor of $\sqrt{2}$ in the noise of measurements, as compared to an ideal photon-counting device.

In case of an access limited to a simple photon, the exit of the electron-multiplying process becomes a curve with exponential decline. When subjecting the camera to low levels of charge where the probability of registering two or less photons per pixel is insignificant, it is possible to consider a distribution with two components, representing the cases when pixels have registered 1 or 0 photoelectrons. If we assume that the readout and multiplication are zero when the pixel does not capture any electron, then the exit probability distribution will be defined as $f(x)$ where:

$$f(x) = \begin{cases} 0 & si \quad x < 1, \\ \frac{\exp^{(\frac{-x}{g_A})}}{g_A} & si \quad x \geq 1. \end{cases} \tag{II.11}$$

So we expect the histogram of pixel values to be similar to the following distribution:

$$P(x) = P(N_{phot} = 0) \times \frac{1}{r}\phi(\frac{x-b}{r}) + P(N_{phot} = 1) \times \left[f(x-b) * \frac{1}{r}\phi(\frac{x-b}{r}) \right], \tag{II.12}$$

where ϕ is the normal distribution, r stands for the standard deviation of the readout noise, b is the bias pedestal, and $*$ represents the convolution. As stated above, this equation is the sum of the distribution of readout noise representing the pixels which have not captured photo-electrons, and an exponential distribution per pixels which detected a photon, both in convolution with the Gaussian readout noise.

When adjusting the histogram of an image of a real dark to this model, we see that the model and reality are similar in the greatest part of the intensity ranges, except the elbow of the curve where the model is beneath the curve. This excess of values of low intensity is due to the CIC, not molded yet.

The CIC can be divided in two phases. On the one hand, there are electrons generated by the charge along the CCD before it passes through the register of gain. We shall call it transit CIC. These electrons cannot be distinguished from those generated by photon events.

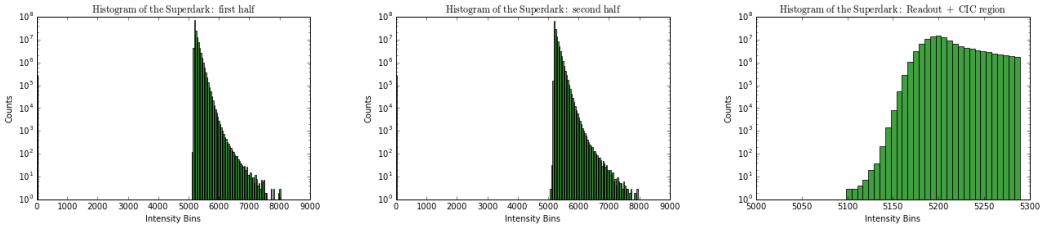

FIGURE II.11: BAO's May-June 2017 superdark histogram

Generated before the gain register, they undergo the same process of multiplication as the photo-electrons of the detected signal. In case of necessity to correct them, we can use images of bias and subtract them from the images of interest. This is carried out when a real estimator of the sky depths is required, which is not usually necessary for the SI but may be needed for the LI.

On the other hand, there are electrons generated when the charge passes through the register of electro-multiplication. The greatest part of these electrons records a smaller gain than the electrons coming from the CCD, because, depending on the register's height, they pass through more or less phases of gain. We shall call them CICIR, standing for CIC in the register. They are responsible for the lack of adjustment between the model histogram and the one obtained with real data. A form of molding their distribution is to assume that they have the same occurrence probability in any gain phase. So the distribution is just the superposition of different curves of exponential decline, each of them representing a different access of electrons passing across a different number of amplification phases, and therefore, undergoing a different gain average. The average contribution to the signal of one of these events would be smaller than that of a photo-electron according to the factor $\frac{1}{\ln(g_A)}$ (Tulloch and Dhillon, 2011).

II.5.3 The OARMA's eMCCD Camera

During the consecutive years after the International Workshop VISUAL DOUBLE STARS, FORMATION, DYNAMICS, AND EVOLUTIONARY TRACKS of 1996, the collaboration with the SAO strengthened in several areas. In particular, permission for observation with the telescope of 6 m for some period was applied for and obtained. Thanks to this period, observation campaigns in Speckle Interferometry were fulfilled, focused on the study of binary stars. The graduate Jose Blanco, co-worker of AORMA, had a stay in the Russian center. Several joint articles were published as a result of this scientific collaboration and the observations obtained.

The OARMA's suggestion to the SAO to prepare and sell an eMCCD camera, twin of the one used by themselves (Maksimov et al., 2009), was accepted. Thus the Observatory of

Santiago achieved an observation tool which would permit to obtain not only binary-related positions, but also the difference of magnitude between their components. This camera became possible to procure finally thanks to the funds supplied by different research projects of OARMA, granted by the Ministry of Education and the Xunta of Galicia.

The camera travelled to Santiago from Nizhny Arkhyz, in the valley of the Greater Zelenchuk River, where the scientific equipments and facilities of the SAO are situated, and it was installed for the first time on the OARMA's telescope of 0.62 m. J. A. Docobo clearly understood that its appropriate scientific performance could not be fully exploited on the urban telescope of the Observatory. After considering it with another frequent partner of OARMA, Professor Norair D. Melikian from Byurakan Astrophysical Observatory (BAO) of Armenia, they started communication in order to transport the camera to the mentioned center of observation where it could be mounted on a telescope of 2.6m.

In January 2010, the Professors H. A. Harutyunyan, Director of the BAO, and J. A. Docobo, Director of the OARMA, signed a cooperation agreement, envisaging the delivery, installation and exploitation of the OARMA's speckle camera connected to the BAO's telescope of 2.6m, appointing minimum one observation campaign per year during five years. The agreement was prolonged after its termination and it remains valid to the present.

The first installation of the camera in the BAO, despite being supervised by the engineer who designed it, A. F. Maksimov, failed for technical reasons. Afterwards, the telescope and the dome of the BAO went through a long period of scientific inactivity, while both were being fine-tuned. It made the start of the campaigns remain at a deadlock. Meanwhile, the SI kept fulfilling annual campaigns at the SAO, as the Time Allocation Comittee accepted the observation programs suggested from the OARMA.

We are proud to say that the first successful installation of this camera in the BAO was conditioned by our hard work between May and June 2016. During this period of approximately a month, I moved to the BAO, trying to instal the camera for the first time. The context was not the best possible. The decease of our dear A. A. Karapetyan, engineer of the BAO in charge of the maintenance of the camera and its components, who was at the same time the Center's representative who took part in the previous installation, helping the engineer who created the camera, A. F. Maksimov, provoked a loss of the know-how accumulated during the first trial. Besides, A. F. Maksimov was not able to move in this case to Armenia because he was recovering after a delicate surgery, so his availability was rather limited, including by telematic communication.

Nevertheless, after a month of works on different components of the camera, it became possible to reinstall correctly the software necessary to control the operation of the eMCCD, the optical mechanical unit, and the guide camera. It became possible also to test in the laboratory the operation of different optical-mechanical parts and the reaction of the camera to the light. Thus we verified that all the components remained in good conditions in spite of their inactivity. The installation on the telescope was delayed until October 2016, because

FIGURE II.12: PhotonMAX located over optical-mechanical cylinder

the last works on the telescope had suffered a small delay, and it was not yet available in June. It is necessary to express our deepest gratitude to D. A. Rastegaev for his commitment to travel to Armenia for a week in order to advise and help in the mentioned works.

The OARMA's eMCCD camera was designed to merge a speckle-oriented optical configuration (Figure II.20) together with a PhotonMax EMCCD detector from Princeton Instruments II.13). Its main components are described below.

Components

First of all we shall enumerate the physical parts from which the camera consists:

- PhotonMAX 512B: the camera has an entrance for the white cable coming from the Data Control Box and another one for the cable supplying energy. This cable is connected to a Power Supply of 100V/240V which shall be fixed on the telescope's structure and connected to a common supply source. Figure II.12.
- TV card: it is used in order to be able to see the image in real time, provided by the guide camera. It is installed inside of the computer, in one of the free slots. The guide camera is not used in the BAO so the installation of this card is not fundamental for the observations.
- Optical-Mechanical Cylinder (OMC): contains filters, microscopic lenses, Risley prisms and the elbow which leads the light to the guide camera. On its lateral side, there are the units of control: Data Control Box (DCB) and Optical Mechanical Control Box (OMCB), connected opposite to each other. Both boxes present a cable of supply which shall be connected to a common supply source. Fig. II.13.
- RS232: serves as a link between the OMCB and the computer. It converts the information arriving through the optical fiber into digital information, and viceversa. Steamoco software lets us manage all the components inside of the OMC from computer. Steamoco allows us implementing the following actions: move the filter wheel towards the selected filter in the interface, locate the prisms in the preferred positions

FIGURE II.13: PhotonMax and control units attached to the optical-mechanical cylinder

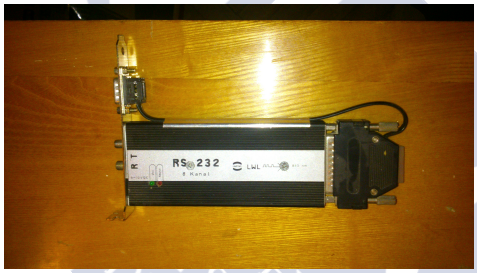

FIGURE II.14: RS232 adapted to receive the electricity directly from the computer. Notice the green and red LEDs

with respect to the separation of the indicated part with zenith, placing the elbow on the path of the light to deviate it towards the guide camera and/or to alternate the microscopic lenses according to our election. Fig. II.14.

- PCI card: it is installed on the computer. It receives information from the DCB and manages the acquisition processes of the camera, as well as the data it sends. PhotonMAX counts with proper software created in the ambient of WinSpec. When everything is correctly connected, WinSpec program recognizes the camera and lets us adjust its parameters (exposure time, gain, ...). Fig. II.15.
- Optical fiber cable: this is a long and thick cable with two black boxes in both ends from where other six shorter and narrower cables follow. One of them has a T-shaped mark which indicates that this end must be situated near the prime focus of the telescope. The second one does not have any mark on its surface and is situated inside of the control room, near the computer which will manage Steamoco and WinSpec programs. Six smaller cables deriving from both boxes have equal cable heads, two each one,

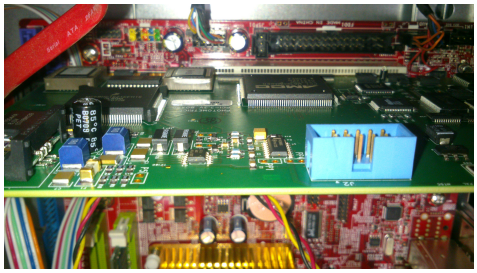

FIGURE II.15: PCI target connected to the motherboard

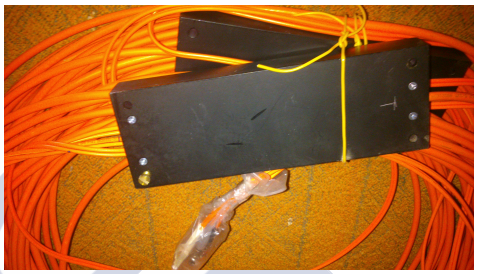

FIGURE II.16: Optical fiber cables and the black boxes that unite the six different heads: two are to be connected to the CDB, two to the OMCB, and two as possible substitutes in case of malfunction

in correlation from end to end. Only two couples from these are cables used, while one pair remains free. This pair exists like a replacement for other pairs in case of the failure of any of them. A pair goes from the DCB to the transponder and then the data travels to the PCI using another kind of wire. The second one communicates the OMCB with the RS232 which, as we said, is connected to the computer. Figures II.16 and II.17.

- Transponder: this is a small grey box, situated in the control room, near the black box with no marks on the end of the thick optical fiber cable. The transponder is connected to the pair of cables with the same head as those connected to the DCB. Its exit leads to the PCI via another cable. This cable has marks, indicating which end corresponds

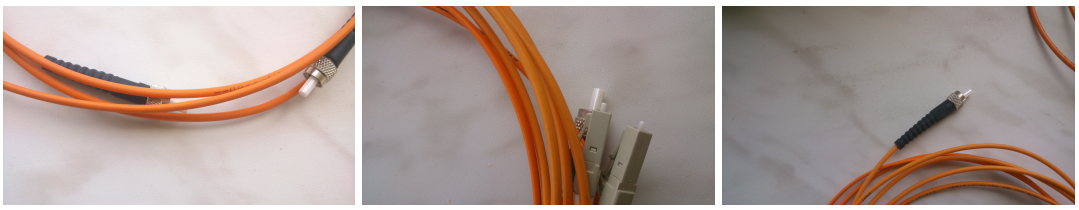

FIGURE II.17: The heads of the optical fiber cables: central image corresponds to the heads that connect to CDB and transponder and right one to the OMCB and RS232

FIGURE II.18: Transponder: orange wires correspond to the optical wires that come from the telescope while the grey wire goes to the RS232

FIGURE II.19: PhotonMAX 512

to the transponder and which one goes to the PCI. Figure II.18.

Description of PhotonMAX 512 Detector

PhotonMAX (Fig. II.19) camera is provided with the technology of on-chip multiplication gain which permits to multiply the signal produced by the photons detected by the CCD. The model of OARMA, PhotnMAX:512B is the first one from the series of Princeton Instruments.

The square detector has a 512 × 512, a pixel size of 16 × 16 μm, so an imaging area of 8.2 × 8.2 mm^2 is covered. The eMCCD pixel back-illuminated with dual amplifiers ensure optimal performance for applications that demand the highest sensitivity and for those requiring a combination of high quantum efficiency and dynamic range. His technical description assure more than 90% quantum efficiency and < $1e^-$ rms read noise. These features allow single photon sensitivity with sufficient multiplication gain. Deep thermoelectric cooling down to -70°C reduces the dark current below 0.01 $e^- s^{-1}$ per pixel. The cooler is integrated inside the PhotonMax. The camera can be operated at 10MhZ for high speed imaging or more slowly for high-precision photometry.

The operations of the camera are regulated by means of the PCI card which is located in the control computer, as indicated in II.5.3. These circuits receive data coming from computer and convert them into signals for the adjustment of different options of the camera. The controlling electronics also collect the analog signal from the CCD, digitalize it, and send it to the computer. It also allows to specify the read rate, binning parameters, and regions of interest.

The system is capable of acquiring and storing 16 bit digitized data at a frame rate of up to 20 fps at full resolution, with ~38 ms readout time per frame. Single photoelectron events are recorded with a signal-to-noise ratio of about 50.

We used the 10Mhz frequency operating readout in Frame Transfer mode and the Low Light option was selected in the controller gain. It sets the relation between the electrons acquired in the CCD and the ADUs generated. The highest multiplication gain value, 4095, were used mostly, except for a few bright objects. It implies a multiplication gain factor in excess of 1000x. Before each exposure the CCD is cleaned two times. No flip or rotation is being applied to the images. More information regarding all the possibilities that the PhotonMax offers in both standard application as normal CCD and in high speed low light level multiplication gain mode can be found in its manual.

Description of the Optical Mechanical Part

The main parts of the optical mechanical configuration of our camera may be observed in the Fig. II.20.

The part marked with 1 would correspond to the shutter which left removed in the definitive version of the camera because the eMCCD, thanks to the frame transfer technology, provides a more appropriate electronic “shutter” for observations with an exposure time in the range of miliseconds that we manage. Number 2 corresponds to the focal plane of the telescope and it is not a physical part of the camera. It can be adjusted by using the focusing capacity of the telescope itself where the camera is installed. The elbow leading the light to the guide camera should be at the height of the focal plane. Neither the guide camera nor the elbow is observed in the image, but its design is similar to that exploited for the same function in the Observatory’s ICCD (Figure II.7).

Number 3 marks two microscopes which permit to adjust the image formed in the prime focus to the detector’s pixel size. Our camera is provided with two Carl Zeiss lesses, a 16-fold and a 2.5-fold, which permit to amend the curvature of the field and to reach for theoretical scales in the BAO’s telescope of 2.6 m, with a focal distance of 10.01 m, 0”0412 per pixel with a microscope of 8x and 0”0165 per pixel for that of 20x resulting in total fields of 21”09 and 8”438, respectively. The large convergence of the 16-fold lens (1:64) permits to place other optical elements (prisms, filters) on the axis between the lens and the detector, without the necessity to include any other optical element.

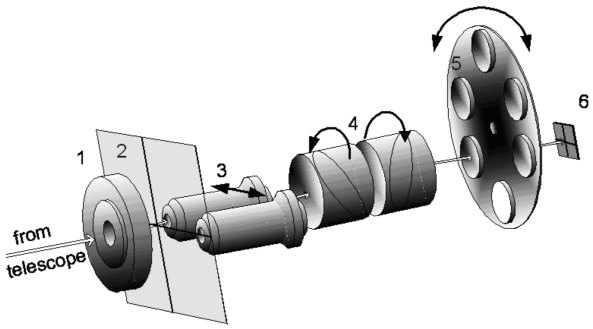

FIGURE II.20: Design of the optical-mechanical configuration

Afterwards, the number 4 indicates the Risley prisms moving above a central thread. They consist from a pair of wedge prisms that are used for beam steering. Rotating one wedge in relation to the other will change the direction of the beam. When the wedges angle in the same direction, the angle of the refracted beam becomes greater. When the wedges are rotated to angle in opposite directions, they cancel each other out, and the beam is allowed to pass straight through. The Risley prisms of our eMCCD camera were configured to allow the correction of the atmospheric distortion based on the angular separation between the source of the light observed and the zenit in sections of 10° getting from 10° to 70°. Each of these positions permits to alleviate the presence of atmospheric distortion in their range of separation.

Immediately after and before the detector eMCCD of our PhotonMAX, there is a wheel with 6 spaces for filters marked with 6 in the Figure II.20. One of them does not contain any filter and lets the light pass unmodified, meanwhile the remaining five contain filters of the manufacturer Andover (USA). All the filters have a diameter of 25 mm, with a light diameter of 21.2 mm, and thickness 6mm. The thickness of the filter dielectric layer is 0.25% throughout the surface. The center wavelength/bandwidth of our filters are 550/20 nm, 600/40 nm, 650/40 nm, 700/80 nm and 800/100 nm (Figure II.21).

Additional information regarding the eMCCD, the filters characteristics, and the Risley prisms for Atmospheric Dispersion Correction can be found in Maksimov et al. (2009).

Just as in case of the ICCD camera, the camera eMCCD must be mounted on the telescope applying some type of physical support adapted to the telescope-cylinder pair, containing optical-mechanical configuration. A thick steel disc was prepared at the BAO with a series of holes in order to be fastened to the telescope, and another series, for setting the camera. The installation of the mentioned support and the setting of the camera produce small variations in the angle from which the eMCCD receives light between installation and installation. In order to arrange this deficiency in all the campaigns, they observe stars with well enough

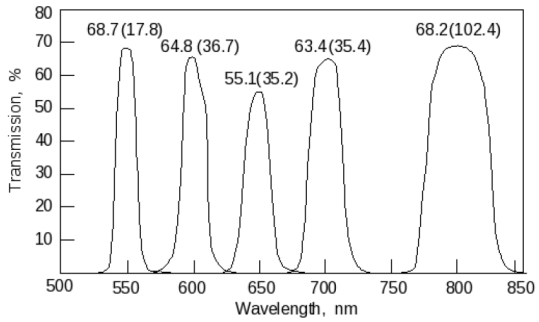

FIGURE II.21: Spectral performance of the interference filters of the OARMA camera: the transmission in maximum and half width (within brackets) are displayed over each curve

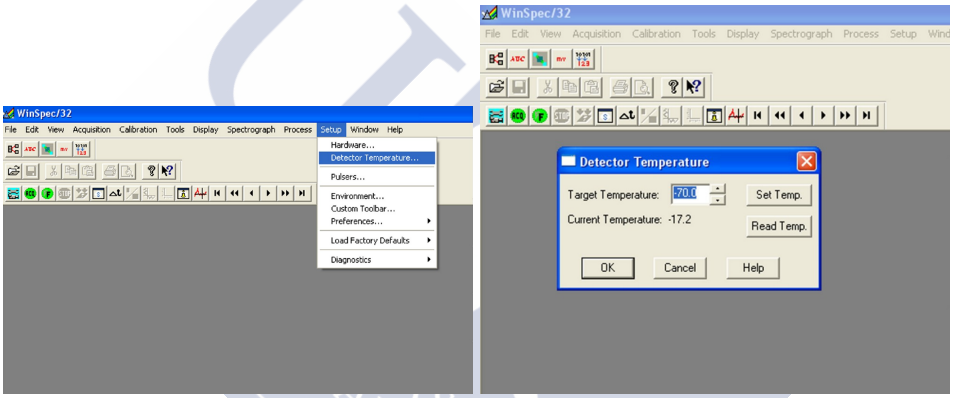

FIGURE II.22: Detector Temperature Setup

determined orbits in order to set the offset of the angle.

In the future it is planned to make a mask which would allow a more precise calibration.

Configuration of the Control Computer

In order to install the camera, we need to place the PCI card inside of the camera that will control the operation of PhotonMAX. This card is similar to the card of the figures: like them, it is directly coupled to one of the slots present in the motherboard (Fig. II.15).

We shall instal the necessary software on the mentioned computer to manage the different processes of the camera. Everything related to the PhotonMAX is managed from WinSpec. If the camera is recognized by software, a specific interface will appear. If it is not recognized, a warning window will be displayed. It will suppose that we made wrong the connections of

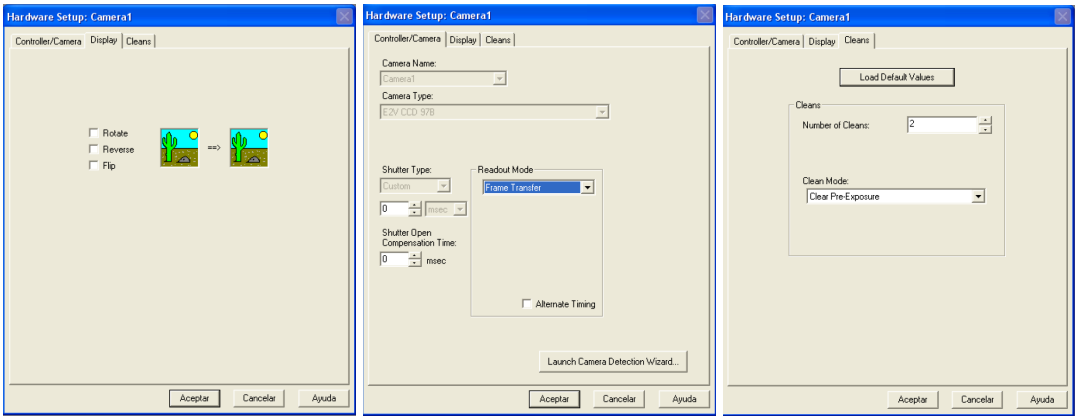

FIGURE II.23: Hardware Setup

different heads of small optical fiber cables to their respective accesses. In this case, we shall amend these connections and try again, until the camera is recognized.

The first thing we have to do is to configure the temperature of the camera. In order to set it up, we shall enter the tab "Setup" and then, "Detector Temperature". Then we shall select -70° and set it, clicking on Set Temperature and Enter in the mentioned order (Fig. III.1). Its evolution is reflected in this section of software. When reached for -70° we shall wait for some fifteen minutes approximately until the temperatura is stabilized.

In the same "Setup" tab, "Hardware..." appears above "Detector temperature...". Once inside, we shall set up different aspects, like the orientation or flip of the image, the CCD's action mode or the cleaning process. In our observations we shall always use the configurations presented in the Fig. II.23, i.e., Frame Transfer; no rotation, reversal nor flipping; Clear Pre Exposure with two cleans. In order to check out the operation of these selections, the readers may look up the manual[3] on the use of PhotonMAX 512B, available online in the ftp archive of the manufacturer (Princeton Instruments).

Afterwards, we shall configure our observations. For that purpose, we shall enter the tab "Acquisition" and then, "Experiment Setup...". Several fields and tabs will appear inside of this emerging window. We shall be configuring by means of the tabs the most important aspects for the realization of observations. In the tab corresponding to "Main", presented in the middle of the Fig. III.3, we shall select the exposure time according to the intensity received from the star. It is better to be conservative before adjusting the time. 5-10 ms would be enough if the star is very brilliant like the stars of calibration, used to carry out the first observation of the night. A more common speckle observation would need exposure time of 20 or 30 ms, according to the intensity detected. In general, we shall use the maximal value of Gain, corresponding to 4095. The rest of the values are as shown in the image,

[3]This link leads directly to the ftp archive and asks for an Access code. I would recommend to google Manual PhotonMAX 512 and to open directly the pdf.

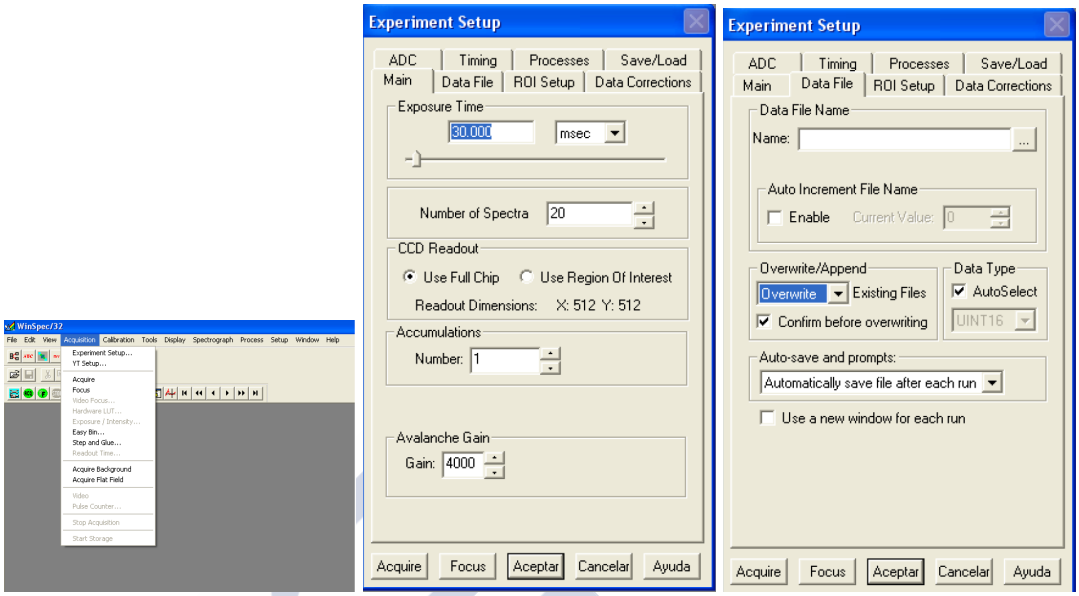

FIGURE II.24: Acquisition Setup

1 accumulation, full chip. The number of spectra does not appear in our configuration of software, the number of images will. We always take 1000 pictures in our observations.

As a rule, we are not going to select Overwrite in "Data File" tab, to the right of Fig. III.3. We shall select from among other options the one we prefer. In general, we shall save and assign a name for every image. The following important tab shown to the right in the Fig. II.25 corresponds to "ADC". We shall select there a rate of 10 MHz and a gain controller of 3: the appropriate one for our type of observations because it requires a smaller number of electrons to generate an ADU and thus minimizes some noise sources. It is better to let the ADC offset fixed along all the campaigns of observation.

The Steamoco software permits to manage the optical-mechanical part of the camera. After opening it, we shall upload a setup archive and restart it. Then we shall move every component, i.e., filters, microscopical lenses/elbow and prisms of Risley to basic position. It is done by clicking the corresponding buttons, waiting for the adjustments to finish and different indicators to turn green (Fig. III.2). If an indicator remains red, it means that the basic position was not succeeded and it is necessary to click again to restart the process. It may take several minutes.

Installation on the Telescope

The BAO's representative in charge of organizing the installation and maintenance of different parts forming the camera of Speckle Interferometry of OARMA is Professor Melikian.

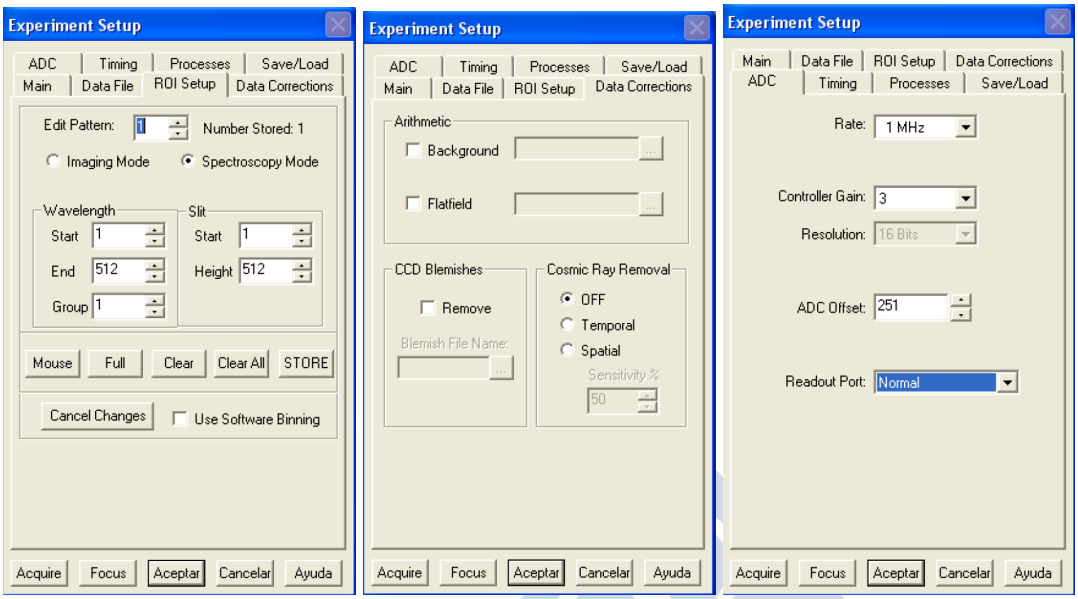

FIGURE II.25: Acquisition Setup

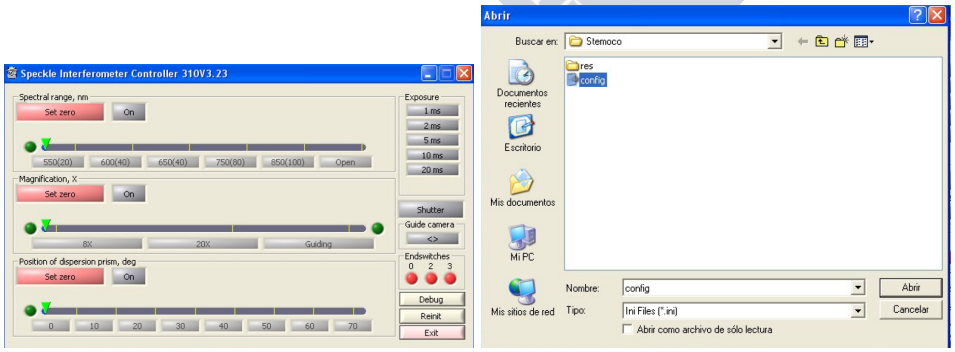

FIGURE II.26: Left, Steamoco main window; right, Steamoco config window

FIGURE II.27: Detail of the PhotonMAX white strip: the red stopper needs to be unscrewed before installing the camera on the OMC

The pieces described above are kept at this office between campaigns, except the Optical Mechanical Cylinder (OMC) and the stand which fastens the latter to the telescope. These parts, due to their size, are kept in the warehouse of the same building which includes the 2.6 m telescope of the BAO. The pieces shall be taken from the office and from the warehouse to the telescope control room before starting the installation process.

As soon as the stand is installed on the prime focus of the telescope, the optical mechanical part of the camera shall be screwed up and fastened to it. The PhotonMAX 512B (Fig. II.12) is placed on it, without the red hat cap that covers the access of the light to the eMCCD, Fig. II.27. PhotonMAX is screwed up to fasteners offered by the OMC in the upper side.

The OMC, which contains optical components inside, offers two metallic boxes in opposite sides (Fig. II.13). The Control Data Box (CDB) manages the transmission of data in the series computer-PhotonMAX-computer, while the other one, the Optical-Mechanical Control Box (OMCB), manages the movements of the components situated inside of the cylinder, i.e., elbow, wheel of filters, prisms of Risley and microscopic lenses. The stand of the camera is also provided with a screw to fasten the black box, marked with T, so that the slim cables of optical fiber can be connected to lateral boxes.

The CDB has a fixed cable, the white one on the left of the Fig. II.12, which serves to connect it to the base of PhotonMAX, meanwhile the information is transferred to the computer situated in the telescope control room by means of an optical fiber cable. Both of them, marked in orange in the Figure II.28, are converted in one only in a metallic box marked with

FIGURE II.28: Detail of the wires connected to the Control Data Box

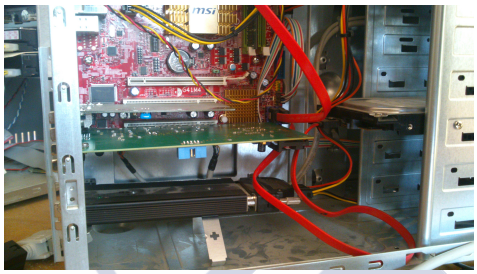

FIGURE II.29: PCI target and RS 232 connected to the motherboard and computer respectively

a T standing for the telescope (Fig. II.16). The signals are transferred through this unique cable between two black boxes. The black box situated in the control room has a couple of optical cables of exit with the same heads as those we fastened to the CDB. They are connected to the transponder (Fig. II.18), where the information coming through the optical fiber is converted into digital information. Another cable deriving from the transponder is connected to the PCI. Both ends of cables correspond to the heads of the central image of II.17.

The RS232 is connected with the OMCB by means of two cables of optical fiber (Fig. II.17 right). They are marked directly in the RS232 and oppositely, in the OMCU, i.e., the cable with the red stopper is connected to the access R of the RS232, meanwhile the one going to OMCB, i.e., deriving from the black box marked with a T, presents an orange mark at its surface, near the head, going to the access L. In this case there is a transponder too, but it is inside the OMCB so it is not visible.

All the cables of optical fiber must be connected to the appropriate entrance in order to ensure the due operation of the camera. In case of a mistake, different illuminated signs will inform us what has caused the failure. Two boxes of control in the OMC, the transponder and the RS232 present the mentioned signs. The most common failure is to invert the position of the pair corresponding to the OMCB (II.17 right image); this is expressed by the activation of a red light on the upper surface of the RS232 (Fig. II.14).

If the heads of the central image of II.17 corresponding to the DCB and the transponder are

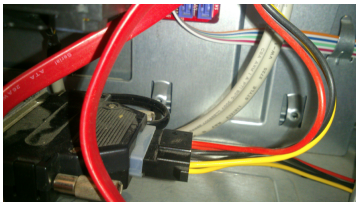

FIGURE II.30: Back of RS 232 to computer

placed wrong, it will provoke a green flickering light instead of a fixed green light. It can occur only in the transponder, because the heads of this type going to the DCB are joint, and it is compulsory to have them introduced in appropriate way. The signs of the DCB and the OMCB are not used in general, because they provide the same information as the previous ones. It is worth remarking that when connecting the heads coming from the box with no marks to the RS232, the cable of optical fiber corresponding to the access R has a red stopper on the side of the head. This detail facilitates the process a lot.

At last, a COM-COM cable deriving from the backside of the computer and reaching for the general COM access is connected to the RS232, contacting its "frontal side" (Fig. II.31). The RS232 obtains the energy directly from the computer or the backside thereof.

To finalize, let us comment that according to our typical installation in the 2.6 m telescope of the BAO, the south is in the top of the frame, the north in the bottom and west/east are in the left/right sides. This will depend on how we will place the PhotonMAX above the OMC. We have situated the lateral presenting a white tape downstairs in all our campaign (Fig. II.27). In the BAO's 2.6m telescope, we observe an angular field of view of 168"7 in the prime focus of the 2.6 m telescope (F/3.85, scale 20"6 mm^{-1}) and a resolution of 0"33 $pixel^{-1}$. With 8x and 20x objective microscopes, angular fields of 21"1 and 8"4 are covered, respectively.

Deinstallation

Once the camera and the computer are disconnected after use, in order to dismount the OARMA tool at the end of the observation campaign, all three power cables that supply the PhotonMAX 512 and the DCB and OMCB boxes are moved away. The mentioned cables are stored with the power supply of the camera.

The slim cables of optical fiber are disconnected from boxes, and their heads are protected. The entrances of optical fiber of the boxes shall be protected with the heads too, in order to avoid the access of dust. The TV cable which takes the image of the guide camera to the memory card is disconnected too. The detector is unscrewed from the optical mechanical part (OMC) and screwed with the red cap which protects the entry of the light inside the camera before packing and saving it (Fig. II.27). All these operations are developed around the main focus of the telescope. To make it possible, it is out in standby position.

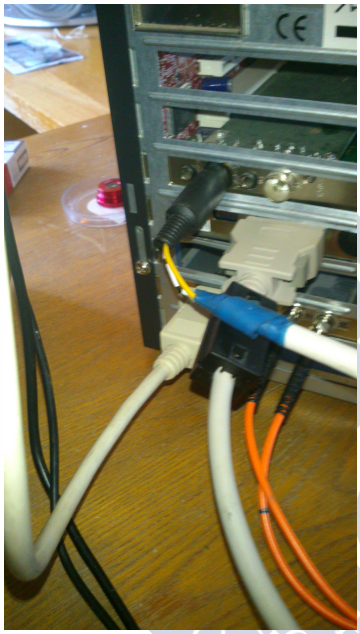

FIGURE II.31: Lower left, cable from RS 232 to computer (COM-COM). Lower right, a couple of orange optical fiber cables from the control room black box to RS232. Lower middle cable from transponder to PCI. Upper cable from guide camera to TV card; this cable comes directly from the telescope and it is a normal TV cable.

The optical mechanical part is moved away from the stand which communicates it with the telescope; the entrance through which the beam of light passes is protected and kept in its box. The stand is also moved away and kept with the OMC in the warehouse assigned for our tool in the same building of the telescope.

The cables of optical fiber and TV are disconnected from the telescope and taken to the control room. The ends of the cables of optical fiber located in the control room are disconnected from the transponder and the RS232, respectively. Their heads and the corresponding entrances both of the transponder and of the RS232 are protected with their respective heads. All the cables are rolled up very carefully and kept in a box meant for that purpose. The transponder and RS232 are kept in the same box together with additional grey cables connected to the PCI and to computer. The TV card and the screws both moved away from the PhotonMAX and those affixing the stand to the OMC are also kept in the mentioned box.

At last, the PCI is put in a protecting bubble wrap and in a cardboard envelope. The PhotonMAX, the cables of supply and the power supply, the envelope with the PCI, the documents of the camera, the box with the cables of optical fiber and the rest of elements connecting them to the computer of control are kept in a safe in the office of Prof. Melikian, looking forward for the next campaign.

USC
UNIVERSIDADE
DE SANTIAGO
DE COMPOSTELA

Chapter III

Observational Campaigns with SI

Although our referent star, the Sun, does not belong to a multiple system, it is common that the great majority of its kind do. Duquennoy and Mayor (1991) conducted a spectroscopic examination about the stars found mainly in the north hemisphere with spectral classes in the interval F7-G9 located to less than 22 pc from the Sun. In addition, they also achieved all the measures of radial velocities available for this type of stars during 13 years, and combined their own detections with the accumulated data from known binaries and with lists of systems with common proper motions. They considered 164 primary stars in search of multiplicity, finding out ratios of S:D:T:Q = 57:38:4:1, with S signifying singular or with no multiplicicty, D double or binary, T triple, and Q quadruple. The results have been corrected because it existed a downward trend given by the instrumental limits of the era in order to detect low mass components, and calculated a multiplicity percentage of 57% increasing the 43% observed.

In his relatively recent doctoral dissertation, Raghavan (2009) determined that the quantity of triple components in G type stars in a distance of 25 pc from the Sun had at least been found in underestimated twice. These new components were detected in previously known double systems, i.e., the number of single stars remain almost changeless. Similar results to those of Duquennoy and Mayor (1991) have also been found for stars belonging to population II, or metal-poor stars, in a radius of 250 pc with respect to the Sun (Rastegaev, 2010). This seems to indicate that the steady multiple systems are the normal outcome in the stellar formation processes, not only when our galaxy was created but also now.

Despite this, approximately 3 out of 4 stars existing in the Milky Way have a ratio of multiplicity of "only" 21-27% (Winters et al., 2015). This high percentage of stars corresponds to the dwarfs of spectral type M, typically called red dwarfs (Henry et al., 2006). If we compare them with those of class O, located opposite to the red dwarfs within the Main Sequence, we can see that the stars of spectral class O present much higher percentages: 43% for the stars called runaway; 59% for field stars, and going up to 75% for stars pinpointed inside clusters or associations of stars (Mason et al., 2009). The explanation for this difference lies on the fact that class O stars, given their great mass, can contain others stars from whatever spectral type as partners, whereas type M dwarfs can only be associated with lower mass

stars: brown dwarfs or even less bright objects. Nowadays, these low brightness objects that accompany a spectral class M dwarf continue to be an observational challenge and it is highly complicated to detect them. This factor shows up that its percentage of multiplicity is being underestimated. As a consequence, the lack of reliable information about the mass margins, radii and multiplicity on this kind of stars makes it impossible to the temperatures of most of the stars in our galaxy.

Not only the statistics of singularity/multiplicity ratios provide useful information about the stellar formation and evolution. Thank to the differences of magnitude and the orbital parameters calculated for binary and multiple systems we can statistically reveal some of the laws of physics that regulate the processes of formation, not only of stars, but also the exoplanets which surround them. In a not very distant future, we should probably be able to detect exosatellites, or even rings as the ones surrounding the giant gaseous planets that we found in our Solar system. This will allow us to deeply understand the galaxy that host us.

One of the most highlighting effects of the stellar multiplicity is its effect on the stellar evolution. To illustrate this, we will review the past and future of the quadruple system Regulus (Rappaport, Podsiadlowski, and Horev, 2009). Regulus is a B7V star, located to 24.3±0.2 pc from the Sun and with an apparent magnitude of 1.36_m, which means that it is one of the brightest stars that we can see in the sky from the surface of Earth. Surprisingly, despite its brilliance, it has been considered a singular star until recent times when it was discovered that it was accompanied by a second component, a white dwarf star with a period of ~ 40.11d (Gies et al., 2008). This lack of awareness about its binary condition affected to the age as well as to its effective temperature and mass. As the mass exchanges between close stars can take place in the different stellar stages of their evolution, the models to predict the evolution are completely different when they are applied to singular stars that will occur in stellar systems. Depending on the efficiency of the mass exchanges, the future between the main component of Regulus and the white dwarf, which orbits it at great velocity, several possible scenarios exist for their interrelationship and evolution (Rappaport, Podsiadlowski, and Horev, 2009). Nevertheless, it almost 100% certain that the development of Regulus as a binary is now completely different than it was a single star. It is a particular example of the importance in detecting new components in stars of astrophysicist interest and how the multiplicity alters our knowledge about them.

In the former case, we point out our lack of information regarding its multiplicity led us to assign incorrect physical parameters. In the case of the single stars, this is due to the fact that mass is assigned using models, and the relationship between mass and luminosity is an indicator of the evolutionary phase of star, and therefore, of its age. For astronomers, it is a great advantage that many stars are configured in systems with multiple components, since the binary stars allow us to derive their masses thanks to Kepler's laws.

From the orbit of a binary system, Kepler's laws enable us to obtain the combined mass of both bodies. In addition, as it is the case of the double-lined spectroscopics binaries, the spectrum

of the system reflects, due to the Doppler effect, the existence of two components, we can determine also the individual masses together with the majority of astrophysicists parameters. It is essential to highlight that thanks to these calculated masses in visual multiple systems, in spectroscopic binaries, and even more important given their high accuracy, in the visual-spectroscopic ones, we can assign mass values to the single stars (Docobo et al., 2014, 2017a).

In the case of Regulus, this multiplicity has allowed researchers to delve into the particularities of different scenarios of its stellar formation as well as its posible evolution. Regulus is an example of the orbital configuration of multiple systems which provides information about the different stages of its past. For interested readers, you can find another illustrative and revealing example in the twins ballerinas of (Tokovinin, 2018a).

From a computational view, the hydrodynamic simulations applied to astronomy, for instance, Bate (2009), as the softwares of stellar evolution, p.e. Paxton et al. (2011, 2013, 2015), help us better understand the formation of multiple and binary systems. During their design, development and refining, they need to be adjusted to the observational data in order to determine the physical processes that a star experiences in its whole life.

Technologically, facing up these observational challenges emerged from the astronomic observation, new technologies such as CCDs (section II.3) have been developed and have changed the way we understand the world. These CCDs, which today are part of our mobile phones, have been created fundamentally for scientific purposes.

All of this knowledge has been achieved thanks to thousands of observations and the possibility of accessing to them. Likewise, the only way of clearing many of the unknowns in astrophysics (e.g, the percentages of multiplicity for red dwarfs, the relationship between their luminosity and mass, the formation and evolution of protoplanetary discs, the relation between multiplicity and mass accretion, etc.) is the detection of secondary components using and analyzing new observations.

As we have previously explained, obtaining highly accurate observations of binary systems is essential to determine their orbits and consequently their masses. Calculating an orbit supposes a massive challenge for researchers such as for those which present long orbital periods. In general, their historic information only covers a little stretch of its trajectory. Also, those systems with components which fulfill its orbit very quickly. In this case, the lack of detailed observations could lead to misunderstand the data. Preliminary orbits are usually estimated in both cases.

Nevertheless, even though certain orbits could be temporarily imprecise, the observational effort is worthy by different reasons. As we have mentioned in the Regulus' case, the detection of new components in a system can radically change the information we have. Possessing precise orbits allows us to predict the position of its components and to understand systems of

great importance in astrophysics. This aspect is highly relevant in the study of stellar systems with surrounding planets.

As already mentioned in previous chapters, in terms of resolution, Speckle Interferometry is a very accurate technique which supplies photometric information and, at the same time, very efficiently collects data. Such observational campaigns can be a great contribution to the astronomic community. The importance of the double systems, which we have been talking in this chapter, give the IS observations an added value, now and in the future.

During the development of this PhD studies regarding SI, the director of this thesis considered of a fundamental importance that the author acquired expertise on the practical challenges of this technique using big telescopes. Thanks to that, it was posible to obtain speckle data using the following telescopes: 2,6m at Byurakan Astrophysical Observatory (BAO), 6m at Special Astrophysical Observatory (SAO RAS, Rusia), and 4.1m at Southern Astrophysical Research (SOAR, Chile).

The tasks to fulfill were, first of all, to start up observational campaigns with the OARMA's speckle camera that were since 2011 in deposit in BAO. Secondly, to accelerate the data reduction workflow related with the 2012-2014 observational campaigns in SAO. And, finally, to acquire data related with southern binaries in SOAR. All these assignments were included in the research plan presented at the very beginning of this PhD project under the supervision of Prof. Docobo. Also, these tasks are contemplated in the ongoing research plan of the OARMA: *Study of close binaries of special dynamical and astrophysical interest in the GAIA era*.

Our main collaborators on those observatories have been: Norair Melikian at BAO; Yuri Balega, Evgeny Malogolovets, Denis Rastegaev, and Vladimir Dyachenko at SAO RAS; René Mendez and Andre Tokovinin at SOAR.

The observational campaigns carried out in Armenia are good for getting a high performance of the OARMA's eMCCD camera (II.5.3). Even though we have suffered many setbacks and the process has not been simple, the experience of our researchers in calculating orbits shall allow us to use the data in future articles and studies. The experience acquired in the observational processes, the reduction and analysis of images are applicable to other imaging techniques and they constitute the basis for future works.

In what follows, we are going to detail how we have developed our observational campaigns together with the staff of SAO and Byurakan. We shall describe an observational night and how data is reduced and analyzed. The theory about reduction has been explained before as we consider it a technical aspect rather than methodological. However, some aspect must been detailed once again so that the reader can understand how workflow runs.

Besides it, the calculus of Power Spectrum (PS) and the function of auto-correlation (ACF) are detailed in this chapter. We explain carefully the physical parameters involved, the understanding and simulation of their characteristics, and how we can obtain astrometric

and photometric information related with stellar components separated over and near the diffraction limit of the telescope employed.

To conclude, we summarize the data acquired in the campaigns until now so that the reader can have an idea as to how productive they can be when the atmospheric conditions are suitable.

III.1 Process of observation, reduction and collection of results with Speckle Interferometry

In order to launch a successful observational project with SI, it is necessary to avail of both hardware and software with full technical capacity required to take and handle pictures. The PhotonMax 512 camera of the Ramon María Aller Astronomical Observatory, as well as the processes of installation and control thereof were already explained above in II.5.3. We shall proceed with the explanation of the objectives and peculiarities of different parts forming the process of collection, reduction and analysis of images. The knowledge of this process allowed me developing software meant to conclude every task.

Along this section, we shall compare different methods of reduction and analysis of the images obtained thanks to the combination of SI with eMCCD detectors. We shall focus on the techniques applied by the main research groups which are developing observational campaigns with SI on a regular basis and, when methodological discrepancies are detected, we shall explain why a certain version was regarded as preferable in every case for the design and development of the code applied on pictures obtained with the 2.6m telescope at Byurakan or with the 6m BTA at SAO RAS.

It is worth emphasizing that the necessities of both observation campaigns are slightly different. In case of the observations at SAO, were performed thanks to the dedication of time by the Time Allocation Committee of the BTA in response to the Prof. Docobo observational proposals. The SAO's speckle team was led by Y. Y. Balega and included D. A. Rastegaev and V. V. Dyachenko as main researchers/observers, as well as A. F. Maksimov as engineer in charge of the instrument. This team provided us with the results obtained for the calibration of the pixel size and the angle offset. Those quantities are determined by a two-hole mask. They usually applied the light coming from Deneb or another very bright star apparent beyond a mask with two dot slits. As for the collection process, the decisions made when observing different objects fell entirely under their competence.

On the other hand, the campaigns implemented with the BAO 2.6 m telescope by means of the AORMA camera PhotonMax 512 have been conducted under the direct responsibility of the author of this text. When collecting data, the choice of the optical configurations and the planning of the observation strategies were based on different experiences of observation that

I shared both with the above-mentioned team of the SAO and with A. Tokovinin at SOAR, Chile. We shall explain below all of the aspects of observation with SI and the way that we developed them on the BAO 2.6 m telescope.

III.1.1 Calculation of the pixel size and mismatch of the installation angle

The theoretical size of pixel in a detector with an equal number of rows and columns is calculated by means of the equation:

$$p_S = \frac{206255L}{FMN}, \tag{III.1}$$

where L stands for the length of one of the detector's sides in meters; F is the focal distance of the used telescope used in meters; M is the magnification applied, and N is the number of rows or columns of the pixels. This measurement might be not as precise as we would like as some of theoretical factors may suppose errors, therefore it is convenient to compare it with other measures obtained in experiments.

The research groups led by Horch (DSSI camera), Balega (Andor camera with the same optical configuration as applied for our PhotonMax 512) and Tolovinin (HRCam) use or have used during some period a mask with slits or narrow holes on the optical path in order to determine both the pixel size and the angle mismatch provoked by the camera's installation. This allowed them to take speckle pictures of very bright stars (with 2 or 3 of magnitude in V band) beyond the mentioned slits. The resulting images present a series of superimposed bands located at a different spatial frequencies. Just as in the pictures of the objects of interest, the data block is converted to the space of frequencies by means of the Fourier transform and their median is calculated. The result is known as Power Spectrum. The Power Spectrum calculation makes the bands turn into very sharp line-shaped structures in the Fourier Plane, where they can be modeled with high accuracy. By using the measure of real distance of the slits, the distance between the mask and the focal plane, the wavelength which we observe on and the focal radius of the telescope, the spatial frequencies obtained from the model represented in cycles per pixel may be transformed in cycles per arcsecond. Introducing this quantity, we get the scale of arcseconds per pixel.

Assuming that the focal radius is known, the other three quantities shall be measured within a due margin of error, usually less than 0.1%: the distance between the mask bearing and the focal plane, the real distance between the mask slits, and the effective wavelength under observation which itself implies a combination of the filter applied, the atmospheric transmission, the quantum efficiency of the detector, and, at last, the spectrum of the star in question.

In order to improve the determination of the effective wavelength by means of the mask, it is convenient to observe stars of different spectral types. The calculation of the effective wavelength is carried out by building models which capture information about the atmospheric transmission in the telescope's site, the filter's features, and the detector's characteristics in order to simulate the distribution of wavelengths for certain spectrum and to compare it with the intensity detected. This may cause errors if the models are not good enough to model the observations. When taking pictures of two or more stars with quite differentiated spectrums (e.g., A-M or A-K) the deduction of two scales obtained should result in no difference.

As for the angle difference, it is usually conditioned by slight variations when mounting the camera on the telescope. The value may slightly change from campaign to campaign if the camera has been demounted and installed again between two observational campaigns, as it is usually done in most cases. The masks themselves do not allow determining it. Normally the masks are provided with parallel slits, installed perpendicularly regarding its central axis. If it is duly carried out, the error of angles (parallel to each other and perpendicular to an axis) shall be very small and easily definable. During the installation it is also important to ensure that the structure on which the mounting is done does not add a variability source to the measures. In the ideal case, it should be fixed, although this is not always possible with all the telescopes.

Another way of calculating the scale and angle mismatch is through the observation of binary stars with quite well-known orbits. WDS ORB6 (Hartkopf, Mason, and Worley, 2001), in its updated online version, provides a list of calibration stars. They are binaries with well determined orbits, definitive or almost definitive ones, and calculated mainly using high precision data, as speckle observations. The list also includes wide binaries showing a slow orbital displacement. After the observation of some of these stars, the process of reduction and analysis is carried out. Afterwards, the obtained results of the apparent position are compared with those expected, i.e. the orbit's ephemeris on the date when each observation was implemented. We can calculate this way the pixel size, the mismatch angle and the related errors.

This approach has been followed to calibrate the OARMA's observations carried out at Calar Alto in collaboration with Balega's team (Docobo et al., 2001, 2004, 2008).

Another option used to calibrate these values, which also has the advantage of not implying night observations, was used by Tokovinin, Mason, and Hartkopf (2010). Guided by this purpose, they placed two light points in the telescope's spider, forming a band pattern. Having the distance between these light points, b, and the wavelength of the lasers in use, the period of bands $\frac{\lambda}{b}$ was calculated. As in the case of masks, the information is recovered as a Power Spectrum through a simple centroid algorithm on the bands detected in the Fourier plane. The study of this Power Spectrum, or calculating its inverse Fourier Transform, allows the determination of the pixel scale and the angle mismatch.

As for our observations, SAO applies microscopic lens, meant to adjust the image on the primary focal point of BTA with the detector pixel size of 16 micrometers. This requires a magnification of 16x, although a fewer magnification is used to observe wider fields. Two high-quality 16-fold and 2.5-fold Carl Zeiss lenses are used to amend the field's curvature and to reach for theoretical scales of 0.055"/pix and 0.0087"/pix for fields of total 28"2×28"2 and 4"5×4"5. The great convergence of the 16-fold lens (1:64) permits to place other optical elements (prisms, filters) on the axis between the lens and the detector, with no need to include any other optical element. Besides, SAO possesses a mask to calculate the pixel size and the angle mismatch. Although we do not count with data of these measures that would coincide with all our campaigns, the values thereof serve as a benchmark when calculating the range of error during the determination of the pixel size and as an average value for the installation angle and its error.

In the BAO's 2.6m telescope, as we employ almost the same optical configuration as SAO, we observe an angular field of view of 168"7 in the prime focus of the 2.6 m telescope (F/3.85, scale 20"6 mm^{-1}) and a resolution of 0"33 $pixel^{-1}$. With 8x and 20x objective microscopes, angular fields of 21"1×21"1 and 8"4×8"4 are covered, respectively, corresponding to pixel sizes of 0.0412"/pixel and 0.0165"/pixel. The main difference between the optical configuration that is mounted in SAO and BAO is that in BAO we use a different magnification microscopes, 20x instead of 16x for the small FOV, to achieve the desired sample of the speckle.

III.1.2 The Acquisition Process

The acquisition process is determined by the following parameters: number of images per block, number of blocks, a certain sampling ratio, calibration images, exposure time, atmospheric distortion and filters. Besides, other aspects such as the obtaining of necessary images to reduce (darks,flats and bias), the level of gain and the use or not of binning must be taken into account.

Each data block is composed by the observations of an object of interest which were taken sequentially. As a reference, SOAR uses two blocks of 400 images, 400×400pixels, or 200×200 applying binning. At SAO, if we employ the full chip, that is, 512×512 pixels, we can get 2000 images in a block. DSSI uses an area of 128×128 pixels and it takes 1000 images for bright stars whereas the observation of 12-13 magnitudes are kept in blocks of 3000-5000 images, depending on the present seeing.

Regarding the ratio of sampling, SOAR employs a magnificacion that divides into two the observed field in its focal plane (F/16.5) in order to get an adequate Nyquist' sampling for the speckles, since the camera has a pixel size of 10 microns. We can achieve this by combining two achromatic lens, a negative one with F=50mm, which is located opposite to the focal point and colimate the light beam, and a positive one with F=+100mm, which focus the

light on the image detector (Tokovinin, 2018b). Generally speaking, it does not matter what detector SOAR mounts on the camera, they always maintain a pixel scale of ~15mas.

DSSI uses an area of 128×128 pixels for observations of 2.8×2.8 arcseconds in the WIYN telescope, although this instrument is also employed at the DCT at the Lowell Observatory, and we can occasionally find it as an invited instrument in both Gemini North and Gemini South which are telescopes of 8.1m with a silvered cover.

Both HRCam, mounted on 4.1m SOAR's telescope, and DSSI, usually obtain blocks of data of single stars, calibration blocks, in order to shape the seeing present in observations of the objects of interest. To achieve this, they take images of singular stars which are moderately bright and are close in time and in the sky to the scientific oriented observations. It is not unusual to use the same reference star to calibrate one or more observations.

Normally, the time used with DSSI in each exposure is 40ms. At SAO, the usual exposure time is 20ms but it can vary if it is combined with the multiplication of eMCCD, depending on the seeing and the magnitude of the star we want to observe. The same happens in SOAR, where the use of binning to get images of separated and bright stars is quite common.

In order to correct the atmospheric distortion, the SOAR group and DSSI use the AO from the telescopes, whereas BAO and SAO use the Risley's prisms which are integrated in the optical-mechanical part of both cameras. A pair of wedge prisms are used for beam steering. Rotating one wedge in relation to the other will change the direction of the beam. When the wedges angle in the same direction, the angle of the refracted beam becomes greater. When the wedges are rotated to angle in opposite directions, they cancel each other out and the beam is allowed to pass straight through.

The Risley's prisms of our eMCCD camera used at BAO have been configured to correct the atmospheric distortion according to the angular distance between the source of light observed and zenith in 10° sections from 10° to 50°. Every position allows the mitigation of atmospheric distortion in its range of zenith distance.

BAO and SAO cameras are fitted with a wheel of different filters. The filters correspond to center wavelengths/bandwidths: 550/20 nm, 600/40 nm, 650/40 nm, 700/80 nm, and 800/100 nm. When choosing a filter for our observation, we want to use the one that presents a smaller bandwidth so that the adequate amount of light can pass through. That is why the most used filters are 550/20mm for bright stars, 650/40nm for stars of medium luminosity and 700/80nm for less bright stars. Filters with 600/40 nm, and 800/100nm are used occasionally and the observations with these filters are preceded or followed by others where one or more of the main filters are used.

The data gathered by the camera of SAO are transferred to us in .dat format and the SAO speckle team provide us with the log of the observations. In order to mix both forms of information, we have written a routine that builds a header from the data of the log and put

it together with the speckle images to become a block in FITS format. This routine must be separately implemented for each image.

The data taken by the speckle camera of OARMA are kept in SPE format. Because of this, we have to delete the part of the block which corresponds to the original heading of that format. Likewise in SAO, we have used a routine composed by the register of our observational campaigns (information about the name of the object, the period of the observation, the filter used, the exposure time, the position of the Risley's prisms, etc.) and the observational data in the form of speckle images. The result is kept in FITS format as well.

The SAO blocks usually consist of 2000 images and their size was a problem because of the computer we used about five years ago. With the computer we have now at OARMA, this is not a problem.

The Acquisition Process in BAO

The blocks obtained at BAO are usually of 1000 images and at least two consecutive blocks are taken by each system and kept separately. First, they are kept in SPE format and passed to FITS, providing the suitable heading for each block according to the observational register. This register is carefully crafted. On one side, the information regarding the configuration of the camera is under the care of the person who runs the control computer. On the other side, the data relating to the telescope such as the declination, the right ascension, zenith distance, and the focus are written down by the operator of the telescope.

The sidereal and local time of each observation are taken twice by the two people in charge of the observations, that is, the person under the care of the control computer and the operator of the telescope.

It is very important to plug it in and turn on the power switches of the PhotonMAX camera and the control boxes before turning on the computer. The camera can never be switched on if the computer is connected. Inversely, we must switch off the computer before disconnecting the camera and boxes. Generally, we follow a there-and-back process. Firstly, we connect the three power supply cables –PhotonMAX,Data Control Box(DCB) and Optical-Mechanical Control Box(OMCB)–, and switch on the PhotonMAX, the DCB and the OMCB. Secondly, the computer that manage the PhotonMax and that is is placed in the control room must to be turn on. Finally, before switching off the system, we must turn off the computer, then the boxes and the PhotoMAX, and then unplug the three cables completing the loop.

Before getting the images, the person who runs the control computer handles the necessary parameters in WinsSpec and Steamoco. Assuming we have previously configured the camera as it was explained in II.5.3. The process to begin an observational night is as described below.

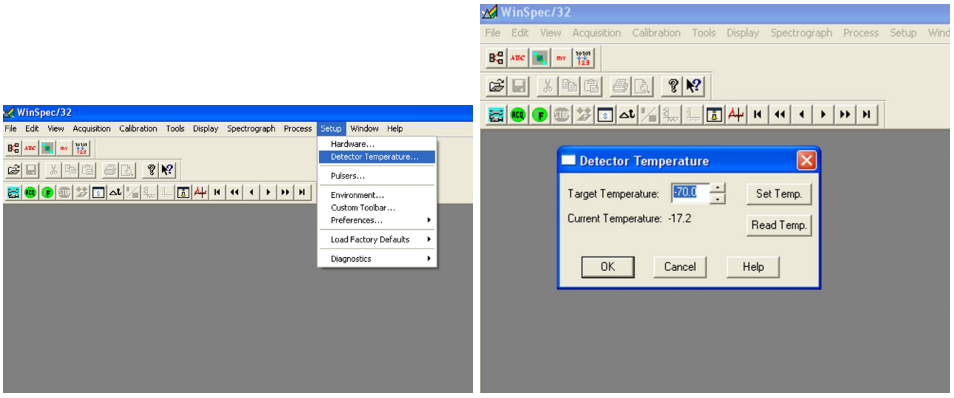

FIGURE III.1: Detector Temperature Setup

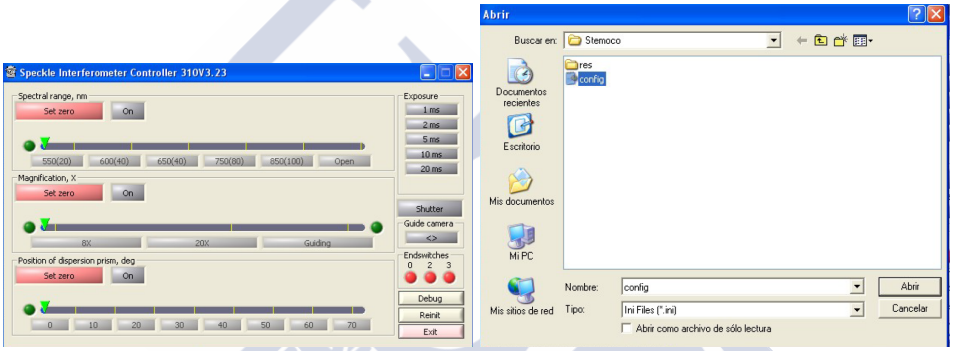

FIGURE III.2: Left, Steamoco main window; right, Steamoco config window

After plugging in the camera and the control boxes, which are called DCB and OMCB (II.5.3) respectively, we turn on the camera and activate the boxes by turning on their power switches. We have to do it in the correct order: PhotonMAX, DCB and OMCB. Then, while the telescope moves out from its position of repose and a luminous singular star is pinpointed next to the zenith, the control computer is switched on and WinSpec and Steammoco windows are opened.

The temperature of the PhotonMAX is established in WinSpec to be -70° (Fig. III.1). In Steamoco, the configuration file is loaded and the optical elements are located (filters, microscopic lens and Risley's prisms) by means of "Set Zero" in its initial position (Figure III.2).

Once the camera has reached a temperature of -70°, we must wait 15 minutes before beginning to observe. After that, we configure the exposure time in WinSpec (Fig. III.3), from 5 to 10 ms, with the telescope pointing to the calibration star. In general, the number of images used is 1000 because of computer memory limitations. [1]

[1]In the menu shown in the image this option pop up as "Number of spectra", whereas in our real software configuration it is marked as "Number of images".

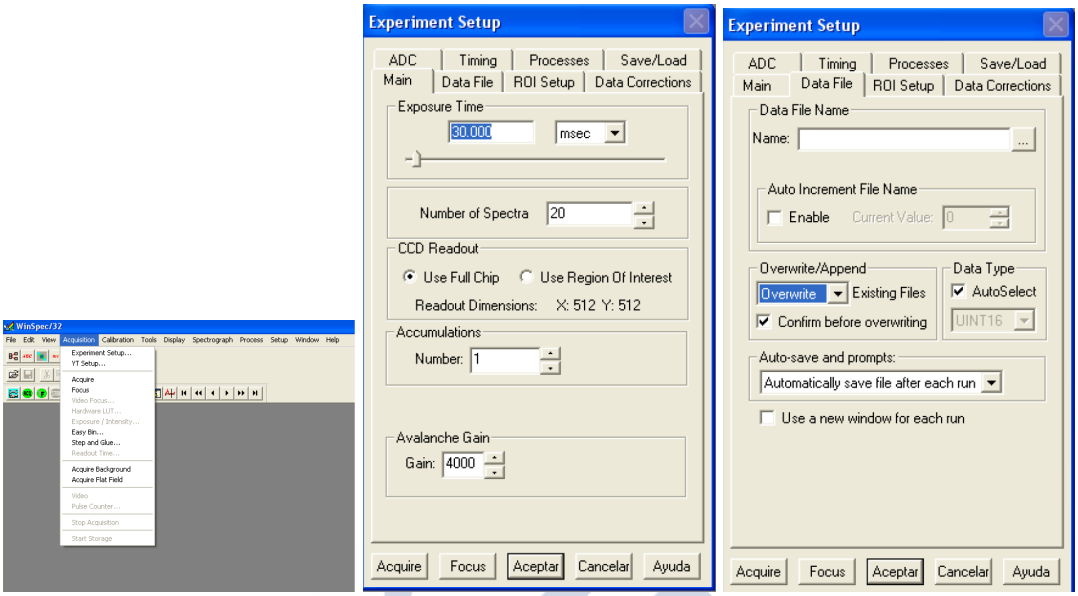

FIGURE III.3: Acquisition Setup

In Steamoco we select the 500/20nm filter, the 8x lens, and the atmospheric dispersion configuration corresponding to the distance between the star and the zenith (in this case, the usual position would be 0 or 10 because the star should be located close to the zenith). Generally, the zenith distance is provided by the person who is pointing the telescope.

After the optical components have been positioned and the indicators are in green in Steamoco, we enter in WinSpec again and click in "Focus", the green button with a **F** visible in the image on the left la Fig. III.1.

This allow us to see what the camera is capturing in "real time", we must check that the image is not saturated, i.e., the detector is not receiving too much light. If we consider it is saturated, we can reduce the exposure time, but this only occurs with very bright stars and nights with perfect atmospheric conditions.

At the present time we would be watching a very bright star with the biggest field of view (FOV). If the star was not shown in the FOV or if it was cut, we can take advantage of this by synchronizing the pointing of the telescope with the centre of the FOV in our camera. Once we have done this, we displace the micrometric lens in Steamoco by selecting that of greatest magnification, 20x. The displacement of the lens causes a shift in the location of the centre of the FOV, so we should synchronize the pointing once again in order to adjust it to the new centre. After this, it is appealing to put the lens back to 8x and memorize where the star is located in the big field so that we can easily locate future stars in the small one centre.

When this process is done, we come back to the 20x FOV and we should close the screen which was opened with Focus and we gather the data in our register log. At that moment,

we write down the name of the star, the filter, the exposure time, the position of the Risley's prism, the date, the focus of the telescope, and the first coordinates of the right ascension and of the declination.

If the operator of the telescope and the observer are ready, we shall proceed to set a starting time of the observation, then make the countdown. In WinSpec, press **ACQ**, the green button which is adjacent to the focus button shown in Fig. III.1). Now, the camera will start to take the image block. We note down the starting time (sidereal and local), the exact coordinates of right ascension and declination and be alert to make a note of the ending time.

The balance of the camera is great. An observation of 1000 images at 10ms of exposure takes 10s, plus another 3.8ms for each image, so we have a total of 48s. An observation of 1000 images a 20ms per image makes up a total of 58s, etc. According to the configuration we have set up, the PhotonMAX needs 38 seconds for a block of 1000 images. This has been tested in hundreds of observations and the error margin in a block of 1000 images is less than 1 second. The information transfer process from the camera to the computer takes 6 extra seconds.

Once that the transfer has been completed successfully, we can keep and name the image. As we have said, we always keep the blocks in an extended file .SPE though also can be done in a TIFF. Format.

Next, we proceed to set up the telescope towards a star with specific and scientific interest. To make this movement is advisable that the light that reaches the PhotoMAX be covered. At BAO, we put the self-guiding camera of the telescope in the optical path of our detector. Once the telescope pinpoints the star on its vision field, we adjust the acquisition and optical parameters conform with the brightness of the star, we distance the self-guiding camera from light path to the detector, we activate Focus mode in WinSpec and we prepare our FOV to locate the star in the centre of it. Finally, we already can observe and gather data until daylight or until the atmospheric conditions prevent us from continuing.

It is essential to localize the self-guiding camera at BAO between the beam of light and our detector when we move the telescope. As it blocks the light pass into the optical-mechanical part, we can also take images of darks. Alternatively, we can take these darks when the optical-mechanical part is in pause mode ("Set Zero" buttons showing green color).

At the end of the observational night, we have to turn off the camera. To do so, we put the telescope in the pause position. Meanwhile, we put Steamoco in initial/reposed position by selecting the three "Set Zeros" on the screen (left side image Fig. III.2) and we wait till the indicators mark the correct position. We shut down Steamoco, WinSpec and the computer. We must never turn off the camera before the computer.

When the telescope reachs its reposed position, we raise its main focus and switch off both control boxes, the DCB first and then the OMCB, and we finish turning off the PhotonMAX. Afterwards, we disconnect the three power supply cables. Later, we go to the control room

and transfer all data gathered during the night to an exterior hard drive and after that we turn off the computer.

III.1.3 Reduction of the Readout Noise

The cleaning process used for the blocks which were obtained through eMCCDs has already been explained in II.5.1 and II.5.2. In this section, we are going to detail what parts of this process are done by our researchers related to the images taken by the 2.6m telescope at BAO and by the 6m BTA at SAO RAS.

SAO Reduction

In general, we usually keep the data from the SAO'S observational campaigns in files whose names indicates the date of the observation. Before starting with the reduction process, we should identified the calibration blocks we are going to need, i.e. darks blocks and flats blocks.

The campaigns developed at SAO have fewer calibration images than the ones developed by OARMA at BAO. A dark is normally available per two or three days of observation. It is for this reason that, given a block to reduce, B, we must identify the closest-in-time dark, D_B. We must remember that to delete the readout noise, this dark must have the same exposure time per image as the one used for B. Once we have located the dark, we shall calculate its median and as a result we shall get an output image that we will subtract for each image within B,

$$B_i^{red} = B_i - Median(D_B). \tag{III.2}$$

Another part of the reduction process would be the flat correction, but this will be explained in the next section since it is done once we have converted the blocks into their power spectrums. We must state that the high performance of the Andor camera used at SAO make the flat reduction unnecessary. However, if we decide to use a flat block, F, in order to improve the reduction, this block must also be corrected by the readout noise, i.e., we also have to diminish the dark median chosen for this flat, which can be distinct from the one used for the block of images to be reduce by the flat,

$$F_i^{red} = F_i - Median(D_F). \tag{III.3}$$

If we consider it necessary for future steps, once that we have reduced the scientific image and its flat, we would calculate their PS as it follows in III.1.4.

BAO Reduction

In the observations we have accomplished in 2.6m telescope at Byurakan, almost every night we have gotten the dark images for the different exposure times. The flats have been taken at dawn and evening of 26 May 2017, 02 June 2017, and 02 November 2017.

At the beginning of each night we usually take images of a very bright star which is pinpointed near to the zenith. We do not consider them scientific targets, but calibration images. These calibrating stars which we have used throughout our campaigns can be seen in a table (llamada a tabla estrellas de calibración). A summary of the other images used to get the reduction are also exposed in a table (llamada tabla darks, bias y flats).

The dark images have been used to determine the threshold of the readout noise with one or none photon events as explained before (II.5.2 and II.5.2). Furthermore, they allow us to calculate the camera gain for the utilized multiplicative regime. The threshold has been used to filter the dark and flat images, just like the calibration and scientific ones. Besides, this process correct the number of death pixels in the camera. The filter assigns the average value of the surrounding pixels to those which do not overtake the intensity threshold. The size of the window has been 3. When there are some pixels which do not overtake the threshold of the window, this is increased to 5 and it is assigned the obtained value to both of them. A second harmless pass through the threshold filter confirms that the cleaning process has been fulfilled.

The dark images with the same exposure time from the same campaign have been combined in order to build a superdark block and its images are used to reduce image by image both the blocks of objects with scientific interest as the blocks of the calibration stars. Darks have been employed belonging to the same campaign to account for the environmental temperature differences. The fact of subtract image by image the superdark to the scientific blocks ensure us that the exponential warming pattern which is shown in the first 400 images (llamada imagen que muestra las medias de los darks) is deleted. If we do not make it like this, the first images lose SNR, whereas in the last images the readout noise would not be deleted successfully.

We have create a routine to clean the darks before to merge them into the superdark. It is carried out as follows:

1. store the intensity and position of the brightest pixel in each image of the block,
2. calculate the average and standard deviation, σ, of the pixels' intensity detected previously,
3. point at the number of image located at 3σ over the average and also the ones located 3σ below,

4. for each of these images out of the 3σ range regarding the average we calculate a median image with the adjacent images. Usually, we will use the previous and next 3 to 5 images,
5. every image detected is substituted by its calculated median image.

Due to high intensity particles, some of the detections are 3σ over the average. These particles show a very intense pixel and leave a small trace, also over-intense, behind itself in the image. Sometimes, it is only an error in the camera operation that is shown in a single over-stimulated pixel. In both cases, what we achieve by replacing the images indicated in the stage 3 for the image resultant from calculating the median of the adjacent ones which it is done in the fourth step, is to delete the most intense pixels and their possible traces without altering the number of images of the block. To maintain the size of the block when we are calculating the superdark simplifies the process during the reduction. Pixels 3σ below average use to be more scarce in the PhotonMAX and their presence is not an issue because we have already corrected the images with the histogram threshold.

Once the blocks are ready, we produce the superdark by calculating the median of all of them, image by image.

The scientific images do not suffer these cleaning processes on pixels which are deflected from the average because they are already minimized in the average of the Power Spectrum. If we detect some death or hot pixels on the camera, i.e. they do not transmit information or they are always too powerful, they shall be eliminated by means of calculating a new value based on the annexed pixels. Some little changes in the routine described previously allow us to detect this kind of pixels.

Once that we have the block of the suprdark, S, in a certain exposure time, we subtract it image by image to the scientific blocks, B, and we make exactly the same with flats, F, which will be used later,

$$B_i^{red} = B_i - S_i, \tag{III.4}$$

and,

$$F_i^{red} = F_i - S_i. \tag{III.5}$$

In the case of the images acquired with the PhotonMAX 512, the camera design provokes an elevated number of counts shown in one of its corners. This is clearly visible in the power spectrum in the uncorrected scientific images and also in the power spectrum of the flats. These images show an open-book shape in addition to the typical zero frequency saturation in both central axes. This is the reason why the correction made by flats is always advisable.

III.1.4 Power Spectrum

We have a large number of images taken with short exposures where the readout noises have being eliminated, as explained in the last section, by using a cleaned dark median image for all images or, using a superdark, image by image.

For each of these reduced images, the quasi-monochromatic incoherent imaging equation applies (Dainty, 1974),

$$I(x,y) = \int_{-\infty}^{\infty}\int_{-\infty}^{\infty} O(x',y')T(x-x',y-y')dx'dy' = O(x,y) * T(x,y), \tag{III.6}$$

being $*$ the convolution operator.

The equation means that the recorded image intensity, $I(x,y)$, is related to the object of interest, $O(x,y)$, by a convolution relationship with the instantaneous transfer point function $T(x,y)$. In the case of a single star being observed its light becomes a "blurred" version of the image of a point source object. The blurred shape and intensity is represented by $T(x,y)$ and depends on the optics involved, both telescope and camera, together with the atmospheric conditions. As we are using speckle interferometry, each speckles present in the specklegrams will reflect this $T(x,y)$. In the case of long exposures, the FWHM and the seeing disk will be the ones that will show it.

The analysis of these images may be carried out in either one of two equivalent ways. Staying in the spatial domain, we could calculate the ensemble average space autocorrelation giving the equation,

$$C(x,y) =< I(x,y) \star I(x,y) >= \{O(x,y) \star O(x,y)\} * \{< T(x,y) \star T(x,y)\}, \tag{III.7}$$

where $\star$ denotes autocorrelation in the spacial domain.

In another way and domain, we can transform the initial equation to the spatial frequency domain using the squared modulus of the Fourier Transform (FT) of the images, i.e., the Wiener Power Spectrum or just the Power Spectrum, represented by $P(f_x, f_y)$. The equation now becomes,

$$P(f_x,f_y) \equiv< |\tilde{I}(f_x,f_y)|^2 >= |\tilde{O}(f_x,f_y)|^2 \cdot < |\tilde{T}(f_x,f_y)|^2) > . \tag{III.8}$$

- $\tilde{I}(f_x, f_y)$ is the Fourier Transform of the image intensity,
- $\tilde{O}(f_x, f_y)$ is the Fourier Transform of the object intensity,
- $\tilde{T}(f_x, f_y)$ is the Fourier Transform of $T(x,y)$,

- $< |\tilde{T}(f_x, f_y)|^2) >$ is called the instantaneous transfer function or the speckle transfer function (STF). We will note it as $S(f_x, f_y)$.

Both equations, III.7 and III.8, are equivalent because $C(x, y)$ and $P(f_x, f_y)$ are Fourier pairs. Equation III.8 indicates that the real object's power spectrum and the power spectrum of the block of images recorded in the camera are linearly related being weighted by the function $S(f_x, f_y)$. This linearity avoid the need to calculate a convolution as we must do in equation III.7.

We will follow the PS option to work with our blocks.

If we have a block with total number of images equal to N, the PS consists of adding the square modulus of the Fourier Transform of each image, those represented by $\tilde{I}_i$,

$$P(f_x, f_y) = \frac{C}{N} \sum_{i=1}^{N} |\tilde{I}_i(f_x, f_y)|^2, \tag{III.9}$$

where f_x,f_y are the elements of square discrete arrays that corresponds to spatial frequencies (Tokovinin, Mason, and Hartkopf, 2010). C acts as a normalization constant that looks forward to achieve the condition $P(0, 0) = 1$, so $C = P(0, 0)$.

Sometimes it will be helpful to restrict the PS till the so-called, cut-off frequency. The cut-off frequency is defined as $f_c = \frac{D}{\lambda}$ so it depends on D, the telescope diameter, and the central wavelength of the filter passband, λ. To restrict the PS in this way, we will use the cut-off normalized frequencies ($\kappa_x = \frac{f_x}{f_c}$,$\kappa_y = \frac{f_y}{f_c}$), and we will ignore the ones that are larger than f_c.

If we analyze the PS of a single star, $P_0(f_x, f_y)$, we will find that we can divide it in two components. At low frequencies, i.e. when $||(f_x, f_y)||^2 < r_0/\lambda$, a strong signal is present. This part corresponds to the seeing-limited image. The other component corresponds to the restriction $r_0/\lambda \leqslant ||(f_x, f_y)||^2 < f_c$, we called it high-frequency term and it is produced by the speckle structure of the speckle images (specklegrams). The term r_0 on previous constrains corresponds to the Fried's parameter.

We will call $P_0(f_x, f_y)$ to the PS of a single star and we will express the two components structure as:

$$P_0(f_x, f_y) \approx |\tilde{T}_{SE}(f_x, f_y)|^2 + 0.435(\frac{r_0}{D})^{-2} T_{DL}(f_x, f_y), \tag{III.10}$$

where $\tilde{T}_{SE}(f_x, f_y)$ is called the seeing-limited short-exposure transfer function that we can calculate as the Fourier Transform of the average recentered image obtained by Shift-and-Add (SAA). Whereas, T_{DL} is the diffraction-limited transfer function of an ideal telescope with the central obstruction ignored,

$$T_{DL}(\kappa) = \frac{2}{\pi}[\arccos\kappa - \kappa\sqrt{1-\kappa^2}], \tag{III.11}$$

and the rightest part of the equation as a whole, $0.435(\frac{r_0}{D})^{-2}T_{DL}(f_x, f_y)$, is called the high-frequency term (Christou et al., 1985; Tokovinin, 2018b). We will see the importance of each part later when we do the analysis of the Autocorrelation Function of a unresolved star.

III.1.5 Power Spectrum Photon Noise

To take also into account the additive noise as well, we need to add it to the original equation III.8 so it becomes,

$$P(f_x, f_y) = |\tilde{O}(f_x, f_y)|^2 \cdot S(f_x, f_y) + N(f_x, f_y). \tag{III.12}$$

Here, $N(f_x, f_y)$ represents the effect on the PS of both the photon noise and the readout noise (Pluzhnik, 2005). We may express it as,

$$N(f_x, f_y) = N_p(f_x, f_y) + N_r(f_x, f_y), \tag{III.13}$$

to separate between the readout noise, it being the $N_r(f_x, f_y)$ term, and the photon noise, $N_p(f_x, f_y)$.

Modern detectors presents a much larger photon bias term than readout noise. Moreover, as we are using previously reduced images where the dark current has being subtracted to calculate and work with the PSs, we can delete the readout term out of the expression III.13. We will focus now on how to correct the photon bias part.

To do that, we will separate the photon bias noise as amplitude, N_0, and normalized photon bias, $n_p(f_x, f_y)$. Then we have:

$$N_p(f_x, f_y) = N_0 n_p(f_x, f_y). \tag{III.14}$$

On one hand, $n_p(f_x, f_y)$ can be determined as the average normalized power spectrum of a flat field block. On the other hand, the amplitude, N_0, can be obtained from the power spectrum beyond the telescope cut-off frequency because, beyond this value, the right part of equation III.8 should be zero. Thus, removing it form III.12

$$P(f_x, f_y) = N(f_x, f_y), \tag{III.15}$$

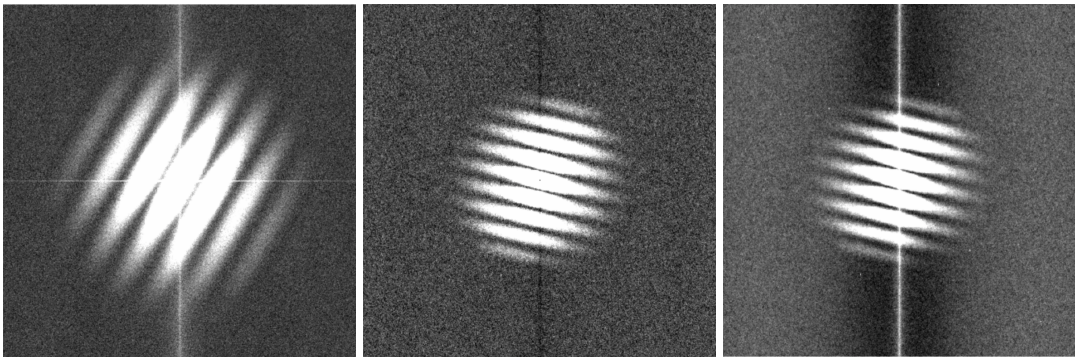

FIGURE III.4: SAO (left) and BAO (center and right) Power Spectrums
Only the center PS has been reduced using a flat

$\forall \mathbf{f} = (f_x, f_y)$ such that $||\mathbf{f}||^2 = ||(f_x, f_y)||^2 > f_c$.

According to that, calculating the average of the PS, $P(f_x, f_y)$, where $||(f_x, f_y)||^2 > f_c$, we obtain the amplitude of the photon noise. Thus, we may remove the amplitude of the photon bias noise, N_0, just subtracting the previous average value from the PS image. In addition, we may mask the region out of the cut-off frequency giving a intensity value of 0 to all those exterior pixels and finally, we may divide the resultant PS by the normalized PS of the flat block to remove the $n_p(f_x, f_y)$ pattern.

The amplitude of the photon noise must always to be dropped for all images. However, as we already mentioned, we will do the flat PS correction for the majority of the data collected in BAO, whereas SAO's blocks do not need it, in general (e.g., III.4).

At the end of previous subsection, III.1.3, we indicated that is common to find central cross features in the PS of the speckle blocks. To avoid them, we will mask the pixels corresponding to central axes of the image. It usually takes two rows and columns and it is rare to need more.

III.1.6 Speckle Transfer Function

The speckle transfer function (STF) indicates the extent to which the different spatial frequency components of the object power spectrum are attenuated by the atmosphere-telescope combination. Dainty and Greenaway (1979) and Korff (1973) calculate for $D \gg r_0$,

$$< |\tilde{T}(f_x, f_y)|^2 > \approx | < \tilde{T}(f_x, f_y) > |^2 + 0.435(\frac{r_0}{D})T_{DL}(f_x, f_y), \qquad \text{(III.16)}$$

where $T_{DL}(f_x, f_y)$ is the diffraction limited transfer function of the telescope, r_0 the Fried's coherent length or parameter (around 5-20cm in good seeing (Dainty, 1981)). The form of

the transfer function can be approximated calculating the power spectrum of an unresolvable star.

Sadly, the STF is not stable in time as it is dependent on seeing conditions, telescope aberrations, vibrations, etc. We can calculate an empirical model following the indications presented in Tokovinin, Mason, and Hartkopf (2010). This model prevents us from obtaining a reference star for each science block and accounts for the changing conditions automatically. To create this model, we could calculate the one-dimensional averaged azimuthally PS, $\bar{\mathrm{P}}(\kappa)$, where $\kappa = (\kappa_x, \kappa_y)$ is the normalized by cut-off frequency pair. The average will remove the fringes and that will result in a good model of the STF when the system presents angular separations between components larger than λ/D (Tokovinin, 2018b).

In another way, Tokovinin, Mason, and Hartkopf (2010) and Tokovinin et al. (2015) suggested a simple 2-parameter synthetic model to be fitted in the range $\kappa_{min} < \kappa < \kappa_{max}$. As κ is normalized, in general, the restrictions become $\kappa_{min} = 0.2$ and $\kappa_{max} = 0.8$. These limits can vary slightly depending on the amount of noise. The model looks like,

$$P_r(\kappa) = \overline{T}_{AD}(\kappa) T_{DL}(\kappa) \cdot 10^{p_0 + p_1 \kappa}, \tag{III.17}$$

where, as before,

$$T_{DL}(\kappa) = \frac{2}{\pi}[\arccos \kappa - \kappa\sqrt{1-\kappa^2}], \tag{III.18}$$

is the diffraction-limited transfer function of an ideal telescope with the central obstruction ignored, p_0 shows the level of the high-frequency component of the PS, and $\overline{T}_{AD}(\kappa)$ is the azimuthally averaged deterministic blur $T_{AD}(f_x, f_y)$ caused by the atmospheric dispersion. In equation III.17 (f_x, f_y) are normalized by the cut-off frequency to (κ_x, κ_y). The authors offer a equation to calculate the dispersion effects,

$$\overline{T}_{AD}(\mathbf{f}) \approx \exp -2\pi^2[(\frac{\mathbf{fx}}{2.506})^2]. \tag{III.19}$$

The blur vector **x** direction is known from the parallactic angle and the detector orientation. Its length in pixels is given by

$$|\mathbf{x}| = [n_{\lambda_1} - n_{\lambda_2}]/p \tan z, \tag{III.20}$$

with z being the zenith distance, n_λ being the refractive index of air at λ wavelength, λ_1 and λ_2 being the bandwidth limits of the filter used to observe, and p is the pixel size.

In our observations we take advantage of the Risley prisms to correct the atmospheric dispersion so the $\overline{T}_{AD}$ factor should be eliminated from our calculations. According to that, the equation III.17 turn out to be,

$$P_r(\kappa) = T_{DL}(\kappa) \cdot 10^{p_0 + p_1 \kappa}. \tag{III.21}$$

The theoretical model predicts

$$(D/r_0)^{-2} = 0.435 \cdot 10^{p_0}. \tag{III.22}$$

The value p_0 matches quite well the half-width of the recentred long-exposure images that can be calculated employing the Shift-and-Add algorithm on the images of the data block, i.e. the specklegrams. So it becomes an useful value to estimate the seeing conditions for each data cube. The other parameter, p_1, shows how the high-frequency component of the PS decrease with the increase in frequency.

This model becomes very useful when the components of the stellar system are close, with separations of order λ/D (Tokovinin, 2018b).

Once we calculare our model, we can divide the masked and reduced block of science's PS by it (Christou et al., 1985),

$$\frac{P(f_x, f_y)}{S(f_x, f_y)} = |\tilde{O}(f_x, f_y)|^2. \tag{III.23}$$

To do this (Wiener-filter) kind of correction, we have to be aware that division by zero could happen, and that would stop our code or something worst. Masking the STF zero intensities, e.g., giving them a very low value different than zero, will solve the issue in most cases.

III.1.7 Autocorrelation Function

The masked and reduced block of science's PS already should give us information about the multiplicity of the light source observed. When we observed a double system over the diffraction limit of the telescope, and the atmospheric conditions did not avoid us to resolved it, we may see a fringe pattern in the PS. But, to detect companions, the auto-correlation function (ACF) is more practical and visual.

As we said, $C(x, y)$ and $P(f_x, f_y)$ are Fourier pairs, being $P(f_x, f_y)$ being the Fourier transform of $C(x, y)$. The Fourier transform can be written as:

$$\tilde{f}(\xi) = \int_{-\infty}^{\infty} f(x) e^{-2\pi x\xi} \partial x, \tag{III.24}$$

for any real number ξ.

So, under suitable conditions f is determined by $\tilde{f}$ via the inverse transform:

$$f(x) = \int_{-\infty}^{\infty} \tilde{f}(\xi) e^{2\pi x\xi} \partial \xi, \tag{III.25}$$

for any real number x.

Thus, if we can calculate the Fourier inverse transform of the PS, we will obtain the ACF. As our PSs are finite and discrete, we can use the Discrete Fourier Transform (DFT) or, even better, the Fast Fourier Transform (FFT). The FFT rapidly computes the DFT of a sequence or its inverse (IFFT) by factorizing the DFT matrix into a product of sparse factors. It manages to reduce the complexity of computing the DFT from $O(n^2)$ to $O(n \lg n)$, where n is the data size.

In our case, n is the total number of pixels per block when we calculate the PS, so n equal to $1000 \times 512 \times 512$ for BAO blocks and $2000 \times 512 \times 512$ for SAO ones. When we calculate the ACF, we just do the inverse Fourier Transform of a single image that can be seen as a 512x512 array. We use numpy.fft library on python to compute both transformations.

When we work on python we need to be careful with the next topic. We consider the origin of the spatial images as the centre of the image and we consider the origin of the frequency images also as the centre of the image. Python did not work with that convention and it usually considers the origin as the top left corner when you use matplotlib to display the image and the user do not flip the y-axis. It is important to be aware of this aspect when you create the code. In this text, we will continue considering the origins as the centres of the images.

Previously, in section III.1.4, we showed how $P_0(f_x, f_y)$, the PS of a single star, has a two components structure expressed by:

$$P_0(f_x, f_y) \approx |\tilde{T}_{SE}(f_x, f_y)|^2 + 0.435(\frac{r_0}{D})^{-2} T_{DL}(f_x, f_y), \tag{III.26}$$

and the first component that we called the seeing-limited short-exposure transfer function is transformed by the FFT into a broad seeing-limited component, called seeing-pedestal. The second part, the high-frequency term, is responsible for the narrow diffraction-limited peak at the origin of the ACF image.

Whereas, when we can observe the characteristic fringes in the PS image that indicatee the duplicity of the system, i.e., the case of a resolved binary star, the ACF images will also show

a narrow origin-located peak as well as two more narrow and equal peaks located 180° to each other at some separation to the centre of the image. The three of them are located over a wide seeing pedestal as in the single case.

This pedestal could be crudely removed adding another mask to the PS. To this end, we mask the centre of the PS image which means that we set zero the low spatial frequencies, e.g., $||f||^2 < 0.2 \cdot f_c$. This filter will cause that the ACF shows a concentric "ringing" structure around its center. To avoid it, we can handle more developed filters like the Butterworth filter or just to divide the PS by its azimuthal average at those low frequencies. The filtered ACFs computed from the filtered and masked PSs can be used together to determine if the star that we are observing is a binary star as well as to provide data related with the position of the secondary component and the magnitude difference between it and the main component.

Our code allows to successful detection the secondary peaks, and to storage their intensity and position. As both peaks has equal intensity, and are located symmetrically 180° confronted, it is only required to detect one of them to know the position of the another. Using the pixel position detected, we calculate the angle between the peak and a fixed reference axis centered in the origin. Also, using the theoretical pixel size that is calculated as we detailed in III.1.1, we calculate the angular separation between the centre of the ACF image and the secondary peak.

The presence of two secondary peaks is due to the fact that we lost the phase information during the calculation of the Fourier Transforms of each image that we add to create the PS. When the IFFT transform the PS back to the space domain it give us the two posible phase options. So, one of the peaks will be located at the position of the secondary component in the case of a binary star and the other is just a phantom detection created during the process.

III.1.8 Differential Magnitude

Once that we have the θ and ρ values provided by the ACF, we can generate a model of the pure fringes that would be generated from two points of light located at the same way. For that, we create a 2D vector, $\mathbf{r}=(\rho\cos\theta, \rho\sin\theta)$, and the theoretical fringes will be the result of:

$$A + B\cos 2\pi(f_x, f_y)\mathbf{r}, \tag{III.27}$$

where A and B are obtained from the Δm information.

In the previous section, we indicated that we storage the intensity of the secondary peak. As we normalized the PS to be one in the center of frequencies, the ratio between the main peak (the intensity of which is equal to one) and the secondary peak will help us to calculate A and B. The contrast of fringes in power spectrum, β, must verify:

$$\beta = \frac{I_{max} - I_{min}}{I_{max} + I_{min}}, \tag{III.28}$$

as theoretically $I_{max} = A + B$ and $I_{min} = A - B$, the equation becomes:

$$\beta = \frac{2B}{2A} = B/A, \tag{III.29}$$

and the ratio between the peaks in the ACF must be equal to $\beta/2$.

So if we calculate the median value in an annular region out of the center seeing peak of the PS the result must be A. If we calculate the contrast in that region as in eq. III.28, we will obtain the β and we can derive B. Another way is to rotate the image θ degrees in order to locate the fringes at perpendicular position in the image, then make a cut where the waves be clearly visible, and calculate A and B directly fitting a 1D model to it.

Once we have $A + B\cos 2\pi(f_x, f_y)\mathbf{r}$ we can create the final model, $P_{mod}(f_x, f_y)$, multiplying by one of the STF models that we called $P_r(f_x, f_y)$,

$$P_{mod}(f_x, f_y) = P_r(f_x, f_y) \cdot [A + B\cos 2\pi(f_x, f_y)\mathbf{r}]. \tag{III.30}$$

This model will allow us to better fit the values of A,B,ρ and θ and calculate their errors.

As we said, the STF can be calculated in several ways. One option is to use the 2-parameter synthetic model once we calculate p_0 and p_1 of the observation. Then we use,

$$P_r(\kappa) = T_{DL}(\kappa) \cdot 10^{p_0 + p_1 \kappa}, \tag{III.31}$$

where $\kappa = (\kappa_x, \kappa_y)$ is the normalized by cut-off frequency pair. To calculate p_0, we just need to calculate the intensity average at $0.2 \cdot f_c$ annular region. p_0 will be the $\lg_{10}$ of this value. Another way is to calculate the Fried's parameter using the seeing disk or the FWHM. p_1 is related to how it drops the intensity to the cut-off frequency. Its value is more stable and a good approximation can be calculated from the set of calibration stars.

This kind of approximation will work well for close systems whereas, for separated systems, we will use the one-dimensional averaged azimuthally PS, $\bar{\mathrm{P}}(\kappa)$. As we said in III.1.6, the average will remove the fringes and that will result in a good model of the STF when angular separations are larger than λ/D (Tokovinin, 2018b).

Another way to calculate the model when the angular separation is small is to use the Fourier Transform of the SAA image obtained from the images of the block that are well centered in the FOV.

Once we have the model, we can use the Levenberg–Marquardt method for non linear least square fitting between the model and the PS. With this method, we can adjust better the values of θ, ρ, A and B (i.e. β).

The error of the measured PS at each point (j_x, j_y) is:

$$\sigma_j^2 = (P(j_x, j_y) + N_0)/N. \tag{III.32}$$

Where N is the total number of images, N_0 is the photon noise amplitude, and $P(j_x, j_y)$ is the value of the PS at the frequency point (j_x, j_y) after remove all the noises. This will be valid for $\kappa_{min} < \kappa = (\kappa_x, \kappa_y) < \kappa_{max}$.

The quality of the fit between model and PS is evaluated with the normalized residuals,

$$\frac{\chi^2}{N_P} = \frac{1}{N_P} \sum_j \frac{(P_j - P_{mod,j})^2}{\sigma_j^2}, \tag{III.33}$$

using the total number of frequency plane points fitted, N_P.

This method of evaluation is being used by Tokovinin, Mason, and Hartkopf (2010) in the campaigns that are developing in SOAR. The authors indicate that for noisy data $\frac{\chi^2}{N_P} \sim 1$, but for bright stars, values could up till 20.

Once that we fit the model and we adjust the final values of A and B, in order to calculate the magnitude difference, we can use both the contrast fringes in the PS $\beta = B/A$ or the ratio of the peaks in the ACF $\beta/2$. As the model provided better adjusted A and B values together with an error estimation, the first option will be usually chosen. The final value for magnitude difference will be equal to:

$$\Delta m = -2.5 \log_{10}[\frac{1 - \sqrt{1 - \beta^2}}{\beta}]. \tag{III.34}$$

III.2 SAO SI campaigns

The observational campaigns at SAO provide us with blocks of speckle images with high resolution as we use a 6m telescope. The campaigns are conducted by a team that is run by Y.Y Balega. We obtained 186 blocks for 176 systems between 2012 and 2014. The number of flats and darks available is fewer than in the campaigns at BAO (compare tables III.2 and III.1). This does not represent a big problem because the Andor iXon DU-897 camera with e2v 512×512 px eMCCD97 which the group of SI at SAO used between 2007 and 2013 is much more modern than our PhotonMAX and the readout and photonic noises are more faint

TABLE III.2: Spetial Astrophysical Observatory SI data

Campaign	Nights	Objects	Science Blocks	Mask Blocks	Dark Blocks	Flat Blocks
June 2012	3	29	29	3	8	0
Nov 2013	2	35	35	0	2	8
April 2014	2	34	34	0	8	0
Dec 2014	2	78	88	0	6	0

and stable. From 2013 on, they used an Andor iXon Ultra 897 that can cooler till -80° and allows a faster readout (20 frames/sec). This leading-edge camera has great stability.

The reader can see the articles published by SAO's speckle research group in the last years in order to get more information about the acquisition process, the instrumentation, the detection limits, etc. (Balega et al., 2017; Rastegaev et al., 2014) as our observations and theirs have been carried through simultaneously in many occasions. Balega et al. (2017) detailed general aspects of the observations made between 2006 and 2016, to where our campaigns also belonged (Docobo et al., 2006, 2010).

It should be noted that among the filters used in these observations, what we call "550" in the table III.3 and which corresponds to $\lambda/\Delta\lambda = 550/20$, is comparable to the H_p filter of Hipparcos. In Balega et al. (2017), we can check that the seeing conditions in these campaigns vary from 0"7 FWHM under the best conditions to 3" FWHM under the worst. According to the authors, if the seeing is in moderated values (1"-1"5), they can achieve the diffraction limit of the telescope for components showing a magnitude difference lower that $\Delta \approx 5$. Nevertheless, when conditions are unfavourable (>2") the quality of the observations do not allow to get definitive measurement. Finally, the detection boundaries reach the angular separations of $\rho > 0''2$ if the difference in magnitude between components exceeds the 5 magnitudes and the system is not excessively closed. However, in closed systems, if the difference in magnitude is below 3, the capacity of detection reaches values between 0"02 y 0"1. Obviously, these limits also depend on the conditions of the seeing.

In order to calibrate the size of pixels and the mismatch in the angle of instalación, SAO uses a double-hole mask installed opposite to primary focus, $f/4$, and the distance to the focal plane is 4007±2mm. The diameter of the both holes is of 15mm and the distance between them is of 833±1mm. The young fringes shown in the images taken with the camera allow to determine the scale and any mistake in the position. The main source of error is the focal distance respect to the primary mirror. In order to correct this, they adapted the value to 24025±15mm. The observations with the mask were made at nights with really good seeing

TABLE III.3: Spetial Astrophysical Observatory SI calibration data

Campaign	Filter 550		Filter 600		Filter 700		Filter 800		Filter 900	
	θ offset °	pixel size arcsec	θ offset °	pixel size arcsec	θ offset °	pixel size arcsec	θ offset °	pixel size arcsec	θ offset °	pixel size arcsec
Oct 2010	1.464 ±0.0559	0.00886 ±1.221e-5	1.489 ±0.0397	0.00892 ±8.712e-6	1.55 ±0.0606	0.00888 ±1.325e-5	1.585 ±0.0497	0.00914 ±1.116e-5	–	–
June 2012	1.204 ±0.0434	0.00887 ±9.455e-6	1.263 ±0.0309	0.00892 ±6.783e-6	–	–	1.315 ±0.0362	0.00917 ±8.161e-6	–	–
Feb 2014	1.214 ±0.237	0.00885 ±5.164e-5	1.229 ±0.0657	0.00889 ±1.437e-5	1.291 ±0.0086	0.00896 ±1.901e-6	1.362 ±0.0162	0.00912 ±3.638e-6	1.362 ±0.0162	0.00909 ±2.714e-6

conditions. The calibrations attain an error of tenth of degree for position angle and 0.1% to scale. It is important to indicate that as the telescope is azimuthal, the measurements of angular position must be corrected by the paralactic angle keeping in mind both the sideral time and the zenith distance.

In Table III.3, the data of calibration for the size of the pixel and for the offset in the position angle of installation of the camera that were supplied by the research team of SAO are included. All of this data comes from the usage of the mask through which bright stars are observed. As we can see, the mismatch in the installation angle does not surpass 1°5 and the pixel size obtained empirically by using the mask is not far from the theoretical size of pixel, 0.0086”/pix. As the distances in pixels that we manage in our observations are of a few dozens, the separation error accumulated is not huge. To obtain the final astrometric results, we take advantage of the calibration values provided in June 2012 for June 2012 campaign and February 2014 for April 2014 campaign. The rest of campaigns use the value resulting to average all the calibrations and errors.

We have had the cooperation of the SAO’s speckle research group in all our campaigns. Y. Y. Balega as its PI, D. A. Rastegaev and V. V. Dyachenko as main observers, as well as A. F. Maksimov as engineer.

III.3 BAO SI campaigns

As we have previously said, one of the main tasks that we have achieved was the start-up and the realization of observational campaigns with SI at the Byurakan Astrophysical Observatory. The description of the observations carried out until November 2017 has already been published in the first volume of the magazine, Communications of the Byurakan

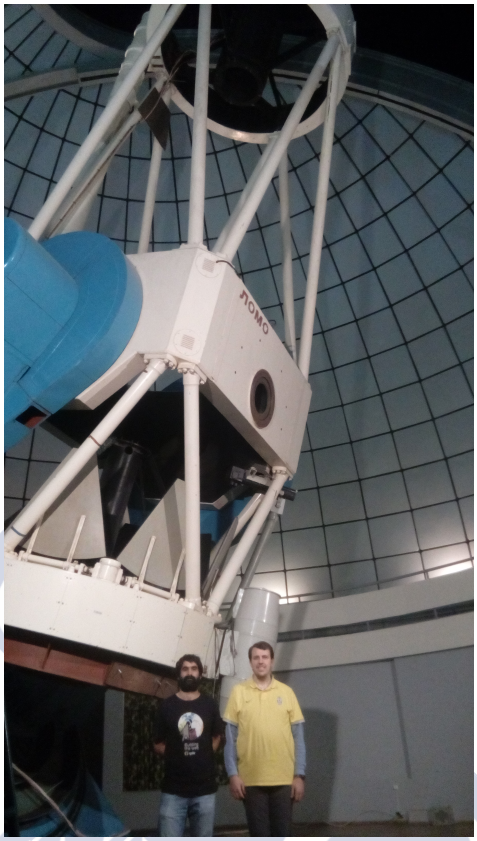

FIGURE III.5: BAO telescope

Astrophysical Observatory. "Speckle Interferometric Observations on 2.6 m telescope of BAO" (Docobo et al., 2017b) is added at the end of this section. This publication has recently been recovered by the personnel of BAO after years of inactivity and yet it is not indexed in the Journal Citation Report.

As stated, in the end of 2017, we had fulfilled 23 observational nights in three different campaigns. Furthermore, we must add two extra nights in the last campaign that was done in May 2018 but they are not reflected in that text. In October 2016, the atmospheric conditions allowed us to observe 5 nights when we could gather images of 67 different systems. During the campaign of May-June in 2017, the number increased to 8 nights and 183 systems. Another doctoral student from OARMA, Luca Piccotti (on the right of the Fig. III.6), also took part in this campaign. From October to November 2017, we observed 183 systems over ten nights. Sadly, from May to June 2018, the atmospheric conditions prevented us from observing. We can only use the telescope and take some images during two nights.

In total we have acquired more than one thousand and one hundred blocks which contain images from stellar systems of scientific interest and also more than a hundred of darks and sixty flats as well. The exact number is shown in table III.1.

The table shows how many observations correspond to the magnification 8x, in the column Wide Field Blocks. These systems can be double-systems that are split up by an angular distance which we cannot cover with the field of view (FOV) provided by the 20x magnifying microscope. However, this configuration with the big FOV was used for triple or multiple systems where the 8x microscope allows the observation of multiple components at the same time. It is quite usual, in these double and triple systems, to obtain other blocks with magnification 20x, which corresponds to the small FOV. We can observe each of the isolated components in the system in these kind of blocks.

Generally, in our observational campaigns, we take at least two blocks per configuration and system. That is, once we have located the star in the centre of the FOV and we have chosen a filter and a magnification, we acquired two blocks in a row. It is not so unusual to take blocks with several configurations but the most common is to have blocks for two different bandwidth.

The data obtained along these campaigns have been reduced partially, even though this process is still ongoing. At present, we have cleaned the noisy blocks, calculated the PSs by cleaning the photon noises, and gotten rid of the ACFs. In those, we have detected the positions of the secondary components and the ratio between the secondary peak and the central one, that is, β. Now, we have to calibrate the results from these images and orbital information in order to detect the error in the accuracy of the pixel and narrow down the mismatch in the installation camera offset. We have to finish the routine that allows to adjust the model to the PS by using Levenberg-Marquardt. Sadly, it has not been possible to improve all the details before the deadline.

Once that we have obtained the final values of the positional parameters, θ and ρ, we will intentionally contrast them with the ephemeris expected from the cases of those systems which have a well defined orbit. Some of these systems corresponds to that ones provided for calibration purposes in the WDS ORB6 (Hartkopf, Mason, and Worley, 2001).

This calibration must be realized in every campaign in order to define the angle mismatch of

TABLE III.1: Byurakan Astrophysical Observatory SI campaigns

Campaign	Nights	Objects	Science Blocks	Wide Field Blocks	Dark Blocks	Flat Blocks	Calibration Blocks
Oct 2016	5	67	228	4	15	0	39
May-June 2017	8	183	429	11	24	14	10
Oct-Nov 2017	10	183	435	19	65	48	22
May 2018	2	7	18	0	23	0	1
Total	25	440	1110	34	127	62	72

FIGURE III.6: BAO's 2.6m telescope building
N. Melikian (center), G. Paronyan (right), and J. Gómez Crespo (left)

each of them. To achieve this, we have observed numerous systems of grade 1 in each of the campaigns. Exceptionally, we can also use systems with grade 2 as long as the quantity of systems with grade 1 are not sufficient.

We have had the cooperation of the 2.6m telescope operators at BAO and of their engineers in all our campaigns, especially Gurgen M. Paronyan (operator), Mkrtich Gevorgyan (engineer and operator), Tigran H. Movsissian (Head of 2.6 m telescope laboratory), and Kamo S. Gigoyan (operator). Although the process of obtaining results is not yet over, the initial and partial results related to the angular position and separation show that the combination of eMCCD and OARMA 2.6m telescope at BAO provide the expected results for binaries with separation angle below 90 miliarcseconds. The magnitude limit is close to 12 in V and the difference in magnitude that we expect is larger than 4. Thank to Dr. Melikian's cooperation in the logistic processes, the timing, the camera setup, and the organization of the campaigns, we may have obtained all such measures that will be reflected in new orbits in a not very distant future. The final results shall show that the sending of the camera to BAO has been a correct decision.

USC
UNIVERSIDADE
DE SANTIAGO
DE COMPOSTELA

Chapter IV

Published articles using SI

IV.1 Introduction

This dissertation was written by Jorge Gomez Crespo as a compendium of research articles according to the standards indicated by the RD 99/2011 and the Escola de Doutoramento Internacional (EDI) of the Universidade de Santiago de Compostela (USC).

In this Chapter, we explain the scientific interest of three papers that have been published or accepted for publication in high impact journals in the fields of Astronomy and Astrophysics. Concretely, two of them can be found in The Astronomical Journal that hold top positions in the second quartile, and the other has been accepted by Monthly Notices of the Royal Astronomical Society a first quartile journal published by Oxford University Press on behalf of the Royal Astronomical Society.

All three articles contribute important information concerning the physical and dynamical properties of double and multiple star systems within the research lines of Commission G1 of the International Astronomical Union, which are those of the research team of the Observatorio Astronómico Ramon María Aller of the University of Santiago de Compostela.

All of those articles were coordinated by the Director of this dissertation within the frame of different international collaborations in which the author of this text actively participated in speckle register programs at important astronomical installations in Russia and Chile as well as worked in the exploitation of said scientific data. Under the direction of Prof. Docobo, the tasks included determining orbits and physical parameters of great value as well as studying the evolutionary tracks of selected objects.

The mathematical apparati utilized has been extensive and includes the algorithms of reduction of the observations themselves as well as the methods of calculus and improvement employed in order to determine orbits and, finally, the procedures used to obtain masses, orbital and dynamical parallaxes, absolute magnitudes, luminosities, and evolutionary tracks.

IV.2 SOAR

In this section, we present two articles that have been published in two different journals, The Astronomical Journal and Monthly Notices of the Royal Astronomical Society.

The articles, *Orbits of 12 Southern Binaries Based on SOAR Speckle Observations* and *Orbits of 14 Binaries Based on 2018 SOAR Speckle Observations* are grounded in the interferometric measurements obtained with the High Resolution Camera (HRCAM) (Tokovinin and Cantarutti, 2008) mounted exclusively at the Southern Astrophysical Research Observatory (SOAR), which is a 4.1 m telescope . This camera has been used on this telescope in Cerro Pachón (Chile) since 2008 (Tokovinin et al., 2018) and, today, it works in conjunction with the SOAR Adaptive Module (SAM, (Tokovinin et al., 2016)). The instrument is operated exclusively by PI Andrei Tokovinin. The manual contains all of the technical characteristics of the camera.

The process of reduction and analysis of the images is performed with software written by A. Tokovinin in IDL. This software was made available to us in order to serve as the basis of what we have constructed to work with the images obtained in our campaigns at the Special Astrophysical Observatory (see III.2) as well as with images acquired with the 2.6 m telescope at the Byurakan Astrophysical Observatory (see III.2). The theoretical fundamentals that support the reduction process are explained in II. Information that pertains to the calculation of the power spectrum, the autocorrelation function, and the magnitude difference is explained in Chapter III. As our construction was based on the Tokovinin software, the majority of the techniques used by the author to simulate the PS and to calculate the difference of magnitude have been explained in III.1.6 and III.1.8.

Our collaborator and a co-author of these articles, R. A. Méndez, was responsible for arranging the observation times and to provide the measurements once they were obtained by A. Tokovinin. The observing time was allocated by the Chilean National Time Allocation Committee (CN2015B-6 and CN2018A-1 programs, respectively). It was necessary for the author to travel to the CTIO installations at La Serena (Chile) in September of 2015 in order to participate in the observations in person as commented in the preceding chapter.

In the two articles, we reported the study of 26 systems of which 23 has austral declinations. These objects were selected after an exhaustive evaluation of a large number of multiple star systems indexed in the Washington Double Star Catalog (WDS) and in the Sixth Catalog of Orbits of Visual Binary Stars (WDS ORB6) (Hartkopf, Mason, and Worley, 2001). For said evaluation, the Director of OARMA, J.A. Docobo worked with the Observatory personnel to compare the orbits of hundreds of systems, the dates of the last observations,

[0]The Southern Astrophysical Research (SOAR) telescope is a joint project of the Ministério da Ciência, Tecnologia, e Inovâçao (MCTI) da República Federativa do Brasil, the U.S.National Optical Astronomy Observatory (NOAO), the University of North Carolina at Chapel Hill (UNC), and Michigan State University (MSU).

their ephemerides, and their position in the celestial sphere at which the observations were going to be conducted. This careful selection process allowed us to find a series of objects for which new observations would be useful in order to considerably improve their orbits.

Ultimately, the following double star systems were observed and recalculated. They are: WDS 01477-4358 (I 52), WDS 01500-0408 (A 2602), WDS 02514-2139 (DON 43), WDS 03189-0101 (BU 1177), WDS 04142-4608 (RST 2338), WDS 06274-2544 (B 114), WDS 18434-5546 (B 398), WDS 20002-5522 (B 459 BC), WDS 20081-3929 (RST 2134), WDS 22007-5002 (I 1450),WDS 22504-1744 (DON 1038 - BD-18 6201), WDS 06478+0020 (STT 157), WDS 07003-2207 (FIN 334Aa,Ab), WDS 07013-0906 (A 671), WDS 10174-5354 (CVN 16Aa,Ab), WDS 12155-3106 (RST 1658), WDS 12572+0818 (FIN 380), WDS 13044-1316 (HU 642), WDS 14243-3838 (RST 1785), WDS 16094-3103 (I 557), WDS 17115-1630 (HU 169), WDS 17119-0151 (LPM 629), WDS 17563+0259 (A 2189), WDS 18464-2755 (RST 2073), and WDS 19035-6845 (FIN 357).

Some of those binaries also presented characteristics that enhanced the importance of their calculated orbits.

- DON 1038: There was no available information concerning the spectrum. With the masses deduced from our orbit along with the dynamical parallax and the available photometric information, we were able to assign an approximate spectral type for it. The orbital parameters, a" (the semiaxis major), P (the period), and the apparent magnitude of the components yielded a table of spectrum-mass by applying the algorithm of Baize-Romani (Baize and Romani, 1946; Heintz, 1978). In the table, the components correspond to the K4-K5 spectral types ranges. Photometrically, the information available in SIMBAD indicated that the most probable spectra for both components corresponds to K4.
- A 671 and RST 2073: There was no information regarding parallax measurements for which the dynamic parallax that we calculated for these systems should be a good approximation.
- DON 43, BU 1177, B 459, RST 2134, I 1450, DON 1038, HU 642, RST 1785, and RST 2073: Until this time, there were no orbits that were calculated using high precision measurements. For that reason, the new orbits obtained using SI measurements significantly improved the previous.
- CHR 232 Aa,Ab: The orbit published in Gomez et al. (2016) is the first calculated for this system although, in an almost simultaneous manner, another orbit was calculated by A. Tokovinin (Tokovinin, 2016).

The orbits published were calculated using the method of Docobo (1985) with which a set of orbits passing through three observations or normal positions are obtained. In the majority of cases, this permits the utilization of more precise observations in order to construct the set. The final orbit is selected from the orbits that fit the three position according to the

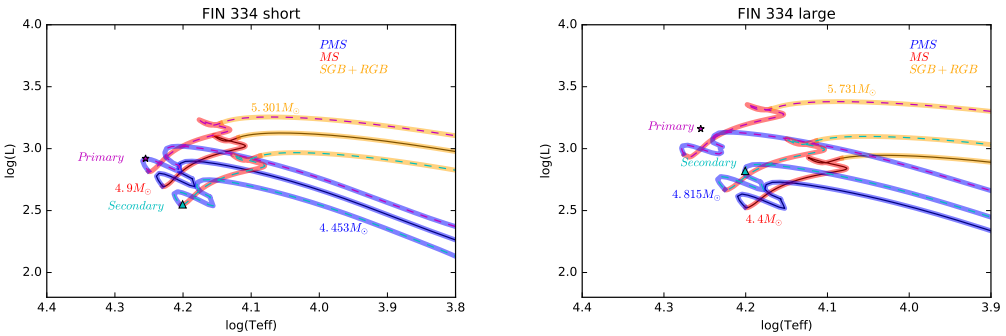

FIGURE IV.1: HR diagram plus evolutionary track for FIN334, short period (left) and long period (right)

criteria detailed by Docobo (2012) that intends to not only minimize the rms with respect to all of the other observations, as do other methods, but also to attempt that the obtained results fit the available system information, as is its spectral type or parallax. The selection of the measurements to be used is made as a function of the historical data presented in Mason et al. (2001c) (interferometric measurements) and in Worley (1997) (micrometric measurements). In order to calculate the rms, a weight is assigned to each observation as explained in Docobo and Ling (2003). Recently, in Docobo, Tamazian, and Campo (2018), a recompilation of the selection criteria for orbits and a new facet in the application of Docobo's method can be seen.

In both articles, we present the orbital parameters of each system (the period in years, the epoch of periastron passage in Besselian years, the eccentricity, the semiaxis major in arcseconds, and the inclination, the angle of the node, and the argument of the periastron in degrees). We also calculated the ephemerides of the following five years and we provided other interesting parameters such as the dynamical parallax and the mass of each component.

In the case of 12 systems studied in the second article (FIN 334Aa,Ab, A 671, RST 1658, FIN 380, HU 642, RST 1785, I 557, HU 169, LPM 629, A 2189, RST 2073, and FIN 357) a section was added in which these objects can be located in the Hertzsprung-Russell diagram. The methodology used could not be applied to two of the systems: STT 157 and CVN 16 Aa,Ab. This is due to the fact that the first contains a class III giant for which the Baize-Romani algorithm is not calibrated while in the case of CVN 16 Aa,Ab, the measurements of the difference of magnitude between the components is not known which impedes the calculation of the absolute difference of magnitude of them.

In order to construct the isochrones that we have used in this article, we have used the interpolator available in the web of MESA Isochrones and Stellar Tracks (MIST) (Choi et al., 2016; Dotter, 2016) using data regarding the metallicity of the system.

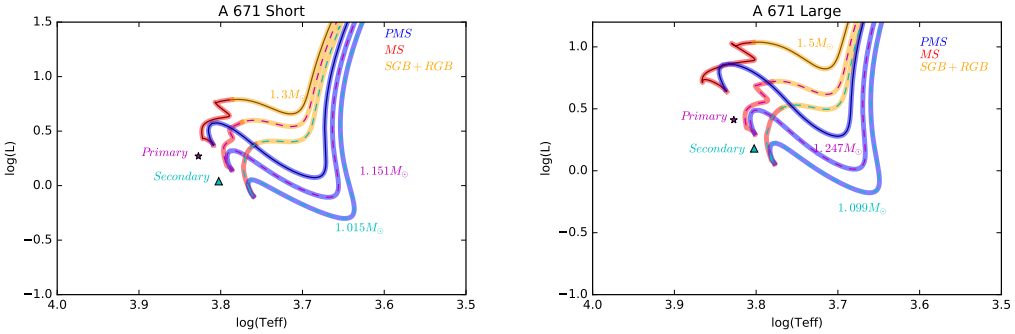

FIGURE IV.2: HR diagram plus evolutionary track for A671, short period (left) and long period (right)

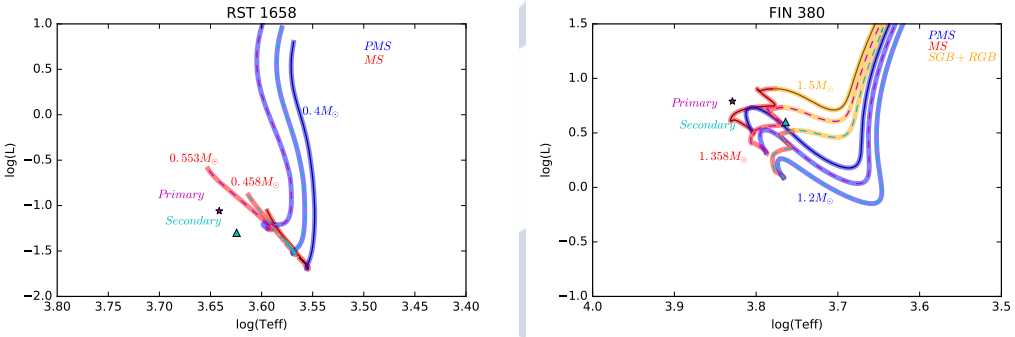

FIGURE IV.3: HR diagram plus evolutionary track for RST1658 (left) and FIN380 (right)

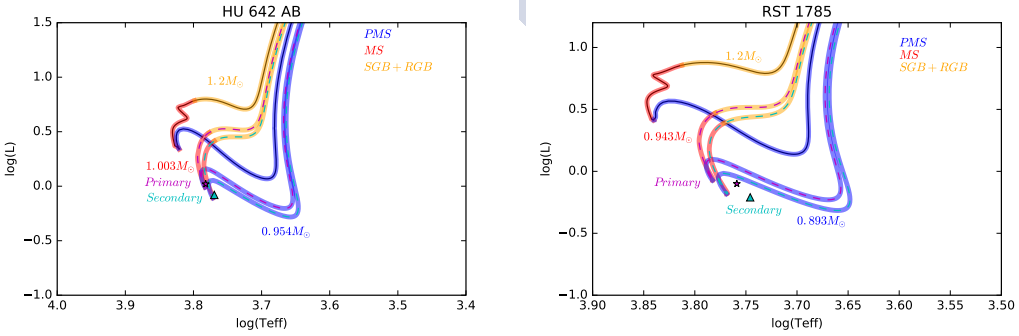

FIGURE IV.4: HR diagram plus evolutionary track for HU642 (left) and RST1785 (right)

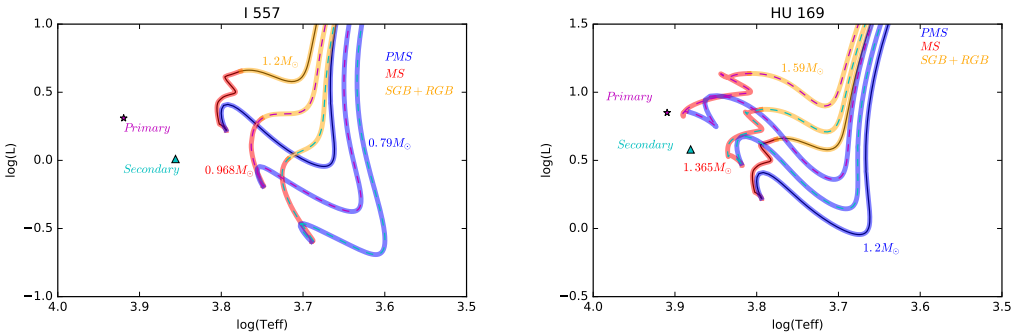

FIGURE IV.5: HR diagram plus evolutionary track for I557 (left) and HU169 (right)

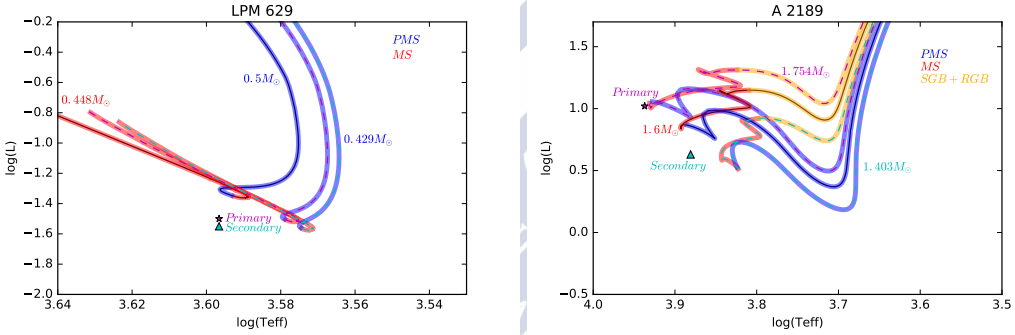

FIGURE IV.6: HR diagram plus evolutionary track for LPM629 (left) and A2189 (right)

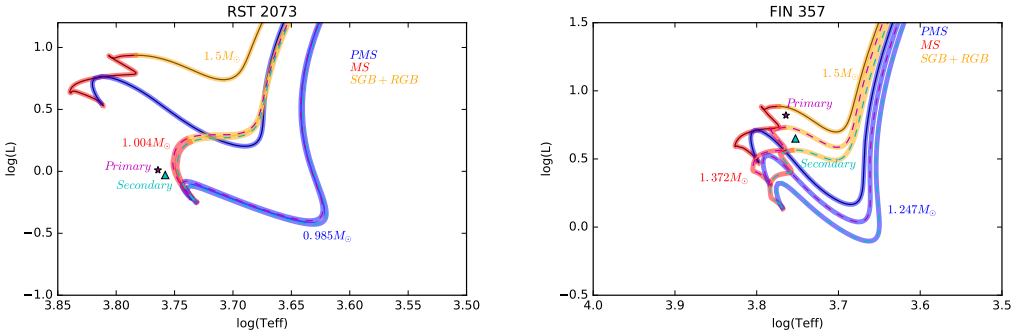

FIGURE IV.7: HR diagram plus evolutionary track for RST2073 (left) and FIN357 (right)

The absolute magnitudes of the components are calculated from the dynamical parallaxes derived from the new orbits, using the formula (Torres, 2010):

$$log\frac{L}{L_\odot} = -0.4(M_V - V_\odot - 31.572 + (BC_V - BC_\odot)), \tag{IV.1}$$

where L is the luminosity, M_V is the absolute magnitude of the star, and $V_\odot$ is the apparent visual magnitude of the Sun (Torres, 2010). BC_V and $BC_\odot$ are the bolometric corrections of the star and the Sun (Straizys and Kuriliene, 1981) with respect to the V band.

We have used the other available interpolator in MIST to calculate the stellar evolutionary tracks based on the derived mass for each component thanks to the new orbits. MIST uses Modules for Experiments in Stellar Astrophysics (MESA) (Paxton et al., 2011, 2013, 2015) for the calculation of the evolutionary tracks. The information related to metallicity was obtained from various catalogs (Ammons et al., 2006; Anderson and Francis, 2012; Gaidos et al., 2014). We used the calibrations of Gray (2005) to calculate the temperature. In order to work with the MIST files, we have altered the script/demo provided on the Web page in Resources. As our intention was to provide the information relative to the age of the systems, we have not published the information provided by the evolutionary tracks.

These diagrams (IV.1, IV.2, IV.3, IV.4, IV.5, IV.6, and IV.7), that, as we have said, we have not published, permit us to locate the components on the HR diagram and to see in which phase of evolution they are.

When it is time to interpret the diagrams, we have to keep in mind that the evolutionary tracks are constructed on the basis of the actual masses of the components and not on the initial masses.

In addition to situating the components in their evolutionary moment, by using the data provided by the evolutionary tracks and obtained from MIST, we are also able to contrast the calculated luminosity with the expected luminosity throughout the evolution of the systems (IV.8, IV.10, IV.12, IV.14, IV.16, IV.18, and IV.20). The same occurs with the effective temperature (IV.9, IV.11, IV.13, IV.15, IV.17, IV.19, and IV.21).

All of these diagrams help us to better understand the systems that we are studying and to infer their age. Nevertheless, the calibration that we have used for the temperature data is from 2005 (Gray, 2005). Moreover, in the cases where there is no available information relative to the metallicity, we have supposed that this corresponds with the solar. We believe that if if we improve the calibration used and if we better infer the metallicity, we would be able to obtain more exact results. The margins of error and the relation between the quality of the orbit and the results of these diagrams are also topics to be treated in future studies.

We should mention the relative importance that these works have at the time of calibration of the results obtained by the Gaia space mission (Gaia Collaboration et al., 2016, 2018). When

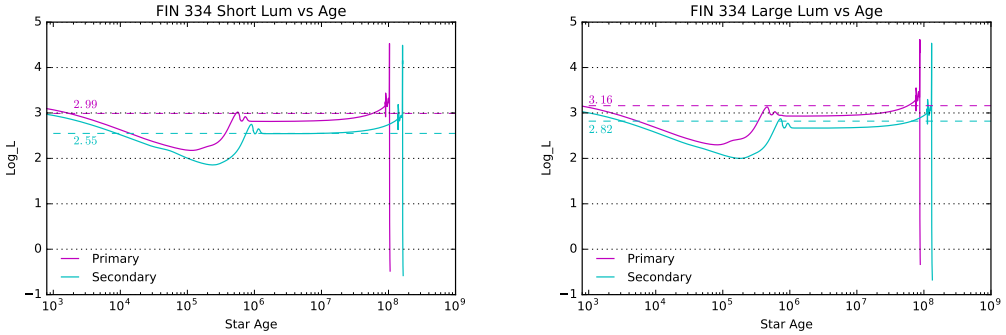

FIGURE IV.8: Luminosity evolution vs Luminosity for FIN334, short period (left) and long period (right)

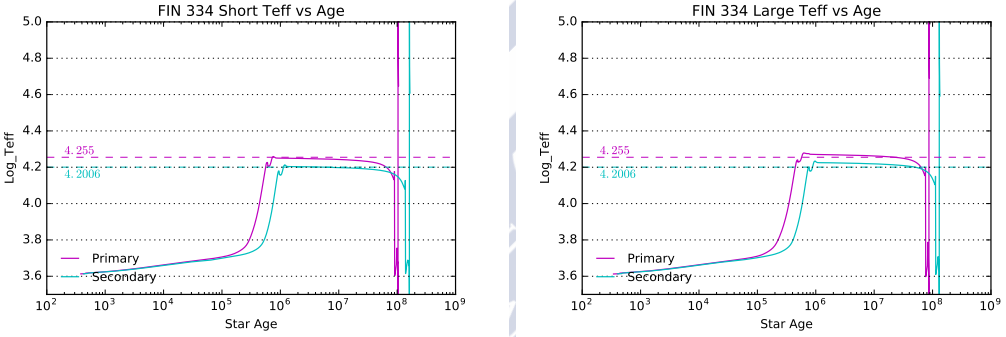

FIGURE IV.9: Teff evolution vs Teff for FIN334, short period (left) and long period (right)

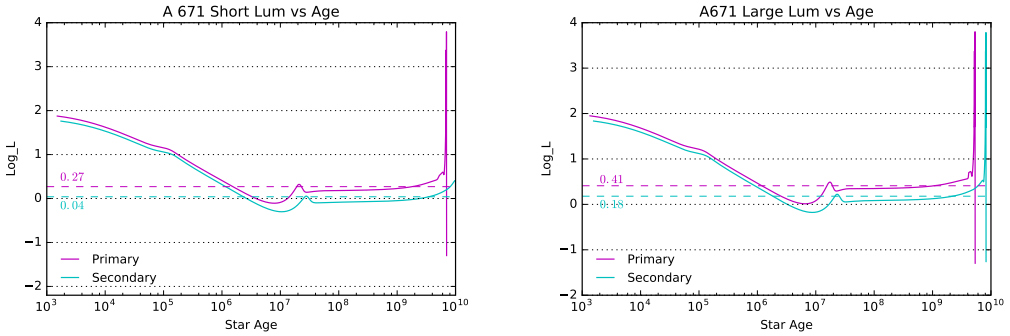

FIGURE IV.10: Luminosity evolution vs Luminosity for A671, short period (left) and long period (right)

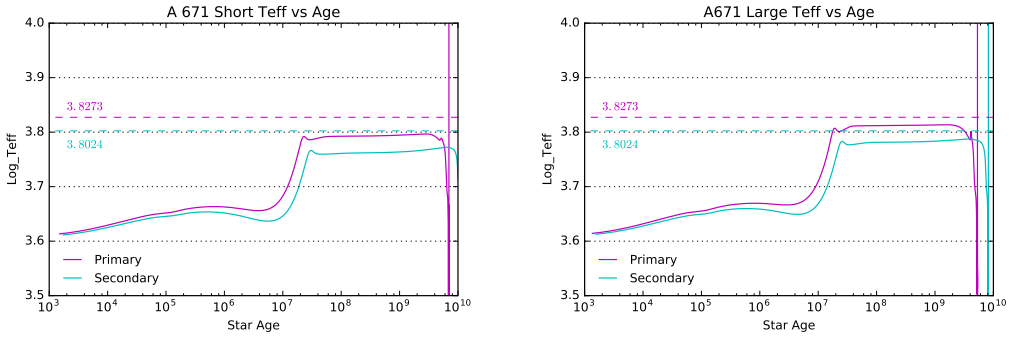

FIGURE IV.11: Teff evolution vs Teff for A671, short period (left) and long period (right)

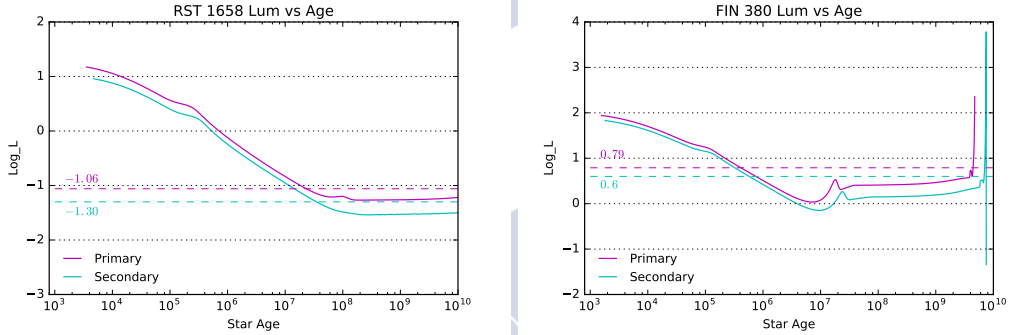

FIGURE IV.12: Luminosity evolution vs Luminosity for RST1658 (left) and FIN380 (right)

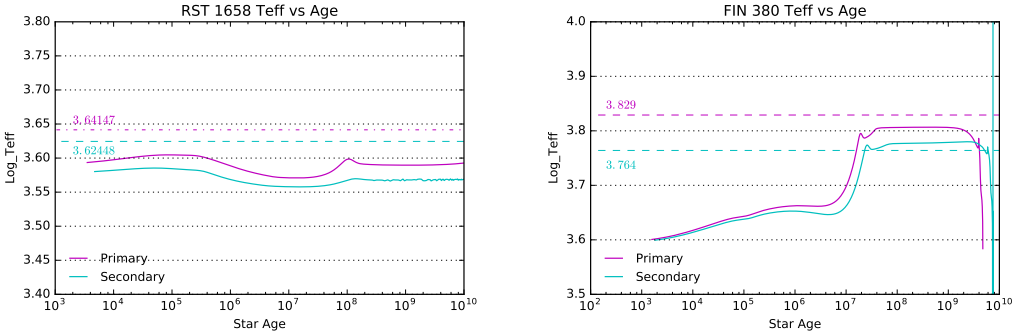

FIGURE IV.13: Teff evolution vs Teff for RST1658 (left) and FIN380 (right)

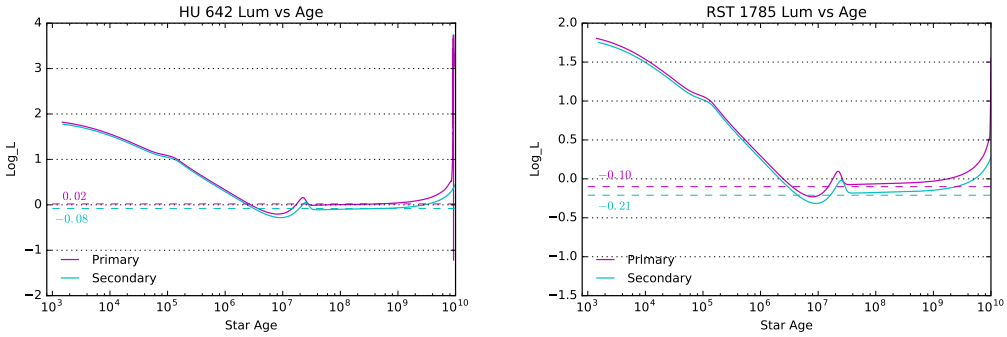

FIGURE IV.14: Luminosity evolution vs Luminosity for HU642 (left) and RST1785 (right)

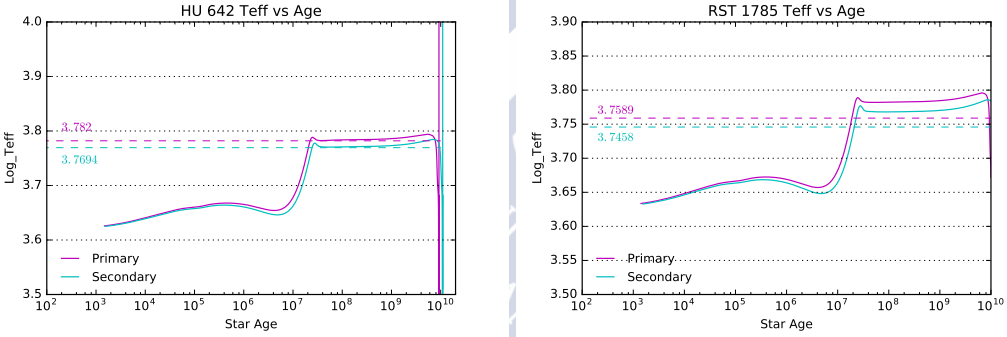

FIGURE IV.15: Teff evolution vs Teff for HU642 (left) and RST1785 (right)

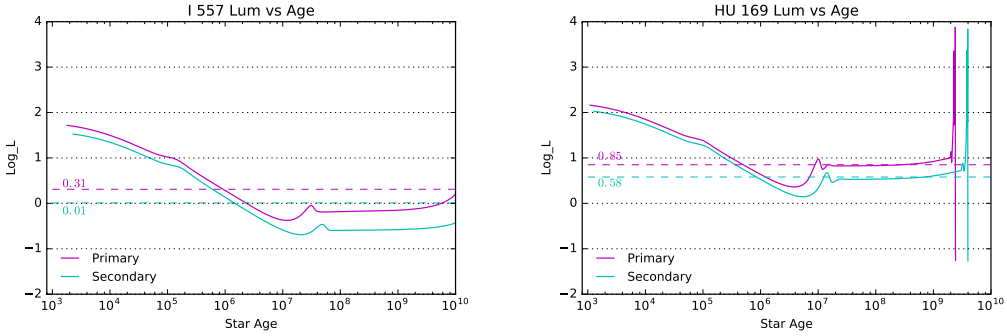

FIGURE IV.16: Luminosity evolution vs Luminosity for I557 (left) and HU169 (right)

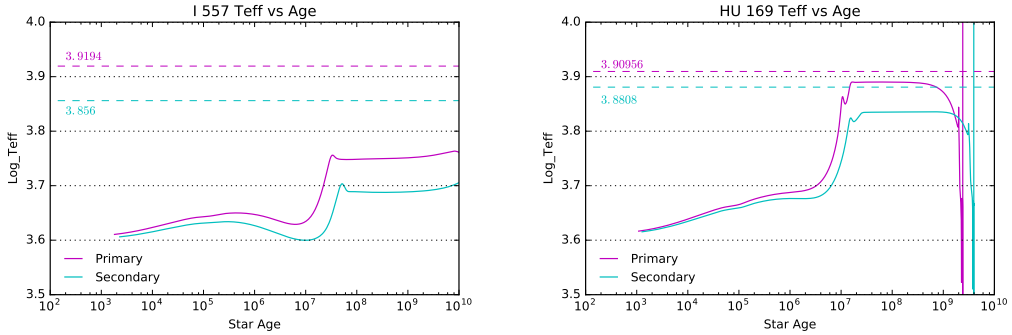

FIGURE IV.17: Teff evolution vs Teff for I557 (left) and HU169 (right)

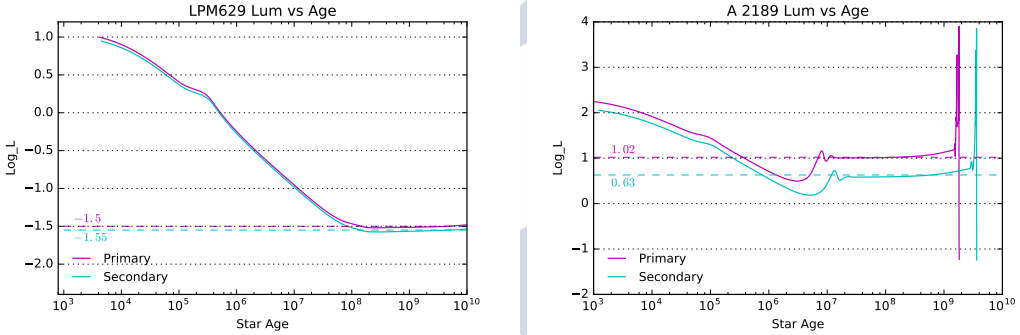

FIGURE IV.18: Luminosity evolution vs Luminosity for LPM629 (left) and A2189 (right)

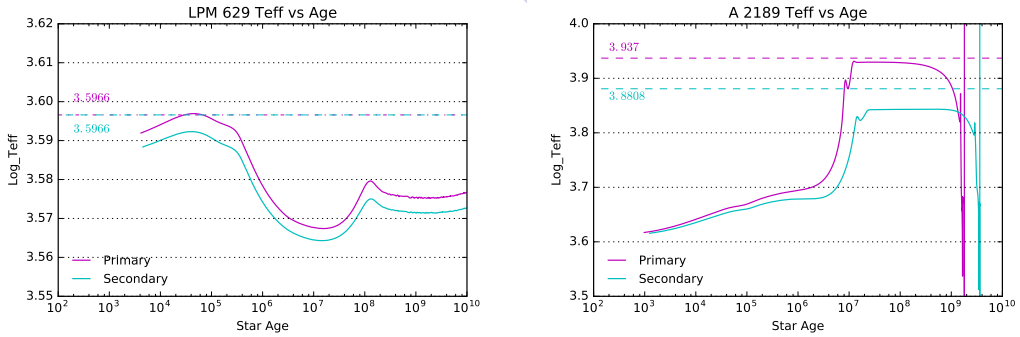

FIGURE IV.19: Teff evolution vs Teff for LPM629 (left) and A2189 (right)

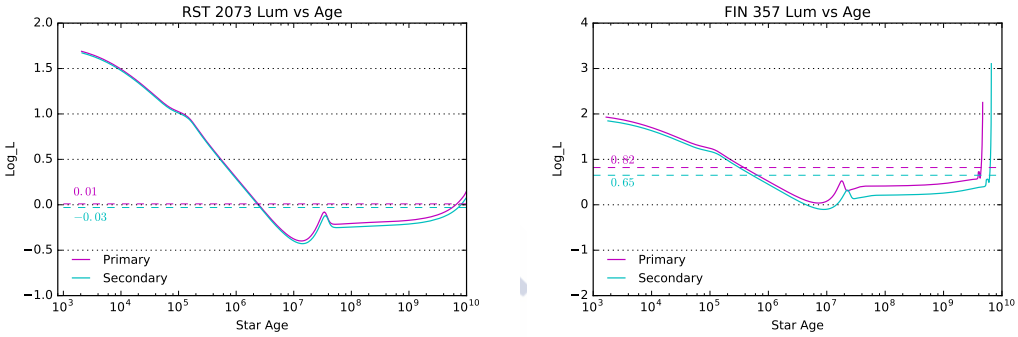

FIGURE IV.20: Luminosity evolution vs Luminosity for RST2073 (left) and FIN357 (right)

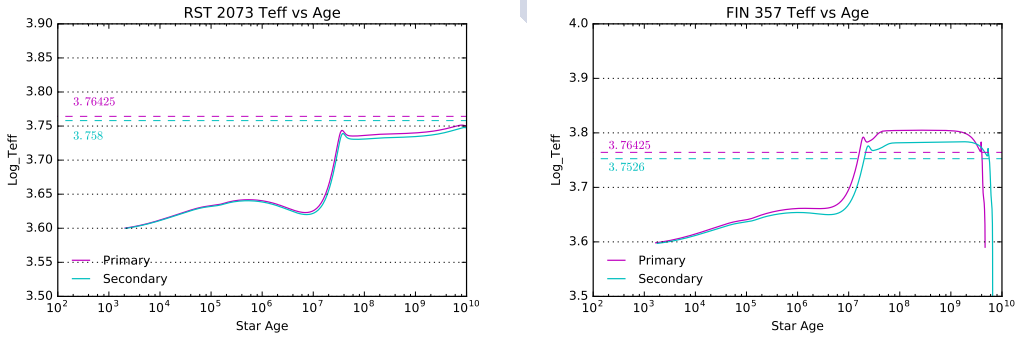

FIGURE IV.21: Teff evolution vs Teff for RST2073 (left) and FIN357 (right)

we wrote the first article, results from Gaia DR2 were not available. For that reason, we used the most precise parallaxes calculated up to that time, i.e., those obtained by Hipparcos (ESA, 1997; van Leeuwen, 2007). For the second article, we were able to use the Gaia parallax data for 6 of the systems (CVN 16 AaAb, RST 1658, I 557, HU 169, A 2189, FIN 357) and the Hipparcos data for 6 other systems. There is no parallax data from either mission for A 671 y RST 2073.

Only in the case of A 2189 did we find that the Gaia results were similar to those provided by the dynamical parallaxes ($\pi_{Gaia} = 0.00511 \pm 0.00042$ vs $\pi_{dyn} = 0.00518 \pm 0.00026$). In the other four cases and given that we have no dynamical parallax for CVN 16 Aa,Ab, the differences are notable as can be seen in Table IV.1. This could be due to the fact that the parallax results in the case of multiple systems are still not definitive in Gaia DR2. In the case of RST 1658, it is obvious that there are still very few orbital measurements and should be considered preliminary.In the cases of I 557, HU 169 and FIN 357, one or two of their quadrants remain to be covered by high precision measurements which implicates that that the orbit may still be improved. System A 2189 also lacks coverage. Nevertheless, the Gaia results correspond significantly with the calculated orbit. In any case, all of these systems should be observed in the future in order to achieve a definite orbit.

As we have seen in this small sample, the results from the orbits do not completely correspond to those provided by Gaia. This could be due to the particularities of these orbits but it could also be due to the fact that, right now, Gaia has still not corrected their results for the effects produced by the stellar multiplicity. The orbital movement causes alterations in the stellar positions that are difficult to detect or to model, which generate errors when the parallax or the spatial velocities are measured. Nevertheless, if the multiple nature of the system is detected and if its orbital movement is modeled correctly, no extra noise should be created although the process of the calculation of the parallax will continue to debilitate as new unknowns are added and they will have to be solved (Bastian and Hefele, 2005). Keeping in mind that the maximum resolution expected by Gaia is a separation of ~0”1, many closed systems are going to have to be revised in the coming years. To observe this type of systems and to calculate their orbits seems to us to be a useful task and it will permit the international astronomical community to be able to take better advantage of the high precision parallax measurements that the ESA satellite will yield.

WDS	name	Π^{Sat}	Π^{dyn}
Hipparcos		e	e
06478+0020	STT157	0.00534^{H}	–
HIP 32572		$\pm0.00094^{H}$	–
07003-2207	FIN334	0.00155^{H}	0.00239
HIP 33721	Aa,Ab$*$	$\pm0.00052^{H}$	±0.00049
07003-2207	FIN334	0.00155^{H}	0.00202
HIP 33721	Aa,Ab$**$	$\pm0.00052^{H}$	±0.0004
07013-0906	A 671$*$	–	0.00825
		–	±0.00049
07013-0906	A 671$**$	–	0.00697
		–	±0.00043
10174-5354	CVN16	0.051	–
	Aa,Ab	±0.0003	–
12155-3106	RST1658	0.03464	0.04326
HIP 59780		±0.00076	±0.00032
12572+0818	FIN380	0.00983^{H}	0.01191
HIP 63221		$\pm0.00071^{H}$	±0.00056
13044-1316	HU642	0.00756^{H}	0.00744
HIP 63789	AB	$\pm0.00214^{H}$	±0.00093
14243-3838	RST 1785	0.0121^{H}	0.00888
HIP 70410		$\pm0.00158^{H}$	±0.00013
16094-3103	I557	0.01535	0.01941
		±0.0007	±0.00224
17115-1630	HU169	0.02007	0.00843
HIP 84092		±0.00116	±0.00022
17119-0151	LPM 629	0.09819^{H}	0.07403
HIP 84123		$\pm0.01209^{H}$	±0.00099
17563+0259	A2189	0.00511	0.00518
HIP 87811		±0.00042	±0.00026
18464-2755	RST 2073	–	0.00828
		–	±0.00051
19035-6845	FIN357	0.01555	0.01769
HIP 93574		±0.00029	±0.00016

TABLE IV.1: Short period orbits are marked with $*$, long period orbits with $**$ The Π^{Sat} column contains Gaia or Hipparcos values of parallaxes: H superscript means that the parallax value comes from Hipparcos, no superscript indicates Gaia

IV.2.1 Articles based on SOAR data

Here we include the two articles. The first, Orbits of 12 Southern Binaries Based on SOAR Speckle Observations, was published in Volume 152 of The Astronomical Journal, an international issue from December 2016 while the second, Orbits of 14 Binaries Based on 2018 SOAR Speckle Observations* (Docobo et al., 2018), has been accepted for publication in October of 2018 in the Monthly Notice of the Royal Astronomical Society. Both are high impact journals of great scientific trajectory that are well known in the field of Astronomy. They have been peer reviewed and have been corrected by the authors as recommended by the referees. Although already expressed, we reiterate our gratitude to A. Tokovinin for the measurements provided as well as to the operators and engineers of SOAR who collaborated in these observation campaigns. We are also grateful for the comments and suggestions that those referees contributed and which improved the articles. Likewise, we are grateful to the editors of both publications.

These articles also serve as a reference to evaluate the importance that these observations at the Byurakan Astrophysical Observatory and the Special Astrophysical Observatory may have. Today we have thousands of observations of hundreds of different systems (see III.2 and III.1) and we hope that their reductions will be concluded and that the astrophysical parameters of interest will be determined. With these measurements, we hope to be able to calculate many new orbits and delve deeper into the study of their systems as we have done with these 26 systems.

IV.3 Spectro-interferometric Binaries

The third article, The Three-Dimensional Orbit, Orbital Parallax, and Individual Masses of the Double-Lined Spectroscopic Binaries HD 183255, HD 114882, AND HD 30712, that we present in this chapter has been accepted for publication in The Astronomical Journal and it is now published on-line. The OARMA researchers, J. A. Docobo, P. P. Campo, and J. Gomez worked together with E.P. Horch who directed his own speckle interferometry observation program in both the Northern and the Southern hemispheres, using a camera named the Differential Speckle Survey Instrument (DSSI, Horch et al. (2009)).

Three spectroscopic double line binary systems: HD 183255, HD 114882, and HD 30712 han were studied using high precision measurements obtained via SI with the following telescopes: the Discovery Channel Telescope, the Gemini North Telescope, and the Special Astrophysical Observatory 6-m Big Alt-azimuth Telescope (SAO BTA). Thanks to these recent speckle measurements, we were able to calculate the visual orbits of those systems using the methodology previously employed by Docobo et al. (2014). In the case of HD 114882, the visual orbit presented in this article is the first visual orbit that has been calculated for this system.

TABLE IV.2: Parallaxes

	HD 183255	HD 114882	HD 30712
Orbital Parallax	0″04201 ± 0″00108	0″00763 ± 0″00030	0″02130 ± 0″00075
Dynamical Parallax	0″04158 ± 0″00090		0″02280 ± 0.00135
Gaia Parallax	0″04121 ± 0″00028	0″00765 ± 0″0004	0″02108 ± 0″00015

These new visual orbits along with the spectroscopic orbits previously known for these systems have allowed us to determine their 3D orbits, the separate masses for each component, and the orbital and dynamical parallaxes. We were also able to carry out a comparison of these with parallaxes provided by Gaia (IV.2).

Keeping in mind that the Data Release 2 of Gaia still considers all of the sources of light to be singular stars, we hope that the value of the parallaxes of the systems studied in our article will vary in the final Data Release and be closer to our calculations.

It is important to highlight that the HD 30712 measurements obtained with the BTA pertain to the set of observations realized by OARMA at SAO as we have described in III.2. The reduction process has been explained in III.1.3 and we used the software that we created for that end and which follows the theory and the recommendations presented in III.1.4-III.1.7 to carry out the astrometric determination. The difference between the magnitudes of the components has not yet been precisely determined.

This article shows that the combination of spectroscopic data along with the Gaia parallaxes and the SI observation programs allow us to obtain high precision in the calculation of masses and other fundamental parameters.

In this line of research of binaries that are both visual and spectroscopic and that has been most recently carried out by OARMA (Docobo et al., 2014, 2017a, 2018b), our objective is to continue with this type of research in the detection of possible double line spectroscopic binaries that can be resolved by high resolution imaging methods. We are also interested in obtaing future spectroscopic measurements of visual orbits with no associated spectrum for its components. This will permit us to spectroscopically classify them and to determine if it is possible to obtain a spectroscopic orbit that will allow us to apply the same methodology that was used in the article concerning the determination of 3D orbits and the individual masses. To that end, we have obtained high resolution spectroscopic observations with GMOS at the Gemini South Telescope for a selection of multiple systems with interferometric visual orbits. At this moment, we are waiting for these data to be reduced and analyzed by the author of this dissertation.

IV.4 Conclusions

In this chapter, we have presented three articles in which speckle interferometric measurements have been used to calculate the orbits of 29 star systems. These orbits permit the determination of their fundamental parameters and, in particular, the masses of the components of each system.

In the case of these three systems, HD 183255, HD 114882, and HD 30712, the visual orbits have been used in combination with the spectroscopic orbits in order to determine the 3D orbits. The orbital parallaxes obtained have been compared with the data provided by the Hipparcos and Gaia space missions.

For 12 of the systems presented in the article Orbits of 14 Binaries Based on 2018 SOAR Speckle Observations*, we have also calculated their isochrones in order to approximate their age based on the absolute luminosities derived from the new orbital data and the difference of magnitude given by the SOAR speckle measurements.

These articles demonstrate the utility of high resolution measurements obtained with SI. In the context of this dissertation, they serve to show the applications and the scientific importance of the observation campaigns realized at SAO and BAO. Thanks to the data obtained in these campaigns, we hope to be able to determine new orbits following the methodologies that we used in these articles. In combination with these speckle measurements, we are also obtaining spectroscopic and photometric measurements for the study of specific double systems.

It is our intention to publish, as soon as possible, the results of the speckle interferometry observations carried out at SAO between 2012 and 2014 and the pertinent observations from the campaigns that OARMA carried out at the Byurakan Astrophysical Observatory using the eMCCD PhotonMAX 512 since 2016. We also hope to publish this year the results obtained thanks to the spectroscopic measurements obtained at Gemini South.

USC
UNIVERSIDADE
DE SANTIAGO
DE COMPOSTELA

Chapter V

Articles about the pohotometric study of stellar regions Cep OB3 and Cyg OB7

V.1 Introduction

This last Chapter will be dedicated to present three articles, developed in cooperation with N. D. Melikyan and published in Astrophysics journal. Two from the mentioned articles were co-written by the late A. A. Karapetyan. These two studies are focused on star formation regions in the stellar associations Cep OB3 and Cyg OB7.

Cep OB3 is a young star formation region (~ 4-8 Myr) where more than hundreds of objects presenting emission lines corresponding to H_α (Mikami and Ogura, 2001) were detected. We published 46 new stars with emissions in H_α in Cep OB3 in "New Hα Emission Stars in Cep OB3 Region. A Rapid Brightness Variation of V 733 Cep" (Melikian, Gomez, and Karapetian, 2014), estimating at the same time the intensity of the mentioned emissions. A color diagram (J-H), (H-K) was made for them showing that they could be T Tau or UV Ceti type variable star of spectral classes later than K0. We also published a rapid variation in the luminous intensity of V733 Cep: a FU Orionis-type star.

V 733 Cep was discovered in 2004 (Persson, 2004), and it is believed to be the last outburst produced between 1953 and 1984 (Reipurth et al., 2007). Roger Persson was examining the digitized versions of the old Palomar Sky Survey, POSS-I, and the new one, POSS-II, when he discovered that this star was visible in an image of POSS-II but not in POSS-I. After his communication, Reipurth and Aspin (2004) confirmed the veracity of his detection.

The stars of the type of FU Orionis (FUors) have certain common spectral features: F-G type low-gravity spectra, strong $Li_I\lambda6707$ line, P Cygni profiles at H_α and Na_I D lines, and a gradual change from earlier to later spectral type from the blue to the infrared (Reipurth et al., 2007). These objects are extremely rare, and the principal feature thereof is the eventual production of outbursts which significantly increase its brightness. The first known outburst corresponds to the case observed in 1936 for the star that gave name to this variety,

FU Orionis, the explosion of which increased its apparent visual magnitude from 16.5 to 9.6 (Herbig, 1966; Wachmann, 1954). These events are considered to be typical of the early stages of stellar evolution, when mass accretion is generated between the star and its circumstellar disc in a varied way (from $\sim 10^{-7}$ to 10^{-4} $M_{\odot}$ yr^{-1}). This variability in the accretion is corresponding to the variability in its ejection. The quantity of the substance ejected in an outburst is of $\sim 10^{-1}$ of the mass accretion rates. Some important aspects, as the question whether any pre-main-sequence star of low mass may present this kind of explosions or if it is experienced only by a part of them, is a subject of debates. Some aspects related to the multiplicity of these systems and the eccentricity of their possible orbits may be important when outbursts are produced (Hartmann and Kenyon, 1996).

Actually hardly a dozen of stars of FUor type are known; the importance and rarity of these objects make their photometric observation so relevant. In the first article presented we studied the rapid variation of its brightness in December 2008, similar to the flare events produced in UV Ceti stars.

Also, we detected during the mentioned research three new variable stars, with variations in R higher than 0.5 magnitudes. The quantity of available observations did not allow us to determine the type of variability.

Cyg OB7 is another area which also includes several stars of T Tauri type, presenting emissions in H_{α}, apart from different nebulas associated to Herbig-Haro objects, and two cometary nebulae. A total quantity of 26 new stars with this kind of emissions was published in "New Emission Stars in B Cyg OB7" Melikian, Karapetian, and Gomez (2016), with their magnitudes in BVRI, being presented in a two-color (J-H),(H-K) diagram. The greatest part of them corresponds to young non-stationary T Tau stars with spectral classes from late K to M5.

In "Photometric Studies of Stars in the Vicinity of Cyg OB7" (Melikian and Gomez, 2017), we continued the research of this area. The mentioned article presented the photometric results of 131 stars in BVRI, some of which were already handled in the first article.

The observations were carried out during 2000, 2002, 2004 and 2011, using the spectral cameras ByuFOSC-2 and SCORPIO, mounted on the telescope of 2.6 m of Byurakan Astrophysical Observatory. We published in this work variations from 0.2 to 2.16 magnitudes, detected in case of 42 stars observed. 31 from them did not present earlier data related to their photometric variability. All of them are situated near the stars T Tau when located on the diagram (J-H), (H-K).

V.2 Conclusions

The papers presented here follow the lines of research made by N. D. Melikian in variable stars, flare stars, nebulas y Herbig-Haro objects in star formation regions (e.g., Abramyan et al. (1990), Melikian (1995, 2014), Melikian and Eritsian (1996), Melikian and Karapetian (1996, 2001, 2003), Melikian, Tamazian, and Karapetian (2006), Melikian, Tamazian, and Samsonyan (2011), Melikian et al. (2011), Melikyan, Natsvlishvili, and Della Valle (1988), Melikyan, Tsvetkov, and Sarkisyan (1994), and Mirzoyan et al. (1977)).

The collaborations between the OARMA's staff and different Directors of the BAO started in 1988 (Docobo et al., 1998; Eritsian et al., 1998; Tamazian, Docobo, and Melikian, 1998) and continue till the date, representing more than 25 joint articles and communications (e.g., Docobo et al. (2003, 2006, 2010, 2017b), Melikian et al. (2010), Tamazian, Docobo, and Melikian (1999), and Tamazian et al. (2000, 2005, 2008)).

During the first year of the PhD, the author of this lines had the opportunity to get an ERASMUS MUNDUS ALRAKIS Action 2 [1] scholarship, thanks to which it became possible to travel to the BAO and study under direction of N. D. Melikian. The stay in Armenia permitted me to visit for the first time the Special Astrophysical Observatory and to take part in observation campaigns with its research group in Speckle Interferometry. BAO's telescope of 2.6 m was under repair during the mentioned year, so it was not possible to perform observations. Therefore, the work realized was focused on learning and mastering the astronomical software IRAF, as well as reducing and analyzing the images taken at Asiago Observatory with AFOSC Tektronix TK1024, which were employed later for one of the articles referred here (Melikian and Gomez, 2017). Besides, Professor Melikian guided me during my investigation in the basic concepts of Astrophysics.

The results presented in three articles show the abundance of objects with H_α emissions, as a rule, of T Tauri character, in the star formation regions Cep OB3 and Cyg OB7. The circumstance that the detection of flares and outbursts is common in these areas does not make their documentation and analysis less significant, as the case of V 377 Cep illustrates. The astrophysical knowledge related to T Tauri, UV Ceti, FUors and Exors stars will be highly useful in my future work. The role that the multiplicity may have when triggering the outbursts of FU Ori type stars is still unknown. Resolving it might help us to predict such events which have seemed accidental till this moment.

The knowledge acquired in the matter of differential photometry was applied in an activity developed during the course of this PhD, although without being presented in the present thesis. During the second year of the PhD research, a stay was realized at the Fabra-ROA Telescope at Monsec during a night of collimation and maintenance. The staff led by J. Nuñez offered us time for observation and helped to administrate the parameters necessary

[1] The original website of the scholarship readdresses now to a page of Académie de trading forex/cryptomonnaies

for observing the objects selected. These objects obtained with Baker-Nunn (Fors et al., 2013), automated and adapted for observation with CCDs, correspond to a field of 4°4×4°4 and with a limit of V ~19.5 magnitudes. Thanks to this, we counted not only with the selected objects of interest, but also with thousands of stars to evaluate. It gave us the possibility to use the Centro de Supercomputación de Galicia (CESGA) to carry out one of the LEMON, (Terrón, 2018). Certain technical details, the quantity of detections and the focus of the work on the Speckle Interferometry delayed the performance of the works described above and they could not be concluded yet.

We hope to be able to calculate the light curves of stars in question during the following months, as a part of works to be fulfilled during the postdoctoral phase.

Conclusions

This dissertation was written by Jorge Gomez Crespo as a compendium of research articles and it was proposed and supervised by J.A. Docobo, a Full Professor in Astronomy, specialist in binaries, and Director of the Ramon Maria Aller Astronomical Observatory (OARMA) of the University of Santiago de Compostela (USC), Spain. Following the research lines suggested by Prof. Docobo, the author, in collaboration with him and other members of OARMA, has continually conducted research since his enrollment in the USC Doctoral program in Mathematics (Astronomy). Thanks to his work and the collaborations with, not only the aforementioned researchers, but also with others prestigious international scientists, such as, Y. Y. Balega, R. A. Méndez, E. P. Horch, and N. D. Melikian, among others, we have been able to accomplish a large part of the tasks that were proposed at the beginning of this educational period. These tasks included the study of:

- Double and multiple stellar systems and the observational techniques used to collect data on those: photometry, spectroscopy, and speckle interferometry.
- Speckle Interferometric, photometric, and spectroscopic data reduction, analysis, and administration.
- Young Stellar Objects (YSOs) such as T Tauri, FU Ori, and UV Ceti type stars.
- Pedagogical methods in astronomy.

As a resume of the main achievements completed and explained in this dissertation we can highlight:

- BAO OARMA collaboration to start and develop several observational campaigns employing OARMA's speckle camera attached to the 2.6m telescope at BAO.
- The development of a software to reduce speckle blocks of images and to obtain astrometric and photometric results.
- Using SOAR speckle interferometric data, 26 orbits of systems accesible from Southern hemisphere has been improved. Some of them presented characteristics (e.g., lack of spectra information, absence of orbit, absence of high resolution measurements, ...) previous to our new determinations that enhance the importance of our solutions.
- An initial study regarding the age and the evolutionary tracks of 12 binary systems.

- Collecting spectroscopic orbital information regarding the double-line spectroscopic binaries HD 183255, HD 114882, and HD 30712, together with new visual measurements obtained with speckle interferometry, we were able to calculate the main physical fundamental parameters of these systems. The orbital parallaxes obtained have been compared with the data provided by the Hipparcos and Gaia space missions.
- A rare flare in V 733 Cep has been detected using differential photometry.
- To obtain time of telescope in Gemini South to use the Gemini Multi-Object Spectrograph (GMOS) to acquire high resolution spectroscopic data related with binary and multiple systems.
- The use of highly efficient softwares in combination with the resources provided by the Center of Supercomputation of Galicia to deal with differential photometry on fields that present a huge amount of detections. The observations used have been provided by the Telescope Fabra-ROA at Monsec (TFRM).

One of the main goals was to increase the output of the speckle eMCCD camera of the OARMA by attaching it to the 2.6m telescope at Byurakan Astrophysical Observatory (BAO) in Armenia, where it had been sent. Beginning in October 2016, we have completed four campaigns where hundreds of stellar systems has been observed. Another goal was to achieve experience participating in speckle runs with the 6m telescope at the Special Astrophysical Observatory of the Russian Academy of Sciences (SAO RAS), and finally, to have access to the southern hemisphere using the Southern Astrophysical Research telescope (SOAR), Chile. In total we were able to organize these runs and to obtain more than 1000 blocks of images using the speckle camera of the OARMA.

These campaigns allow to the OARMA and BAO collaboration to be included between the few centers in the world that are currently working in speckle interferometry. The main task for future months is to complete the reduction and analysis software that the author of this dissertation is creating to be applied on the data blocks. Not only the data collected in BAO will be reduced with this software, the blocks that we have obtained between 2012 and 2015 thanks to the time of telescope assigned in the 6m Big Alt-azimuth Telescope (BTA) of the SAO RAS will also be reduced.

In this dissertation, we have included relevant information related with different imaging techniques and technologies, emphasizing the literature related with Speckle Interferometry (SI). Previously, we have explained the difficulties involved in astronomical observation from Earth's surface. The reader will find that this text supplies a list of published SI articles. This articles show the importance as well as the different applications of this technique since 1970 to the present.

We have explained the micrometers that astronomers have used since more than two centuries ago to obtain data reflecting the orbital movement of thousands of binary and multiple systems. The current devices that we employ to observe, i.e., the CCDs, ICCDs and eMCCDs, has

also been explained in detail. The knowledge related with the technical characteristics of these devices, their noises, and capabilities allows the reader to understand the reduction process that the astronomers execute on the images obtained with them. The mathematical apparati needed to reduce the data is provided as well as we included all the theory related with process of analysis of the speckle blocks.

The software created was already used to reduce two observations obtained with the 6m BTA that have beed employed in one of our articles. In this dissertation, we have included all of the relevant theoretical information that the reader needs to know in order to understand the workflow that the software realize. This software was designed based on that created by A. Tokovinin for SOAR speckle campaigns but also it uses other approaches such as the ones introduced by Pluzhnik and Dainty. The mathematical tools employed to create this software required a deep understanding of different research fields as: Fourier Optics, Image Treatment, Image Quality, SNR calculation, and others.

The main chapter of this dissertation explains the key position that binary stars have in Astronomy. After that, we introduce the articles that we have published using speckle information obtained mainly from SOAR, but also from SAO and Gemini during the past years. These articles were published in two high impact journals located one, Monthly Notices of the Royal Astronomical Society, in the first quartile and the other, The Astronomical Journal, at the top of the second quartile of the JSON. In those papers, we used Docobo's analytical method and other algorithms developed by J. A. Docobo and his collaborators to determine the orbits presented. In one of them, we also carried out an additional brief study regarding the age of the components and its location in the HR diagram.

The final chapter shows the three collaborations that the author has completed during his doctoral studies with the BAO's researchers N. D. Melikian and A. A. Karapetian. In those projects, we detected new H_α emission stars in Cep OB3 and Cyg OB7, we revealed photometrical information regarding a rare flare in V 733 Cep (one of the few FU Orionis type stars known), as well as photometry regarding other variable stars. Most of the stars studied are close to the T Tau region. All of those articles has been published in the journal, Astrophysics.

Regarding our future prospects, our work objectives are, as follows:

- reduce and publish all of the speckle data collected at SAO between 2012 and 2015,
- reduce and publish all of the speckle data collected at BAO during the observational campaigns that we carried out using OARMA's eMCCD camera,
- determine new orbits for some of those systems observed during our speckle campaigns,
- improve the part of our research that includes the age calculation and the evolutionary study of double and multiple systems,

- continue to develop our speckle interferometric observational campaigns with BAO's 2.6m telescope,
- continue to develop our reduction and analysis software created to deal with speckle blocks,
- reduce and study the spectra obtained with GMOS in order to provide of spectra classification regarding the systems and the subcomponents observed, and
- complete the photometrical light curves of the thousands of detections within three different sky regions that the TFRM images provide. These regions were selected because of the presence of an eclipsing binary or a YSO. These object are located at the centre of the field of view.

BIBLIOGRAPHY

Abad, C., J. A. Docobo, and F. della Prugna (1998). "CCD and micrometric observations of visual double stars". In: A&AS 133, pp. 71–79.

Abad, C., J. A. Docobo, V. Lanchares, J. F. Lahulla, P. Abelleira, J. Blanco, and C. Alvarez (2004). "Reduction of CCD observations of visual binaries using the "Tepui" function as PSF". In: A&A 416, pp. 811–814.

Abramyan, G. V., S. V. Zaratsyan, N. D. Melikyan, S. Y. Mel'Nikov, and V. S. Shevchenko (1990). "The Herbig Ae-Star V517-CYGNI". In: *Astrophysics* 32, p. 24.

Afanas'jev, V. L., V. L. Afanas'ev, I. I. Balega, Y. Y. Balega, Y. Y. Balega, V. A. Vasyuk, and V. G. Orlov (1988). "Speckle interferometry and speckle spectroscopy with the 6-m telescope." In: *European Southern Observatory Conference and Workshop Proceedings*. Ed. by F. Merkle. Vol. 29. European Southern Observatory Conference and Workshop Proceedings, pp. 127–141.

Aime, C., G. Ricort, and J. Harvey (1978). "One-dimensional speckle interferometry of the solar granulation". In: ApJ 221, pp. 362–367.

Allen, D. A., J. R. Barton, and P. T. Wallace (1981). "The size of a Wolf-Rayet star's dust shell measured by speckle interferometry". In: MNRAS 196, pp. 797–800.

Aller, R. M. (1930). "Doppelsternbeobachtungen". In: *Astronomische Nachrichten* 238, p. 71.

– (1934). "Doppelsternbeobachtungen". In: *Astronomische Nachrichten* 251, p. 273.

– (1935a). "Beobachtungen des Kometen 1935 a (Johnson)". In: *Astronomische Nachrichten* 255, p. 187.

– (1935b). "Orbita de la estrella doble OΣ 77". In: *Astronomische Nachrichten* 256, p. 245.

– (1936). "Doppelsternbeobachtungen". In: *Astronomische Nachrichten* 259, p. 133.

– (1939). "Orbita de la estrella doble Σ 1932 (ADS 9578 β 7214)". In: *Astronomische Nachrichten* 268, p. 23.

Ammons, S. M., S. E. Robinson, J. Strader, G. Laughlin, D. Fischer, and A. Wolf (2006). "The N2K Consortium. IV. New Temperatures and Metallicities for More than 100,000 FGK Dwarfs". In: ApJ 638, pp. 1004–1017. eprint: astro-ph/0510237.

Anderson, E. and C. Francis (2012). "XHIP: An extended hipparcos compilation". In: *Astronomy Letters* 38, pp. 331–346. arXiv: 1108.4971.

Anderson, J. and I. R. King (2000). "Toward High-Precision Astrometry with WFPC2. I. Deriving an Accurate Point-Spread Function". In: PASP 112, pp. 1360–1382. eprint: astro-ph/0006325.

Anderson, J. A. (1920). "Application of Michelson's interferometer method to the measurement of close double stars." In: ApJ 51.

Argue, A. N., J. C. Hebden, B. L. Morgan, and H. A. Vine (1984). "Speckle interferometry of HIPPARCOS link stars". In: MNRAS 206, pp. 669–672.

Argue, A. N., J. C. Hebden, B. L. Morgan, C. Standley, and H. A. Vine (1985). "Speckle interferometry of HIPPARCOS link stars. II". In: MNRAS 216, pp. 447–451.

Artigau, É., B. A. Biller, Z. Wahhaj, M. Hartung, T. L. Hayward, L. M. Close, M. R. Chun, M. C. Liu, G. Trancho, F. Rigaut, D. W. Toomey, and C. Ftaclas (2008). "NICI: combining coronagraphy, ADI, and SDI". In: *Ground-based and Airborne Instrumentation for Astronomy II*. Vol. 7014. Proc. SPIE, 70141Z. arXiv: 0809.3012.

Bagnuolo Jr., W. G., B. D. Mason, D. J. Barry, W. I. Hartkopf, and H. A. McAlister (1992). "Absolute quadrant determinations from speckle observations of binary stars". In: AJ 103, pp. 1399–1407.

Baier, G., N. Hetterich, and G. Weigelt (1982). "Digital speckle interferometry of Juno, Amphitrite and Pluto's moon Charon". In: *The Messenger* 30, pp. 23–26.

Baier, G., R. Ladebeck, and G. Weigelt (1985). "Speckle interferometry of the central object in the giant H II region NGC 3603". In: A&A 151, pp. 61–63.

Baier, G. and G. Weigelt (1983). "Speckle interferometry observations of the asteroids Juno and Amphitrite". In: A&A 121, pp. 137–141.

– (1987). "Speckle interferometric observations of Pluto and its moon Charon on seven different nights". In: A&A 174, pp. 295–298.

Baier, G., U. Bastian, E. Keller, R. Mundt, and G. Weigelt (1985). "Speckle interferometry of T Tauri stars and related objects". In: A&A 153, pp. 278–280.

Baize, P. and L. Romani (1946). "Formules nouvelles pour le calcul des parallaxes dynamiques des couples orbitaux". In: *Annales d'Astrophysique* 9, p. 13.

Balega, I. I., Y. Y. Balega, and V. A. Vasyuk (1990). "A first catalogue of speckle-interferometric measurements of binary stars made with the 6-m telescope of the USSR AS." In: *Soobshcheniya Spetsial'noj Astrofizicheskoj Observatorii* 65, pp. 5–31.

– (1991a). "Speckle-interferometric measurements of binaries on the 6-m telescope in 1987 - 1988." In: *Bulletin of the Special Astrophysics Observatory* 31, pp. 77–78.

– (1991b). "Speckle-interferometry measurements of binaries using the 6-m telescope in 1986." In: *Bulletin of the Special Astrophysics Observatory* 28, pp. 102–105.

Balega, I. I., Y. Y. Balega, V. V. Vasyuk, and A. A. Tokovinin (1991). "Speckle Interferometry of Stars in the Gliese Catalog". In: *Soviet Astronomy Letters* 17, p. 226.

Balega, I. I., Y. Y. Balega, H. Falcke, R. Osterbart, T. Reinheimer, M. Schöller, and G. Weigelt (1997). "Speckle interferometry of the spectroscopic binaries Gliese 150.2 and 41 Draconis". In: *Astronomy Letters* 23, pp. 172–176.

Balega, I. I., Y. Y. Balega, K.-H. Hofmann, A. A. Tokovinin, and G. P. Weigelt (1999). "Parameters of four multiple systems from speckle interferometry". In: *Astronomy Letters* 25, pp. 797–801.

Balega, I. I., Y. Y. Balega, L. T. Gasanova, V. V. Dyachenko, A. F. Maksimov, E. V. Malogolovets, D. A. Rastegaev, and Z. U. Shkhagosheva (2013). "Speckle interferometry of nearby multiple stars. V. 2002-2006 positional measurements". In: *Astrophysical Bulletin* 68, pp. 53–56.

Balega, Y. Y. and N. A. Tikhonov (1977). "Speckle interferometry of some bright stars with the 6 meter telescope." In: *Soviet Astronomy Letters* 3, pp. 272–273.

Balega, Y. Y., V. V. Dyachenko, A. F. Maksimov, E. V. Malogolovets, D. A. Rastegaev, and I. I. Romanyuk (2011). "Speckle interferometry of magnetic Ap/Bp stars at the BTA 6-m telescope (new binary and multiple systems)". In: *Astronomische Nachrichten* 332, pp. 978–982.

Balega, Y. Y., V. V. Dyachenko, A. F. Maksimov, E. V. Malogolovets, and D. A. Rastegaev (2017). "Multiplicity Survey of Bright Stars in the Nearby OB Associations". In: *Stars: From Collapse to Collapse*. Ed. by Y. Y. Balega, D. O. Kudryavtsev, I. I. Romanyuk, and I. A. Yakunin. Vol. 510. Astronomical Society of the Pacific Conference Series, p. 325.

Baranec, C., R. Riddle, N. M. Law, M. R. Chun, J. R. Lu, M. S. Connelley, D. Hall, D. Atkinson, and S. Jacobson (2014). "Second generation Robo-AO instruments and systems". In: *Adaptive Optics Systems IV*. Vol. 9148. Proc. SPIE, p. 914812. arXiv: 1407.0094 [astro-ph.IM].

Barlow, M. J., B. L. Morgan, C. Standley, and H. Vine (1986). "The determination of the mass of a Magellanic Cloud planetary nebula by speckle interferometry". In: MNRAS 223, pp. 151–172.

Barr, J. M. (1900). "The System of Capella". In: ApJ 11, p. 248.

Basden, A. G., C. A. Haniff, and C. D. Mackay (2003). "Photon counting strategies with low-light-level CCDs". In: MNRAS 345, pp. 985–991. eprint: astro-ph/0307305.

Bastian, U. and H. Hefele (2005). "Astrometric Limits Set by Surface Structure, Binarity, Microlensing". In: *The Three-Dimensional Universe with Gaia*. Ed. by C. Turon, K. S. O'Flaherty, and M. A. C. Perryman. Vol. 576. ESA Special Publication, p. 215. eprint: astro-ph/0411225.

Bate, M. R. (2009). "Stellar, brown dwarf and multiple star properties from hydrodynamical simulations of star cluster formation". In: MNRAS 392, pp. 590–616. arXiv: 0811.0163.

Beletic, J. W. (1988). "Comparison of Knox-Thompson and bispectrum algorithms for reconstructing phase of complex extended objects." In: *European Southern Observatory Conference and Workshop Proceedings*. Ed. by F. Merkle. Vol. 29. European Southern Observatory Conference and Workshop Proceedings, pp. 357–371.

Biller, B., É. Artigau, Z. Wahhaj, M. Hartung, M. C. Liu, L. M. Close, M. R. Chun, C. Ftaclas, D. W. Toomey, and T. Hayward (2008). "Observing strategies for the NICI campaign to directly image extrasolar planets". In: *Adaptive Optics Systems*. Vol. 7015. Proc. SPIE, 70156Q. arXiv: 0809.3020.

Biller, B. A., L. M. Close, R. Lenzen, W. Brandner, D. McCarthy, E. Nielsen, S. Kellner, and M. Hartung (2006). "Suppressing Speckle Noise for Simultaneous Differential Extrasolar Planet Imaging (SDI) at the VLT and MMT". In: *IAU Colloq. 200: Direct Imaging of*

Exoplanets: Science & Techniques. Ed. by C. Aime and F. Vakili, pp. 571–576. eprint: astro-ph/0601059.

Blazit, A., D. Bonneau, L. Koechlin, and A. Labeyrie (1977). "The digital speckle interferometer: preliminary results on 59 stars and 3C 273." In: ApJ 214, pp. L79–L84.

Bonneau, D. and R. Foy (1980a). "Speckle interferometric observations of binary systems with the Haute-Provence 1.93 M telescope". In: A&A 86, pp. 295–298.

– (1980b). "Speckle interferometry with the 3.60 M CFH telescope. I - Resolution of the Pluto-Charon system". In: A&A 92, pp. L1–L4.

Bonneau, D. and A. Labeyrie (1973). "Speckle Interferometry: Color-Dependent Limb Darkening Evidenced on Alpha Orionis and Omicron Ceti". In: ApJ 181, p. L1.

Bonneau, D., A. Blazit, R. Foy, and A. Labeyrie (1980). "Speckle interferometric measurements of binary stars." In: A&AS 42, pp. 185–188.

"Book Review: Adaptive optics for astronomical telescopes / Oxford U Press, 1998" (2000). In: *Physics Today* 53.6, p. 69.

"Book Review: Electronic imaging in astronomy: detectors and instrumentation / Wiley, 1997" (1997). In: *Journal of the British Astronomical Association* 107, p. 223.

Bowell, E., B. L. Morgan, K. Lumme, J. C. Dainty, H. A. Vine, and M. Poutanen (1981). "Speckle Interferometric Observations of Ceres, Vesta, Hebe, and Victoria." In: *Bulletin of the American Astronomical Society*. Vol. 13. BAAS, p. 719.

Brown, R. H. (1968). "Measurement of Stellar Diameters". In: ARA&A 6, p. 13.

Brown, R. H. and R. G. Twiss (1954). "A New type of interferometer for use in radio astronomy". In: *Philosophical Magazine* 45, pp. 663–682.

Brown, R. H. and R. Q. Twiss (1956). "Correlation between Photons in two Coherent Beams of Light". In: Nature 177, pp. 27–29.

– (1957). "Interferometry of the Intensity Fluctuations in Light. I. Basic Theory: The Correlation between Photons in Coherent Beams of Radiation". In: *Proceedings of the Royal Society of London Series A* 242, pp. 300–324.

– (1958). "Interferometry of the Intensity Fluctuations in Light. III. Applications to Astronomy". In: *Proceedings of the Royal Society of London Series A* 248, pp. 199–221.

Chen, W. P., M. Simon, A. J. Longmore, R. R. Howell, and J. A. Benson (1990). "Discovery of five pre-main-sequence binaries in Taurus". In: ApJ 357, pp. 224–230.

Choi, J., A. Dotter, C. Conroy, M. Cantiello, B. Paxton, and B. D. Johnson (2016). "Mesa Isochrones and Stellar Tracks (MIST). I. Solar-scaled Models". In: ApJ 823, 102, p. 102. arXiv: 1604.08592 [astro-ph.SR].

Christou, J. C., A. Y. S. Cheng, E. K. Hege, and C. Roddier (1985). "Seeing calibration of optical astronomical speckle interferometric data". In: AJ 90, pp. 2644–2651.

Chun, M., D. Toomey, Z. Wahhaj, B. Biller, E. Artigau, T. Hayward, M. Liu, L. Close, M. Hartung, F. Rigaut, and C. Ftaclas (2008). "Performance of the near-infrared coronagraphic imager on Gemini-South". In: *Adaptive Optics Systems*. Vol. 7015. Proc. SPIE, p. 70151V. arXiv: 0809.3017.

Ciardi, D. R., C. A. Beichman, E. P. Horch, and S. B. Howell (2015). "Understanding the Effects of Stellar Multiplicity on the Derived Planet Radii from Transit Surveys: Implications for Kepler, K2, and TESS". In: ApJ 805, 16, p. 16. arXiv: 1503.03516 [astro-ph.EP].

Cid Palacios, R. (1958). "On the necessary and sufficient observations for determination of elliptic orbits in double stars". In: AJ 63, p. 395.

Cobb, M. L. and J. D. Fix (1987). "Infrared speckle interferometry and imaging of several OH/IR stars". In: ApJ 315, pp. 325–336.

Costa, J. M. and J. A. Docobo (1983). "New orbit of WDS 14243-3838." In: *Circ. d'Inf.* 91, pp. 1–1.

Couteau, P., J. A. Docobo, and J. Ling (1993). "Measurements of close binaries performed at PIC du Midi". In: A&AS 100, pp. 305–310.

Couteau, P., J. A. Docobo, A. Eliped, and J. F. Ling (1989). "Measurements of binaries made with the 152-cm telescope at Calar Alto". In: A&AS 78, pp. 483–486.

Crossfield, I. J. M., D. R. Ciardi, E. A. Petigura, E. Sinukoff, J. E. Schlieder, A. W. Howard, C. A. Beichman, H. Isaacson, C. D. Dressing, J. L. Christiansen, B. J. Fulton, S. Lépine, L. Weiss, L. Hirsch, J. Livingston, C. Baranec, N. M. Law, R. Riddle, C. Ziegler, S. B. Howell, E. Horch, M. Everett, J. Teske, A. O. Martinez, C. Obermeier, B. Benneke, N. Scott, N. Deacon, K. M. Aller, B. M. S. Hansen, L. Mancini, S. Ciceri, R. Brahm, A. Jordán, H. A. Knutson, T. Henning, M. Bonnefoy, M. C. Liu, J. R. Crepp, J. Lothringer, P. Hinz, V. Bailey, A. Skemer, and D. Defrere (2016). "197 Candidates and 104 Validated Planets in K2's First Five Fields". In: ApJS 226, 7, p. 7. arXiv: 1607.05263 [astro-ph.EP].

Dainty, J. C. (1973). "Diffraction-limited imaging of stellar objects using telescopes of low optical quality." In: *Optics Communications* 7, pp. 129–134.

– (1974). "The transfer function, signal-to-noise ratio, and limiting magnitude in stellar speckle interferometry". In: MNRAS 169, pp. 631–641.

– (1981). "Speckle interferometry in astronomy". In: *Recent Advances in Observational Astronomy*. Ed. by H. L. Johnson and C. Allen, pp. 95–109.

Dainty, J. C. and A. H. Greenaway (1979). "Estimation of spatial power spectra in speckle interferometry". In: *Journal of the Optical Society of America (1917-1983)* 69, p. 786.

Dayton, D., R. Pierson, B. Spielbusch, and J. Gonglewski (1992). "Atmospheric Phase Structure Function Measurements with a Shack-Hartmann Wavefront Sensor". In: *European Southern Observatory Conference and Workshop Proceedings*. Ed. by J. M. Beckers and F. Merkle. Vol. 39. European Southern Observatory Conference and Workshop Proceedings, p. 1047.

Devaney, M. N. (1992). "Speckle Interferometric Observations of Binary Stars from La-Palma". In: *European Southern Observatory Conference and Workshop Proceedings*. Ed. by J. M. Beckers and F. Merkle. Vol. 39. European Southern Observatory Conference and Workshop Proceedings, p. 93.

Devaney, M. N., E. Thiebaut, R. Foy, A. Blazit, D. Bonneau, J. Bouvier, B. de Batz, and C. Thom (1995). "The Hα environment of T Tauri resolved by speckle interferometry." In: A&A 300, p. 181.

Djokić, M. (1996). "The invention of micrometer and its use in astronomical observations." In: *Publications de l'Observatoire Astronomique de Beograd* 54, pp. 191–192.

Docobo, D. A. and C. Prieto (1995). "New orbit for WDS 06053+7400". In: *IAU Commission on Double Stars* 126, p. 1.

Docobo, J. A. (1985). "On the analytic calculation of visual double star orbits". In: *Celestial Mechanics* 36, pp. 143–153.

– (1988). "New orbits for WDS 005943617, WDS 23075+0209". In: *IAU Commission on Double Stars* 104, p. 1.

– (1991a). *La obra cintífica de Aller Ulloa*. Fundación Alfredo Brañas.

– (1991b). "New orbits for WDS 10282-2549, WDS 23078+6338". In: *IAU Commission on Double Stars* 115, p. 1.

– (1996). "New orbit for WDS 15262-2819". In: *IAU Commission on Double Stars* 129, p. 1.

– (1998). "Micrometer measurements of double stars from the Spanish observatories at Calar Alto and Santiago de Compostela." In: A&AS 130, p. 117.

– (2000). "New orbit for WDS 00243+5201". In: *IAU Commission on Double Stars* 141, pp. 1–1.

– (2012). "The use of Docobo's analytic method for calculating visual double star orbits". In: *Orbital Couples: Pas de Deux in the Solar System and the Milky Way*. Ed. by F. Arenou and D. Hestroffer, pp. 119–123.

– (2016). *Ramón María Aller Ulloa, Astrónomo y matemático*. Ed. Ouvirmos.

Docobo, J. A. and M. Andrade (2013). "Dynamical and physical properties of 22 binaries discovered by W. S. Finsen". In: MNRAS 428, pp. 321–339.

Docobo, J. A. and Y. Y. Balega (1998). "New orbit for WDS 13320+3109". In: *IAU Commission on Double Stars* 135, p. 2.

Docobo, J. A. and J. M. Costa (1986). "First orbits for the visual double stars ADS 328, ADS 9043, and ADS 13048". In: ApJS 60, pp. 945–948.

– (1987a). "New orbit for WDS 21397+2817". In: *IAU Commission on Double Stars* 103, p. 1.

– (1987b). "New orbits for WDS 08568+4733, WDS 08568+4733". In: *IAU Commission on Double Stars* 101, p. 1.

– (1987c). "New orbits for WDS 20166+3905". In: *IAU Commission on Double Stars* 102, p. 1.

– (1988a). "New orbit for WDS 18508+0319". In: *IAU Commission on Double Stars* 106, p. 1.

– (1988b). "New orbits for WDS 00463+2205, WDS 03555+0448". In: *IAU Commission on Double Stars* 105, p. 1.

– (1989a). "New orbit for WDS 00550+2337". In: *IAU Commission on Double Stars* 109, p. 1.

– (1989b). “New orbit for WDS 00593-0040”. In: *IAU Commission on Double Stars* 107, p. 1.
– (1989c). “New orbit for WDS 04256+1852”. In: *IAU Commission on Double Stars* 108, p. 1.
– (1990a). “New orbits for WDS 01050+3649, WDS 04432+5932, WDS 23115+3813.” In: *IAU Commission on Double Stars* 111, p. 1.
– (1990b). “New orbits for WDS 14159-0704, WDS 17323+2849.” In: *IAU Commission on Double Stars* 112, p. 1.
– (1990c). “New orbits for WDS 17505+0715, WDS 22575+4728.” In: *IAU Commission on Double Stars* 110, p. 1.
– (1990d). “Orbit of the visual binary WDS No. 00550N2338 (ADS 755 AB)”. In: PASP 102, pp. 1400–1405.
– (1991). “New orbits for WDS 17366+0722, WDS 17533-3444, WDS 17563+0259.” In: *IAU Commission on Double Stars* 113, p. 1.
– (1992). “First orbits for the visual double stars WDS 00516N2238, WDS 17366NJ0722, WDS 17563N0259, and WDS 23020N4800”. In: ApJS 82, pp. 323–327.
Docobo, J. A., A. Elipe, and H. McAlister, eds. (1997). *Visual double stars : formation, dynamics and evolutionary tracks*. Vol. 223. Astrophysics and Space Science Library.
Docobo, J. A. and J. F. Ling (1991). “New orbits for WDS 15428+5059, WDS 16515+0113”. In: *IAU Commission on Double Stars* 115, p. 1.
– (1992a). “New orbit for WDS 07573+0108”. In: *IAU Commission on Double Stars* 117, p. 1.
– (1992b). “New orbit for WDS 15416+1941”. In: *IAU Commission on Double Stars* 118, p. 1.
– (1992c). “New orbit for WDS 20232+2052”. In: *IAU Commission on Double Stars* 116, p. 1.
– (1993a). “New orbit for WDS 01497-1414”. In: *IAU Commission on Double Stars* 120, p. 1.
– (1993b). “New orbits for WDS 03310+2937, WDS 20311+3332”. In: *IAU Commission on Double Stars* 121, p. 1.
– (1993c). “New orbits for WDS 04262+3443, WDS 08267+2433.” In: *IAU Commission on Double Stars* 119, p. 1.
– (1994a). “Micrometer measurements of visual double stars made at PIC du Midi Observatory”. In: A&AS 105, pp. 337–339.
– (1994b). “New orbit for WDS 20494+1124”. In: *IAU Commission on Double Stars* 123, p. 1.
– (1994c). “New orbits for WDS 01039+3528, WDS 05411+1632, WDS 21000+4005”. In: *IAU Commission on Double Stars* 124, p. 1.
– (1995a). “New orbits for WDS 00596-0111,WDS 17575+1057,WDS19471-0810”. In: *IAU Commission on Double Stars* 127, p. 1.

Docobo, J. A. and J. F. Ling (1995b). "New orbits for WDS 10585+1711, WDS 15370+6427". In: *IAU Commission on Double Stars* 125, p. 1.
– (1996a). "New orbit for WDS 19172-6640". In: *IAU Commission on Double Stars* 130, p. 1.
– (1996b). "New orbit for WDS 19487+1503". In: *IAU Commission on Double Stars* 128, p. 1.
– (1997a). "New orbit for WDS 19055+3352". In: *IAU Commission on Double Stars* 132, p. 1.
– (1997b). "New orbitS for WDS 17103-1544, WDS 22401+0112". In: *IAU Commission on Double Stars* 133, p. 1.
– (1997c). "New orbits for WDS 23506-5142,WDS 23529-0313". In: *IAU Commission on Double Stars* 131, p. 1.
– (1998a). "New orbits for WDS 05413+1632, WDS16384+3514,WDS 20311+3333, WDS 20494+1124, WDS 23517-0637". In: *IAU Commission on Double Stars* 135, p. 3.
– (1998b). "New orbits for WDS 15390+2545,17075+3810". In: *IAU Commission on Double Stars* 136, p. 1.
– (1998c). "New orbits for WDS 19180+2012,WDS 23382+5514". In: *IAU Commission on Double Stars* 134, p. 2.
– (1999a). "New orbit for WDS 22077+2622". In: *IAU Commission on Double Stars* 137, p. 1.
– (1999b). "New orbits for WDS 01450+2703 and WDS 23199+2844". In: *IAU Commission on Double Stars* 138, pp. 1–2.
– (1999c). "Orbits of Five Visual Double Stars". In: ApJS 120, pp. 41–48.
– (2000a). "New orbits for WDS 00593-0040,WDS 01233+5808, WDS 02039+4220." In: *IAU Commission on Double Stars* 142, pp. 1–1.
– (2000b). "New orbits for WDS 03320+4341, WDS 18043+4206." In: *IAU Commission on Double Stars* 141, pp. 2–2.
– (2000c). "New orbits for WDS 03423+3141, WDS 06503+2410, WDS 19411+1349." In: *IAU Commission on Double Stars* 140.
– (2003). "Orbits and masses of twenty double stars discovered by Paul Couteau". In: A&A 409, pp. 989–992.
Docobo, J. A., J. F. Ling, and C. Prieto (1994). "Orbits of six visual double stars". In: ApJS 91, pp. 793–798.
Docobo, J. A. and C. Prieto (1991a). "New orbit for WDS 07079-1542". In: *IAU Commission on Double Stars* 113, p. 1.
– (1991b). "New orbit for WDS 08214-0136". In: *IAU Commission on Double Stars* 114, p. 1.
– (1992). "New orbit for WDS 19549+5049". In: *IAU Commission on Double Stars* 118, p. 1.
– (1993a). "Micrometer measurements of visual double stars made at the Spanish observatories at Calar Alto and Fabra". In: A&AS 100, pp. 641–646.

– (1993b). “New orbit for WDS 05482+0137”. In: *IAU Commission on Double Stars* 120, p. 1.
– (1994). “New orbit for WDS 19398-2326”. In: *IAU Commission on Double Stars* 122, p. 1.
– (1996a). “New orbit for WDS 05276-2055”. In: *IAU Commission on Double Stars* 128, p. 1.
– (1996b). “New orbit for WDS 09001-1228”. In: *IAU Commission on Double Stars* 130, p. 1.

Docobo, J. A. and V. S. Tamazian (1998). “New orbit for WDS 14310-0548”. In: *IAU Commission on Double Stars* 135, p. 2.

Docobo, J. A., V. S. Tamazian, and P. P. Campo (2018). “On the orbit calculation of visual binaries with a very short arc: application to the PMS binary system, FW Tau AB”. In: MNRAS 476, pp. 2792–2800.

Docobo, J. A. and V. A. Vasyuk (2000). “New orbit for WDS 02537+3820.” In: *IAU Commission on Double Stars* 141, pp. 1–1.

Docobo, J. A., J. F. Ling, V. Lanchares, A. C. Elipe, and A. J. Abad (1991). “Orbita de la binaria espectro-interferométrica 94 Aquarii.” In: *Boletin de la Astronomico Observatorio de Madrid* 12, pp. 170–183.

Docobo, J. A., N. D. Melikian, V. S. Tamazian, M. H. Eritsian, and A. A. Karapetian (1998). “Photometric and polarimetric observations of double and multiple stars.” In: *Astrophysics* 41, pp. 254–260.

Docobo, J. A., V. Tamazian, P. Abelleira, J. Blanco, V. Lanchares, Y. Balega, A. Maximov, and V. Vasyuk (1999). “New orbits for WDS 16584+3943, WDS 16584+3943, WDS 18035+4032.” In: *IAU Commission on Double Stars* 139, pp. 2–2.

Docobo, J. A., C. Alvarez, J. F. Lahulla, V. Lancharesi, and A. Aguirre (2000a). “CCD measurements of visual double stars from the German-Spanish Astronomical Center at Calar Alto”. In: *Astronomische Nachrichten* 321, pp. 53–57.

Docobo, J. A., Y. Y. Balega, J. F. Ling, V. Tamazian, and V. A. Vasyuk (2000b). “Orbits of Visual Binaries WDS 13320+3109, 14310-0548, 14492+1013, and 16384+3514”. In: AJ 119, pp. 2422–2427.

Docobo, J. A., V. S. Tamazian, Y. Y. Balega, J. Blanco, A. F. Maximov, and V. A. Vasyuk (2001). “Binary star speckle measurements at Calar Alto. I.” In: A&A 366, pp. 868–872.

Docobo, J. A., V. S. Tamazian, M. Andrade, and N. D. Melikian (2003). “Orbit and System Mass for the Visual Binary WDS 23186+6807AB”. In: AJ 126, pp. 1522–1525.

Docobo, J. A., M. Andrade, J. F. Ling, C. Prieto, V. S. Tamazian, Y. Y. Balega, J. Blanco, A. F. Maximov, J. F. Lahulla, and C. Alvarez (2004). “Binary Star Speckle Interferometry: Measurements and Orbits”. In: AJ 127, pp. 1181–1186.

Docobo, J. A., V. S. Tamazian, Y. Y. Balega, and N. D. Melikian (2006). “Speckle Measurements and Differential Photometry of Visual Binaries with the 6 Meter Telescope of the Special Astrophysical Observatory”. In: AJ 132, pp. 994–998.

Docobo, J. A., V. S. Tamazian, M. Andrade, J. F. Ling, Y. Y. Balega, J. F. Lahulla, and A. A. Maximov (2008). “First Results of the Optical Speckle Interferometry with the 3.5

m Telescope at Calar Alto (spain): Measurements and Orbits of Visual Binaries". In: AJ 135, pp. 1803–1809.

Docobo, J. A., V. S. Tamazian, Y. Y. Balega, and N. D. Melikian (2010). "EMCCD Speckle Interferometry with the 6 m Telescope: Astrometric Measurements, Differential Photometry, and Orbits". In: AJ 140, pp. 1078–1083.

Docobo, J. A., P. P. Campo, M. Andrade, and E. P. Horch (2014). "An analytic algorithm to calculate the inclination, ascending node, and semimajor axis of spectroscopic binary orbits using a single speckle measurement and the parallax". In: *Astrophysical Bulletin* 69, pp. 461–471.

Docobo, J. A., M. Andrade, P. P. Campo, and J. F. Ling (2016). "A 3D model for α Gem AB: orbits and dynamics". In: Ap&SS 361, 46, p. 46.

Docobo, J. A., R. F. Griffin, P. P. Campo, and A. A. Abushattal (2017a). "Precise orbital elements, masses and parallax of the spectroscopic-interferometric binary HD 26441". In: MNRAS 469, pp. 1096–1100. arXiv: 1704.03245 [astro-ph.SR].

Docobo, J. A., J. Gomez, N. D. Melikian, and G. M. Paronyan (2017b). "Speckle Interferometric Observations on 2.6 m telescope of BAO". In: *Communications of the Byurakan Astrophysical Observatory* 64, pp. 84–91.

Docobo, J. A., P. P. Campo, J. Gomez, and E. P. Horch (2018a). "The Three-dimensional Orbit, Orbital Parallax, and Individual Masses of the Double-lined Spectroscopic Binaries HD 183255, HD 114882, and HD 30712". In: AJ 156, 185, p. 185.

Docobo, J. A., V. S. Tamazian, P. P. Campo, and L. Piccotti (2018b). "Visual Orbit and Individual Masses of the Single-lined Spectroscopic Binary 94 AQR A (HD 219834A; MCA 74)". In: AJ 156, 85, p. 85.

Docobo, José A, Jorge Gomez, Pedro P Campo, Manuel Andrade, Elliott P Horch, Edgardo Costa, and Rene A Mendez (2018). "Orbits of 14 Binaries Based on 2018 Soar Speckle Observations*". In: *Monthly Notices of the Royal Astronomical Society*, sty2704. eprint: /oup/backfile/content_public/journal/mnras/pap/10.1093_mnras_sty2704/1/sty2704.pdf.

Dotter, A. (2016). "MESA Isochrones and Stellar Tracks (MIST) 0: Methods for the Construction of Stellar Isochrones". In: ApJS 222, 8, p. 8. arXiv: 1601.05144 [astro-ph.SR].

Douglass, G. G., R. B. Hindsley, and C. E. Worley (1993). "Three Years of Speckle Interferometry at the U.S. Naval Observatory". In: *American Astronomical Society Meeting Abstracts*. Vol. 25. Bulletin of the American Astronomical Society, p. 1426.

– (1997). "Speckle Interferometry at the US Naval Observatory. I." In: ApJS 111, pp. 289–334.

Douglass, G. G., B. D. Mason, M. E. Germain, and C. E. Worley (1999). "Speckle Interferometry at the US Naval Observatory. IV." In: AJ 118, pp. 1395–1405.

Douglass, G. G., B. D. Mason, T. J. Rafferty, E. R. Holdenried, and M. E. Germain (2000). "Speckle Interferometry at the US Naval Observatory. V." In: AJ 119, pp. 3071–3083.

Druesne, P., J. Borgnino, F. Martin, G. Ricort, and C. Aime (1989). "Speckle interferometric study of the solar granulation from centre to limb". In: A&A 217, pp. 229–236.

Drummond, J. D., W. J. Cocke, E. K. Hege, and P. A. Strittmatter (1982). "The Size, Shape, and Rotational Pole of 433 Eros from Speckle Interferometry." In: *Bulletin of the American Astronomical Society*. Vol. 14. BAAS, p. 725.

Duquennoy, A. and M. Mayor (1991). "Multiplicity among solar-type stars in the solar neighbourhood. II - Distribution of the orbital elements in an unbiased sample". In: A&A 248, pp. 485–524.

Duquennoy, A., A. A. Tokovinin, C. Leinert, A. Glindemann, J.-L. Halbwachs, and M. Mayor (1996). "Spectroscopic and speckle interferometric orbit of Gliese 692.1." In: A&A 314, pp. 846–848.

Dyck, H. M. and R. R. Howell (1982). "Speckle interferometry of molecular cloud sources at 4.8 microns". In: AJ 87, pp. 400–403.

Dyck, H. M., B. Zuckerman, C. Leinert, and S. Beckwith (1984). "Near-infrared speckle interferometry of evolved stars and bipolar nebulae". In: ApJ 287, pp. 801–813.

Ebersberger, J. and G. Weigelt (1979). "Speckle interferometry and speckle holography with the 1.5 M and 3.6 M ESO telescopes". In: *The Messenger* 18, pp. 24–27.

Eritsian, M. A., J. A. Docobo, N. D. Melikian, and V. S. Tamazian (1998). "Photometric and polarimetric observations of U Ophiuchi". In: A&A 329, pp. 1075–1079.

ESA, ed. (1997). *The HIPPARCOS and TYCHO catalogues. Astrometric and photometric star catalogues derived from the ESA HIPPARCOS Space Astrometry Mission*. Vol. 1200. ESA Special Publication.

Esposito, S., A. Riccardi, L. Fini, A. T. Puglisi, E. Pinna, M. Xompero, R. Briguglio, F. Quirós-Pacheco, P. Stefanini, J. C. Guerra, L. Busoni, A. Tozzi, F. Pieralli, G. Agapito, G. Brusa-Zappellini, R. Demers, J. Brynnel, C. Arcidiacono, and P. Salinari (2010). "First light AO (FLAO) system for LBT: final integration, acceptance test in Europe, and preliminary on-sky commissioning results". In: *Adaptive Optics Systems II*. Vol. 7736. Proc. SPIE, p. 773609.

Evans, D. S. (1955). "An occultation of Antares observed at the Union Observatory". In: MNRAS 115, p. 468.

Finsen, W. S. (1964a). "Interferometer Measures of Double Stars". In: *Republic Observatory Johannesburg Circular* 123, pp. 53–58.

– (1964b). "SYMPOSIUM ON INSTRUMENTAL ASTRONOMY: Interferometer observation of binary stars". In: AJ 69, p. 319.

– (1971). "Twenty Years of Doubles-Star Interferometry and its Lessons". In: Ap&SS 11, p. 13.

Fors, O., E. P. Horch, and J. Núñez (2004). "Application of fast CCD drift scanning to speckle imaging of binary stars". In: A&A 420, pp. 397–404. eprint: astro-ph/0403107.

Fors, O., J. Núñez, and A. Richichi (2001). "CCD drift-scan imaging lunar occultations: A feasible approach for sub-meter class telescopes". In: A&A 378, pp. 1100–1106. eprint: astro-ph/0108415.

Fors, O., A. Richichi, J. Núñez, and A. Prades (2004). "Infrared and visual lunar occultations measurements of stellar diameters and new binary stars detections at the Calar Alto 1.5 m telescope". In: A&A 419, pp. 285–290. eprint: astro-ph/0401638.

Fors, O., J. Núñez, J. L. Muiños, F. J. Montojo, R. Baena-Gallé, J. Boloix, R. Morcillo, M. T. Merino, E. C. Downey, and M. J. Mazur (2013). "Telescope Fabra ROA Montsec: A New Robotic Wide Field Baker-Nunn Facility". In: PASP 125, p. 522. arXiv: 1211.5581 [astro-ph.IM].

Fraquelli, D. A., A. B. Schultz, H. Bushouse, H. M. Hart, and P. Vener (2004). "NICMOS Coronagraphy". In: PASP 116, pp. 55–64.

Fried, D. L. (1965). "Statistics of a Geometric Representation of Wavefront Distortion". In: *Journal of the Optical Society of America (1917-1983)* 55, pp. 1427–1431.

– (1978). "Probability of getting a lucky short-exposure image through turbulence". In: *Journal of the Optical Society of America (1917-1983)* 68, pp. 1651–1658.

Fruchter, A. S. and R. N. Hook (2002). "Drizzle: A Method for the Linear Reconstruction of Undersampled Images". In: PASP 114, pp. 144–152. eprint: astro-ph/9808087.

Furlan, E., D. R. Ciardi, M. E. Everett, M. Saylors, J. K. Teske, E. P. Horch, S. B. Howell, G. T. van Belle, L. A. Hirsch, T. N. Gautier III, E. R. Adams, D. Barrado, K. M. S. Cartier, C. D. Dressing, A. K. Dupree, R. L. Gilliland, J. Lillo-Box, P. W. Lucas, and J. Wang (2017). "The Kepler Follow-up Observation Program. I. A Catalog of Companions to Kepler Stars from High-Resolution Imaging". In: AJ 153, 71, p. 71. arXiv: 1612.02392 [astro-ph.SR].

Gaia Collaboration, A. G. A. Brown, A. Vallenari, T. Prusti, J. H. J. de Bruijne, F. Mignard, R. Drimmel, C. Babusiaux, C. A. L. Bailer-Jones, U. Bastian, and et al. (2016). "Gaia Data Release 1. Summary of the astrometric, photometric, and survey properties". In: A&A 595, A2, A2. arXiv: 1609.04172 [astro-ph.IM].

Gaia Collaboration, A. G. A. Brown, A. Vallenari, T. Prusti, J. H. J. de Bruijne, C. Babusiaux, and C. A. L. Bailer-Jones (2018). "Gaia Data Release 2. Summary of the contents and survey properties". In: *ArXiv e-prints*. arXiv: 1804.09365.

Gaidos, E., A. W. Mann, S. Lépine, A. Buccino, D. James, M. Ansdell, R. Petrucci, P. Mauas, and E. J. Hilton (2014). "Trumpeting M dwarfs with CONCH-SHELL: a catalogue of nearby cool host-stars for habitable exoplanets and life". In: MNRAS 443, pp. 2561–2578. arXiv: 1406.7353 [astro-ph.SR].

Germain, M. E., G. G. Douglass, and C. E. Worley (1999a). "Speckle Interferometry at the US Naval Observatory. II." In: AJ 117, pp. 1905–1920.

– (1999b). "Speckle Interferometry at the US Naval Observatory. III." In: AJ 117, pp. 2511–2527.

Gezari, D. Y., A. Labeyrie, and R. V. Stachnik (1972). "Speckle Interferometry: Diffraction-Limited Measurements of Nine Stars with the 200-INCH Telescope". In: ApJ 173, p. L1.

Gies, D. R., B. D. Mason, W. I. Hartkopf, H. A. McAlister, R. A. Frazin, M. E. Hahula, L. R. Penny, M. L. Thaller, A. W. Fullerton, and M. M. Shara (1993). "Binary star orbits from

speckle interferometry. 5: A combined speckle/spectroscopic study of the O star binary 15 Monocerotis". In: AJ 106, pp. 2072–2080.

Gies, D. R., S. Dieterich, N. D. Richardson, A. R. Riedel, B. L. Team, H. A. McAlister, W. G. Bagnuolo Jr., E. D. Grundstrom, S. Štefl, T. Rivinius, and D. Baade (2008). "A Spectroscopic Orbit for Regulus". In: ApJ 682, p. L117. arXiv: 0806.3473.

Gliese, W. (1969). "Catalogue of Nearby Stars. Edition 1969". In: *Veroeffentlichungen des Astronomischen Rechen-Instituts Heidelberg* 22.

Gliese, W. and H. Jahreiß (1979). "Nearby Star Data Published 1969-1978". In: A&AS 38.

Golbraikh, E., H. Branover, N. S. Kopeika, and A. Zilberman (2006). "Non-Kolmogorov atmospheric turbulence and optical signal propagation". In: *Nonlinear Processes in Geophysics* 13, pp. 297–301.

Gomez, J., J. A. Docobo, P. P. Campo, and R. A. Mendez (2016). "Orbits of 12 Southern Binaries Based on Soar Speckle Observations". In: AJ 152, 216, p. 216.

Gough, P. T. and R. H. T. Bates (1974). "Speckle holography." In: *Optica Acta* 21, pp. 243–254.

Gray, D. F. (2005). *The Observation and Analysis of Stellar Photospheres*.

Grec, C., C. Aime, M. Faurobert, G. Ricort, and F. Paletou (2007). "Differential speckle interferometry: in-depth analysis of the solar photosphere". In: A&A 463, pp. 1125–1136.

Greenwood, D. P. (1977). "Bandwidth specification for adaptive optics systems". In: *Journal of the Optical Society of America (1917-1983)* 67, pp. 390–393.

Guyon, O., B. Gallet, E. A. Pluzhnik, H. Takami, and M. Tamura (2006). "High contrast imaging with focal plane wavefront sensing for ground based telescopes". In: *Society of Photo-Optical Instrumentation Engineers (SPIE) Conference Series*. Vol. 6272. Proc. SPIE, p. 62723C.

Harris III, D. L., K. A. Strand, and C. E. Worley (1963). "Empirical Data on Stellar Masses, Luminosities, and Radii". In: *Basic Astronomical Data: Stars and Stellar Systems*. Ed. by K. A. Strand. the University of Chicago Press, p. 273.

Hartkopf, W. I. (1992). "Twenty Years of Speckle Interferometry". In: *IAU Colloq. 135: Complementary Approaches to Double and Multiple Star Research*. Ed. by H. A. McAlister and W. I. Hartkopf. Vol. 32. Astronomical Society of the Pacific Conference Series, p. 459.

Hartkopf, W. I. and B. D. Mason (2011). "Speckle Interferometry at the USNO Flagstaff Station: Observations Obtained in 2008 and Nine New Orbits". In: AJ 142, 56, p. 56.

– (2015). "Speckle Interferometry at the U.S. Naval Observatory. XX". In: AJ 150, 136, p. 136.

Hartkopf, W. I., B. D. Mason, and H. A. McAlister (1996). "Binary Star Orbits From Speckle Interferometry. VIII. Orbits of 37 Close Visual System". In: AJ 111, p. 370.

Hartkopf, W. I., B. D. Mason, and T. J. Rafferty (2008). "Speckle Interferometry at the USNO Flagstaff Station: Observations Obtained in 2003-2004 and 17 New Orbits". In: AJ 135, pp. 1334–1342.

Hartkopf, W. I., B. D. Mason, and C. E. Worley (2001). "The 2001 US Naval Observatory Double Star CD-ROM. II. The Fifth Catalog of Orbits of Visual Binary Stars". In: AJ 122, pp. 3472–3479.

Hartkopf, W. I. and H. A. McAlister (1984). "Binary stars unresolved by speckle interferometry. III". In: PASP 96, pp. 105–116.

– (1991). "The GSU/CHARA program of binary star speckle interferometry - Recent results". In: Ap&SS 177, pp. 161–167.

Hartkopf, W. I., H. A. McAlister, and O. G. Franz (1989). "Binary star orbits from speckle interferometry. II - Combined visual-speckle orbits of 28 close systems". In: AJ 98, pp. 1014–1039.

Hartkopf, W. I., B. D. Mason, D. J. Barry, H. A. McAlister, W. G. Bagnuolo, and C. M. Prieto (1993). "ICCD speckle observations of binary stars. VIII - Measurements during 1989-1991 from the Cerro Tololo 4 M telescope". In: AJ 106, pp. 352–360.

Hartkopf, W. I., B. D. Mason, H. A. McAlister, N. H. Turner, D. J. Barry, O. G. Franz, and C. M. Prieto (1996). "ICCD Speckle Observations of Binary Stars. XIII. Measurements During 1989- 1994 From the Cerro Tololo 4 M Telescope". In: AJ 111, p. 936.

Hartmann, L. and S. J. Kenyon (1996). "The FU Orionis Phenomenon". In: ARA&A 34, pp. 207–240.

Harvey, J. W. and J. B. Breckinridge (1973). "Solar Speckle Interferometry". In: ApJ 182, p. L137.

Harvey, J. W. and M. Schwarzschild (1975). "Photoelectric speckle interferometry of the solar granulation". In: ApJ 196, pp. 221–226.

Hege, E. K., E. N. Hubbard, P. A. Strittmatter, and S. P. Worden (1981). "Speckle interferometry observations of the triple QSO PG 1115 + 08". In: ApJ 248, pp. L1–L3.

Heintz, W. D. (1978). "Double stars /Revised edition/". In: *Geophysics and Astrophysics Monographs* 15.

Henry, T. J. and D. W. McCarthy Jr. (1990). "A systematic search for brown dwarfs orbiting nearby stars". In: ApJ 350, pp. 334–347.

Henry, T. J., W.-C. Jao, J. P. Subasavage, T. D. Beaulieu, P. A. Ianna, E. Costa, and R. A. Méndez (2006). "The Solar Neighborhood. XVII. Parallax Results from the CTIOPI 0.9 m Program: 20 New Members of the RECONS 10 Parsec Sample". In: AJ 132, pp. 2360–2371. eprint: astro-ph/0608230.

Herbig, G. H. (1966). "On the interpretation of FU orionis". In: *Vistas in Astronomy* 8, pp. 109–125.

Herbst, T. M., S. V. Beckwith, C. Birk, S. Hippler, M. J. McCaughrean, F. Mannucci, and J. Wolf (1993). "MAGIC: a new near-infrared camera for Calar Alto". In: *Infrared Detectors and Instrumentation*. Ed. by A. M. Fowler. Vol. 1946. Proc. SPIE, pp. 605–609.

Herriot, G., S. Morris, S. Roberts, J. M. Fletcher, L. K. Saddlemyer, G. Singh, J.-P. Veran, and E. H. Richardson (1998). "Innovations in Gemini adaptive optics system design". In: *Adaptive Optical System Technologies*. Ed. by D. Bonaccini and R. K. Tyson. Vol. 3353. Proc. SPIE, pp. 488–499.

Hetterich, N. and G. Weigelt (1983). "Speckle interferometry observations of Pluto's moon Charon". In: A&A 125, pp. 246–248.

Hippler, S., C. Bergfors, Brandner Wolfgang, S. Daemgen, T. Henning, F. Hormuth, A. Huber, M. Janson, B. Rochau, R.-R. Rohloff, and K. Wagner (2009). "The AstraLux Sur Lucky Imaging Instrument at the NTT". In: *The Messenger* 137, pp. 14–17.

Hirsch, L. A., D. R. Ciardi, A. W. Howard, M. E. Everett, E. Furlan, M. Saylors, E. P. Horch, S. B. Howell, J. Teske, and G. W. Marcy (2017). "Assessing the Effect of Stellar Companions from High-resolution Imaging of Kepler Objects of Interest". In: AJ 153, 117, p. 117. arXiv: 1701.06577 [astro-ph.EP].

Hodapp, K.-W., J. Hora, E. Graves, E. M. Irwin, H. Yamada, J. W. Douglass, T. T. Young, and L. Robertson (2000). "Gemini near-infrared imager (NIRI)". In: *Optical and IR Telescope Instrumentation and Detectors*. Ed. by M. Iye and A. F. Moorwood. Vol. 4008. Proc. SPIE, pp. 1334–1341.

Hofmann, K.-H., Y. Balega, M. Scholz, and G. Weigelt (2000). "Multi-wavelength bispectrum speckle interferometry of R Cas and comparison of the observations with Mira star models". In: A&A 353, pp. 1016–1028.

Horch, E., O. G. Franz, and Z. Ninkov (2000). "CCD Speckle Observations of Binary Stars from the Southern Hemisphere. II. Measures from the Lowell-Tololo Telescope during 1999". In: AJ 120, pp. 2638–2648.

Horch, E., Z. Ninkov, and O. G. Franz (2001). "CCD Speckle Observations of Binary Stars from the Southern Hemisphere. III. Differential Photometry". In: AJ 121, pp. 1583–1596.

Horch, E., J. S. Morgan, G. Giaretta, and D. B. Kasle (1992a). "A new-speckle interferometry system for the MAMA detector". In: PASP 104, pp. 939–948.

Horch, E., J. G. Timothy, G. Giaretta, and D. Kasle (1992b). "The Stanford University Speckle Interferometer System". In: *American Astronomical Society Meeting Abstracts*. Vol. 24. Bulletin of the American Astronomical Society, p. 1220.

Horch, E., W. F. van Altena, T. M. Girard, C. E. Lopez, and O. Franz (1995a). "Speckle Interferometry of Double Stars from the Southern Hemisphere". In: *Astronomical and Astrophysical Objectives of Sub-Milliarcsecond Optical Astrometry*. Ed. by E. Hog and P. K. Seidelmann. Vol. 166. IAU Symposium, p. 392.

Horch, E., D. Dinescu, T. Girard, W. van Altena, C. Lopez, O. Franz, and J. G. Timothy (1995b). "The First Year of Observations on the Yale-San Juan Double Star Project". In: *American Astronomical Society Meeting Abstracts*. Vol. 27. Bulletin of the American Astronomical Society, p. 1325.

Horch, E. P., Z. Ninkov, and R. W. Slawson (1997). "CCD Speckle Observations of Binary Stars From the Southern Hemisphere". In: AJ 114, p. 2117.

Horch, E. P., D. I. Dinescu, T. M. Girard, W. F. van Altena, C. E. Lopez, and O. G. Franz (1996). "Speckle Interferometry of Southern Double Stars.I.First Results of the Yale-San Juan Speckle Interferometry Program". In: AJ 111, p. 1681.

Horch, E. P., B. J. Baptista, D. R. Veillette, and O. G. Franz (2006). "CCD Speckle Observations of Binary Stars from the Southern Hemisphere. IV. Measures during 2001". In: AJ 131, pp. 3008–3015.

Horch, E. P., D. R. Veillette, R. Baena Gallé, S. C. Shah, G. V. O'Rielly, and W. F. van Altena (2009). "Observations of Binary Stars with the Differential Speckle Survey Instrument. I. Instrument Description and First Results". In: AJ 137, pp. 5057–5067.

Horch, E. P., S. C. Gomez, W. H. Sherry, S. B. Howell, D. R. Ciardi, L. M. Anderson, and W. F. van Altena (2011a). "Observations of Binary Stars with the Differential Speckle Survey Instrument. II. Hipparcos Stars Observed in 2010 January and June". In: AJ 141, 45, p. 45.

Horch, E. P., W. F. van Altena, S. B. Howell, W. H. Sherry, and D. R. Ciardi (2011b). "Observations of Binary Stars with the Differential Speckle Survey Instrument. III. Measures below the Diffraction Limit of the WIYN Telescope". In: AJ 141, 180, p. 180.

Horch, E. P., D. I. Casetti-Dinescu, M. A. Camarata, A. Bidarian, W. F. van Altena, W. H. Sherry, M. E. Everett, S. B. Howell, D. R. Ciardi, T. J. Henry, D. A. Nusdeo, and J. G. Winters (2017). "Observations of Binary Stars with the Differential Speckle Survey Instrument. VII. Measures from 2010 September to 2012 February at the WIYN Telescope". In: AJ 153, 212, p. 212. arXiv: 1703.06253 [astro-ph.SR].

Horch, E. P., J. Löbb, S. B. Howell, W. F. van Altena, T. J. Henry, and G. T. van Belle (2018). "Speckle Imaging at Gemini and the DCT". In: *Revista Mexicana de Astronomia y Astrofisica Conference Series*. Vol. 50. Revista Mexicana de Astronomia y Astrofisica Conference Series, pp. 19–22.

Hormuth, F., W. Brandner, S. Hippler, and T. Henning (2008). "AstraLux - the Calar Alto 2.2-m telescope Lucky Imaging Camera". In: *Journal of Physics Conference Series*. Vol. 131. Journal of Physics Conference Series, p. 012051. arXiv: 0807.0504.

Howell, S. B. (2000). *Handbook of CCD Astronomy*.

Howell, S. B., M. E. Everett, W. Sherry, E. Horch, and D. R. Ciardi (2011). "Speckle Camera Observations for the NASA Kepler Mission Follow-up Program". In: AJ 142, 19, p. 19.

Howell, S. B., M. E. Everett, E. P. Horch, J. G. Winters, L. Hirsch, D. Nusdeo, and N. J. Scott (2016). "Speckle Imaging Excludes Low-mass Companions Orbiting the Exoplanet Host Star TRAPPIST-1". In: ApJ 829, L2, p. L2. arXiv: 1610.05269 [astro-ph.EP].

Hubbard, G., K. Hege, M. A. Reed, P. A. Strittmatter, N. J. Woolf, and S. P. Worden (1979). "Speckle interferometry. I - The Steward Observatory speckle camera". In: AJ 84, pp. 1437–1442.

Jennison, R. C. and M. K. Das Gupta (1953). "Fine Structure of the Extra-terrestrial Radio Source Cygnus I". In: Nature 172, pp. 996–997.

Karbelkar, S. N. (1988). "Atmospheric noise on the bispectrum: limiting faintness for binary stars." In: *European Southern Observatory Conference and Workshop Proceedings*. Ed. by F. Merkle. Vol. 29. European Southern Observatory Conference and Workshop Proceedings, pp. 217–223.

Karbelkar, S. N. and R. Nityananda (1987). "Atmospheric Noise on the Bispectrum in Optical Speckle Interferometry". In: *Journal of Astrophysics and Astronomy* 8, p. 271.

Knox, K. T. and B. J. Thompson (1974). "Recovery of images from atmospherically degraded short-exposure photographs". In: ApJ 193, pp. L45–L48.

Kolmogorov, A. (1941). "The Local Structure of Turbulence in Incompressible Viscous Fluid for Very Large Reynolds' Numbers". In: *Akademiia Nauk SSSR Doklady* 30, pp. 301–305.

Korff, D. (1973). "Analysis of a method for obtaining near-diffraction-limited information in the presence of atmospheric turbulence". In: *Journal of the Optical Society of America (1917-1983)* 63, p. 971.

Korff, D., G. Dryden, and M. G. Miller (1972). "Information Retrieval from Atmospheric Induced Speckle Patterns". In: *Optics Communications* 5, pp. 187–192.

Krieg, J., F. Kneer, M. Koschinsky, and C. Ritter (2000). "Granular velocities of the Sun from speckle interferometry". In: A&A 360, pp. 1157–1162.

Labeyrie, A. (1970). "Attainment of Diffraction Limited Resolution in Large Telescopes by Fourier Analysing Speckle Patterns in Star Images". In: A&A 6, p. 85.

Labeyrie, A., D. Bonneau, R. V. Stachnik, and D. Y. Gezari (1974). "Speckle Interferometry. III. High-Resolution Measurements of Twelve Close Binary Systems". In: ApJ 194, p. L147.

Lafrenière, D., R. Doyon, É. Artigau, C. Marois, M. Beaulieu, D. Nadeau, and R. Racine (2006). "Simultaneous spectral differential imaging with a focal plane holographic diffuser". In: *Society of Photo-Optical Instrumentation Engineers (SPIE) Conference Series*. Vol. 6269. Proc. SPIE, 62692H.

Lafrenière, D., C. Marois, R. Doyon, D. Nadeau, and É. Artigau (2007a). "A New Algorithm for Point-Spread Function Subtraction in High-Contrast Imaging: A Demonstration with Angular Differential Imaging". In: ApJ 660, pp. 770–780. eprint: astro-ph/0702697.

Lafrenière, D., R. Doyon, D. Nadeau, É. Artigau, C. Marois, and M. Beaulieu (2007b). "Improving the Speckle Noise Attenuation of Simultaneous Spectral Differential Imaging with a Focal Plane Holographic Diffuser". In: ApJ 661, pp. 1208–1217. eprint: astro-ph/0703093.

Law, N. M., S. T. Hodgkin, and C. D. Mackay (2008). "The LuckyCam survey for very low mass binaries - II. 13 new M4.5-M6.0 binaries". In: MNRAS 384, pp. 150–160. arXiv: 0704.1812.

Law, N. M., C. D. Mackay, and J. E. Baldwin (2006). "Lucky imaging: high angular resolution imaging in the visible from the ground". In: A&A 446, pp. 739–745. eprint: astro-ph/0507299.

Leinert, C. and M. Haas (1989a). "Detection of an infrared companion to Haro 6-10". In: ApJ 342, pp. L39–L42.

– (1989b). "Near-infrared speckle observations of the Red Rectangle". In: A&A 221, pp. 110–122.

Leinert, C., T. Henry, A. Glindemann, and D. W. McCarthy Jr. (1997). "A search for companions to nearby southern M dwarfs with near-infrared speckle interferometry." In: A&A 325, pp. 159–166.

Linfoot, E. H. and R. C. Witcomb (1972). "Random wave-front perturbations and telescopic star images." In: MNRAS 158, pp. 199–231.

Ling, J. F. and V. Lanchares (1993). "Micrometer measurements of visual double stars at Calar Alto". In: *Astronomische Nachrichten* 314, pp. 303–305.

Ling, J. F. and C. Prieto (2000). "Micrometer measurements of double stars made at the Côte D'Azur and Calar Alto observatories". In: A&AS 143, pp. 335–342.

Liu, C. Y. C. and A. W. Lohmann (1973). "High resolution image formation through the turbulent atmosphere." In: *Optics Communications* 8, pp. 372–377.

Liu, M. C. (2004). "Substructure in the Circumstellar Disk Around the Young Star AU Microscopii". In: *Science* 305, pp. 1442–1444. eprint: astro-ph/0408164.

Lu, P. K., P. Demarque, W. van Altena, H. McAlister, and W. Hartkopf (1987). "ICCD speckle observations of binary stars. III - A survey for duplicity among high-velocity stars". In: AJ 94, pp. 1318–1326.

Lynds, C. R., S. P. Worden, and J. W. Harvey (1976). "Digital image reconstruction applied to alpha Orionis". In: ApJ 207, pp. 174–180.

Macintosh, B., J. R. Graham, P. Ingraham, Q. Konopacky, C. Marois, M. Perrin, L. Poyneer, B. Bauman, T. Barman, A. S. Burrows, A. Cardwell, J. Chilcote, R. J. De Rosa, D. Dillon, R. Doyon, J. Dunn, D. Erikson, M. P. Fitzgerald, D. Gavel, S. Goodsell, M. Hartung, P. Hibon, P. Kalas, J. Larkin, J. Maire, F. Marchis, M. S. Marley, J. McBride, M. Millar-Blanchaer, K. Morzinski, A. Norton, B. R. Oppenheimer, D. Palmer, J. Patience, L. Pueyo, F. Rantakyro, N. Sadakuni, L. Saddlemyer, D. Savransky, A. Serio, R. Soummer, A. Sivaramakrishnan, I. Song, S. Thomas, J. K. Wallace, S. Wiktorowicz, and S. Wolff (2014). "First light of the Gemini Planet Imager". In: *Proceedings of the National Academy of Science* 111, pp. 12661–12666. arXiv: 1403.7520 [astro-ph.EP].

Maksimov, A. F., Y. Y. Balega, V. V. Dyachenko, E. V. Malogolovets, D. A. Rastegaev, and E. A. Semernikov (2009). "The EMCCD-based speckle interferometer of the BTA 6-m telescope: Description and first results". In: *Astrophysical Bulletin* 64, pp. 296–307. arXiv: 0909.1119 [astro-ph.IM].

Marois, C., B. Macintosh, and J.-P. Véran (2010). "Exoplanet imaging with LOCI processing: photometry and astrometry with the new SOSIE pipeline". In: *Adaptive Optics Systems II*. Vol. 7736. Proc. SPIE, 77361J.

Marois, C., D. W. Phillion, and B. Macintosh (2006). "Exoplanet detection with simultaneous spectral differential imaging: effects of out-of-pupil-plane optical aberrations". In: *Society of Photo-Optical Instrumentation Engineers (SPIE) Conference Series*. Vol. 6269. Proc. SPIE, p. 62693M. eprint: astro-ph/0607002.

Marois, C., R. Doyon, D. Nadeau, R. Racine, and G. A. H. Walker (2003a). "Effects of Quasi-Static Aberrations in Faint Companion Searches". In: *EAS Publications Series*. Ed. by C. Aime and R. Soummer. Vol. 8. EAS Publications Series, pp. 233–243. eprint: astro-ph/0212039.

Marois, C., D. Nadeau, R. Doyon, R. Racine, and G. A. H. Walker (2003b). "Searching for Faint Companions with the TRIDENT Differential Simultaneous Imaging Camera". In:

Scientific Frontiers in Research on Extrasolar Planets. Ed. by D. Deming and S. Seager. Vol. 294. Astronomical Society of the Pacific Conference Series, pp. 103–106. eprint: astro-ph/0211636.

Marois, C., D. Lafrenière, R. Doyon, B. Macintosh, and D. Nadeau (2006). "Angular Differential Imaging: A Powerful High-Contrast Imaging Technique". In: ApJ 641, pp. 556–564. eprint: astro-ph/0512335.

Marois, C., C. Correia, R. Galicher, P. Ingraham, B. Macintosh, T. Currie, and R. De Rosa (2014). "GPI PSF subtraction with TLOCI: the next evolution in exoplanet/disk high-contrast imaging". In: *Adaptive Optics Systems IV*. Vol. 9148. Proc. SPIE, 91480U. arXiv: 1407.2555 [astro-ph.IM].

Mason, B. D. (1997). "Binary Star Orbits from Speckle Interferometry. XI. Orbits of Twelve Lunar Occultation Systems." In: AJ 114, pp. 808–818.

Mason, B. D., G. G. Douglass, and W. I. Hartkopf (1999). "Binary Star Orbits from Speckle Interferometry. I. Improved Orbital Elements of 22 Visual Systems". In: AJ 117, pp. 1023–1036.

Mason, B. D. and W. I. Hartkopf (2017). "Speckle Interferometry at the U.S. Naval Observatory. XXII." In: AJ 154, 183, p. 183. arXiv: 1707.06060 [astro-ph.SR].

Mason, B. D., W. I. Hartkopf, and E. A. Friedman (2012). "Speckle Interferometry at the U.S. Naval Observatory. XVIII". In: AJ 143, 124, p. 124.

Mason, B. D., W. I. Hartkopf, and H. M. Hurowitz (2013). "Speckle Interferometry at the U.S. Naval Observatory. XIX". In: AJ 146, 56, p. 56.

Mason, B. D., W. I. Hartkopf, and G. L. Wycoff (2008). "Speckle Interferometry at the U.S. Naval Observatory. XIV." In: AJ 136, pp. 2223–2226.

– (2010). "Speckle Interferometry at the U.S. Naval Observatory. XV." In: AJ 140, pp. 480–482. arXiv: 1006.5676 [astro-ph.SR].

– (2011a). "Speckle Interferometry at the U.S. Naval Observatory. XVI." In: AJ 141, 157, p. 157.

– (2011b). "Speckle Interferometry at the U.S. Naval Observatory. XVII." In: AJ 142, 46, p. 46.

Mason, B. D., H. A. McAlister, and W. I. Hartkopf (1996). "Binary Star Orbits From Speckle Interferometry. IX. The Nearby Solar-Type Speckle-Spectroscopic Binary Fin 347 AA". In: AJ 112, p. 276.

Mason, B. D., H. A. McAlister, W. I. Hartkopf, and M. M. Shara (1995). "Binary star orbits from speckle interferometry. 7: The multiple system XI Ursae Majoris". In: AJ 109, pp. 332–340.

Mason, B. D., H. A. McAlister, W. I. Hartkopf, R. F. Griffin, and R. E. M. Griffin (1997). "Binary Star Orbits From Speckle Interferometry. X. Speckle-Spectroscopic Orbits of HR 233, 36 Tau, and 73 Leo." In: AJ 114, p. 1607.

Mason, B. D., C. Martin, W. I. Hartkopf, D. J. Barry, M. E. Germain, G. G. Douglass, C. E. Worley, G. L. Wycoff, T. ten Brummelaar, and O. G. Franz (1999). "Speckle Interferometry of New and Problem HIPPARCOS Binaries". In: AJ 117, pp. 1890–1904.

Mason, B. D., W. I. Hartkopf, E. R. Holdenried, T. J. Rafferty, G. L. Wycoff, G. S. Hennessy, D. M. Hall, S. E. Urban, and T. E. Corbin (2000). "Speckle Interferometry at the US Naval Observatory. VI." In: AJ 120, pp. 1120–1132.

Mason, B. D., W. I. Hartkopf, G. L. Wycoff, E. R. Holdenried, I. Platais, T. J. Rafferty, D. M. Hall, G. S. Hennessy, S. E. Urban, and B. L. Pohl (2001a). "Speckle Interferometry at the US Naval Observatory. VII." In: AJ 122, pp. 1586–1601.

Mason, B. D., W. I. Hartkopf, E. R. Holdenried, and T. J. Rafferty (2001b). "Speckle Interferometry of New and Problem Hipparcos Binaries. II. Observations Obtained in 1998-1999 from McDonald Observatory". In: AJ 121, pp. 3224–3234.

Mason, B. D., G. L. Wycoff, W. I. Hartkopf, G. G. Douglass, and C. E. Worley (2001c). "The 2001 US Naval Observatory Double Star CD-ROM. I. The Washington Double Star Catalog". In: AJ 122, pp. 3466–3471.

Mason, B. D., W. I. Hartkopf, S. E. Urban, G. L. Wycoff, D. Pascu, D. M. Hall, G. S. Hennessy, I. Platais, T. J. Rafferty, and E. R. Holdenried (2002). "Speckle Interferometry at the US Naval Observatory. VIII." In: AJ 124, pp. 2254–2272.

Mason, B. D., W. I. Hartkopf, G. L. Wycoff, D. Pascu, S. E. Urban, D. M. Hall, G. S. Hennessy, T. J. Rafferty, L. Flagg, D. Kang, P. Ries, and E. Holdenried (2004a). "Speckle Interferometry at the US Naval Observatory. IX." In: AJ 127, pp. 539–548.

Mason, B. D., W. I. Hartkopf, G. L. Wycoff, T. J. Rafferty, S. E. Urban, and L. Flagg (2004b). "Speckle Interferometry at the US Naval Observatory. X." In: AJ 128, pp. 3012–3018.

Mason, B. D., W. I. Hartkopf, G. L. Wycoff, and T. J. Rafferty (2006a). "Speckle Interferometry at the US Naval Observatory. XI." In: AJ 131, pp. 2687–2694.

Mason, B. D., W. I. Hartkopf, G. L. Wycoff, and E. R. Holdenried (2006b). "Speckle Interferometry at the US Naval Observatory. XII." In: AJ 132, pp. 2219–2230.

Mason, B. D., W. I. Hartkopf, G. L. Wycoff, and G. Wieder (2007). "Speckle Interferometry at the US Naval Observatory. XIII." In: AJ 134, pp. 1671–1678.

Mason, B. D., W. I. Hartkopf, D. R. Gies, T. J. Henry, and J. W. Helsel (2009). "The High Angular Resolution Multiplicity of Massive Stars". In: AJ 137, pp. 3358–3377. arXiv: 0811.0492.

Mason, B. D., W. I. Hartkopf, G. Bredthauer, E. W. Ferguson, C. T. Finch, C. M. Kilian, T. J. Rafferty, T. J. Ragan, and G. D. Wieder (2017). "Speckle Interferometry at the U.S. Naval Observatory. XXI." In: AJ 153, 20, p. 20.

Matsuo, K., M. C. Teich, and B. E. A. Saleh (1985). "Noise properties and time response of the staircase avalanche photodiode". In: *IEEE Transactions on Electron Devices* 32, pp. 2615–2623.

McAlister, H., W. I. Hartkopf, and O. G. Franz (1990). "ICCD speckle observations of binary stars. V - Measurements during 1988-1989 from the Kitt Peak and the Cerro Tololo 4 M telescopes". In: AJ 99, pp. 965–978.

McAlister, H. A. (1976a). "Speckle interferometry of eta Orionis." In: PASP 88, pp. 957–959.

– (1976b). "Spectroscopic binaries as a source for astrometric and speckle interferometric studies." In: PASP 88, pp. 317–322.

– (1977a). “Speckle interferometric measurements of binary stars. I”. In: ApJ 215, pp. 159–165.
– (1977b). “Speckle interferometry of the Hyades spectroscopic binary 51 Tauri.” In: ApJ 212, pp. 459–461.
– (1978a). “Binary stars unresolved by speckle interferometry”. In: PASP 90, pp. 288–296.
– (1978b). “Masses and luminosities for the spectroscopic/speckle interferometric binary 12 Persei”. In: ApJ 223, pp. 526–529.
– (1978c). “Speckle interferometric measurements of binary stars. II”. In: ApJ 225, pp. 932–938.
– (1979a). “Speckle interferometric measurements of binary stars. IV”. In: ApJ 230, pp. 497–501.
– (1979b). “Speckle Interferometry of the Spectroscopic Binary ϵ Cephei”. In: *Bulletin of the American Astronomical Society*. Vol. 11. BAAS, p. 405.
– (1981). “Speckle interferometry of Tau Persei”. In: AJ 86, pp. 1397–1400.
– (1983). “Five years of double star interferometry and its lessons”. In: *Lowell Observatory Bulletin* 9, pp. 125–143.
– (1988). “The GSU/CHARA optical telescope array project.” In: *European Southern Observatory Conference and Workshop Proceedings*. Ed. by F. Merkle. Vol. 29. European Southern Observatory Conference and Workshop Proceedings, pp. 971–979.
McAlister, H. A. and K. A. Degioia (1979). “Speckle interferometric measurements of binary stars. III.” In: ApJ 228, pp. 493–496.
McAlister, H. A. and F. C. Fekel (1980). “Speckle interferometric measurements of binary stars. V”. In: ApJS 43, pp. 327–337.
McAlister, H. A. and W. I. Hartkopf (1982). “Speckle interferometry of the spectroscopic binary 94 Aquarii A”. In: PASP 94, pp. 832–834.
– (1983). “Standard stars for binary-star interferometry”. In: PASP 95, pp. 778–781.
– (1984). *Catalog of interferometric measurements of binary stars*.
McAlister, H. A., W. I. Hartkopf, and B. D. Mason (1992). “Binary star orbits from speckle interferometry. IV - The old disk population star HR 1071”. In: AJ 104, pp. 1961–1967.
McAlister, H. A. and E. M. Hendry (1981). “Binary Stars Unresolved by Speckle Interferometry - Part Two”. In: PASP 93, p. 221.
– (1982a). “Speckle interferometric measurements of binary stars. VI”. In: ApJS 48, pp. 273–278.
– (1982b). “Speckle interferometric measurements of binary stars. VII”. In: ApJS 49, pp. 267–272.
McAlister, H. A., W. G. Robinson, and S. L. Marcus (1982). “Development of a Dual Microchannel Plate Intensified Charge-Coupled Device CCD Speckle Camera”. In: *Instrumentation in Astronomy IV*. Vol. 331. Proc. SPIE, p. 113.
McAlister, H. A., E. M. Hendry, W. I. Hartkopf, B. G. Campbell, and F. C. Fekel (1983). “Speckle interferometric measurements of binary stars. VIII”. In: ApJS 51, pp. 309–320.

McAlister, H. A., W. I. Hartkopf, B. J. Gaston, E. M. Hendry, and F. C. Fekel (1984). "Speckle interferometric measurements of binary stars. IX". In: ApJS 54, pp. 251–257.

McAlister, H. A., W. I. Hartkopf, D. J. Hutter, and O. G. Franz (1985). "Interferometric Measurements of Binary Stars with the GSU ICCD Speckle Camera". In: *Bulletin of the American Astronomical Society*. Vol. 17. BAAS, p. 551.

McAlister, H. A., W. I. Hartkopf, D. J. Hutter, M. M. Shara, and O. G. Franz (1987a). "ICCD speckle observations of binary stars. I - A survey for duplicity among the bright stars". In: AJ 93, pp. 183–194.

McAlister, H. A., W. I. Hartkopf, D. J. Hutter, and O. G. Franz (1987b). "ICCD speckle observations of binary stars. II - Measurements during 1982-1985 from the Kitt Peak 4 M telescope". In: AJ 93, pp. 688–723.

McAlister, H. A., W. I. Hartkopf, W. G. Bagnuolo Jr., J. R. Sowell, O. G. Franz, and D. S. Evans (1988). "Binary star orbits from speckle interferometry. I - The Hyades binary Finsen 342 (70 Tauri)". In: AJ 96, pp. 1431–1438.

McAlister, H. A., W. I. Hartkopf, J. R. Sowell, E. G. Dombrowski, and O. G. Franz (1989). "ICCD speckle observations of binary stars. IV - Measurements during 1986-1988 from the Kitt Peak 4 M telescope". In: AJ 97, pp. 510–531.

McAlister, H. A., W. I. Hartkopf, B. D. Mason, F. C. Fekel, P. A. Ianna, A. A. Tokovinin, R. F. Griffin, and R. B. Culver (1995). "Binary Star Orbits from Speckle Interferometry. VI. The Nearby Solar-Type Speckle-Spectroscopic Binary HR 6697". In: AJ 110, p. 366.

McCarthy, D. W., F. J. Low, S. G. Kleinmann, and F. C. Gillett (1982). "Infrared speckle interferometry of the nucleus of NGC 1068". In: ApJ 257, pp. L7–L11.

Meikle, W. P. S., S. J. Matcher, and B. L. Morgan (1987a). "Optical speckle interferometric observations of supernova 1987A." In: *Bulletin of the American Astronomical Society*. Vol. 19. BAAS, p. 950.

– (1987b). "Optical Speckle Interferometry of Supernova 1987A". In: *European Southern Observatory Conference and Workshop Proceedings*. Ed. by I. J. Danziger. Vol. 26. European Southern Observatory Conference and Workshop Proceedings, p. 197.

Melikian, N. D. (1995). "Appearance of a nebula near Y Ori". In: *Astrophysics* 38, pp. 307–308.

– (2014). "Spectra of Stellar Flares. Continuum Emission". In: *Astrophysics* 57, pp. 77–89.

Melikian, N. D. and M. A. Eritsian (1996). "Polarimetric observations of pulsating variable stars". In: *Astrophysics* 39, pp. 216–220.

Melikian, N. D. and J. Gomez (2017). "Photometric Studies of Stars in the Vicinity of Cyg OB7". In: *Astrophysics* 60, pp. 520–531.

Melikian, N. D., J. Gomez, and A. A. Karapetian (2014). "New Hα Emission Stars in Cep OB3 Region. A Rapid Brightness Variation of V 733 Cep". In: *Astrophysics* 57, pp. 500–509.

Melikian, N. D. and A. A. Karapetian (1996). "New H_α objects in dark nebulae. I." In: *Astrophysics* 39, pp. 27–32.

– (2001). "New Hα Stars, HHL Objects, and a Cometary Nebula". In: *Astrophysics* 44, pp. 216–221.
– (2003). "New T-Association in the Cyg OB7 Region". In: *Astrophysics* 46, pp. 282–290.
Melikian, N. D., A. A. Karapetian, and J. Gomez (2016). "New Emission Stars in B Cyg OB7". In: *Astrophysics* 59, pp. 484–491.
Melikian, N. D., V. S. Tamazian, and A. A. Karapetian (2006). "Spectral and photographic studies of the known T association in the neighborhood of Cyg OB7". In: *Astrophysics* 49, pp. 320–332.
Melikian, N. D., V. S. Tamazian, and A. L. Samsonyan (2011). "Variation in the flare activity of the star UV Ceti". In: *Astrophysics* 54, pp. 469–475.
Melikian, N. D., V. S. Tamazian, J. A. Docobo, A. A. Karapetian, G. R. Kostandian, and A. A. Henden (2010). "Spectral and photometric observations of TT Ari. III." In: *Astrophysics* 53, pp. 373–386.
Melikian, N. D., V. S. Tamazian, A. A. Karapetian, and A. L. Samsonyan (2011). "Emission stars in Cyg OB7. new flare stars. III". In: *Astrophysics* 54, pp. 377–383.
Melikyan, N. D., R. S. Natsvlishvili, and M. Della Valle (1988). "Observations of the long-period variable star Y Ori". In: *Astrophysics* 28, pp. 193–197.
Melikyan, N. D., M. K. Tsvetkov, and R. A. Sarkisyan (1994). "Simultaneous Photoelectric and Spectral Observations of the Star Ev-Lacertae". In: *Astrophysics* 37, p. 312.
Merrill, P. W. (1922). "Interferometer observations of double stars." In: ApJ 56.
Michelson, A. A. (1920). "On the Application of Interference Methods to Astronomical Measurements". In: ApJ 51, p. 257.
Michelson, A. A. and F. G. Pease (1921). "Measurement of the Diameter of α Orionis with the Interferometer." In: ApJ 53.
Mikami, T. and K. Ogura (2001). "Hα Emission Stars in the Cepheus OB3 Region". In: Ap&SS 275, pp. 441–462.
Mirzoyan, L. V., O. S. Chavushyan, L. K. Erastova, G. B. Oganyan, N. D. Melikyan, R. S. Natsvlishvili, and M. K. Tsvetkov (1977). "Flare stars in the pleiades. V". In: *Astrophysics* 13, pp. 105–116.
Morgan, B. L., G. K. Beckmann, and R. J. Scaddan (1980). "Observations of binary stars by speckle interferometry. II". In: MNRAS 192, pp. 143–151.
Morgan, B. L., D. R. Beddoes, R. J. Scaddan, and J. C. Dainty (1978). "Observations of binary stars by speckle interferometry. I". In: MNRAS 183, pp. 701–710.
Muller, P. (1949). "Sur Un Nouveau Micrometre a Double Image, Ses Possibilites, et Quelques Questions Connexes." In: *Bulletin Astronomique* 14, pp. 257–313.
Nicholls, T. W., G. D. Boreman, and J. C. Dainty (1995). "Use of a Shack-Hartmann wave-front sensor to measure deviations from a Kolmogorov phase spectrum". In: *Optics Letters* 20, pp. 2460–2462.
Nightingale, N. S. and D. F. Buscher (1991). "Interferometric seeing measurements at the La Palma Observatory". In: MNRAS 251, pp. 155–166.

Nulsen, P. E. J., P. R. Wood, P. R. Gillingham, M. S. Bessell, M. A. Dopita, and C. McCowage (1990). "Speckle interferometry of SN 1987A - Final measurements". In: ApJ 358, p. 266.

Orlov, V. G. (2015). "Speckle Interferometry of the Solar Neighborhood". In: *Revista Mexicana de Astronomia y Astrofisica Conference Series*. Vol. 46. Revista Mexicana de Astronomia y Astrofisica Conference Series, pp. 47–49.

Paxton, B., L. Bildsten, A. Dotter, F. Herwig, P. Lesaffre, and F. Timmes (2011). "Modules for Experiments in Stellar Astrophysics (MESA)". In: ApJS 192, 3, p. 3. arXiv: 1009.1622 [astro-ph.SR].

Paxton, B., M. Cantiello, P. Arras, L. Bildsten, E. F. Brown, A. Dotter, C. Mankovich, M. H. Montgomery, D. Stello, F. X. Timmes, and R. Townsend (2013). "Modules for Experiments in Stellar Astrophysics (MESA): Planets, Oscillations, Rotation, and Massive Stars". In: ApJS 208, 4, p. 4. arXiv: 1301.0319 [astro-ph.SR].

Paxton, B., P. Marchant, J. Schwab, E. B. Bauer, L. Bildsten, M. Cantiello, L. Dessart, R. Farmer, H. Hu, N. Langer, R. H. D. Townsend, D. M. Townsley, and F. X. Timmes (2015). "Modules for Experiments in Stellar Astrophysics (MESA): Binaries, Pulsations, and Explosions". In: ApJS 220, 15, p. 15. arXiv: 1506.03146 [astro-ph.SR].

Persson, R. (2004). "Variable Star in Cepheus". In: IAU Circ. 8441.

Petrov, R. G., Y. Y. Balega, A. Blazit, V. A. Vasyuk, S. Lagarde, and R. Foy (1996). "Rotational velocity of the cool component of Capella from differential speckle interferometry". In: *Astronomy Letters* 22, pp. 348–353.

Pluzhnik, E. A. (2005). "Differential photometry of speckle-interferometric binary and multiple stars". In: A&A 431, pp. 587–596.

Prieur, J.-L., M. Scardia, L. Pansecchi, R. W. Argyle, A. Zanutta, and E. Aristidi (2017). "Speckle observations with PISCO in Merate (Italy): XV". In: *Astronomische Nachrichten* 338, pp. 74–90.

Racine, R. (2006). "The Strehl Efficiency of Adaptive Optics Systems". In: PASP 118, pp. 1066–1075.

Racine, R., G. A. H. Walker, D. Nadeau, R. Doyon, and C. Marois (1999). "Speckle Noise and the Detection of Faint Companions". In: PASP 111, pp. 587–594.

Raghavan, D. (2009). "A survey of stellar families: Multiplicity of solar-type stars". PhD thesis. Georgia State University.

Rappaport, S., P. Podsiadlowski, and I. Horev (2009). "The Past and Future History of Regulus". In: ApJ 698, pp. 666–675. arXiv: 0904.0395 [astro-ph.SR].

Rastegaev, D. A. (2010). "Multiplicity and Period Distribution of Population II Field Stars in Solar Vicinity". In: AJ 140, pp. 2013–2024. arXiv: 1009.4596 [astro-ph.SR].

Rastegaev, D. A., Y. Y. Balega, V. V. Dyachenko, A. F. Maksimov, and E. V. Malogolovets (2014). "Speckle interferometry of magnetic stars with the BTA. II. Results of 2010-2012 observations". In: *Astrophysical Bulletin* 69, pp. 296–304.

Reipurth, B. and C. Aspin (2004). "The FU Orionis Binary System and the Formation of Close Binaries". In: ApJ 608, pp. L65–L68.

Reipurth, B., C. Aspin, T. Beck, C. Brogan, M. S. Connelley, and G. H. Herbig (2007). "V733 Cep (Persson's Star): A New FU Orionis Object in Cepheus". In: AJ 133, pp. 1000–1011.

Ricort, G. and C. Aime (1979). "Solar seeing and the statistical properties of the photospheric solar granulation. III - Solar speckle interferometry". In: A&A 76, pp. 324–335.

Ricort, G., C. Aime, F. Deubner, and W. Mattig (1981). "Solar granulation study in partial eclipse conditions using speckle interferometric techniques". In: A&A 97, pp. 114–121.

Roddier, F. (1981). "The effects of atmospheric turbulence in optical astronomy". In: *Progress in optics. Volume 19. Amsterdam, North-Holland Publishing Co., 1981, p. 281-376.* 19, pp. 281–376.

Rogalski, A. (2005). "HgCdTe infrared detector material: history, status and outlook". In: *Reports on Progress in Physics* 68, pp. 2267–2336.

Rothman, J., E. de Borniol, S. Bisotto, L. Mollard, and F. Guellec (2009). "HgCdTe APD-Focal Plane Array development at DEFIR for low flux and photon-counting applications." In: *Proceedings of the Quantum of Quasars workshop. December 2-4, 2009. Grenoble, France. Published online at Quantum of Quasars workshop*, p. 9.

Schertl, D., Y. Balega, T. Hannemann, K.-H. Hofmann, T. Preibisch, and G. Weigelt (2000). "Diffraction-limited bispectrum speckle interferometry and speckle polarimetry of the young bipolar outflow source S140 IRS1". In: A&A 361, pp. L29–L32. eprint: astro-ph/0009456.

Schneider, G. and M. D. Silverstone (2003). "Coronagraphy with HST: detectability is a sensitive issue". In: *High-Contrast Imaging for Exo-Planet Detection.* Ed. by A. B. Schultz. Vol. 4860. Proc. SPIE, pp. 1–9.

Schoeller, M., I. I. Balega, Y. Y. Balega, K.-H. Hofmann, T. Reinheimer, and G. Weigelt (1998). "Diffraction-limited speckle masking interferometry of binary stars with the SAO 6-m telescope". In: *Astronomy Letters* 24, pp. 283–287.

Schwarzschild, K. (1896). "Über Messung von Doppelsternen durch Interferenzen". In: *Astronomische Nachrichten* 139, p. 353.

Selby, M. J., R. Wade, and C. Sanchez Magro (1979). "Speckle interferometry in the near-infrared". In: MNRAS 187, pp. 553–566.

Shannon, C. E. (1949). "Communication in the Presence of Noise". In: *IEEE Proceedings* 37, pp. 10–21.

Soummer, R., L. Pueyo, and J. Larkin (2012). "Detection and Characterization of Exoplanets and Disks Using Projections on Karhunen-Loève Eigenimages". In: ApJ 755, L28, p. L28. arXiv: 1207.4197 [astro-ph.IM].

Straizys, V. and G. Kuriliene (1981). "Fundamental stellar parameters derived from the evolutionary tracks". In: Ap&SS 80, pp. 353–368.

Tamazian, V. S., J. A. Docobo, and N. D. Melikian (1998). "Flare Activity of Visual Binary COU 14". In: Ap&SS 261, pp. 95–100.

– (1999). "Spectral, Photometric, and Polarimetric Study of Visual Binary COU 14". In: ApJ 513, pp. 933–940.

Tamazian, V. S., J. A. Docobo, N. D. Melikian, N. Baba, and V. H. Chavushyan (2000). "Spectral, photometric and speckle observations of visual binary WDS 00550+2338". In: A&A 363, pp. 1019–1025.

Tamazian, V. S., J. A. Docobo, N. D. Melikian, Y. Y. Balega, and A. A. Karapetian (2005). "Orbit, Dynamical Mass, and MK Type of Visual Binary WOR 2". In: AJ 130, pp. 2847–2851.

Tamazian, V. S., J. A. Docobo, Y. Y. Balega, N. D. Melikian, A. F. Maximov, and E. V. Malogolovets (2008). "Preliminary Orbit and Differential Photometry of the Nearby Flare Star CR Dra". In: AJ 136, pp. 974–979.

Tango, W. J., J. Davis, R. J. Thompson, and R. Hanbury (1979). "A 'Narrabri' binary star resolved by speckle interferometry". In: *Proceedings of the Astronomical Society of Australia* 3, p. 323.

Tatarskii, V. I. (1961). *Wave Propagation in Turbulent Medium*. McGraw-Hill.

Terrón, V. (2018). *LEMON: Differential photometry pipeline*. Astrophysics Source Code Library. ascl: 1809.001.

Texereau, J. (1962). "Turbulence et structure d'images photographiques dans un grand télescope". In: *L'Astronomie* 76, p. 159.

Thiebaut, E., Y. Balega, I. Balega, I. Belkine, J. Bouvier, R. Foy, A. Blazit, and D. Bonneau (1995). "Orbital motion of DF Tauri from speckle interferometry." In: A&A 304, p. L17.

Thiele, T. N. (1883). "Neue Methode zur Berechung von Doppelsternbahnen". In: *Astronomische Nachrichten* 104, p. 245.

Tokovinin, A. (2002). "From Differential Image Motion to Seeing". In: PASP 114, pp. 1156–1166.

– (2016). "New Orbits Based on Speckle Interferometry at SOAR". In: AJ 152, 138, p. 138.

– (2018a). "Dancing Twins: Stellar Hierarchies That Formed Sequentially?" In: AJ 155, 160, p. 160. arXiv: 1802.06445 [astro-ph.SR].

– (2018b). "Ten Years of Speckle Interferometry at SOAR". In: PASP 130.3, p. 035002. arXiv: 1801.04772 [astro-ph.IM].

Tokovinin, A. and R. Cantarutti (2008). "First Speckle Interferometry at SOAR Telescope with Electron-Multiplication CCD". In: PASP 120, pp. 170–177.

Tokovinin, A., B. D. Mason, and W. I. Hartkopf (2010). "Speckle Interferometry at the Blanco and SOAR Telescopes in 2008 and 2009". In: AJ 139, pp. 743–756. arXiv: 0911.5718 [astro-ph.SR].

Tokovinin, A., B. D. Mason, W. I. Hartkopf, R. A. Mendez, and E. P. Horch (2015). "Speckle Interferometry at SOAR in 2014". In: AJ 150, 50, p. 50. arXiv: 1506.05718 [astro-ph.SR].

Tokovinin, A., R. Cantarutti, R. Tighe, P. Schurter, M. Martinez, S. Thomas, and N. van der Bliek (2016). "SOAR Adaptive Module (SAM): Seeing Improvement with a UV Laser". In: PASP 128.12, p. 125003. arXiv: 1608.05593 [astro-ph.IM].

Tokovinin, A. A., A. Duquennoy, J.-L. Halbwachs, and M. Mayor (1994). "Duplicity in the solar neighborhood. 7: Spectroscopic orbits of three K-dwarf stars". In: A&A 282, pp. 831–834.

Tokovinin, Andrei, Brian D. Mason, William I. Hartkopf, Rene A. Mendez, and Elliott P. Horch (2018). "Speckle Interferometry at SOAR in 2016 and 2017". In: AJ 155, 235, p. 235.

Torres, G. (2010). "On the Use of Empirical Bolometric Corrections for Stars". In: AJ 140, pp. 1158–1162. arXiv: 1008.3913 [astro-ph.SR].

Trujillo, I., J. A. L. Aguerri, J. Cepa, and C. M. Gutiérrez (2001a). "The effects of seeing on Sèrsic profiles". In: MNRAS 321, pp. 269–276. eprint: astro-ph/0009097.

– (2001b). "The effects of seeing on Sérsic profiles - II. The Moffat PSF". In: MNRAS 328, pp. 977–985. eprint: astro-ph/0109067.

Tulloch, S. M. and V. S. Dhillon (2011). "On the use of electron-multiplying CCDs for astronomical spectroscopy". In: MNRAS 411, pp. 211–225. arXiv: 1009.3403 [astro-ph.IM].

Vakulik, V. G., V. N. Dudinov, A. P. Zheleznyak, S. B. Novikov, E. A. Pluzhnik, and V. S. Tsvetkova (1989). "Speckle Interferometry of Vesta at its 1988 Opposition - Preliminary Results". In: *Soviet Astronomy Letters* 15, p. 159.

Van Altena, W. F., E. Horch, and D. I. Casetti-Dinescu (2017). "Sixteen Years of Speckle Interferometry at the WIYN Observatory". In: *AAS/Division of Dynamical Astronomy Meeting #48*. Vol. 48. AAS/Division of Dynamical Astronomy Meeting, p. 203.03.

van den Bos, W. H. (1926). "Orbital Elements of Binary Stars". In: *Circular of the Union Observatory Johannesburg* 68, pp. 352–359.

– (1932). "Orbital Elements of Binary Stars". In: *Circular of the Union Observatory Johannesburg* 86, pp. 261–270.

– (1953). "A Study of Finsen's Interferometer Measures of Double Stars". In: *Circular of the Union Observatory Johannesburg* 113, pp. 183–184.

van Leeuwen, F. (2007). "Validation of the new Hipparcos reduction". In: A&A 474, pp. 653–664. arXiv: 0708.1752.

Velasco, S., C. Colodro-Conde, R. L. López, A. Oscoz, L. Labadie, Y. Martín-Hernando, A. Pérez Garrido, C. Mackay, and R. Rebolo (2018). "The adaptive optics lucky imager (AOLI): presentation, commissioning, and AIV innovations". In: *ArXiv e-prints*. arXiv: 1807.09759 [astro-ph.IM].

Vidal, E. (1979). *Hombres que hicieron Galicia*. Ed. Banco Noroeste.

Wachmann, A. (1954). "Das bisherige Verhalten von FU Orionis. Mit 7 Textabbildungen". In: ZAp 35, p. 74.

Weigelt, G., G. Baier, and R. Ladebeck (1985). "R136a and the central object in the giant H II region NGC 3603 resolved by holographic speckle interferometry". In: *The Messenger* 40, pp. 4–6.

Weigelt, G., Y. Balega, T. Bloecker, A. J. Fleischer, R. Osterbart, and J. M. Winters (1998). "76mas speckle-masking interferometry of IRC+10216 with the SAO 6m telescope: Evidence for a clumpy shell structure". In: A&A 333, pp. L51–L54. eprint: astro-ph/9805022.

Weigelt, G., Y. Balega, T. Preibisch, D. Schertl, M. Schöller, and H. Zinnecker (1999a). "Bispectrum speckle interferometry of the Orion Trapezium stars: detection of a close (33 mas) companion of Theta (1) ORI C". In: A&A 347, pp. L15–L18. eprint: astro-ph/9906233.

Weigelt, G., T. Blöcker, K.-H. Hofmann, R. Osterbart, Y. Y. Balega, A. J. Fleischer, and J. M. Winters (1999b). "Diffraction-limited 76 mas speckle-masking interferometry of the carbon star IRC + 10 216 and related AGB objects with the SAO 6 m telescope". In: *Asymptotic Giant Branch Stars*. Ed. by T. Le Bertre, A. Lebre, and C. Waelkens. Vol. 191. IAU Symposium, p. 273. eprint: astro-ph/9811276.

Weigelt, G. P. (1977). "Modified astronomical speckle interferometry 'speckle masking'". In: *Optics Communications* 21, pp. 55–59.

– (1978a). "Speckle interferometry measurements of 12 binary stars". In: A&A 68, p. L5.

– (1978b). "Speckle interferometry with a 1 m-telescope". In: A&A 67, p. L11.

Winters, J. G., T. J. Henry, J. C. Lurie, N. C. Hambly, W.-C. Jao, J. L. Bartlett, M. R. Boyd, S. B. Dieterich, C. T. Finch, A. D. Hosey, P. A. Ianna, A. R. Riedel, K. J. Slatten, and J. P. Subasavage (2015). "The Solar Neighborhood. XXXV. Distances to 1404 m Dwarf Systems Within 25 pc in the Southern Sky". In: AJ 149, 5, p. 5. arXiv: 1407.7837 [astro-ph.SR].

Wöger, F., O. von der Lühe, and K. Reardon (2008). "Speckle interferometry with adaptive optics corrected solar data". In: A&A 488, pp. 375–381.

Wood, P. R., M. S. Bessell, and M. A. Dopita (1985). "Angular diameters of Magellanic Cloud planetary nebulae obtained using speckle interferometry". In: *Proceedings of the Astronomical Society of Australia* 6, p. 54.

Wood, P. R., P. E. J. Nulsen, P. R. Gillingham, M. S. Bessell, M. A. Dopita, and C. McCowage (1989). "Speckle interferometry of SN 1987A up to one year after explosion". In: ApJ 339, pp. 1073–1077.

Worley, C. E. (1997). "The Visual Double Star Database". In: *Baltic Astronomy* 6, pp. 248–250.

Worley, C. E. and G. G. Douglass (1992). "Speckle Interferometry at the U.S. Naval Observatory". In: *IAU Colloq. 135: Complementary Approaches to Double and Multiple Star Research*. Ed. by H. A. McAlister and W. I. Hartkopf. Vol. 32. Astronomical Society of the Pacific Conference Series, p. 583.

J. A. Docobo (right) and J. Gómez Crespo (left) at OARMA's library